University of Alberta
Department of Civil &
Environmental Engineering

Structural Engineering Report No. 55

An Elastic Stress Analysis of a Gentilly Type Containment Structure Volume 1

by

D.W. Murray

and

M. Epstein

April, 1976

University of Alberta

Department of Civil Engineering

An Elastic Stress Analysis of a Gentilly Type Containment Structure

- Volume 1 -

by

D.W. Murray

M. Epstein

Faculty Investigators:

Professor J.G. MacGregor

Professor D.W. Murray

Professor S.H. Simmonds

A Technical Report to the
Atomic Energy Control Board
Nuclear Plant Licensing Directorate
P.O. Box 1046
Ottawa, Canada K1P 5S9

July 1976 Revision

Acknowledgements

The authors wish to acknowledge the cooperation of the following agencies which provided technical information and/or financial support for this study.

The Atomic Energy Control Board

Atomic Energy of Canada, Limited

Hydro-Québec

Canatom Limited

Ontario Hydro

The interpretation of technical data and any opinions or conclusions arising in this report are those of the authors only and do not necessarily reflect those of the cooperating agencies.

NOTE ON JULY 1976 REVISION

A revision to this report was carried out in July 1976 in an effort to eliminate, as far as possible, any inaccuracies. Many minor alterations were carried out but some revisions of substance were included. These revisions center around the analysis of the structure in the region of the base detail. In particular, the effects of vertical prestressing were modified to include an upward vertical prestressing force at the bottom of the perimeter wall, the effect of pressure on the base slab was included, and minor corrections were made to uniform temperature changes in the structural components. The primary effect of these alterations is with respect to the stress conditions in the region of the connection of the cylinder wall to the base. This necessitated a substantial revision of Appendix M.

Subsequent to this revision, the authors received specific comments relating to the definitions of influence loadings, the effect of thickening the structure at the springing line of the upper dome, and the correlation of analyses with tests results. These factors are examined briefly in an ADDENDUM, and the inclusion of this material has resulted in a delay in issuing the revised report.

D. W. Murray
September 13, 1976

TABLE OF CONTENTS

* Appendices B to F are bound separately as Volume 2 of this report.

LIST OF TABLES

LIST OF FIGURES

LIST OF FIGURES IN APPENDICES OF VOLUME 1

APPENDIX G Stress-Resultants for Reference States — Page

APPENDIX K Interaction Curves at Selected Locations

LIST OF FIGURES IN APPENDICES OF VOLUME 2

APPENDIX B - Stress Resultants for Dead Loads of Portions of the Structure

APPENDIX C - Stress Resultants for Prestress Influence Loadings

1. INTRODUCTION

1.1 Background

This report is the first technical report in a continuing program, sponsored by the Atomic Energy Control Board of Canada, to investigate the overpressure response of nuclear containment structures. The prototype building for the report is the Gentilly-2 Nuclear Power Station Reactor Building, which is considered to be representative of the containment buildings for housing 600 MWe CANDU-PHW type nuclear reactors.

A description of the prototype building, as extracted from Ref. 4, is as follows.

> "The Reactor Building houses the reactor, the auxiliary equipment, the heat transport system and the fuel handling equipment and instrumentation. It essentially consists of two distinct parts (See Fig. 1.1):
>
> a) the containment structure
>
> b) the internal structure.
>
> The major design criteria of the structures are based on safety requirements with application of appropriate safety coefficients.
>
> a) structural safety
>
> b) containment requirements
>
> c) radiation protection

The building design is based on an internal pressure of 18 psig, and a maximum permissible leakage rate of 0.5% per day. The basic data values will be specified during a detailed safety analysis which will include all information from various conditions of operation, accidents, climate, earthquakes, etc.

The containment structure is a prestressed concrete building overall height 168' and comprising:

a) a circular base slab, 5'0" thick and about 155'0" in diameter;

b) a perimeter wall about 3'6" thick, having an inner radius of 68'0";

c) a spherical dome, 2'0" thick at center and a radius of 136'0".

The perimeter wall and dome are independent of the internal structure, which provides a greater flexibility in the overall construction.

Beneath the dome is located a second, reinforced concrete spherical dome with an opening at its centre. This structure constitutes a water tank having a 560,000 imperial gallon capacity.

The base slab is built over a reinforced concrete sub-base slab. A peripheral gallery forms an integral part of the sub-base slab and is designed to allow the tensioning of the cylindrical wall vertical prestressing. It is also used for drainage and inspection. In order to withstand horizontal seismic forces, a system of shear keys connect the base slab to the sub-base slab. (See Figures 1.2 and 1.3).

The internal containment surfaces are covered with an impermeable lining to provide building leak-tightness. The number of penetrations necessary for the passage of water and steam pipes, ventilation ducts and instrumentation and electric cables is minimized and they are built and installed so as to reduce leakage. The largest of these is the equipment airlock.

The perimeter wall is constructed by means of a sliding formwork. Two temporary openings will be provided to allow the entrance of large, heavy elements such as the calandria and steam generators.

Instrumentation devices will be located at appropriate places to measure the distortion and behaviour of various structure components, especially during periodic leakage rate tests."

1.2 Scope of Investigation

The scope of the investigation, of which this report is a part, is outlined in a Proposal for Research (Nov. 15, 1974), submitted by the University of Alberta to the Atomic Energy Control Board, and other supporting documents. The complete investigation outlined in this proposal consists of a series of subphases involving both analytical and experimental investigations and spanning a time period of approximately four and one-half years.

The objective of the study, briefly stated, is to determine the response of nuclear containment structures to internal pressure which may occur as a result of a failure in the piping associated with either the primary or secondary cooling system housed within the structure. The study, in the initial phases, is to concentrate on an examination of the structural response to a hypothetical internal pressure which may increase to the point where it results in complete structural collapse, without regard to the feasibility of such pressures being produced by any postulated series of events which may, or may not, occur within the structure. The primary motivation for investigating such response is to determine the stage in the load deformation history of a containment structure at which an overpressure may result in damage to the safety systems.

Under such a hypothetical pressure increase it is possible to define a series of limit states which are indicative of the deterioration of the structure and may influence its capacity to perform either its containment function or its function of preserving the integrity of the systems which it houses. The limit states which may be of interest in the response of the structure are considered to be the following (not necessarily in chronological order):

1. The pressure at which stress initiates cracking over a significant area of the internal surface.

2. The pressure at which cracks may penetrate through the wall.
3. The maximum pressure from which a prestressed structure can reseal itself upon pressure relief.
4. The pressure at which mild steel reinforcing begins to yield and beyond which permanent residual strains will be retained.
5. The pressure at which yield lines may form to initiate a structural mechanism.
6. The conditions under which rupture of the reinforcing or concrete may lead to sudden failure.
7. The pressure at which relative displacements within the structure may cause significant distress to the systems which are housed within the structure.
8. The pressure at which bond failure or spalling of the concrete may lead to debris falling within the structure.

1.3 Scope of Report

Any attempt to predict structural response over the complete range of hypothetical internal pressure up to the point of structural collapse must necessarily involve the inclusion of nonlinear material and geometric effects. The effect of these nonlinearities on the distribution of forces throughout the structure is beyond the scope of the present report but will be the subject of subsequent reports.

The object of this report is to examine the analysis of a Gentilly-type containment structure by classical linear elastic theory and to develop methodology, subject to the limitations of linear elastic analysis, to estimate the internal pressure at which some of the limit states itemized in Sec. 1.2 may be expected to be attained. For this purpose an approach similar to the "strength design" approach to reinforced concrete has been adopted. That is, although the distribution of forces (i.e. - the "structural analysis") will be determined on the basis of linear elastic response, the effect of these forces on any cross-section (herein called a "section analysis") will be investigated by recognizing the inelastic material response that must occur prior to the development of the full capacity of the section. This approach, as it applies to containment structures, is examined in more detail in the following section.

1.4 General Assumptions, Stress Classification and Loading

"Strength design" is based on two fundamental assumptions. The first is that the distribution of forces throughout the structure may be determined from a superposition of analyses for separate loading effects. This implies the distribution pattern associated with each forcing effect is independent of the level of the loads. The structure as a whole may, therefore, be analyzed elastically to determine each distribution pattern. The second assumption is that forces determined by the above superposition will increase linearly with the loads until they develop the full ultimate strength capacity of the section. A determination of the ultimate strength capacity of the section requires inclusion of nonlinear material response. It can be shown that the load carrying capacity of a ductile structure computed by such a technique is a lower bound on the actual carrying capacity (11, 14). The development of adequate ductility in a reinforced concrete structure to ensure this conclusion is highly dependent on proper detailing of the reinforcement and good construction practices.

A feature of containment structures which must be recognized in order to obtain a realistic assessment of structural response is the "self-limiting" characteristic of some of the stress-resultants which may be significant under service conditions. In normal building design this type of stress resultant is either omitted or, at best, considered only in an indirect manner. Consequently, there is no mechanism in strength design, other than the explicit variation of individual load factors, to account for their effects. In the prediction of behavior, as opposed to design, load factors are derived from the analysis and the self-limiting characteristic of the loading must be explicitly recognized in the analytical process if the computation of these load factors is to have any validity.

The writers have adopted the definitions of Article CC-3136 of Ref. 1, in which loading effects are classified as producing either 'primary' or 'secondary' stresses. These definitions are as follows:

"<u>Primary Stress.</u> Primary stress is any normal stress or a shear stress developed by imposed loading which is necessary to satisfy the laws of equilibrium of external and internal forces and moments. The basic characteristic of a primary stress is that it is not self-limiting. Primary stresses which considerably exceed the yield strength in a steel member or gross cracking in concrete will result in failure or gross distortion. Thermal stress is not classified as a primary stress. The following are examples of primary stresses:

(a) stresses due to internal pressure or to distributed live loads.

(b) bending stress in the central portion of a flat slab due to pressure."

"<u>Secondary Stress.</u> Secondary stress is a normal stress or a shear stress developed by the constraint of adjacent material or by self constraint of the structure. The basic characteristic of a secondary stress is that it is self limiting. Local yielding, minor distortions, and concrete cracking can satisfy the conditions which cause the stress to occur and failure is not to be expected. The following are examples of secondary stresses:

(a) general thermal stress

(b) bending stress at a gross structural discontinuity."

In general it is necessary to consider both primary and secondary stress resultants when considering serviceability conditions, but only primary stress resultants when considering collapse conditions. The results contained in Chapters 3 and 4 of this report can be examined in the light of this expectation.

The following load sources have been included in this report:

(a) gravity forces

(b) internal pressure

(c) shrinkage strains

(d) thermal strains

(e) prestressing forces

A consideration of the effects of these load sources in relation to the above classification indicates the following division for Gentilly-type structures:

(A) Primary stress resultants.

(a) membrane forces from gravity loads

(b) membrane forces from internal pressure

(B) Secondary stress resultants.

(a) bending moments from gravity loads*

(b) bending moments from internal pressure*

(c) all shrinkage effects

(d) all thermal effects

(e) all prestressing effects

(*Note: The total static moment in the base slab is a primary stress resultant, while moments in the shell structure are secondary.)

If one now considers the stress resultants as they relate to the limit states itemized in Sect. 1.2 it would be expected that both primary and secondary stress resultants would be significant for limit states 1 and 4 while only primary stress resultants would be of significance for limit states 2, 6 and 8. The results of the analyses in the remainder of this report should be examined with a view to establishing the validity of these expectations and the degree to which secondary stress resultants may influence the limit states.

1.5 Structure of Report

The report is aimed at determining the nature of the overall response of a Gentilly-type structure. The model of the structure that has been used for this purpose does not consider many features that could influence the response of the actual structure. The structure is assumed axisymmetric and therefore the effect of the vertical pilasters for anchorage of prestressing cables, the rows of penetrations, temporary openings, airlocks and stress concentration effects have not been determined. These items must await a more detailed study.

Chapter 1 has dealt with the general background for the report. Chapter 2 deals with a load superposition analysis of an elastic axisymmetric structural model. Chapter 3 deals with the methodology of the cross-section analysis. Chapter 4 summarizes the results obtained by applying the techniques of Chapter 3 to the Gentilly-2 containment structure subjected to overload pressures. Chapter 5 contains a brief summary and conclusions.

2. LOAD SUPERPOSITION ANALYSIS

2.1 Choice of Structural Analysis Procedure

As indicated in Sect. 1.5 the structure has been modelled as axisymmetric. There are many methodologies which can be used to predict the stress resultants in such a structure. Among these are:

(a) An analysis based on classical shell theory that considers the structure to be broken into component parts, namely, the base, the cylinder, the ring beam and the upper and lower domes, and establishes the forces of interaction between these parts on the basis of a flexibility analysis. A 'closed form' solution is then available to determine stress resultants in each component.

(b) A computer analysis based on approximating the classical shell equations in terms of displacement variables at discrete points throughout the structure. Discretization can be carried out through either the finite difference or finite element technique.

(c) Finite element three-dimensional continuum models for axisymmetric problems.

In view of the fact that the shell components have thickness to radius ratios of approximately 0.015 while the cylindrical component has a thickness to radius ratio of 0.050, a classical thin shell approach would be expected to produce reliable results for linear elastic response. The investigators, therefore, decided to opt for the second of the above types of analyses and selected the BOSOR4 computer code (7,8) to carry out the analysis. This code has a number of desirable features which are described briefly in the following section.

2.2 A Description of the BOSOR4 Computer Code (7,8)

The BOSOR4 computer code (BOSOR is an acronym for buckling of shells of revolution) is a program that is generally available to the engineering profession through its developer, Dr. David Bushnell*. As the name would indicate, this code has been developed primarily to predict buckling (and vibrations) of shell structures but can be specialized easily to linear static analysis. It has a number of features such as the ability to consider stiffening rings, the capability of offsetting components to form eccentric connections, the capability of treating branched shells, and the capability of treating variations of thickness which make it an attractive general purpose program to employ in the analysis of a Gentilly-type structure.

The following is a short description of the scope and capabilities of BOSOR4, based on Ref. 8. The capabilities of BOSOR4 for solving buckling, large deformation, and dynamics problems are not discussed.

---

* Dr. David Bushell, Lockheed Palo Alto Research Laboratory 3251 Hanover Street, Palo Alto, California, 94304.

"The BOSOR4 computer program was developed in response to the need for a tool which would help the engineer to design practical shell structures. An important class of such shell structures includes segmented, ring-stiffened branched shells of revolution. These shells may have various meridional geometries, wall constructions, boundary conditions, ring reinforcements and types of loading, including thermal loading."

With respect to the geometry of the meridian, "the entire shell structure may consist of a number of shell segments joined together in series or branched. The reference surfaces of adjacent segments need not be continuous. Both axial and radial discontinuities are permitted."

The basic types of segments included are: cylindrical, conical, flat circular, spherical, toroidal and ogival segments. Additional shell types can be accommodated by the insertion of other subroutines to calculate parameters for a specific geometry where dummy subroutines are now provided. Alternatively, for completely general shapes, BOSOR4 allows the direct input of relevant geometric data (e.g. curvature radii) at selected mesh points. Reference surfaces can be located anywhere inside or outside the shell walls.

BOSOR4 uses an energy formulation in conjunction with the method of finite differences (6) in a similar fashion as in the finite element method. Each shell segment is divided by means of a mesh which need not be uniform. Points can therefore be concentrated in areas where the solution is expected to vary rapidly.

Three kinds of constraint conditions exist in BOSOR4:

(1) constraints to ground (e.g., boundary conditions)

(2) juncture compatibility conditions

(3) regularity conditions at poles (where radius $r = 0$)

All constraint conditions are written in terms of global variables u^*, v^*, w^* and χ, which are shown in Fig. 2.1(a).

Three groups of data are specified for each constraint condition:

(1) the location of the constraint

(2) the particular variables u^*, v^*, w^*, χ which are constrained.

(3) axial and radial components of a reference surface discontinuity or of a support point eccentric with respect to the reference surface.

Note that BOSOR4 does not allow one to prescribe

a) linear combinations of the displacement variables,

b) linear combinations between displacements and forces,

c) non-homogeneous boundary conditions of displacement.

This is regrettable since these three features are so common in structural applications. On the other hand, the possibility of specifying eccentric connections between segments is a valuable element in BOSOR4 and has been exploited fully in the present analysis of the Gentilly-2 containment vessel.

Each segment may be reinforced by any number of rings. These rings are treated as discrete elastic structures in the analysis. The rings serve also the purpose of allowing the application of line loads.

The rings may be connected eccentrically to any mesh point. They may be composed of up to three rectangles arranged as in a I. Alternatively, their geometric and elastic properties (moments of inertia, etc.) may be specified externally.

"With regard to type of wall construction, the following special branches calling for simple input data are provided:

(1) Monocoque shells

(2) Shells with skew stiffeners

(3) Fiber-reinforced shells laid up in layers (fiberglass)

(4) Layered shells with orthotropic layers

(5) Corrugated shells

(6) Shells with one corrugated and one smooth skin

(7) Layered shells with orthotropic layers, each layer of which has temperature-dependent material properties.

Any of these types of shells can be reinforced by two types of stiffeners. (1) rings and stringers which are "smeared out" in the analysis and (2) by the addition of rings which are treated as discrete elastic structures".

"Mechanical or thermal line loads or distributed loads (pressures) are permitted in the analysis. These loads may be axisymmetric or may vary around the circumference, and the temperature may vary through the thickness. In cases involving non-symmetric loading a linear analysis is used. The program finds the Fourier series for the loads, calculates the shell response in each harmonic to the load components with that harmonic, and superposes the results for all harmonics. The superposed displacements and stress resultants are printed and plotted for selected meridional and circumferential stations. Line loads and moments are assumed to be applied at ring centroids. Thermal line loads arise from the presence of discrete rings which may be heated above their zero-stress states. Distributed thermal loads arise from temperature distributions over the shell surface and through the shell wall thickness".

The variation of distributed thermal and mechanical loads along the meridian is specified by giving their values at selected mesh points. BOSOR4 interpolates linearly between the values given.

The variation of distributed thermal loads through the thickness of the shell is given by specifying the values of constants T1, T2, T3 in one of the following expressions:

$$T1 + T2 \cdot Z + T3 \cdot Z^2$$

$$T1 + T2 \cdot Z^{T3}$$

$$T1 + T2 \cdot \exp (Z \cdot T3)$$

where Z is the thickness coordinate.

2.3 Structural Modelling

The principal dimensions of the Gentilly-2 containment structure are shown in Fig. 2.2. The structure and supporting foundation have been modelled as 11 shell segments and one ring (the perimeter wall at the interior edge of the reservoir). The reference surfaces for the shell segments have been specified as the middle surfaces of the segments. A continuous coordinate, starting at the axis of symmetry at the base of the structure, is used to reference any location in the structure.

The centerline geometry of the model is shown in Fig. 2.3, where the shell segements are identified together with their starting and finishing coordinates. The program sets up geometric constraint equations between the segments which may be visualized as rigid links. Schematic representations of the connections between the shell segments are shown in Fig. 2.4.

The base support has been simulated as an axisymmetric Winkler foundation. That is, the subgrade at a point of support is assumed elastic, and the reaction is therefore proportional to the vertical displacement, but there is no coupling of the reactive forces with displacements of adjacent supporting points. The base was assumed supported at 5 points as shown in Fig. 2.5. Each support was modelled as an axisymmetric annulus and a short shell segment, with axial stiffness proportional to the area of the respective annulus, was attached to the bottom of the base slab. A load of 120 k/ft. was then applied to the perimeter at the wall line and the stiffness of all support segments was adjusted proportionately until the displacement at the base of the wall was 0.15 inches. This displacement corresponds to that obtained from measured base slab settlements of the Gentilly-1 reactor building (Plate 5 of Ref. 16).

The connection of the wall into the top of the base slab has been modelled by a segment one foot in length which tapers from a width of 1.0 ft. at the hinge to 3.5 ft. where it meets the wall as shown in Fig. 2.4.

2.4 Influence Analyses

In a linear elastic analysis the final set of stress resultants can be obtained from a superposition of individual effects. It is convenient, therefore, to carry out analyses to determine the effect of a unit loading of any particular type on the structure. In this manner the influence of a particular loading can be examined prior to a load superposition that reflects the aggregate effect of a combination of loads.

When dealing with any structural analysis there are a number of secondary loadings which contribute to the state of stress at service loads but which are not normally explicitly included in an analysis because they have little or no effect on the ultimate strength of the structure. However, in view of the importance of cracking in a containment structure, and the possible influence of these secondary loadings on the limit states itemized in Sect. 1.2, an attempt has been made to include them. The construction sequence is one of the factors which can be of significance.

The construction sequence for Gentilly-2, as determined from Ref. (12) and discussions with the designers, may be described as follows.

1. Pour base slab
2. Apply 20% of base slab prestressing
3. Pour cylindrical wall
4. Apply remaining 80% of base prestressing and 20% of horizontal cylinder prestressing.
5. Pour lower segment of ring beam and lower dome.
6. Prestress lower ring beam.
7. Pour upper segment of ring beam and upper dome.
8. Apply upper ring beam prestressing, upper dome prestressing and the remainder of the cylinder prestressing.

Since this construction sequence takes place over an extended period, the effect of shrinkage between the completion of different segments of the building could induce stresses that might be of significance. Shrinkage effects have been simulated by an equivalent uniform temperature change in each structural segment that produces the desired inelastic strain. Prestressing effects have been simulated by an equivalent distributed pressure which produces the desired membrane forces in the structural segments. Gravity loads, shrinkage strains and prestressing forces have been applied to the partial structures which exist at the time the loading effects are applied, in a manner consistent with the above construction sequence, in order to determine the effects of the construction sequence on the secondary stress resultants.

In order to simulate the effect of the construction sequence it has been considered sufficient to consider two partial structures in addition to the completed structure. These structures are shown schematically in Table 2.1. The structures are designated as BW (base and wall), BD (base to lower dome) and C (complete). In addition, at high internal pressures the junction between the base and the wall may behave as a hinged connection. For this reason some loading effects have been considered to act on a structure designated as CH (complete with hinge).

Table 2.1 itemizes the influence loads for which each of the structures have been analyzed. The source of the influence loading has been designated by a lower case letter (or a combination thereof). Eight types of influence loadings, designated by the letters f, d, u, g, hf, vf, p and w have been considered. A description of this symbology is given in Table 2.1. Since these influence loads may act on only portions of the structure it is necessary to associate a structure segment with the loading. Seven structural segments designated as B (base), W (wall), LB(lower ring beam), UB (upper ring beam), RB (complete ring beam), LD (lower dome) and UD (upper dome) are necessary to identify the segment of the structure on which a loading effect acts. An influence load may then be described by prefixing the structural segment designation to the load source designation. Finally, the influence loading designation may be prefixed by the partial structure designation to which the loading is applied. Thus C:UBu indicates a uniform strain applied to the upper ring beam when it is a component of the complete structure, while BD:LDd indicates dead load of the lower dome applied to the 'base-to-lower-dome' structure.

In light of the above description the reader should be able to identify the thirty-eight influence loadings itemized in Table 2.1. The stress resultants arising from these influence loadings analyses are contained in graphical form in Appendices B to F.

Appendix B contains plots of stress resultants due to partial gravity loadings. Appendix C contains plots of stress resultants due to the unit distributed pressures which were used to simulate the effect of prestressing. Appendix D contains plots of stress resultants arising from uniform unit strains which were used in the simulation of thermal and shrinkage effects. Appendix E contains plots of the influence of unit strain gradients through the wall thickness which were used in the analysis for thermal gradients. Appendix F contains plots of the stress resultants arising from unit internal pressure and other live load effects.

In these Appendices and in the remainder of this chapter the stress resultants N1 and M1 arise from stresses parallel to the coordinate axis traversing the section in Fig. 2.3. The stress resultants N2 and M2 arise from stresses in the tangential direction. Positive axial stress resultants are tensile and positive moments produce tension on the inside of the structure as shown in Figure 2.1. The plots are divided into segments corresponding to the structural components itemized in Table 2.1, and the abcissa represents the length coordinate of Fig. 2.3. The stress resultants M2 are ν times those for M1 in all cases except for the strain gradient loading cases in which they are equal to M1. However, plots of all stress resultants have been included for completeness (unless the resultant is essentially zero). A list of figures has been included at the beginning of each of these Appendices.

Appendices B to F have been bound separately, as VOLUME 2 of this report, in order to maintain a reasonable size for VOLUME 1.

The reader is cautioned to check the scales on all plots before attempting an interpretation since the plotting program adjusts the scale to fill the width of the page and therefore a high ordinate on one plot may be less significant than a low ordinate on another.

2.5 Reference States for Long Term Loading

The distribution of forces throughout the structure may now be obtained by a proper superposition of the influence loadings itemized in Sect. 2.4. For this purpose thermal and internal pressure loads may be considered to be live loads in the sense that they may be applied in various combinations over short periods of time. On the other hand, gravity, creep, shrinkage and prestressing effects are continuous long term effects which combine to produce a given 'reference state' onto which live loads may be superimposed. Therefore the effect of each of these continuous load sources is considered independently in this Section and these are then superimposed to obtain suitable reference states which represent the state of the structure immediately prior to the application of live loads. Stress plots for these reference states are presented in Appendix G.

2.5.1 Gravity Loads

As discussed in Sect. 2.4 the influence of gravity loading has been determined on the partial structures. The load combination indicated in Column 2 of Table 2.2 represents a straight forward accumulation of these gravity loads. The application of these loads depends on the construction procedure. The load combination in Column 2 of Table 2.2 assumes the shoring below the lower dome will remain effective in carrying the shoring and dead load of the upper dome, and that stripping of both domes occurs after the structure has been completed. However, if it is assumed that prestressing of the lower ring beam lifts the lower dome from its form-work, or that shoring is removed from the lower dome prior to casting the upper dome, the lower dome may be expected to carry the weight of the upper dome until stripping of the upper dome is completed. In this case the load combination of Column 3 of Table 2.2 is more realistic. These load combinations will be referred to as reference states Rd1 and Rd2, respectively.

The normal technique of structural analysis is to analyze for dead loads applied to the completed structure (sometimes referred to as "switched-on gravity"). This load condition will be referenced, in the notation of Sect. 2.4, as C:Cd. Plots of stress resultants from the three different dead load analyses are contained in Figs. G1 to G12 of Appendix G. A comparison of C:Cd with Rd1 indicates only minor discrepancies in the stress resultants and the "switched-on-gravity" analysis appears to be perfectly adequate to represent the construction sequence of Rd1. A comparison of Rd1 with Rd2 indicates that the N1 stress resultant is affected very little by the shoring technique used for the upper dome. The moments in the vicinity of the ring beam are substantially affected, as are the N2 stress resultants. However, the increases in these effects are generally in the opposite sense to those created by internal pressure (see Figs. F3 and F4) and therefore would appear to have little or no detrimental effect.

2.5.2 Prestressing Forces

The load superposition indicated in Column 4 of Table 2.2 represents the sequencing of prestressing on the partial structures. The partial prestressing as the construction progresses is intended to prevent shrinkage cracking and cracking from construction loads. The final prestressing is intended to produce compressive stresses in the concrete which are sufficient to prevent cracking or to limit the tensile stress under the factored loading conditions specified in the design critieria. In the case of Gentilly-2 the design criteria were no tension on the inner surface of the structure under the proof pressure test and no cracking on the inner surface of the structure under design basis accident conditions (3).

The plots for the superposition of prestressing effects are shown in Figs. G13 to G16. These effects are only significant when superimposed on the dead load forces. The superposition of the prestress forces on reference states Rd1 and Rd2 results in the reference states referred to as Rf1 and Rf2, respectively, which are plotted in Figs. G25 to G28 and G33 to G36 respectively.

It is interesting to compare the final prestressing forces from the staged prestressing sequence (G13 to G16) with those obtained by 'switching-on' the prestress forces in the final structure (G17 to G20). Except for the N2 stress resultant, the 'switched-on' prestress forces differ substantially from the staged prestressing forces only in the vicinity of the ring beam.

The primary variable which may affect the prestressing forces is the effect of creep. It is usual to account for creep by allowing a factor for stress relaxation in design such that the design is carried out for the net prestressing force which results after all relaxation has occurred. It can be argued that creep is proportional to the stress level in the concrete and that since these stresses have been determined from a compatibility analysis, the resulting creep strains will increase deflections but will not result in a redistribution of stress resultants from one portion of the structure to another. Although this argument ignores the stiffening effect of reinforcing steel it is considered to be sufficiently valid for the effect of creep to be disregarded in determining the magnitude of the stress resultants. The effect of creep has been implicitly considered in the load superposition by employing the net prestressing forces which should result after all losses, and will be explicitly considered in all section cracking analyses (Chaps. 3 and 4) by allowing for a transfer of stress between steel and concrete.

2.5.3 Shrinkage

Shrinkage is a secondary effect which depends primarily on the quantity of water in the concrete mix. The rate of shrinkage is influenced by the rate at which water is lost to the surrounding medium. There is, therefore, a significant non-uniformity in shrinkage strains between the surface layers and the interior of a concrete section. If the flow of water to the atmosphere is similar on each surface of the section, however, the effect of shrinkage for the purposes of determining stress resultants is simply that of a uniform strain. (The stress distribution across a section resulting from differential shrinkage can be examined by the techniques presented in Sect. 3.4.) Stress resultants arising from shrinkage may be determined by superimposing the different values of this uniform inelastic strain associated with each of the segments of the structure. Shrinkage strains have been computed by the technique recommended by the Comité Européen du Béton in Ref. 17. A summary of these computations is contained in Appendix H and the resulting uniform strains are shown in Column 5 of Table 2.2.

A linear combination of the uniform shrinkage strains of Appendix D, combined as indicated in Column 5 of

Table 2.2 produces the stress resultants arising from shrinkage as plotted in Figs. G21 to G24. It should be noted that these stress resultants are generally very small except for the N2 stress resultant of Fig. G22.

Superposition of the shrinkage analysis on the reference states Rf1 and Rf2 yields the reference states Rs1 and Rs2, respectively, which include the effects of dead load, prestressing and shrinkage. Stress resultants of these reference states are presented in Figs. G29 to G32 and G37 to G40, respectively. A comparison of the Rs reference states with the corresponding Rf reference states indicates that shrinkage effects can be neglected in the calculation of the reference state forces and moments without significant error, except as noted in Sect. 5.1.3.

2.6 Short Term Loadings (Live Loads)

The effect of short term or live loads can now be superimposed on the long term reference states of Sect. 2.5. Since the magnitudes of the live loads can vary in proportion depending on the conditions one wishes to simulate, the combination of live loads with the reference states will be carried out in Chapter 3. In the present Chapter the live load effects are examined individually.

Stress resultants for a unit internal pressure (influence loadings C:Cp and CH:Hp) are presented in Figs. F1 to F6 of Appendix F.

Thermal analyses are obtained from a linear combination of the unit uniform strain effects of Appendix D and the unit gradient strain effects of Appendix E. Thermal analyses have been carried out for the stress resultants arising from the summer shut down temperatures (SST), winter operating temperatures (WOT) and summer operating temperatures (SOT), specified in reference 16 (Plate No. 4). The results are contained in Figs. F7 to F15, inclusive.

The effect of the water loading in the reservoir above the lower dome is contained in Figs. F16 to F21, inclusive.

2.7 Numerical Summary of Stress Resultants

The load superpositions of this Chapter provide the distribution of forces for which the response of the various sections of the structure will be determined in Chapter 4. For this purpose a number of locations have been selected. These locations are indicated on Fig. 2.6, as W1 to W5, which are locations in the cylinder wall; UD1 to UD3, which are locations in the upper dome; and LD1 to LD3, which are locations in the lower dome. Table 2.3 lists numerical values of the reference state stress resultants associated with these locations. Table 2.4 lists the values for live loadings at these locations. Unless otherwise stated, all tables and figures in this report present forces in pounds and moments in foot-pounds.

3. SECTION ANALYSIS

3.1 Introduction to Section Analysis

The gross distribution of forces throughout the structure has been determined in Chapter 2 on the assumption that the structure responds in a linear elastic manner. It remains to determine the material response to this distribution of forces at any given point within the structure, i.e. - to find the effect of these forces on a section through any of the structural elements. It must be recognized that the material will respond in an inelastic manner once the loads exceed the proportional limits of the constituent materials, and this in turn will cause some redistribution of the gross distribution of forces. However, since a complete nonlinear analysis is beyond the scope of this report, the investigation will continue in the manner described in Sections 1.3 and 1.4.

The purpose of this Chapter is to investigate the methodology of determining the response at a particular section to the stress resultants arising from the analysis in Chapter 2. Stress concentrations and the effects of discontinuities are not considered and the response of the section should, therefore, be representative of the behavior to be expected over a significant region in the area of the section.

Two different analyses of cross-sectional behavior are presented herein:

1. A linear elastic cracking analysis is presented in Sections 3.3 and 3.4. This analysis makes it possible to study the progression of cracking through the section and can be used to illustrate the dissipation of secondary stresses such as thermal stresses or shrinkage stresses when cracking occurs. Some results of this analysis are presented in Section 3.5.

2. Interaction diagrams for the wall and dome sections are derived in Sections 3.6 using realistic stress-strain properties for concrete and reinforcement. Some results of this analysis are presented in Section 3.7. The relationship between the cracking and interaction analyses is discussed in Section 3.8.

The material properties assumed in these studies are presented in Section 3.2.

3.2 Material Properties

The response of the section depends on the materials used in its construction. The three materials associated with the basic structure are reinforcing steel (ASTM A615 - Grade 60), prestressing steel (ASTM A421-65 Type BA) and concrete (5000 psi).

The reinforcing steel is assumed to respond in an elastic-perfectly plastic manner with a modulus of elasticity (E) of 29.6 x 10^6 psi and a yield stress (f_y) of 60000 psi. These properties are illustrated in Fig. 3.1.

The prestressing cables are assumed to have a minimum ultimate strength (f_{pu}) of 255 ksi, to reach a 0.2% offset yield strength at 80% of f_{pu}, and to have an effective modulus of elasticity of 29.6 ksi. These properties are consistent with the prestressing wires that were used in Gentilly-2 (5, 12). Since a behavioral analysis requires the specification of a stress-strain relationship up to the point of failure, the relationship shown in Fig. 3.2 was assumed. This curve assumes a proportional limit at 0.7 f_{pu} and a parabolic relationship above the proportional limit. It is described by the equations:

$$\varepsilon = \sigma/E \qquad 0 < \sigma < 0.7\, f_{pu} \qquad (3.1)$$

$$\varepsilon = \frac{\sigma}{E} + 0.2\,\{\frac{\sigma}{f_{pu}} - 0.7\}^2 \qquad 0.7\, f_{pu} < \sigma < f_{pu} \qquad (3.2)$$

Eq. 3.2 satisfies the following criteria:

(a) It branches from Eq. 3.1 at 0.7 f_{pu}.

(b) It is tangent to Eq. 3.1 at 0.7 f_{pu}.

(c) It passes through the 0.2% offset at 0.8 f_{pu}.

For the properties itemized above, the stress-strain curve intersects the ultimate strength at a strain of 0.0266 and the following analyses assume fracture at this point. This ultimate strain is not incompatible with a minimum guaranteed elongation of 4% in a 10 inch gage length (5) and is judged to be conservative.

The concrete is considered to have a 28 day cylinder strength (f'_c) of 5000 psi. The stress-strain curve for ultimate strength evaluations is assumed to follow the uniaxial stress-strain curve of Fig. 3.3. In compression this curve is similar to that suggested by Hognestad (10) with the modification that no decrease in stress is assumed to occur between ε_o and ε_u. This modification has been made in order to eliminate anomolies in the interaction curves of Sect. 3.6. The resulting stress-strain curve closely resembles the curve presented by the European Concrete Committee (9, 15). The following material characteristics have been used for compressive response.

$$E = 57000 \sqrt{f'_c} \tag{3.3a}$$

$$f''_c = 0.85 \, f'_c \tag{3.3b}$$

$$\varepsilon_o = \frac{1.5 \, f'_c}{E} \tag{3.3c}$$

$$\varepsilon_u = 0.0038 \tag{3.3d}$$

Then for

$$0 < \varepsilon < \varepsilon_o \quad , \quad \sigma = f''_c \left\{2 \frac{\varepsilon}{\varepsilon_o} - \left(\frac{\varepsilon}{\varepsilon_o}\right)^2\right\} \tag{3.3e}$$

and for

$$\varepsilon_o < \varepsilon < \varepsilon_u \quad , \quad \sigma = f''_c \tag{3.3f}$$

Concrete has been assumed to fracture in tension at $k_t\sqrt{f'_c}$. The currently accepted value of k_t is 6 (2) but, by setting k_t to zero, analyses which neglect the tensile strength of concrete may be carried out.

Poisson's ratio for concrete has been taken to be 0.15. The effect of biaxial stress conditions on stiffness has generally been accounted for only to the extent of a Poisson's ratio coupling with plane strain boundary conditions on the element. This alters the effective E for use in the uniaxial stress-strain relationship to $E_e = E/(1-\nu^2)$. The interaction relationships for the ultimate strength of concrete under biaxial conditions have been investigated by Kupfer, Hilsdorf and Rüsch (13) who measured the biaxial strength envelope shown by solid lines in Figure 3.4. In this stage of the investigation the effects of biaxial stresses on the tensile strength and crushing strength have been disregarded and the square ultimate strength envelope shown by the dashed lines in Fig. 3.4 has been assumed. In those portions of the structure where both stress components are tensile or both are compressive on one face of the wall this assumption is sufficiently accurate.

The effect of creep on the stress distribution at a section has been included using the Reduced Modulus procedure in which the value of E for sustained loads is taken as E/ϕ where ϕ is a creep coefficient which was taken to be 2.5 (17). This allows an assessment of the local effects of creep.

3.3 Rationale for Linear Elastic Cracking Analysis

Although nonlinear concrete response is significant in establishing the failure conditions at any section, concrete compressive stresses at service loads will generally be low and hence a linear elastic concrete cracking model should give a reasonable estimate of response to short term loading prior to crushing of the concrete. This section considers the context within which a linear elastic cracking analysis has been developed for this report.

One of the difficulties in predicting behavior of a section from the load superposition analysis of Chapter 2 is that the self-limiting stresses are relieved by cracking within the section. Unless a complete nonlinear analysis is carried out, which is beyond the scope of this report, some mechanism should be built into the section analysis to permit this stress relief. The mechanism employed herein is very simple but believed to be a reasonable approximation. It has been assumed that the direct membrane forces (primary effects) increase proportionally with internal pressure, and that the section curvatures (rather than moments, which are secondary effects) increase proportionally with internal pressure. It is argued that the curvatures are geometric effects constrained by the adjacent structural elements and therefore cannot increase locally in an unconstrained fashion until the capacity of the structure has been fully developed. This assumption provides a mechanism for stress release.

3.4 Formulation of Linear Elastic Cracking Equations

Consider a typical segment of the structure as shown in Fig. 3.5. It is assumed that an arbitrary (linear) initial stress distribution exists in the section resulting from the long term effects of gravity, prestressing, shrinkage and creep (Fig. 3.6(b)). For short term response, including both thermal and internal pressure effects, the constraints on the element may be expressed as

$$\Delta P = P^* \tag{3.4.1}$$

$$\Delta \phi = \phi^* \tag{3.4.2}$$

where P^* is the specified change in membrane force and ϕ^* is the specified change in curvature, resulting from pressure or pressure and thermal loads. The resulting <u>changes</u> in strain over the cross-section may be expressed as

$$\varepsilon^E = \varepsilon - \varepsilon^I \tag{3.4.3}$$

where ε^E is the elastic strain, ε is the total strain and ε^I is the (short term) inelastic strain. If ε_o represents the change in strain at face b_1 of Fig. 3.5, then for plane sections remaining plane, we may also write

$$\varepsilon = \varepsilon_o + x\,\phi^* \tag{3.4.4}$$

and the change in concrete stress (shown shaded in Fig. 3.6) at any point within the cross-section may be written as

$$\Delta f_c = E_e \cdot \{\varepsilon_o + x\,\phi^* - \varepsilon^I\} \tag{3.4.5}$$

where E_e is the effective modulus of elasticity and ε^I is the inelastic strain associated with thermal effects ($\varepsilon^I = \varepsilon^T = \alpha\,\Delta T$, with α being the coefficient of thermal expansion and ΔT the change in temperature).

If the section cracks, the change in stress from the reference stresses are no longer given by Eq. (3.4.5) over the entire cross-section but are simply the negative of the initial stresses on that portion of the section which cracks (Fig. 3.6(d)). Assuming the section cracks to a depth x_c, (Fig. 3.6(e)), and substituting Eq. (3.4.5) into Eq. (3.4.1), results in

$$\begin{aligned} P^* = {} & E_e \varepsilon_o \{v_1 + v_2 + n\,(A_{s1} + A_{s2} + A_f - v_{1c} - v_{2c}\} \\ & + E_e\{(\phi^* d - \beta\varepsilon^T_{c2})\,v_2 - \beta\varepsilon^T_{c1}\,v_1 + n(\phi^* x_1 - \varepsilon^T_{s1})A_{s1} \\ & + n\,(\phi^* x_f - \varepsilon^T_f) + n(\phi x_2 - \varepsilon^T_{s2})\,A_{s2}\} \\ & - v_{1c}(f^i_{c1} - E_e \beta\varepsilon^T_{c1}) - v_{2c}\,f_{t2} \end{aligned} \tag{3.4.6}$$

where additional terms are defined in Appendix A and the equation represents the summation of the stress blocks illustrated in Fig. 3.6.

The unknown appearing explictly in this equation is ε_o (Fig. 3.5(c)) but v_{1c} and v_{2c} (the volumes of the cracked stress blocks) are influenced by the depth of cracking x_c. An additional equation is therefore needed and this comes from the requirement that the concrete tensile stress f_t is attained at the depth of the crack x_c. Assuming a linear variation of change in strain across the section, the distance x_c may be expressed as

$$x_c = \frac{\{E_e \varepsilon_o - \beta E_e \varepsilon^T_{c1} + f^i_{c1} - f_t\} d}{f^i_{c1} - f^i_{c2} + \beta E_e (\varepsilon^T_{c2} - \varepsilon^T_{c1}) - E_e \phi^* d} \qquad (3.4.7)$$

Equations (3.4.6) and (3.4.7) are two nonlinear algebraic equations which may be solved iteratively for x_c and ε_o. A computer program has been written to carry out this solution and is contained in Appendix I.

The program of Appendix I has been generalized to the extent that it accounts for yielding of the mild steel reinforcing. It is therefore possible to analyze a section from any arbitrary initial set of stresses (with a linear variation of concrete stress) up to the point of rupture of the prestressing strand, subject to the assumption of linear response in the concrete and prestressing steel, but including the effects of thermal strains, cracking of the concrete and yielding of the reinforcing. Some typical results are contained in Sect. 3.5.

3.5 Illustrative Applications of Cracking Analysis

The cracking analysis formulated in Sect. 3.4 will be illustrated here by considering the response of horizontal sections at the locations W3 (mid-height of the wall) and UD1 (the springing of the upper dome) indicated in Fig. 2.6. (Note that the term 'horizontal' in the dome will imply a circumferential section as opposed to a vertical section.) In the remainder of this report a suffix of H or V will be attached to the location designation to indicate whether a horizontal or vertical section is being considered through the location.

3.5.1 Response of Section W3H

The conditions at this location are typical of those over a considerable range of the cylinder wall. The reference state forces (Rdl) may be obtained from Table 2.3 and indicate a gravity load of 67.6 kips. After prestressing the net effective force on the section is 267.1 kips and the prestressing force is the difference between these, namely, 199.5 kips.

The section properties of the selected sections, as obtained from the design drawings, are tabulated in Table 3.1. It is assumed that the long term loading of 267.1 kips has been in effect for a considerable length of time and the long term stiffness of the concrete is 1/2.5 that of the short term, so that a redistribution of stress between the steel and concrete has taken place. (This effect is accounted for by increasing the n value from that for an elastic distribution.) Moment at this section is negligible and has been disregarded.

The initial stresses arise from the following computations.

$$E_c = 57000 \sqrt{f'_c} = 4.03 \times 10^6 \text{ psi}$$

$$\text{Short term } E_e = \frac{E_c}{1-\nu^2} = 4.12 \times 10^6 \text{ psi}$$

$$\text{Long term } E_e = \frac{E_e}{2.5} = 1.65 \times 10^6 \text{ psi}$$

$$\text{Short term } n = E_s/E_e = 29.6/4.12 = 7.18$$

$$\text{Long term } n = E_s/E_e = 29.6/1.65 = 17.95$$

Short term transformed area

$$= 7.18 \times (1.58 + 1.30) + 12 \times 42 = 524.7 \text{ in}^2$$

Long term transformed area

$$= 17.95 \times 1.58 + 12 \times 42 = 532.4 \text{ in}^2$$

Initial concrete stress = 267.1/532.4 = -502 psi

Initial steel stress = 17.95 x 502 = -9005 psi

Initial prestressing stress = 199.5/1.30 = +153.5 ksi

These initial stresses are computed in the program from the input data. The effect of live loads is then superimposed on this initial stress condition using the short term properties.

The program of Appendix I may be used to study the response under a number of assumptions. The results from typical analyses are shown in Fig. 3.7, as a plot of the superimposed pressure force per unit of width vs the axial strain.

Assuming no tensile strength of the concrete (k_t=0) and no thermal gradient the response is as shown by line O-a-b-c. 'Through-the-wall-cracking', hereafter called through-cracking, occurs suddenly at a, first yielding of the mild steel occurs at b, and rupture of the prestressing strand occurs at c. The design basis accident load (corresponding to 18 psig) is indicated as P_d on the figure. The load factor for cracking is 3.1, for first yield is 5.3 and for rupture is 5.7.

Assuming a tensile strength of concrete of 424 psi (k_t=6) and no thermal gradient gives the response shown as O-d-e-c. This response could be cause for concern since a sudden fracture at a load of 485^k would probably release sufficient energy to immediately rupture the prestressing strand resulting in a brittle type of behavior (at a load factor of 5.6). However, this sudden fracture results only when there is little or no stress gradient on the section. If it is assumed that the section is subjected to a thermal gradient at the time of pressurization the behavior is as shown by line O-f-b-c for the case of k_t=0, and O-g-h-b-c for the case of k_t=6. The thermal gradient for these responses is that of WOT. In this case the section cracks on the exterior surface prior to internal pressurization. A nondimensional plot of the depth of cracking (x_c/d) for the four cases presented on Fig. 3.7 is shown on the right of the figure. The cracking behavior corresponding to line O-a-b-c is O'-a'-a"-c"; to line O-d-e-c is O'-d'-d"-c"; to line O-f-b-c is k-f'-c"; and to line O-g-h-b-c is j-h'-c". Thus through-cracking occurs at points a", d", f' and h', respectively, where cracking points corresponding to points on the P-ε curve have been indicated by the corresponding primed letter(s).

The above analysis confirms the intuitive judgement that cracking conditions are highly dependent on secondary effects while ultimate strength states are independent of them. It also indicates that, providing a significant stress gradient is present, an analysis with k_t=0 yields a reasonable prediction of the behavior of the section except for prediction of cracking.

3.5.2 Response of Section UD1H

In contrast to section W3H, section UD1H is subjected to a significant moment resulting from pressurization. The long term stress resultants for construction sequence one, obtained from Table 2.3, are a gravity force of 15.36 kips, a total force of 346.4 kips and a net prestress force of 331 kips. The section property details are summarized in Table 3.1.

The initial stress conditions, using the same material properties as for W3H are obtained as follows.

Long term area = $17.95\ (2.20) + 24 \times 12 = 327.5\ \text{in}^2$

Long term moment of inertia

$$= 17.95 \times 2.20 \times (9.3)^2 + \frac{12 \text{x} 24^3}{12} = 17240\ \text{in}^4$$

Short term moment of inertia

$$= 7.18 \times 2.20 \times 9.3^2 + \frac{12 \text{x} 24^3}{12} = 15190\ \text{in}^4$$

Initial concrete stress equation

$$= \frac{346400}{327.5} - \frac{104900 \text{x} 12}{17240}\ z$$

$$= 1058 - 73.02\ z\ \text{psi}$$

where z is the distance from the mid-plane of the dome.

Initial stress in steel and concrete

$f^i_{c1} = 1058 - 73.02 \times 12 = 182$ psi (-) (exterior face)

$f^i_{c2} = 1058 + 73.02 \times 12 = 1933$ psi (-) (interior face)

$f^i_{s1} = 17.95\ (1058 - 73.02 \times 9.3) = 6800$ psi (-)

$f^i_{s2} = 17.95\ (1058 + 73.02 \times 9.3) = 31170$ psi (-)

Pressure load axial force	= 48.26 p lb. (p in psf.)
Pressure load moment	= 79.28 p ft. lb. (p in psf)
WOT axial force	= 10450 lb.
WOT moment	= -176800 ft. lb.

$$\text{Curvature from pressure} = \frac{79.28 \times 144}{15190 \times 4.12 \times 10^6}\, p$$

$$= 0.1824\, p \times 10^{-6} \text{ rad/lb./ft}^2$$

Starting with the above initial stresses, the response under increasing internal pressure is shown as the lower curve in Fig. 3.8. The curvature has been increased linearly with the load in determining this response. The abrupt changes of stiffness characterizing the behavior of W3H are no longer present and some cracking is initiated prior to the design basis accident pressure. Load factors corresponding to cracking, yield, through cracking and rupture are 0.8 for k_t=0 (1.0 for k_t=6), 3.9, 4.7 and 5.8.

This section also exhibits cracking on the exterior surface under WOT conditions. When pressurization is superimposed upon these thermal conditions the response is as shown by the upper curve in Fig. 3.8. As pressure is increased the exterior crack closes and the interior surface crack initiates at a load substantially higher than that for which no thermal conditions exist. Through cracking occurs at a load somewhat below that for no thermal loading. This cracking history, for k_t=0, is shown on the right side of Fig. 3.8.

For both of these loadings in which curvatures increase with pressure there is no discernible difference between overall response as k_t varies from 0 to 6, although there is a difference in the depth of cracking. It is apparent, however, that thermal stress again has a substantial effect on crack initiation. To a lesser extent it also influences the pressures at which yielding is initiated and through the wall cracking occurs.

3.6 Interaction Curves

In predicting the ultimate strength capacity of concrete members it is often convenient to construct curves which are the locus of all combinations of bending and axial effects that produce a given condition. Such curves are referred to as interaction curves and are generally constructed to establish the ultimate capacity of the section. The procedure is an indirect one but is easier to implement than the type of analysis of Sect. 3.5 and gives the complete set of all failure points. In this Section a technique of constructing interaction curves for initial cracking, initial yielding, through-cracking, and ultimate strength is described and a detailed explanation of one such curve is given.

Interaction curves in this report have been constructed using the program in Appendix J. Forces and moments have been computed relative to the zero stress condition in the concrete. Under these conditions the initial strain (ε_f^i) in the prestressing steel may be computed as

$$\varepsilon_f^i = \frac{1}{E_f} \{f_f - N_\ell / A_T \, E_e\} \tag{3.6.1}$$

where f_f is the stress in the prestressing steel after all losses, N_ℓ is the long term axial stress resultant (R_f), A_T

is the short term transformed area, E_f is the modulus of the prestressing steel, and E_e is the effective modulus of elasticity of the concrete. Changes in strain may now be imposed on this state (i.e. - the state of zero concrete strain and a strain of ε_f^i in the prestressing steel) and the total axial force and moment computed for the resulting stresses.

The technique of constructing a complete interaction curve may best be described by using an illustrative example. For this purpose the vertical section at location UD1 has been selected. This section is slightly asymmetric in that the reinforcing steel is not the same on the different faces. The prestressing steel is assumed to be concentrated at the center of the section although there are three layers of prestressing in the structure. Thermal effects and redistribution of long term stress effects between the concrete and reinforcing steel are not included. For all interaction curves the concrete was assumed to have a tensile strength of $6\sqrt{f_c'}$. This in effect ignores any prior cracking which may have occurred due to thermal or shrinkage stresses. The idealized section is shown in Fig. 3.9a and the interaction curve is shown in Fig. 3.10.

The failure curve is determined as follows. Assuming a strain of ε_u across the entire section the stress resultants plot as point a of Fig. 3.10. Pivoting about ε_u at x = 0 as shown in Fig. 3.9b, the forces reduce to point b of Fig. 3.10 when the strain at x = d reaches ε_o of Fig. 3.3.

As the strain is further reduced the stress resultants follow the path b-c, point c representing the condition for first cracking (ε_c at x = d). Continuing to pivot about ε_u, and reducing the strain at x = d still further, the stress resultants follow the path c-d, point d representing the condition for which the mild steel yields. Reducing the strain still further, the curve traces d-e, point e representing the point at which the second layer of reinforcing steel yields. The curve e-f is then traced as the pivoting is continued, point f representing the point at which the rupture strain is reached in the prestressing steel. Curve a-b-c-d-e-f of Fig. 3.10 therefore represents the set of combinations of axial force and moment which produce failure by crushing of the concrete for a strain of ε_u at x = 0. The pivoting procedure for this curve is shown in Fig. 3.9b. The curve f-g-h is obtained by pivoting about the rupture strain in the prestressing strands as shown in Fig. 3.9.c.

The other curves shown on Fig. 3.10 may be obtained as follows. Pivoting about x=d (the tensile face) with a strain of ε_c^- yields the curve for first cracking (line c-m); about x=d with a strain of ε_c^+ yields the curve for through the wall cracking (line n-i-k); about x_2 with a strain of ε_y yields the curve for initial yielding of steel at this location (line d-i-j): and, about $x=x_1$ with ε_y yields the curve for yielding of the second steel layer (line e-k). The set of pivots, and the strain conditions for the points identified on Fig. 3.10 are shown in Table 3.2. The 'mirror image' curves are obtained in the same manner. The slight skewness of the diagram is due to the slight asymmetry of the section and reinforcement.

Complete interaction curves for locations W3, W5, UD1, UD2, UD3, LD1, LD2 and LD3 are contained in Appendix K. Curves for sections in which the prestressing is eccentric to the section centerline, such as the horizontal prestressing in the cylinder, can become quite complex (See, for example, the plot for W3V in Fig. K2.) All interaction curves in this report are for a tensile strength of $k_t\sqrt{f'_c}$ with k_t=6.

3.7 Illustrative Applications of Interaction Curves

With interaction curves of the type described in Sect. 3.6, it is possible to predict the pressurization loading that will produce cracking, first yield, through-cracking and failure, providing it is assumed that the ratio of live load moment to axial force remains constant throughout the loading procedure. The technique for doing this is illustrated in Fig. 3.11 for Section UD1H and is described in the next paragraph.

From Table 2.3 the stress resultants for reference state Rs1 on the horizontal section are N_1 = -345.8 kips and M_1 = -104.6 ft.kips. This reference state may be located on Fig. 3.11 as point a. From Table 2.4, pressurization produces stress resultants of N_1 = 48.26 p lbs. and 79.28p ft.lb. (p in psf). Constructing a line on the plot with the proper slope, and reflecting it about the line of symmetry, indicates the loading conditions at b, c and d represent the states of first cracking, first yield and failure, respectively, for this load path. The changes in the N_1 stress resultant from the reference state, as scaled from Fig. 3.11, are 135 kips, 216 kips and 250 kips, respectively, or pressures of 19.5, 31.1 and 36.0 psi, at first cracking, first yield and failure, respectively. These represent load factors on the design basis accident condition of 1.1, 1.7 and 2.0.

A similar analysis to that in Fig. 3.11 is carried out for section W3H in Fig. 3.12. Since there is essentially no moment on the section the loading path is practically vertical and intersects the cracking and rupture lines at points a and e, respectively, corresponding to pressurization loads of 475 and 482 kips, respectively, or internal pressures of 99.5 and 101 psi.

3.8 Comparison of Interaction and Cracking Analyses

A comparison of the two techniques presented in Sections 3.5 and 3.7 is rather interesting. For W3H (Fig. 3.12), a section subjected to practically no moment, the loads of 475 kips and 482 kips compare favorably with those of 485 kips and 496 kips predicted by the cracking analysis.

However, for UD1H (Fig. 3.11) which is subjected to a substantial moment, only the cracking condition shows good agreement. An examination of Fig. 3.8 indicates that through-cracking occurs at 584 kips and the section continues to deform until rupture of the prestressing strands occurs at 720 kips. The interaction plot of Fig. 3.11 indicates that through-cracking does not occur and failure is by crushing of the concrete. The difference, is, of course, due to the different assumptions relating the ratio of axial load to moment. It is interesting to note that a straight line joining b to e on Fig. 3.11 would predict through cracking at a load of 505 kips (cf. 484) and failure at 720 kips (cf. 720 kips).

It is apparent that the difficulty with interaction plots is that the loading path is unknown after initial cracking. To determine the loading path requires a full nonlinear analysis of the structure. However, the two types of solutions examined in this Chapter are expected to provide bounds on the nonlinear solution.

4. STRUCTURAL RESPONSE TO PRESSURIZATION

4.1 Load Factor Determination

The two different types of section analysis developed in Chapter 3 may now be used to estimate the load factors on the design basis accident pressure (18 psi) at which the limit states of initial cracking, first yield, through-cracking and section failure may be reached at various locations throughout the structure. This Chapter will be concerned with the determination of these load factors and a comparison of some of the results.

The limit state capacities of the sections will be determined for cracking analyses by the technique described in Sect. 3.5, and for the interaction analyses by the graphical technique described in Sect. 3.7. Dividing the limit state capacities of the section by the forces produced at the section due to a pressurization of 18 psig yields load factors for the particular limit states. It is convenient at this time to tabulate membrane forces in kips, rather than pounds (which have been used in the previous tables and have been used in all the figures in this report).

The investigation will be confined to the locations itemized in Sect. 2.7 and illustrated in Fig. 2.6. To facilitate the computation of load factors, the membrane forces at these sections produced by pressurization (loading C:Cp of Table 2.4) are tabulated for internal pressures of 1 psig and 18 psig in Table 4.1.

Plots of cracking analyses on selected sections are presented in Appendix L. Plots of interaction curves on selected sections are contained in Appendix K. The loading paths on the interaction plots are constructed from the conditions for reference state Rs1 (indicated by point S1), at a slope consistent with the C:Cp stress resultants (Table 2.4), and the point representing conditions at an internal pressurization of 18 psig is denoted as P18. Where the reference state stress resultants for Rs2 differ significantly from those for Rs1, the point representing this reference state is indicated as S2. Normally, these two points are indistinguishable in the plot and only one has been shown. If the cross-section is symmetrical, only one-half of the interaction plot is shown and, where necessary, the loading path has been reflected about the M=0 axis or the sign of the moment has been reversed.

It should be recalled that the load factors computed in this Chapter do not account for the features itemized in Sect. 1.5 and are, therefore, indicative of the overall response of the structure rather than lower bound values at critical points.

4.2 Lower Dome Sections

Interaction plots, with load paths determined as described in Sect. 4.1, are presented in Figs. K11 to K14 for the lower dome sections. These sections are not prestressed. For the horizontal sections the change in membrane force is small and the effect of internal pressurization at these locations is primarily to increase moments, resulting in a flexural type of response. It can be seen from Table 2.4 that the membrane forces at locations LD1 and LD2 increase in a compressive sense. Therefore a cracking analysis at these locations is inappropriate and failure is by crushing of the concrete. The forces required to produce the limit states have been determined graphically from the Figures and are tabulated, with the resulting load factors, in Table 4.2. Since pressurization has little effect on these sections the load factors are generally very high and indicate that there should be no concern over the safety of the reservoir.

4.3 Interaction and Cracking Analyses at Selected Sections

The limit state membrane forces, obtained from the cracking analyses presented in Appendix L, and the interaction plots in Appendix K, are tabulated for locations W3, W5, UD1, UD2 and UD3 in Table 4.3. In contrast to the LD sections of Sect. 4.2, all sections tabulated have a significant tensile membrane force arising from pressurization. Load factors, obtained by dividing the limit state forces by the appropriate membrane forces of Table 4.1, are also tabulated.

Considering first location UD1, section UD1V has been omitted because it is subject to a compressive membrane force as shown in Fig. K6. Section UD1H (Fig. K5) has a high moment to force ratio and is the example of Sect. 3.8

where the reasons for the discrepancy between cracking analyses and interaction analyses were discussed. The load factors for first cracking are comparable but for all other limit states there is a wide discrepancy. It was pointed out in Chapter 3 that to trace a realistic loading path on the interaction plot would require a complete nonlinear analysis. It is anticipated that the results of such an analysis would conform more closely with the cracking analysis contained herein than with the interaction analysis but that the interaction analysis will produce lower bounds on the load factors. Scanning the load factors in Table 4.3 indicates that, except for first cracking, the interaction load factors are always less than those from the cracking analyses.

The load factors for first cracking should be similar for both types of analyses. However, they should not be expected to be identical since the cracking analysis takes into account stress redistribution between steel and concrete resulting from creep (Sect. 3.5). This will lower the cracking analysis loads below those produced by the interaction analyses providing the pressurization effects are in an opposite sense to the long term effects. This is seen to be the case in Table 4.3 where first cracking loads from the cracking analyses are essentially equal to or less than those from the interaction analyses for all sections except W5H. The discrepancy at this section occurs because the cracking analyses of Appendix L have been carried out from reference state Rf1, while the interaction results tabulated in Table 4.3 are for loading paths originating from reference state Rs1. An examination of Table 2.3 indicates that the difference in these reference states, for the sections tabulated in Table 4.3, is small (generally less than 5%) except for location W5. With the loading path for Sect. W5H arising from the Rf1 point, (point F1 of Fig. K3) rather than the Rs1 point, the interaction cracking load rises to 130 kips, which corresponds to that for the cracking analysis. The load factors of Table 4.3 for first cracking should not be considered as reliable, however, since these factors are sensitive to the thermal conditions, as discussed in the next section.

It should be noted that some of the loads and factors tabulated for the interaction analyses in Table 4.3 are fictitious. This may be illustrated by considering the interaction plot of Fig. K1 for section W3H. Since this section is the example of Chapter 3 it is more convenient to refer to Fig. 3.12 which is an enlargement of the lower portion of Fig. K1. The limit state forces for first cracking, first yield, through-cracking and ultimate, shown in the FC, FY, TC and U columns of Table 4.3, respectively, are indicated on the figure, as the distances to points a, c, b and e, respectively. If the load path of Fig. 3.12 were to be followed, the load would increase to a, drop to b, increase to c and then increase through d and e. However, unless substantial rapid pressure release were to occur, the actual response of the structure would require through-cracking and first yield to occur rapidly, immediately after first cracking. Points b and c may, therefore, be regarded as fictitious. Fictitious loads obtained from the interaction plots are indicated by brackets in Table 4.3 and could be replaced by first cracking loads.

4.4 Cracking Analyses at Selected Sections

The complete set of cracking analyses carried out in this investigation is presented in graphical form in Appendix L. Membrane forces for these analyses are summarized in Tables 4.4 and 4.5, while load factors are summarized in Tables 4.6 and 4.7. Cracking analyses were, in general, run for four different conditions, namely, (a) for no thermal effects with k_t=0 and k_t=6, and (b) for WOT thermal effects with k_t=0 and k_t=6. As can be seen from the tables, not all analyses were run for every section. Let us first consider all locations but W1 (the hinge at the base).

It can be seen from Tables 4.6 and 4.7 that, if there is no strain gradient due to thermal effects, k_t has a significant influence on the load factors at first cracking and through-cracking but has practically no influence on first yield.

It was found that without pressurization the summer shutdown thermal condition (SST), which is critical in producing tensile effects on the internal face, did not produce cracking. This is to be expected because of the no cracking design requirement that was imposed under these conditions. Since it is not physically possible to realize an internal pressurization together with summer shutdown thermal gradients, the most severe thermal condition, namely the winter operating condition (WOT), was selected to determine load factors to first cracking under pressurization.

An examination of Tables 4.6 and 4.7 and the x_c/d cracking plots of Appendix L, indicates that all cylinder wall sections crack under WOT for both $k_t=0$ and $k_t=6$. With thermal effects, first yield generally occurs at loads slightly lower than without thermal effects (sections in the dome, where thermal effects oppose pressurization effects, are the expection to this rule) and is not affected by k_t. Cylinder wall through-cracking generally occurs at loads slightly higher than for no thermal stress if $k_t=0$ and slightly lower if $k_t=6$. In the dome, thermal stress increases the through-cracking loads for both values of k_t.

None of the parameters included in this study affect the ultimate strength capacity of the section. The ultimate strength load factors of the structure are generally substantially higher than for most civil engineering structures. The lowest ultimate strength load factor arising from the cracking analyses is the 3.7 occurring at W4V. It should be noted that this is substantially higher than the lowest interaction load factor of Table 4.3, which is 2.0 arising at section UD1H. However, while the lowest ultimate strength load factor is 3.7, the lowest through-cracking load factor is 1.9 arising at sections W4V and UD3H. The capacity of the structure to relieve itself of internal pressure between these limits, and thus avoid an ultimate structural failure, is a subject for further study.

4.5 Analyses in the Vicinity of the Base Connection

The hinged connection between the base of the wall and the slab (i.e. - section W1) is a special detail where the assumptions imposed in the cracking analysis used in this report are not directly applicable. However it is interesting to examine the response at the hinge in the light of the present assumptions. All the steel at this section passes through the centroid of the area and, since there is no continuity of concrete across the section, $k_t=0$.

The results of a cracking analysis at the hinge are shown in Figs. L1 and L2. From Fig. L2 it can be seen that the analysis predicts a crack depth (on the exterior) greater than one quarter the thickness of the section in the reference state prior to pressurization. When subjected to pressurization this crack closes and an interior crack opens at a load factor of approximately 1.2 (Table 4.6). The ultimate strength of the section is developed as a tendon failure without through-cracking occurring.

The reference state forces have been computed in the BOSOR analysis on the assumption that complete continuity is maintained through a 12" contact thickness with the base.

The depth of crack predicted from the cracking analysis on the basis of an 18" thickness results in a contact area of approximately that assumed in the BOSOR analysis which is indicative that the reference state stress resultants are reasonably accurate in this area within the limits of the 'plane section' assumptions. Since the hinge area is of particular interest, a more detailed approximate examination of this section is carried out in Appendix M.

The behavior at the hinge has an influence on the distribution of forces arising during pressurization. If the base connection were a pure hinge, the M1 moment at location W1 would be zero and consecuently the stress resultants in the lower section of the wall would be affected.

The set of stress resultants arising from a pressurization analysis assuming continuity at the hinge is shown in Figs. F1 to F4 (C:Cp stress resultants), while the set for an ideal hinge at the base connection is shown in Figs. F5 to F8 (CH:Hp stress resultants). A comparison of these figures indicates that the only significant differences are in the stress resultants in the immediate vicinity of the hinge. This is also evident in Table 2.4 where significant differences in the stress resultants for C:Cp and CH:Hp occur only at section W1 and W2. It is apparent from Table 2.4 that the horizontal N2 stress resultant at section W2V is considerably greater for CH:Hp than for C;Cp, and the load factors of Table 2.4 are not, therefore, conservative for this section. Cracking analyses using the CH:Hp stress resultants at section W2V are shown in Figs. L31 and L32 and the corresponding limit state loads and load factors (for sections W2V and W2H) are shown in square brackets in Tables 4.4 to 4.7. These load factors are somewhat lower than those for the C:Cp analysis but remain generally high in comparison with those at other locations in the structure.

5. SUMMARY AND CONCLUSIONS

5.1 Load Superposition Summary and Conclusions

The load superposition analysis in this report has taken into account the staging of construction and prestress application, and shrinkage effects, as well as the live load effects of temperature and internal pressurization. The results of this analysis are summarized in Tables 2.3 and 2.4. An examination of these results indicates the following general conclusions may be drawn.

5.1.1 Analysis for Self-Weight

A 'switched-on-gravity' analysis produces dead load stress resultants very similar to those of a staged fully-supported construction sequence except for the moments at locations immediately below the ring beam (Figs. G1 to G8). Since moments in the structure are secondary effects, and the difference in dead load moments at these locations is less than 10% of the live load moment for the design basis accident, 'switched-on-gravity' appears to be a sufficiently accurate analysis on which to base the design for forces arising from gravity loads.

5.1.2 Shoring of Upper Dome from Lower Dome

The effect of supporting the upper dome from the lower dome has been investigated. This construction sequence produces significant differences in dead load moments at the top of the cylinder wall and in all stress resultants throughout the lower dome (except near the center of this dome). This may be seen by comparing results for Rd2 with those for Rd1 in Table 2.3. Although the lower dome is not itself prestressed, the application of the ring beam prestressing has a major influence on the stress resultants arising in the lower dome.

The effect of this construction procedure on structural response can be put in perspective by examining Figs. K3 and K11 to K14. In these figures, S_1, S_2, F1 and F2 correspond to the stress resultants arising in reference states Rs1, Rs2, Rf1 and Rf2, respectively. The only significant shifts in the reference state occur for sections W5H, LD1H and LD1V. In all cases the shift in reference state is such that the apparent load factors are increased. It may, therefore, be concluded that the procedure of shoring the upper dome from the lower dome will not have any detrimental effects on the completed structure. In future reports it will be assumed that the shoring sequence can be ignored. This corresponds to the switched on gravity assumption.

5.1.3 Differential Shrinkage Strains

The effect of gross differential shrinkage between structural components, resulting from the time sequence of construction, has been computed (Appendix H and Table 2.2). The influence of this shrinkage on the stress resultants is generally small (less than 5%) except in the vicinity of the base of the cylinder wall, where the N2 stress resultant in the prestressed structure has been reduced by approximately 10% (compare Rf1 and Rs1 or Rf2 and Rs2 in Table 2.3), and in the vicinity of the interior edge beam around the opening in the lower dome.

Since the interior lower dome sections are not designed as prestressed sections, remain in a state of compression (Table 2.3), and are subject to small stress resultants upon pressurization (Figs. K12 to K14), the effect of shrinkage in this dome is not significant.

The effect of shrinkage on section W2V is to produce an N2 stress resultant of approximately 30% of that due to the design basis accident. This is a significant effect that has been anticipated by the designers. The additional reinforcement and the reduced pressurization effect at this section due to base restraint (Table 2.4), combine to yield relatively high load factors at this location, except for the initial cracking condition.

It should be noted (Fig. G22) that shrinkage strains produce considerably higher N2 stress resultants in the vicinity of the ring beam than anywhere else, but are a smaller fraction of the reference state and pressurization effects at these locations. These stress resultants are compressive in the top of the wall and tensile in the bottom of the dome.

5.1.5 Live Load Deflections

Displacements associated with the C:Cp and CH:Hp pressurization influence loadings (1 psf) are plotted in

Figs. 5.1 to 5.4, where w and u indicate the local coordinate normal and meridional displacements, respectively, as shown in Fig. 2.1(b). Two points of interest emerge.

First, the normal displacement, w, indicates an inward rotation of the ring beam about its bottom elevation. This probably results from the inward reactive force of the upper dome on the top of the ring beam and the outward shear exerted on the bottom of the ring beam by the more flexible cylinder wall. The result of this deformation is to produce compressive pressurization membrane stress resultants at section UD1V and at locations LD1 and LD2. The fact that pressurization membrane forces at these locations are compressive, rather than tensile, appears to be generally beneficial in terms of overall behavior.

The second point of interest is the large component of the vertical wall deflection (Fig. 5.2) which arises from deformations of the base. The vertical displacement at the base of the wall for the design basis accident may be predicted from Fig. 5.2 as $2.83 \times 10^{-5} \times 18 \times 144 = 0.073$ inches. The relative displacement at locations above the base connection can be easily computed from the plots with good accuracy in the elastic response range. However, relative deflections which include base movements may be less reliable because these are closely tied to the technique used to model the foundation stiffness, and the internal structure of the building has been neglected. (Preliminary finite elements analyses indicate a substantially smaller base deformation).

5.2 Section Analysis Summary and Conclusions

The effect of the distribution of loads at specific locations throughout the structure has been determined by two approximate techniques, namely:

(a) load paths on interaction plots for which the ratio of pressurization stress resultants is assumed to remain constant, and

(b) section analyses for which the ratio of pressurization membrane force to curvature is assumed to remain constant.

Except for initial cracking these analyses predict load factors at the various limit states which differ significantly (Table 4.3). The reasons for this discrepancy have been discussed in Sect. 3.8.

Within the limitations of the techniques explored within this report the following conclusions appear to be warranted.

(1) Except for initial cracking a realistic assessment of the load factors for the various limit states cannot be made without performing a non-linear structural analysis.

(2) Interaction plots with straight line load paths appear to be a simple, but unverified, technique of establishing load factors in regions where the membrane forces are compressive.

(3) A cracking section analysis with a constant curvature-force ratio appears to be a useful, but unverified, technique for establishing load factors in regions where membrane forces are tensile.

(4) The level of prestress is such that, in all reference states, the outer structure remains in an uncracked condition except at the base junction.

(5) The design of the structure has been carried out in such a way that interior cracking does not occur during summer shut down conditions.

(6) Cracking occurs over most of the exterior of the structure under winter operating conditions.

(7) Cracking analyses indicate that the ultimate strength of the structure is not significantly affected by thermal or shrinkage effects.

(8) The pressure at which first cracking, through-cracking and first yield occur are all dependent on thermal conditions.

(9) When significant thermal gradient exists, first yield is not significantly affected by the tensile strength of the concrete.

(10) The ultimate strength load factors on the design basis accident pressure are significantly higher than those for normal engineering structures.

(11) There appears to be no cause for concern with respect to the safety of the dousing reservoir shell because, at critical sections, internal pressure causes compressive membrane stress resultants.

(12) The behavior of the structure in the area of the hinged connection between the wall and the base should be subjected to a more detailed examination.

5.3 Closure

This report has explored the application of a strength design approach to assess the behavior of a Gentilly type nuclear powerhouse containment structure. A principal conclusion of this investigation must be that, in the absence of further verification, these techniques are inadequate to realistically assess the behavior of the structure, when subjected to a hypothetical pressurization, in that the loading path at any section is undetermined beyond the initiation of first cracking. Linear shell analysis cannot adequately account for changes in stiffness due to cracking or yielding. These changes lead to a redistribution of forces and moments for which nonlinear structural analyses are required.

Furthermore, the analytical techniques applied in this report are incapable of distinguishing between benign and nonbenign failures in the sense that the succession of events in a hypothetical failure are dependent on the capacity of the structure to relieve itself of internal pressure. At what stage this capacity is developed is a complex problem which will be the subject of future investigations. In the absence of such information the assessment of behavior may rely on the traditional concept of ductility and the energy relationships between cracking and ultimate strengths. These subjects remain to be explored.

The analyses in this report are also confined to the classical assumption that 'normals to the middle surface remain normal'. This is generally a good assumption for the type of geometric ratios associated with this structure, except in the vicinity of the ring beam and at points of geometric discontinuity. In regions where geometric discontinuities exist, such as the hinged connection at the base of the wall and those areas which depart from axisymmetric assumptions as itemized in Sect. 1.5, both linear and nonlinear finite element analyses would be beneficial.

The investigation of shrinkage has been carried out only for gross effects and a more detailed examination to predict surface cracking resulting from differential shrinkage through the thickness could be undertaken. Creep has been explicitly accounted for in local analyses by the reduced modulus procedure, the global effects being confined to a reduction in the net prestressing force. If it were thought necessary a more involved global creep analysis including the effect of construction sequence could be undertaken.

Regardless of the type of analyses which are carried out it would be desirable to verify the analytical results experimentally. This is particularly true in regions where shear capacity may be of significance (an effect which is difficult to predict by any analytical means), such as at the base detail, and where construction practice may be of significance, as may be the case in the vicinity of lapped bar splices where additional tensile splitting forces could be developed.

REFERENCES

1. American Concrete Institute, "Code for Concrete Reactor Vessels and Containments", ACI Standard 359-74, American Concrete Institute, P.O. Box 4754, Redford Station, Detroit, Michigan, 48219, 1974.

2. American Concrete Institute, "Building Code Requirements for Reinforced Concrete", ACI Standard 318-71, American Concrete Institute, P.O. Box 4754, Redford Station, Detroit, Michigan, 48219, 1971.

3. Atomic Energy of Canada Limited, "Containment Structure Design Loading Requirements, Engineering Design Guide (Civil Engineering)", Revision 2, August, 1975, (DG-XX-21000-1).

4. Atomic Energy of Canada Limited, "Safety Report: Gentilly-2 600 MW Nuclear Power Station", Report to the Atomic Energy Control Board for Hydro-electrique de Québec.

5. BBR Limited, "Engineered Post Tensioning", BBR Limited P.O. Box 37, Agincourt, Ontario.

6. Bushnell, D., "Finite-Difference Energy Models vs Finite-Element Models: Two Variational Approaches in One Computer Program", Numerical and Computer Methods in Structural Mechanics, edited by S.J. Fenves, et.al., Academic Press, New York, 1973.

7. Bushnell, D., "Thin Shells", Structural Mechanics Computer Programs: Surveys, Assessments, and Availability, edited by W. Pilkey, et. al, University of Virginia Press, Charlottesville, 1974.

8. Bushnell, D., "Stress, Stability and Vibration of Complex Branched Shells of Revolution: User's Manual for BOSOR4", Lockheed Missiles and Space Company, Inc., Sunnyvale, California.

9. Comité Européen du Béton, "International Recommendations for the Design and Construction of Concrete Structures", Paris, 1970.

10. Hognestad, E., "A Study of Combined Bending and Axial Load in Reinforced Concrete Members", University of Illinois Engineering Experiment Station, Bulletin No. 399, Vol. 49, No. 22, November, 1951.

11. Hodge, P.G., "Plastic Analysis of Structures", McGraw-Hill Book Co., Inc., New York, 1959.

12. Hydro-Québec, "Call for Tenders CCH-73-10142: Gentilly-2 Nuclear Station", Document No. TS-1666-20034, Hydro-Québec, Montreal, March, 1973.

13. Kupfer, H., Hilsdorf, H., and Rüsch, H., "Behavior of Concrete Under Biaxial Stress," Proc., American Concrete Inst., Vol. 66, Aug. 1969, pp. 656-666.

14. Neal, B.G., "The Plastic Methods of Structural Analysis", John Wiley and Sons, Inc., 1956.

15. Rüsch, H., Grasser, E. and Rao, P.S., "Fundamentals of Design for Uniaxial Stress-Conditions in Concrete Structures", Deutscher Ausschuss für Stahlbeton, Wilhelm Ernst und Sohn, Berlin, 1963.

16. Surveyer, Nenninger, & Chennevert, Inc., "Instrumentation Studies on Deformation, Thermal Response, and Mechanical Properties of Material (Gentilly Nuclear Power Station Containment Building)", AECL REf. 61-21200, Feb., 1971.

17. Comité Européen du Béton, "Manuel de Calcul, Effets Structuraux du Fluage et des Déformations Différées", CEB Bulletin d'Information, No. 94, Paris, August 1973.

TABLES

TABLE 2.1 - INFLUENCE LOADINGS

Column	(1)	(2)	(3)	(4)
Structure	BW	BD	C	CH
	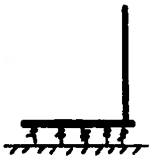	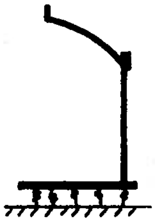	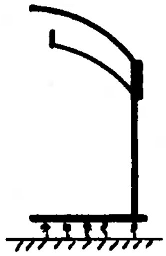	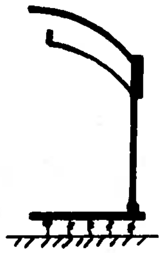
Completion Time	t_2	t_3	t_4	
Dead Load	Wd LBd	UBd LDd LDd*	UDd LDd LDd*	Hd
Prestress	Bf Whf	LBf	UBf UDf Wvf Whf	Hf
Uniform Strain	Bu Wu	Bu Wu LDu LBu	Bu Wu LDu UDu UBu RBu	
Strain Gradient			Bg Wg RBg LDg UDg	
Live Loads			Cp Cw	Hp Hw

<u>Load Designation</u>: General Form - $U\ell$
where U = upper case letters designating structural component(s)
and ℓ = lower case letters designating nature of load

<u>Load Type</u>

f = prestress force
d = dead load
u = uniform strain
g = gradient strain
hf = horizontal prestress
vf = vertical prestress
p = internal pressure
w = water
s = snow
t = wind (tornado)

<u>Structural Component</u>

B = base } BW } BD } C or CH
W = wall
LB = lower beam
LD = lower dome
UB = upper beam
UD = upper dome
RB = ring beam (UB+LB)
H = C with hinge at base of wall

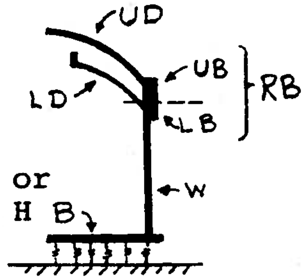

TABLE 2.2 - LOAD COMBINATIONS FOR REFERENCE STATES

Struct. (time)†	(1) Infl. Load	(2) Basic D.L.	(3) Alt. D.L.	(4) Prestress	(5) Shrinkage Time†	(5) Shrinkage Value$\times 10^{-5}$
B (t_1)						
BW (t_2)	Wd	1	1			
	LBd	1	1			
	Bf			0.8		
	Whf			0.2		
	Bu				t_{32}, t_1	-0.63
	Wu				t_{32}, t_2	-1.6
BD (t_3)	LDd*		1			
	UBd	1	1			
	LDd		1			
	LBf			1		
	Bu				t_{43}, t_1	-0.42
	Wu				t_{43}, t_2	-0.88
	LBu				t_{43}, t_3	-1.53
	LDu				t_{43}, t_3	-4.5
C (t_4)	LDd	1				
	LDd*		-1			
	UDd	1	1			
	UBf			1		
	Whf			0.8		
	Wvf			1		
	UDf			1		
	Bu				t_{f4}, t_1	-8.82
	Wu				t_{f4}, t_2	-8.43
	RBu				t_{f4}, t_3	-8.97
	UBu				t_{f4}, t_4	-1.53
	LDu				t_{f4}, t_3	-7.65
	UDu				t_{f4}, t_4	-11.55

Reference States

Rd_1 = Col. (2)

Rd_2 = Col. (3)

Rf_1 = Col. (2) + Col. (4)

Rf_2 = Col. (3) + Col. (4)

Rs_1 = Col. (2)+Col. (4)+Col. (5)

Rs_2 = Col. (3)+Col. (4)+Col. (5)

Note:

t_1 = Time of completion of base slab

t_2 = Time of completion of wall

t_3 = Time of completion of lower dome

t_4 = Time of completion of upper dome

t_{ij}, t_k = shrinkage in interval $t_i - t_j$ for concrete poured at time t_k

Table 2.3 - Numerical Values of Reference State Stress Resultants at Selected Sections

Section		Rd1	Rf1	Rs1	Rd2	Rf2	Rs2
W1	N1	-104100	-303600	-303600	-104100	-303600	-303600
	N2	-7775	-91140	-85670	-7775	-91140	-85670
	M1	-82800	-129500	-135600	-82790	-129500	-135600
	M2	-12440	-19470	-20390	-12430	-19460	-20380
W2	N1	-101700	-301200	-301200	-101700	-301200	-301200
	N2	+30070	-232300	-218900	+30070	-232300	-218900
	M1	-47100	-34070	-32770	-47090	-34070	-32670
	M2	-7289	-5722	-5572	-7289	-5772	-5572
W3	N1	-67550	-267100	-267000	-67540	-267000	-267000
	N2	12	-368900	-369100	145	-368800	-368800
	M1	698	3013	2976	747	3062	3025
	M2	-43	-135	-140	-36	-127	-133
W4	N1	-44980	-244500	-244500	-44970	-244500	-244500
	N2	-1732	-356600	-352700	-7080	-362000	-358000
	M1	+4223	13140	11230	4618	13530	+11630
	M2	535	1435	1148	594	1494	1207
W5	N1	-33720	-233200	-233200	-33710	233200	-233200
	N2	23140	-328500	-344700	32230	-319400	-335600
	M1	6604	-84720	-106800	39050	-52270	-74330
	M2	917	-13220	-16530	5785	-8355	-11670
UD1	N1	-15360	-346400	-345800	-16270	-347300	-346700
	N2	21940	-170200	-162600	11900	-180200	-172600
	M1	-25170	-104900	-104600	-24600	-104400	-104000
	M2	-3891	-13760	-13330	-4237	-14110	-13680
UD2	N1	-21210	-378700	-379000	-20930	-378400	-378700
	N2	-8445	-337100	-337400	-8531	-337200	-337400
	M1	5312	28550	29510	4022	27260	28220
	M2	2285	11200	11440	1931	10850	11090
UD3	N1	-20730	-377700	-377700	-20860	-377900	-377800
	N2	-20730	-377700	-377700	-20860	-377900	-377800
	M1	-188	-1321	-1384	-97	-1229	-1292
	M2	-188	-1321	-1384	-97	-1229	-1292
LD1	N1	-9635	-28450	-28900	-6548	-25360	-25810
	N2	12880	-113600	-112800	30580	-95920	-95110
	M1	-10180	48920	51680	-20880	38220	40980
	M2	-1602	8034	8638	-3465	6171	6775
LD2	N1	-11900	-13540	-13750	-11490	-13130	-13340
	N2	-3326	-49530	-51570	4836	-41360	-43410
	M1	1787	-8122	-8065	3087	-6822	-6765
	M2	720	-3006	-3029	1272	-2454	-2477
LD3	N1	-5444	-5262	-4796	-5483	-5301	-4835
	N2	-17660	-15560	-5233	-18020	-15920	-5593
	M1	1231	2196	7684	1086	2051	7538
	M2	-245	112	-971	-301	56	-1027

Units are pounds and feet. Sign convection as in Fig. 2.1.

Table 2.4
Numerical Values of Live Load Stress
Resultants at Selected Locations

Section		SST	WOT	SOT	C:Cp*	C:Cw	CH:Hp*	CH:Hw
	N1	0	0	0	33.15	-11630	33.15	-11630
	N2	-54130	87950	-47960	3.856	-867	0.525	-341
W1	M1	101800	-292300	-42230	58.39	-9217	0.0	0
	M2	17820	-50790	-6977	8.764	-1385	0.0	-2
	N1	0	0	0	33.15	-11630	33.15	-11630
	N2	-110000	176100	-100200	10.98	3355	19.63	1990
W2	M1	60910	229900	-82540	17.81	-5235	-21.06	902
	M2	118800	-332100	-39790	2.745	-811	-3.087	110
	N1	0	0	0	33.15	-11630	33.15	-11630
	N2	1373	-4251	-891	67.72	7	67.62	22
W3	M1	129100	-350300	-32080	-0.218	-34	-0.349	-14
	M2	129000	-350000	-32210	0.004	-31	0.002	-28
	N1	0	0	0	33.15	-11630	33.15	-11630
	N2	804	-1747	252	73.85	2220	73.85	2220
W4	M1	129000	-349700	-31720	-4.781	6654	-4.778	6653
	M2	129000	-350100	-32170	-0.645	973	-0.644	973
	N1	0	0	0	33.15	-11630	33.15	-11630
	N2	3631	-7407	1644	35.34	35350	35.34	35350
W5	M1	135300	-370600	-37230	-30.99	-21830	-30.99	-21830
	M2	129900	-353200	-32990	-4.576	-3301	-4.576	-3301
	N1	-4691	14200	2705	48.26	3622	48.26	3622
	N2	-152900	50910	13640	-39.51	12630	-39.51	12630
UD1	M1	68170	-189900	-22120	79.28	7012	79.28	7013
	M2	47350	-129200	-12530	12.95	1263	12.95	1263
	N1	-324	804	0	68.38	656	68.38	656
	N2	-8946	25920	3948	41.01	6562	41.01	6562
UD2	M1	39650	-106300	-8566	-15.39	817	-15.39	817
	M2	40750	-110100	-9696	-6.309	707	-6.309	707
	N1	666	-1927	-290	69.35	-282	69.34	-281
	N2	666	-1927	-290	69.35	-282	69.34	-281
UD3	M1	42530	-115500	-10750	1.338	-163	1.338	-163
	M2	42530	-115500	-10750	1.338	-163	1.338	-163
	N1	9878	-25830	-1445	-1.733	-19740	-1.733	-19740
	N2	74730	-195400	-10960	-6.909	9881	-6.909	9881
LD1	M1	-28030	73430	4243	+7.168	-29960	7.168	-29960
	M2	-4224	11080	655	1.365	-4444	1.365	-4444
	N1	498	-1285	-56	-0.359	-20250	-0.359	-20250
	N2	22540	-58710	-3054	-5.263	-41650	-5.263	-41650
LD2	M1	6130	-15780	-635	-0.401	8836	-0.401	8836
	M2	2110	-5513	-300	-0.256	2008	-0.256	2008
	N1	-173	-473	-938	0.041	-1266	0.041	-1266
	N2	-3714	-11660	-21730	0.263	-9715	0.263	-9715
LD3	M1	-2012	-6196	-11650	0.067	-3423	0.067	-3423
	M2	98	2020	2359	0.0296	-1343	0.0296	-1343

* These loading cases are for an internal pressurization of 1 psf.
Units are in pounds and feet. Sign convection as in Fig. 2.1.

TABLE 3.1 - SECTION DETAILS

Location	Sect.	d	b_1	b_2	x_1	x_2	x_f	A_{s1}	A_{s2}	A_f
W1	W1H	18	12	12	9	9	9	0.85	0.85	1.30
	W1V	42	12	12	2.5	28	34	0.96	0.99	2.41
					16	39.5		1.49	1.49	
W2	W2H	42	11.70	12.30	3.5	38.5	21	0.96	0.99	1.30
					15	29		0.10	0.11	
	W2V	42	12	12	2.5	28	34	1.23	1.23	2.41
					16	39.5		1.23	1.23	
W3	W3H	42	11.70	12.30	3.5	38.5	21	0.77	0.81	1.30
	W3V	42	12	12	2.5	39.5	34	0.60	1.27	2.41
W4	W4H	42	11.70	12.30	3.5	38.5	21	0.77	0.81	1.30
	W4V	42	12	12	2.5	39.5	34	0.60	1.27	2.41
W5	W5H	42	11.70	12.30	3.5	38.5	21	1.52	1.58	1.30
	W5V	42	12	12	2.5	39.5	34	1.56	1.56	2.41
UD1	UD1H	24	12	12	2.7	21.3	12	1.10	1.10	2.33
	UD1V	24	12	12	4.1	19.9	12	1.27	1.69	2.33
UD2	UD2H	24	12	12	2.7	21.3	12	1.17	1.34	2.33
	UD2V	24	12	12	4.1	19.9	12	1.02	1.02	2.33
UD3	UD3H	24	12	12	2.7	21.3	12	2.67	2.67	2.33
	UD3V	24	12	12	4.1	19.9	12	2.03	2.03	2.33
LD1	LD1H	15	12	12	2.6	12.4	-	2.08	1.28	-
	LK1V	15	12	12	3.9	11.1	-	0.99	0.99	-
LD2	LD2H	15	12	12	2.6	12.4	-	1.91	1.91	-
	LD2V	15	12	12	3.9	11.1	-	0.99	0.99	-
LD3	LD3H	15	12	12	2.6	12.4	-	1.91	1.91	-
	LD3V	15	12	12	3.9	11.1	-	0.99	0.99	-

x is measured from the interior face

Curve	Pivot	Point On Fig. 3.10	Control Strains At 0	x_1	x_f	x_2	d
Concrete Crushing Failure	$x=0$	a	ε_u				ε_u
		b	ε_u				ε_o
		c	ε_u				ε_c
		d	ε_u			ε_y	
		e	ε_u	ε_y			
		f	ε_u		ε_r		
Tendon Rupture	$x=x_f$	f	ε_u		ε_r		
		g	ε_r		ε_r		
		h			ε_r		ε_u
First Cracking	$x=d$	c	ε_u				ε_c^-
		m	ε_c^-				ε_c^-
Through Cracking	$x=0$	n	ε_c^+				ε_c^+
		i	ε_c^+			ε_y	
		k	ε_c^+	ε_y			
		g	ε_c^+		ε_r		
First Yield at x_2	$x=x_2$	d	ε_u			ε_y	
		i	ε_c			ε_y	
		j		ε_y		ε_y	
		k				ε_y	ε_c
		l				ε_y	ε_u

TABLE 3.2 - STRAIN CONDITIONS AT CRITICAL POINTS OF FIG. 3.10

Table 4.1 - Membrane Forces at Selected Locations Arising From Internal Pressure

Location	Membrane Forces in kips/ft/psi		Membrane Forces in kips/ft at 18 psi	
	N1	N2	N1	N2
W1	4.774	0.553	85.93	9.99
W2	4.774	1.581	85.93	28.46
W3	4.774	9.752	85.93	175.54
W4	4.774	10.634	85.93	191.41
W5	4.774	5.089	85.93	91.60
UD1	6.949	-5.689	125.09	-102.41
UD2	9.846	5.905	177.24	106.30
UD3	9.986	9.986	179.76	179.76
LD1	-0.250	-0.995	-4.49	-17.91
LD2	-0.051	-0.758	-0.93	-13.64
LD3	0.006	0.038	0.11	0.68

Table 4.2 - Pressurization Forces and Load Factors
For Lower Dome Sections

Location	Sect.	Membrance Force (kips) at				Pressure Load Factor			
		FC	FY	TC	U	FC	FY	TC	U
LD1	H	0	-	NA	-21	0	-	NA	4.7
	V	-447	NA	NA	-507	>20	NA	NA	>20
LD2	H	-16	-121	NA	-131	17	>20	NA	>20
	V	NA	NA	NA	-754	NA	NA	NA	>20
LD3	H	5	45	NA	50	>20	>20	NA	>20
	V	62	-	32	109	>20	-	>20	>20

FC = first cracking
FY = first yield
TC = through-cracking
U = ultimate strength
NA = not applicable

Table 4.3 - Comparison of Interaction and Cracking Analyses at Selected Sections

Location	Section and Anal.		Membrane Force At FC	FY	TC	U	Pressure Load Factor FC	FY	TC	U
W3	H	C	480	480	480	490	5.6	5.6	5.6	5.7
		I	475	(405)	(282)	482	5.5	(4.7)	(3.3)	5.6
	V	C	600	660	600	720	3.4	3.8	3.4	4.1
		I	590	(445)	(370)	500	3.4	(2.5)	(2.1)	2.8
W5	H	C	130	460	290	550	1.5	5.4	3.4	6.4
		I	108	233	NA	295	1.3	2.7	NA	3.4
	V	C	440	680	450	770	4.8	7.4	4.9	8.4
		I	465	645	(405)	675	5.1	7.0	(4.4)	7.4
UD1	H	C	130	510	590	700	1.0	4.1	3.2	5.6
		I	135	216	NA	250	1.1	1.7	NA	2.0
UD2	H	C	270	700	390	750	1.5	3.9	2.2	4.2
		I	360	500	-	624	2.0	2.8	NA	3.5
	V	C	340	630	380	710	3.2	5.9	3.6	6.7
		I	374	457	NA	598	3.3	4.3	NA	5.6
UD3	H	C	470	880	470	920	2.6	4.9	2.6	5.1
		I	499	763	(408)	898	2.8	4.2	(2.3)	5.0
	V	C	470	810	470	840	2.6	4.5	2.6	4.7
		I	499	680	(418)	830	2.8	3.8	(2.3)	4.6

NOTES:

1. FC = first cracking TC = through-cracking
   FY = first yield U = ultimate strength

2. In column 3, C = cracking analysis
   I = interaction analysis

3. NA = not applicable

4. All results are for k_t = 6, with no thermal effects

5. Forces in kips

6. ( ) = fictitious loads (See Sect. 4.3)

Table 4.4 - Membrane Forces at Horizontal Sections for Various Cracking Analyses (in kips)

	Limit State	W1H	W2H	W3H	W4H	W5H	UD1H*	UD2H	UD3H
k=0	FC	0-(45)-100	190 [120]	260	210	40	110	270	330
	FY	470	510 [500]	460	430	460	510	700	880
	TC	NA	310 [320]	270	250	260	580	390	350
k=0	FC	NA		0	0	0	0-(75)-160	40	0
(WOT)	FY	NA		440	410	430	540	670	890
	TC	NA		290	270	300	560	440	400
k=6	FC	NA	300 [210]	480	390	130	130	350	470
	FY	NA	510 [500]	480	430	460	510	700	880
	TC	NA	360 [350]	480	390	290	590	420	470
k=6	FC	NA		0	0	0	0-(50)-180	12	75
WOT	FY	NA		450	410	430	540	670	890
	TC	NA		320	290	320	560	450	430
ULTIMATE		515	570 [570]	490	470	550	700	750	920

FC = first cracking　　FY = first yield　　TC = through cracking

() = crack closure　　k = tensile strength coefficient

NA = not applicable　　[ ] = results for hinged base connection

WOT = winter operating temperature

* = See ADDENDUM, Sect. AD.3

Table 4.5 - Membrane Forces at Vertical Sections for Various Cracking Analyses (in kips)

Limit State		W1V	W2V		W3V	W4V	W5V	UD1V	UD2V	UD3V
k=0	FC	30	160	[170]	370	360	250	Compressive Membrane Force	250	340
	FY	390	670	[680]	660	650	680		630	810
	TC	120	230	[230]	370	360	330		380	360
k=0 WOT	FC				0	0	0		0	0
	FY				650	630	660		610	820
	TC				420	410	390		430	400
k=6	FC	80	330	[350]	600	580	440		340	470
	FY	390	670	[680]	660	650	680		630	810
	TC	160	330	[350]	600	580	450		380	470
k=6 WOT	FC				0	0	0		90	100
	FY				650	630	660		610	820
	TC				450	440	410		400	420
ULTIMATE		640	780	[780]	720	710	770		710	840

FC = first cracking FY = first yield TC = through-cracking
[ ] = results for hinged base connection WOT = winter operating temperature

Table 4.6 - Load Factors on Horizontal Sections for Various Cracking Analyses

	Limit State	W1H	W2H	W3H	W4H	W5H	UD1H*	UD2H	UD3H
k=0	FC	0-(0.5)-1.2	2.2 [1.4]	3.0	2.4	0.5	0.9	1.5	1.8
	FY	5.5	5.9 [5.8]	5.4	5.0	5.4	4.1	3.9	4.9
	TC	NA	3.6 [3.7]	3.1	2.9	3.0	4.6	2.2	1.9
k=0 WOT	FC			0	0	0	0	0.2	0
	FY			5.1	4.8	5.0	4.3	3.8	5.0
	TC			3.4	3.1	3.5	4.5	2.5	2.2
k=6	FC	0	3.5 [2.4]	5.6	4.5	1.5	1.0	2.0	2.6
	FY	5.5	5.9 [5.8]	5.6	5.0	5.4	4.1	3.9	4.9
	TC	NA	4.2 [4.1]	5.6	4.5	3.4	4.7	2.4	2.6
k=6 WOT	FC			0	0	0	0	0.1	0.4
	FY			5.2	4.8	5.0	4.3	3.8	5.0
	TC			3.7	3.4	3.7	4.5	2.5	2.4
ULTIMATE		6.0	6.6 [6.6]	5.7	5.5	6.4	5.6	4.2	5.1

FC = first cracking FY = first yield TC = through-cracking

k = tensile strength coefficient WOT = winter operating temperature

* See ADDENDUM, Sect. AD.3

Table 4.7 - Load Factors on Vertical Sections for Various Cracking Analyses

	Limit State	W1V	W2V	W3V	W4V	W5V	UD1V	UD2V	UD3V
k=0	FC	3.0	5.6 [3.3]	2.1	1.9	2.7	Compressive Membrane Force	2.4	1.9
	FY	39.0	23.5 [13.4]	3.8	3.4	7.4		5.9	4.5
	TC	12.0	8.1 [4.5]	2.1	1.9	3.6		3.6	2.0
k=0 WOT	FC			0	0	0		0	0
	FY			3.7	3.3	7.2		5.7	4.6
	TC			2.4	2.1	4.3		4.0	2.2
k=6	FC	8.0	11.6 [6.9]	3.4	3.0	4.8		3.2	2.6
	FY	39.0	23.5 [13.4]	3.8	3.4	7.4		5.9	4.5
	TC	16.0	11.6 [6.9]	3.4	3.0	4.9		3.6	2.6
k=6 WOT	FC			0	0	0		0.8	0.6
	FY			3.7	3.3	7.2		5.7	4.6
	TC			2.6	2.3	4.5		3.8	2.3
ULTIMATE		64.0	27.4 [15.3]	4.1	3.7	8.4		6.7	4.7

FC = first cracking FY = first yield TC = through-cracking

[ ] = results for hinged base connection k = tensile strength coefficient

WOT = winter operating temperature

FIGURES

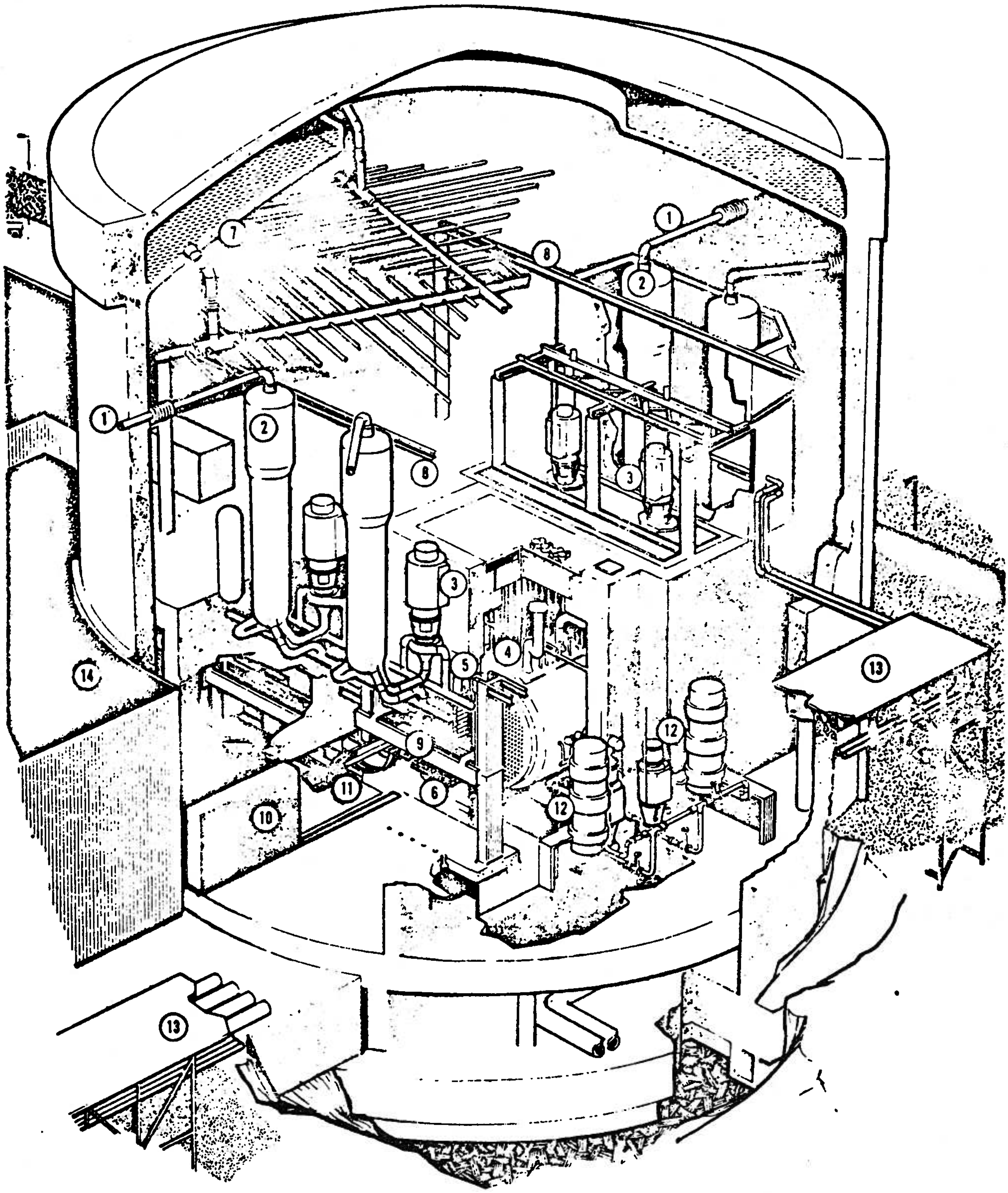

1 MAIN STEAM SUPPLY PIPING
2 STEAM GENERATORS
3 MAIN PRIMARY SYSTEM PUMPS
4 CALANDRIA ASSEMBLY
5 FEEDERS
6 FUEL CHANNEL ASSEMBLY
7 DOUSING WATER SUPPLY
8 CRANE RAILS
9 FUELLING MACHINE
10 FUELLING MACHINE DOOR
11 CATENARY
12 MODERATOR CIRCULATION SYSTEM
13 PIPE BRIDGE
14 SERVICE BUILDING

FIGURE 1.1 Reactor Building Cutaway

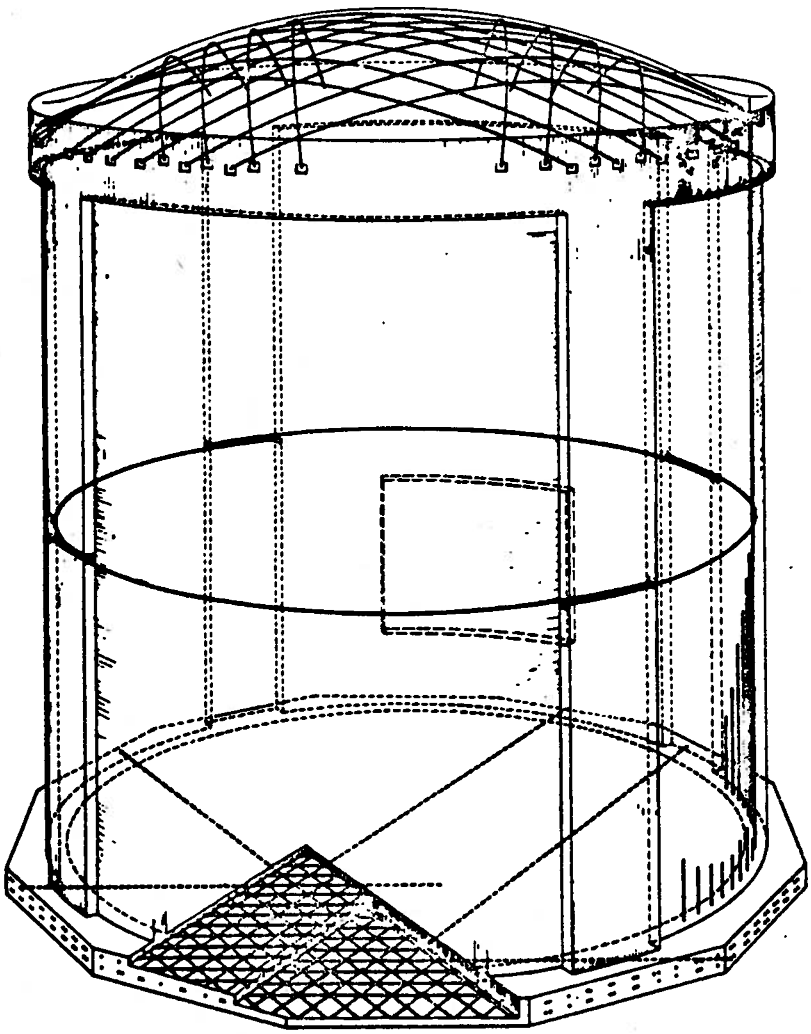

FIGURE 1.2 Reactor Building Prestressing
Cable Arrangement

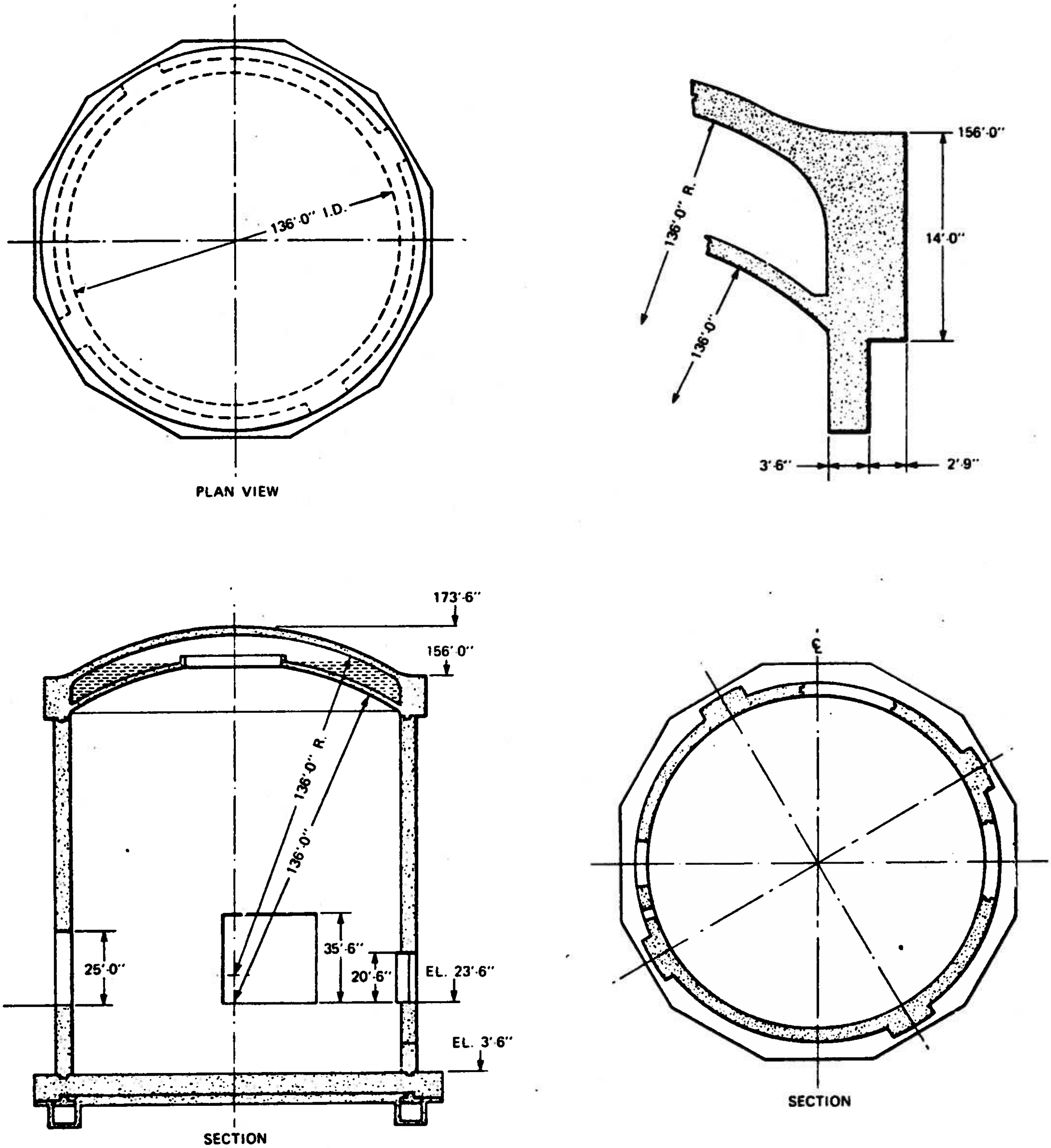

FIGURE 1.3 Reactor Building Structural Arrangement

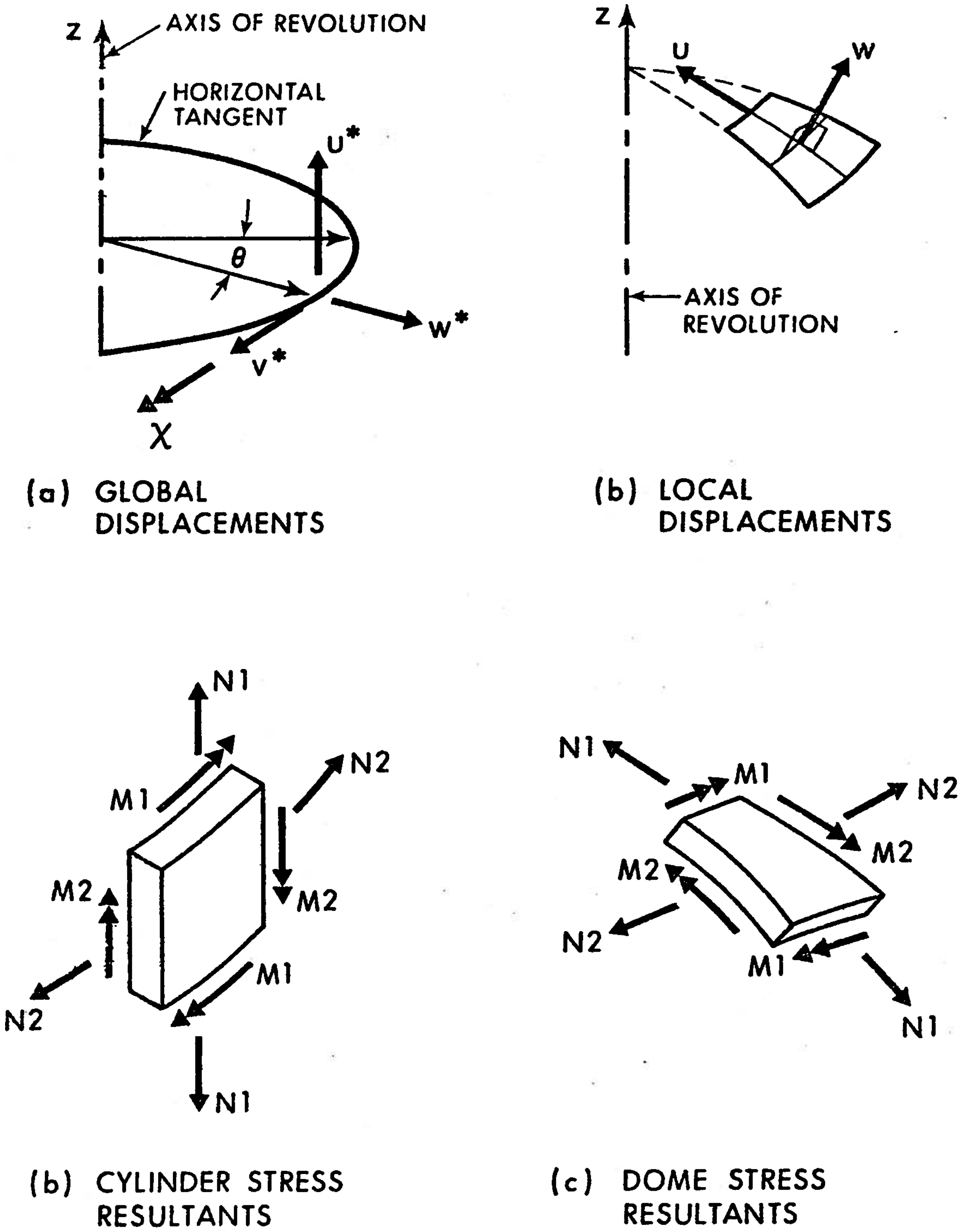

FIGURE 2.1 Positive Displacements and Stress Resultants in BOSOR4

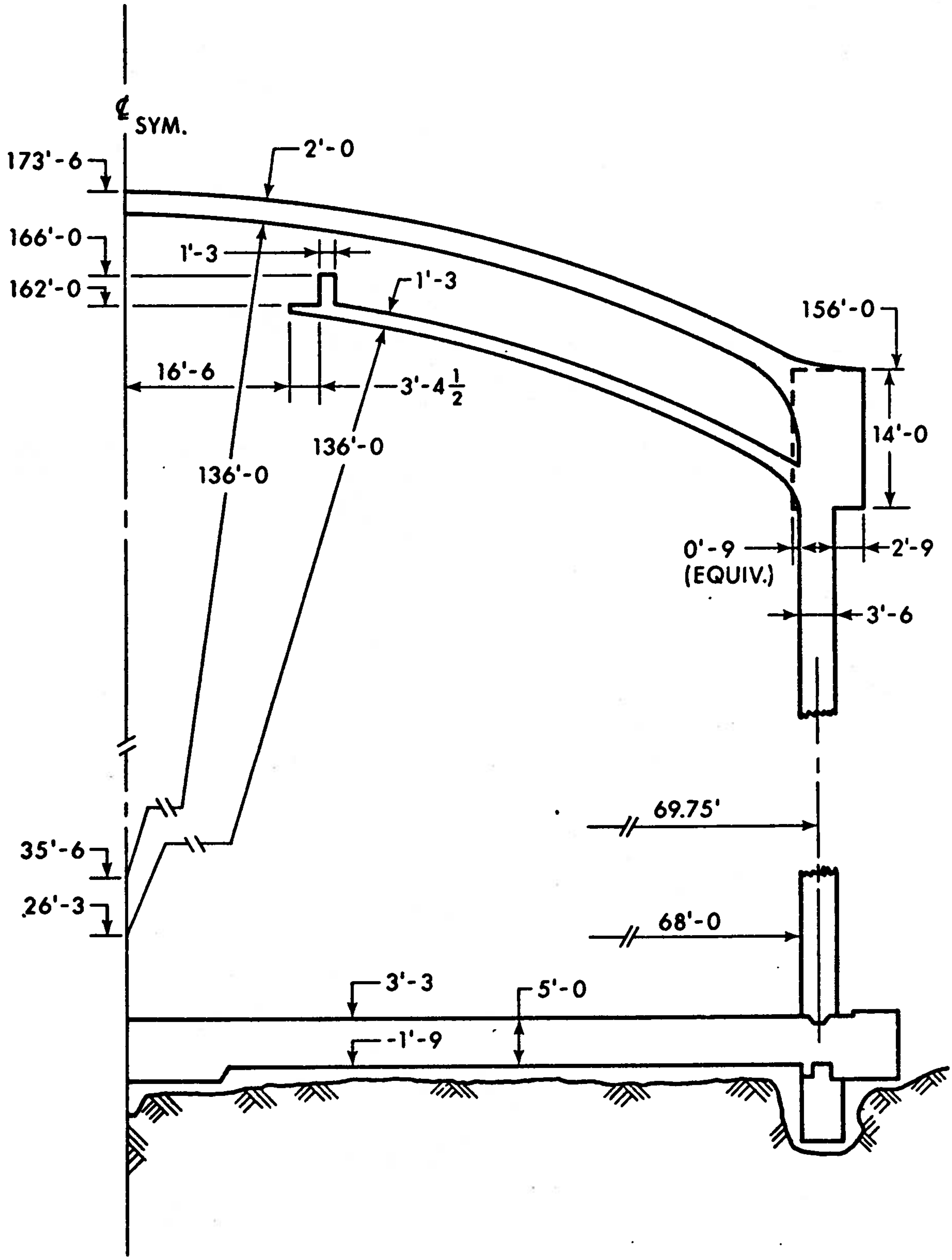

FIGURE 2.2 Principal Dimensions of GENTILLY-2

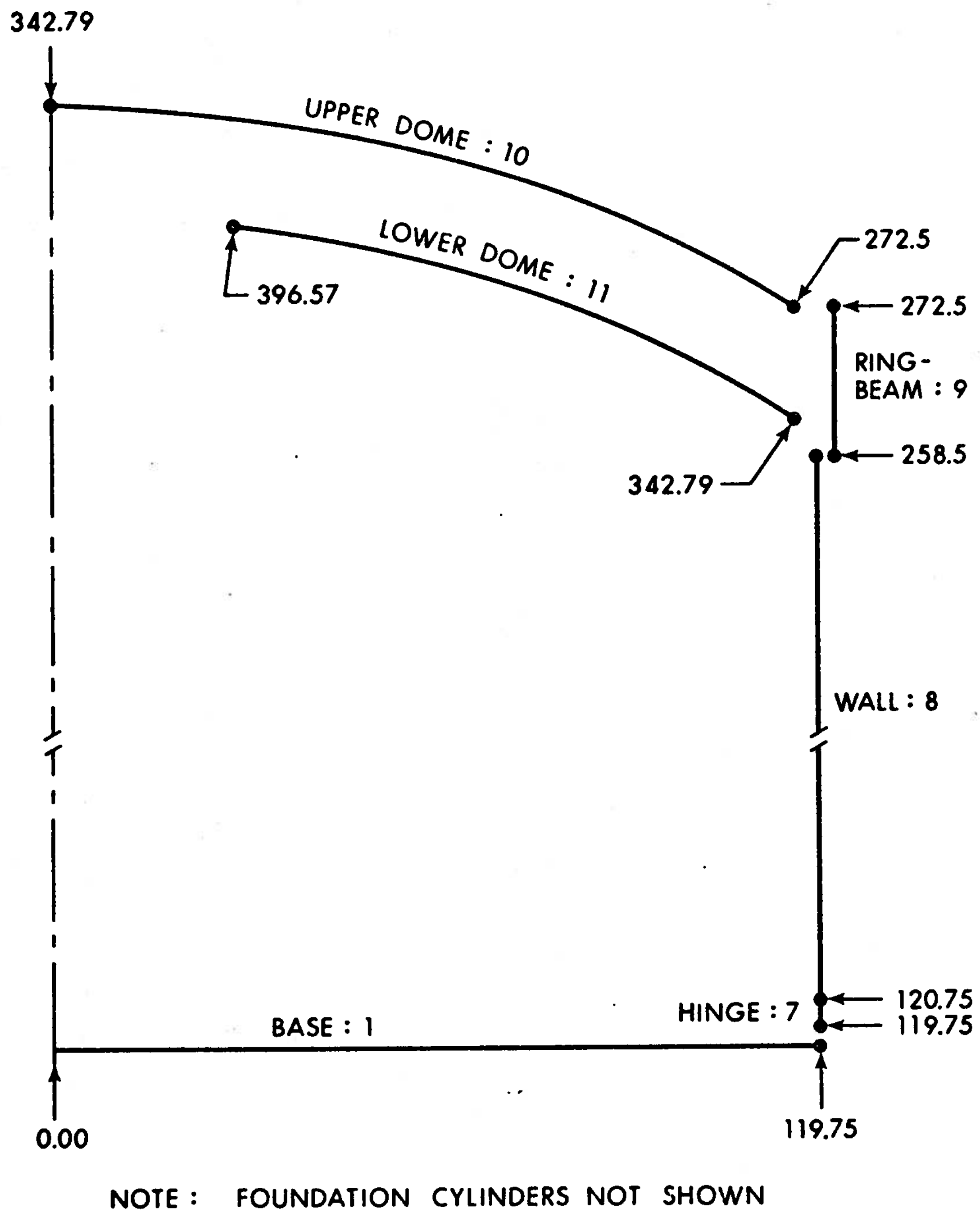

FIGURE 2.3 BOSOR4 MODEL: Meridional Coordinates and Segment Numbering

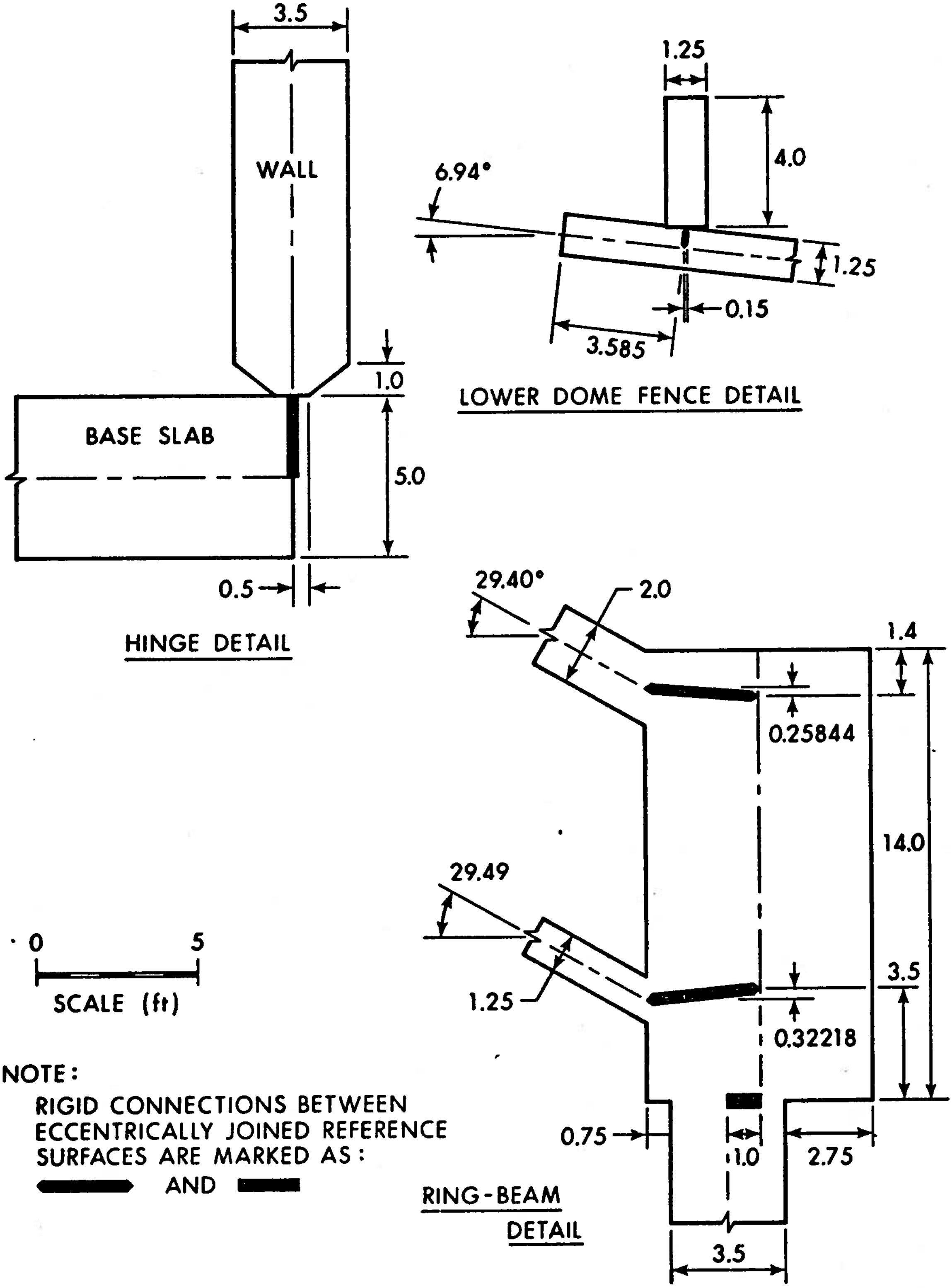

FIGURE 2.4 Connectivity Between Shell Segments

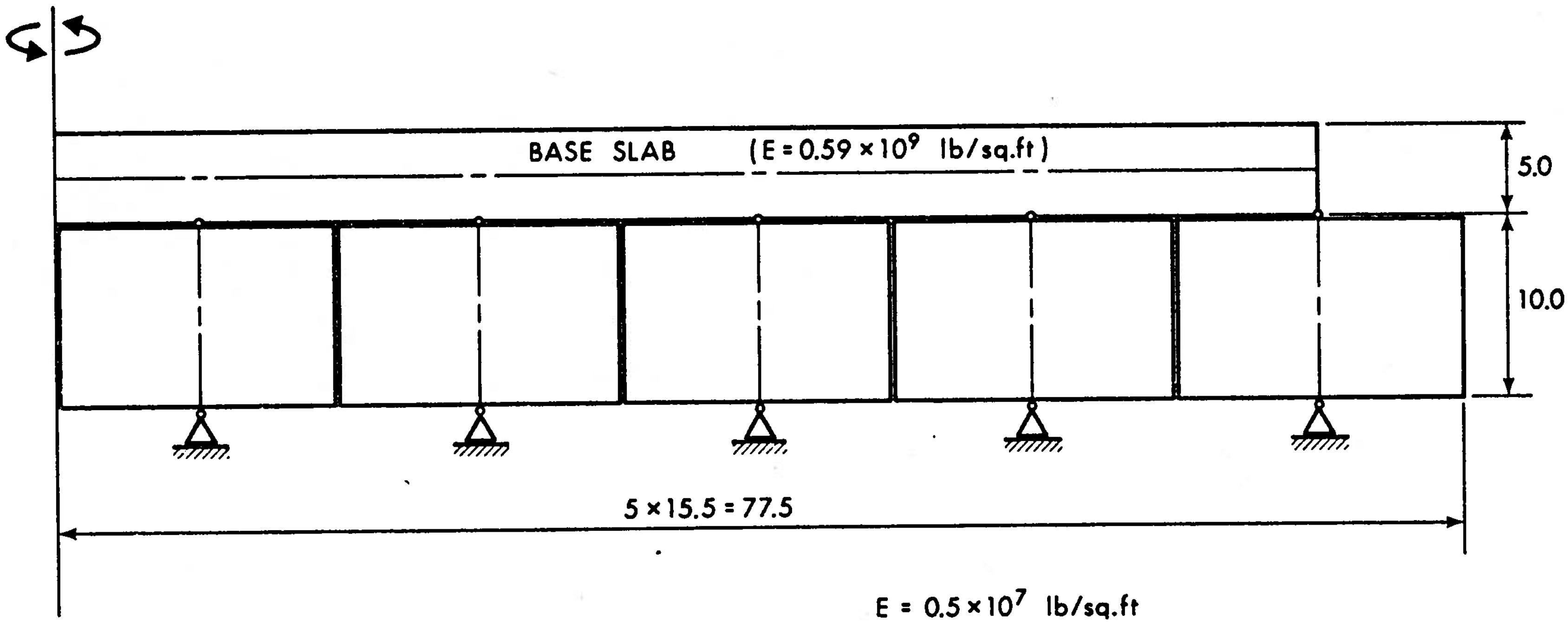

FIGURE 2.5 Modelling of Elastic Foundation

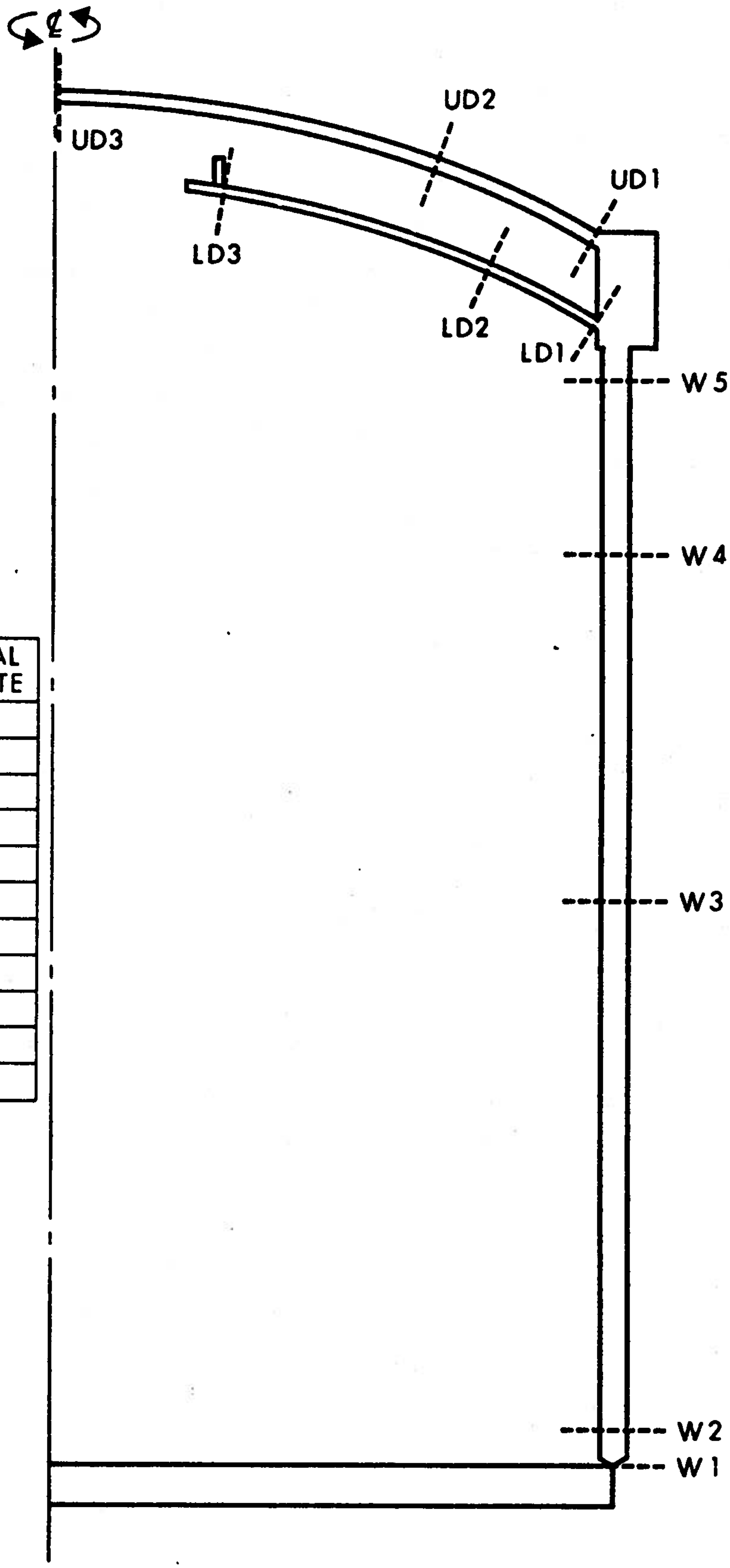

SECTION	MERIDIONAL COORDINATE
W 1	119.75
W 2	124.57
W 3	189.70
W 4	232.70
W 5	254.15
UD 1	272.50
UD 2	293.59
UD 3	342.79
L D 1	342.79
L D 2	357.13
L D 3	391.19

NOTE :
FOR DEFINITION OF MERIDIONAL COORDINATE REFER TO FIG. 2.3

FIGURE 2.6 Location of Reference Sections

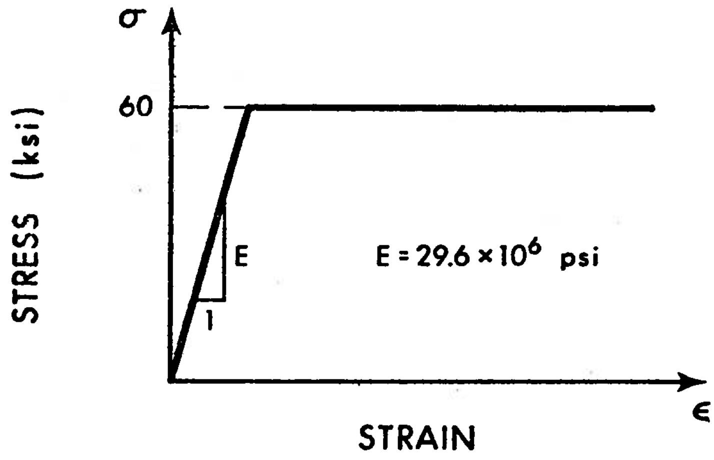

FIGURE 3.1 Stress-Strain Diagram for Reinforcing Steel

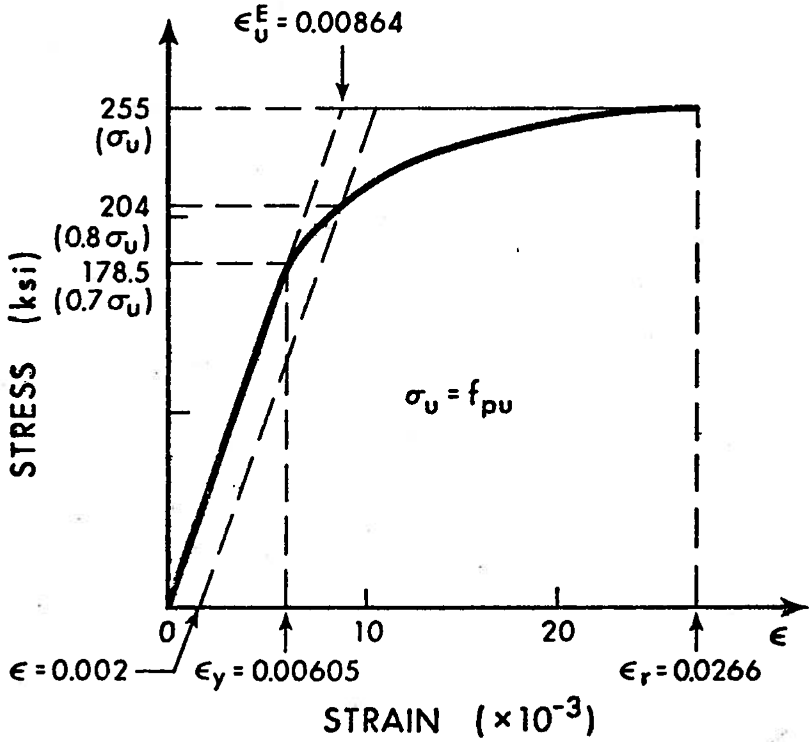

FIGURE 3.2 Stress-Strain Diagram for Prestressing Steel

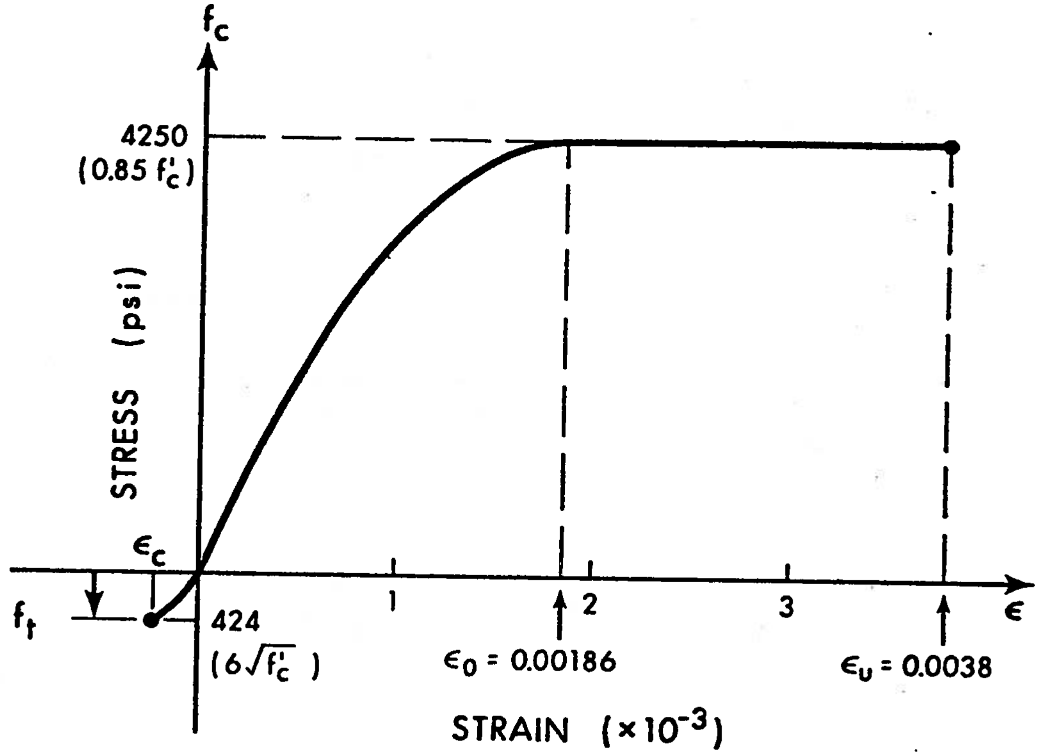

FIGURE 3.3 Stress-Strain Diagram for Concrete

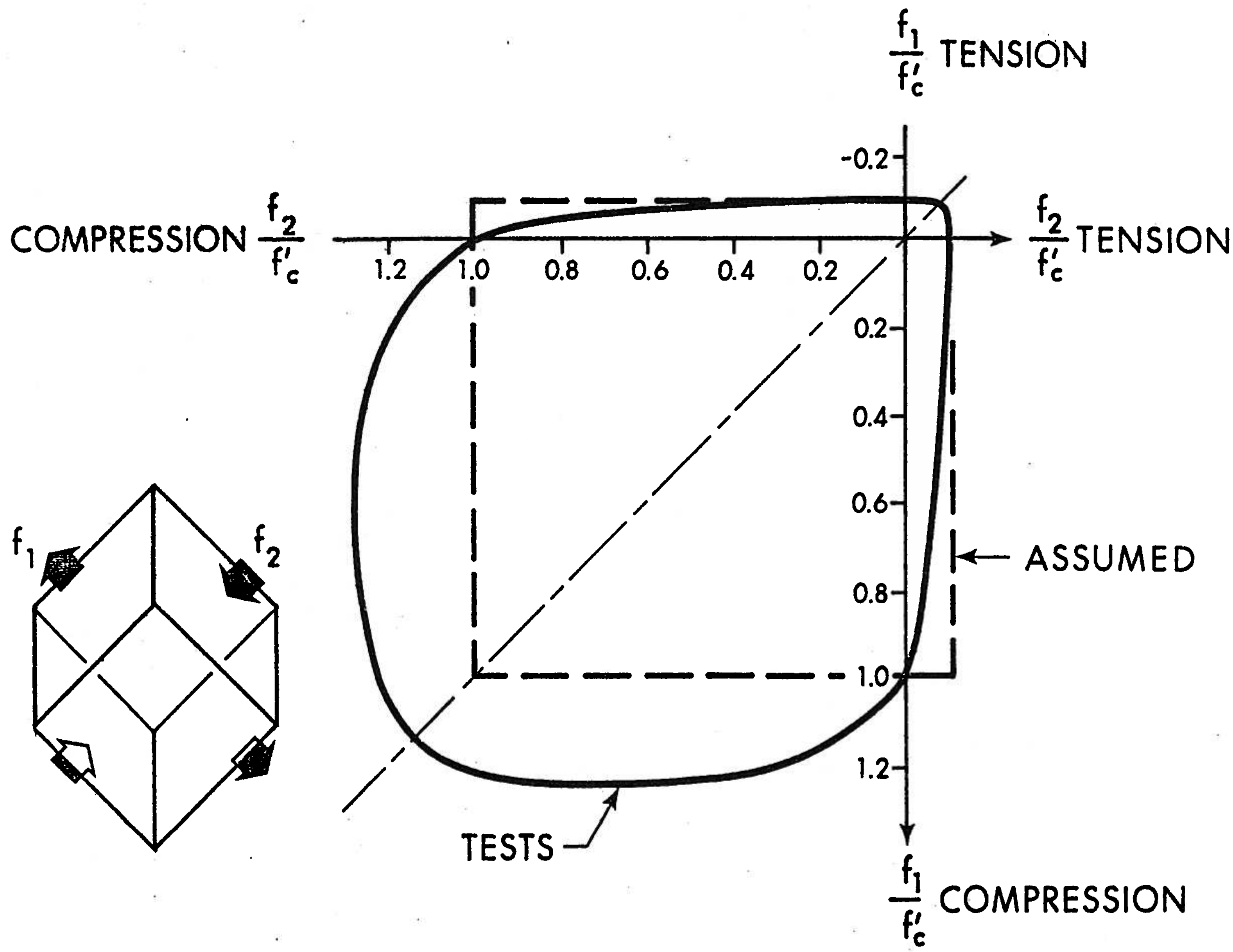

FIGURE 3.4 Biaxial Failure Criterion for Concrete

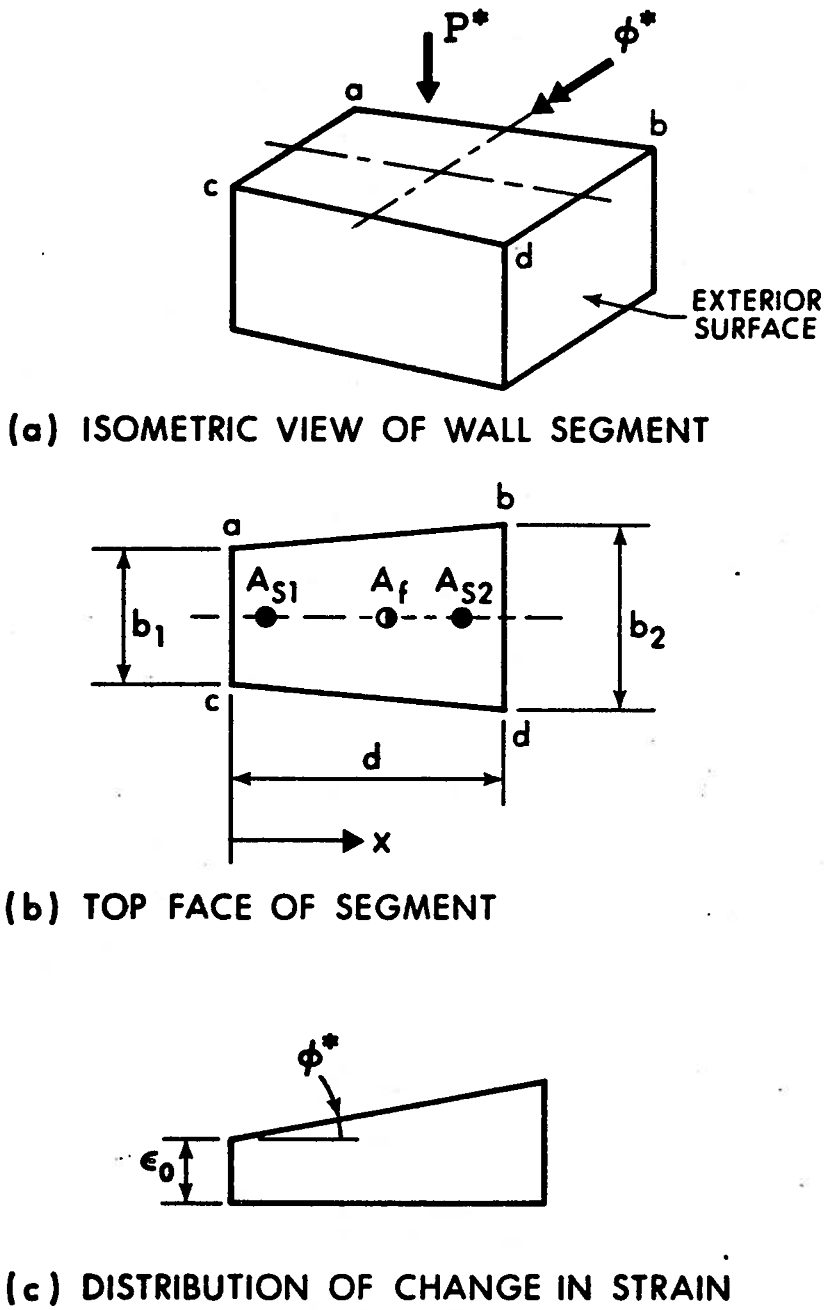

FIGURE 3.5 Typical Wall Segment

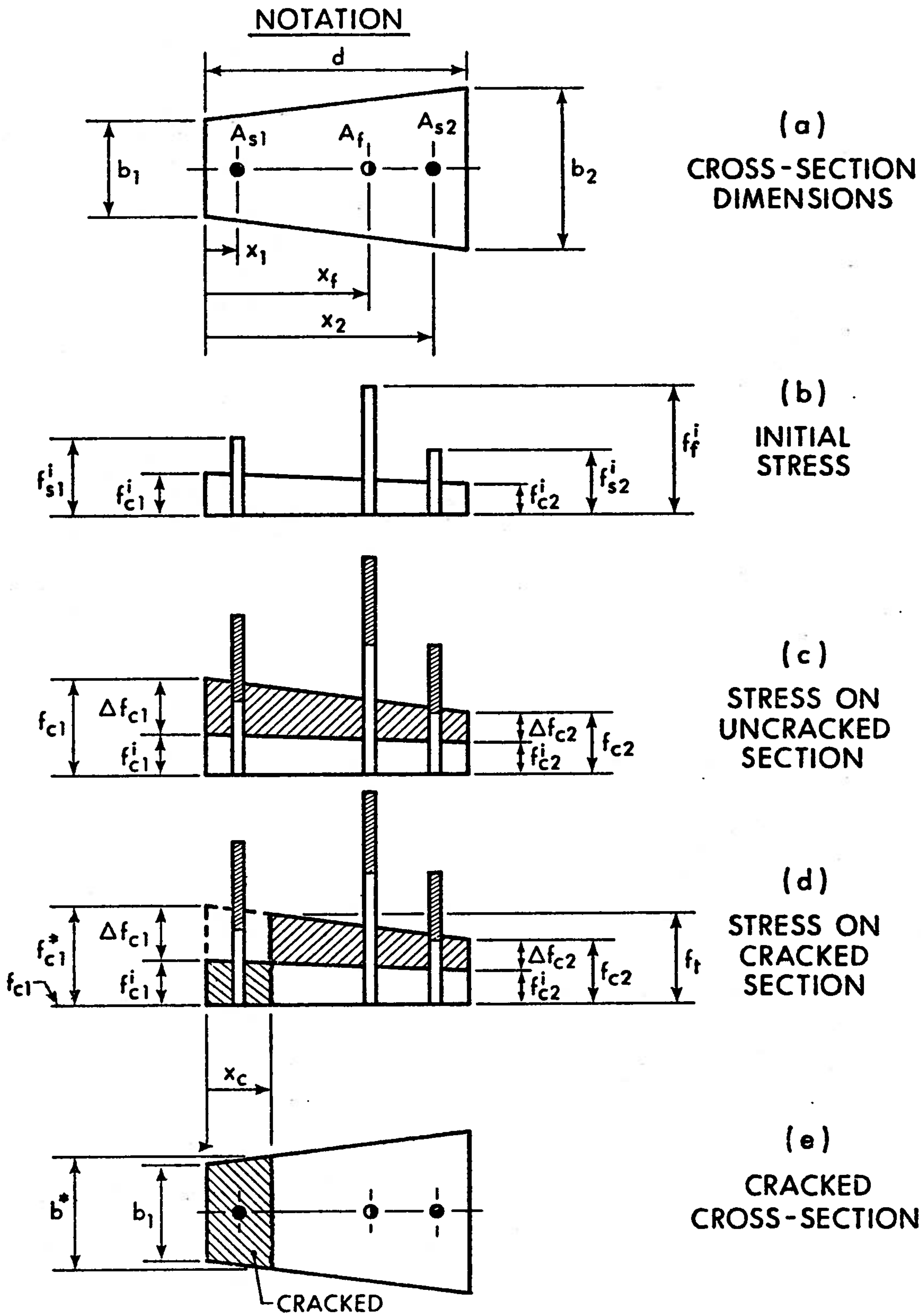

FIGURE 3.6 Stress Distribution for Cracking Analysis

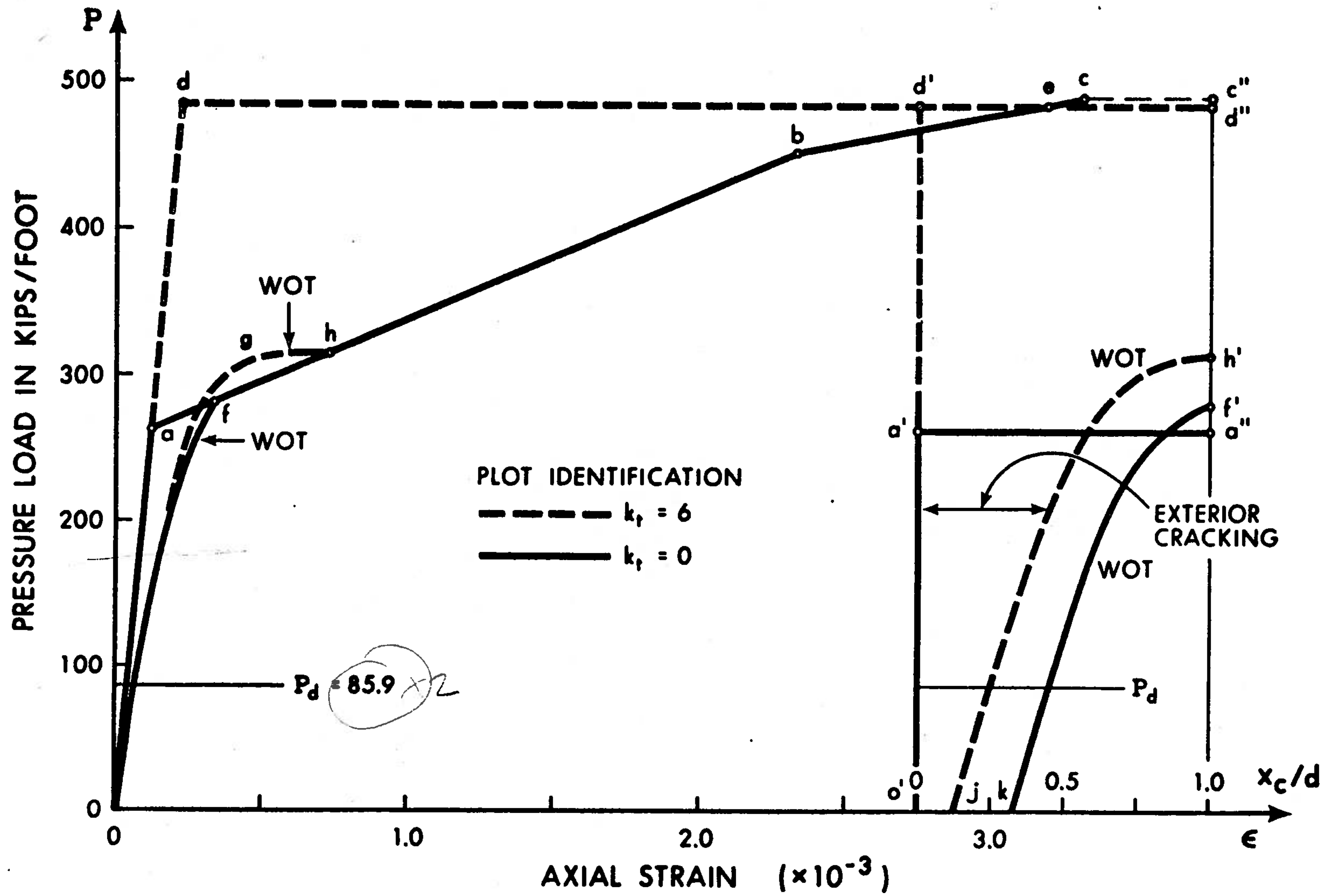

FIGURE 3.7 Response of Section W3H to Pressure Load

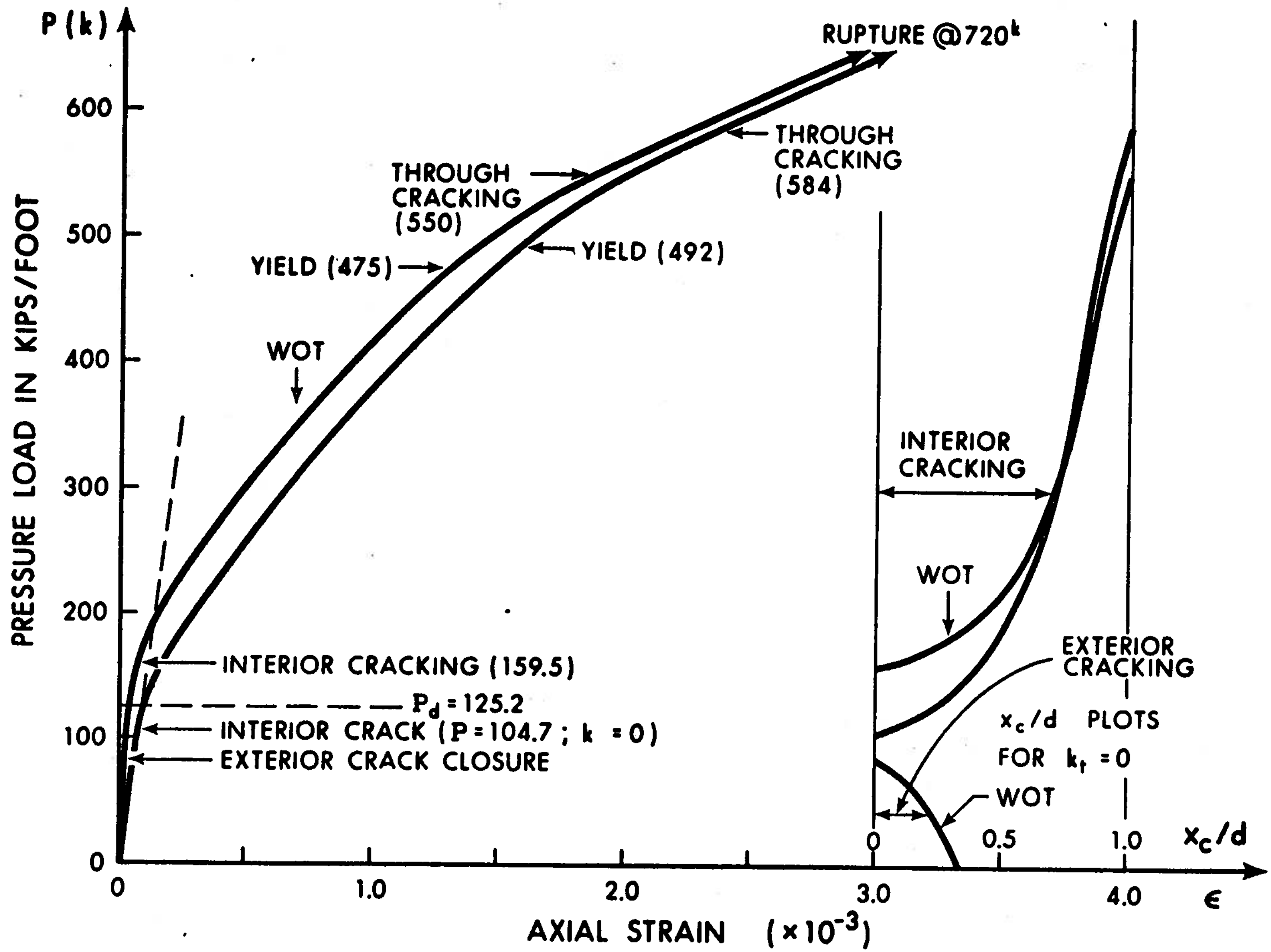

FIGURE 3.8 Response of Section UD1H to Pressure Load

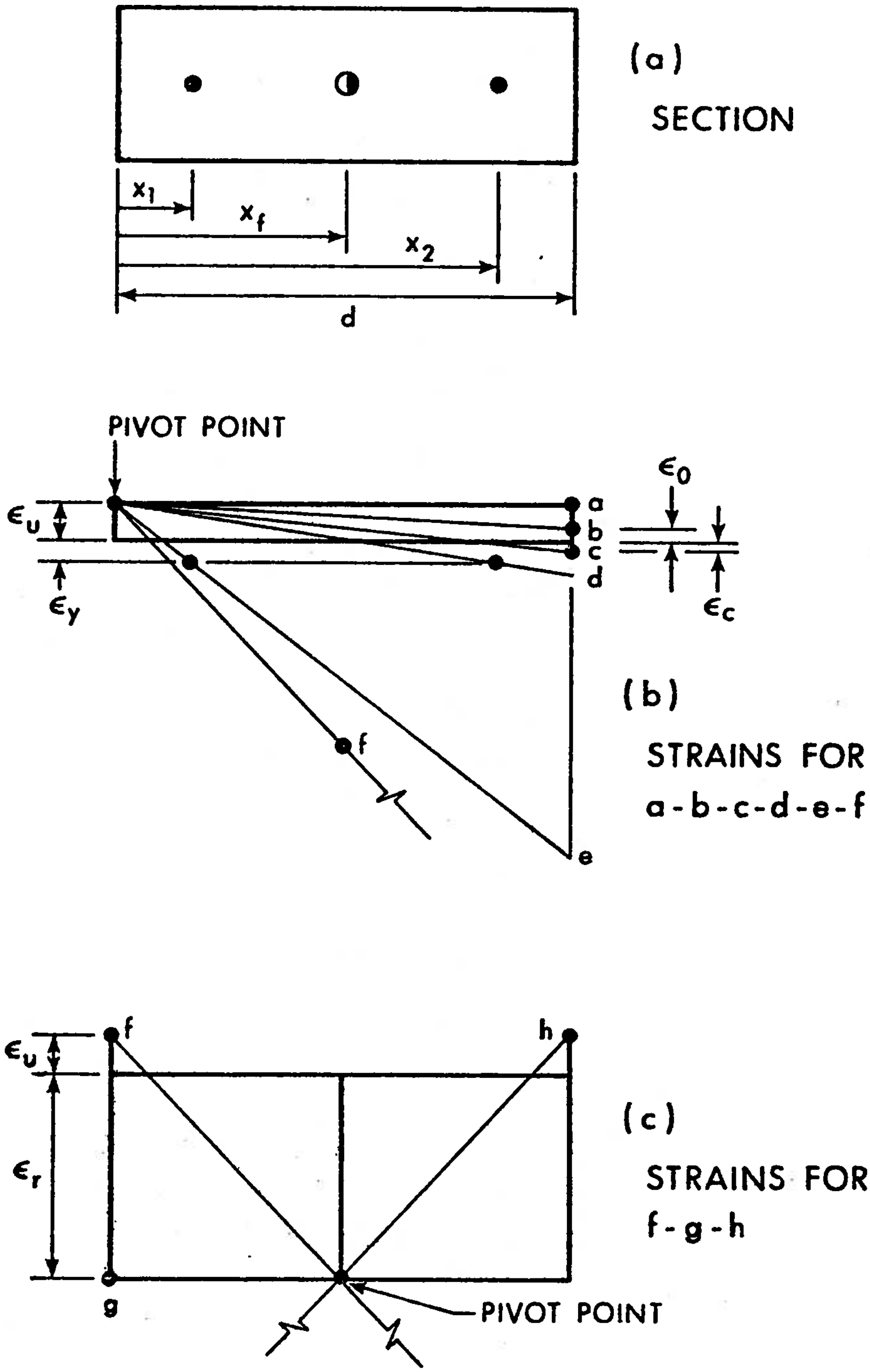

APPROXIMATE STRAIN VALUES :

$\epsilon_u = 0.0038$ $\quad$ $\epsilon_c = 0.0010$ $\quad$ $\epsilon_r = 0.0214$

$\epsilon_0 = 0.00186$ $\quad$ $\epsilon_y = 0.00203$

FIGURE 3.9 Strain Distributions for Ultimate Strength Conditions

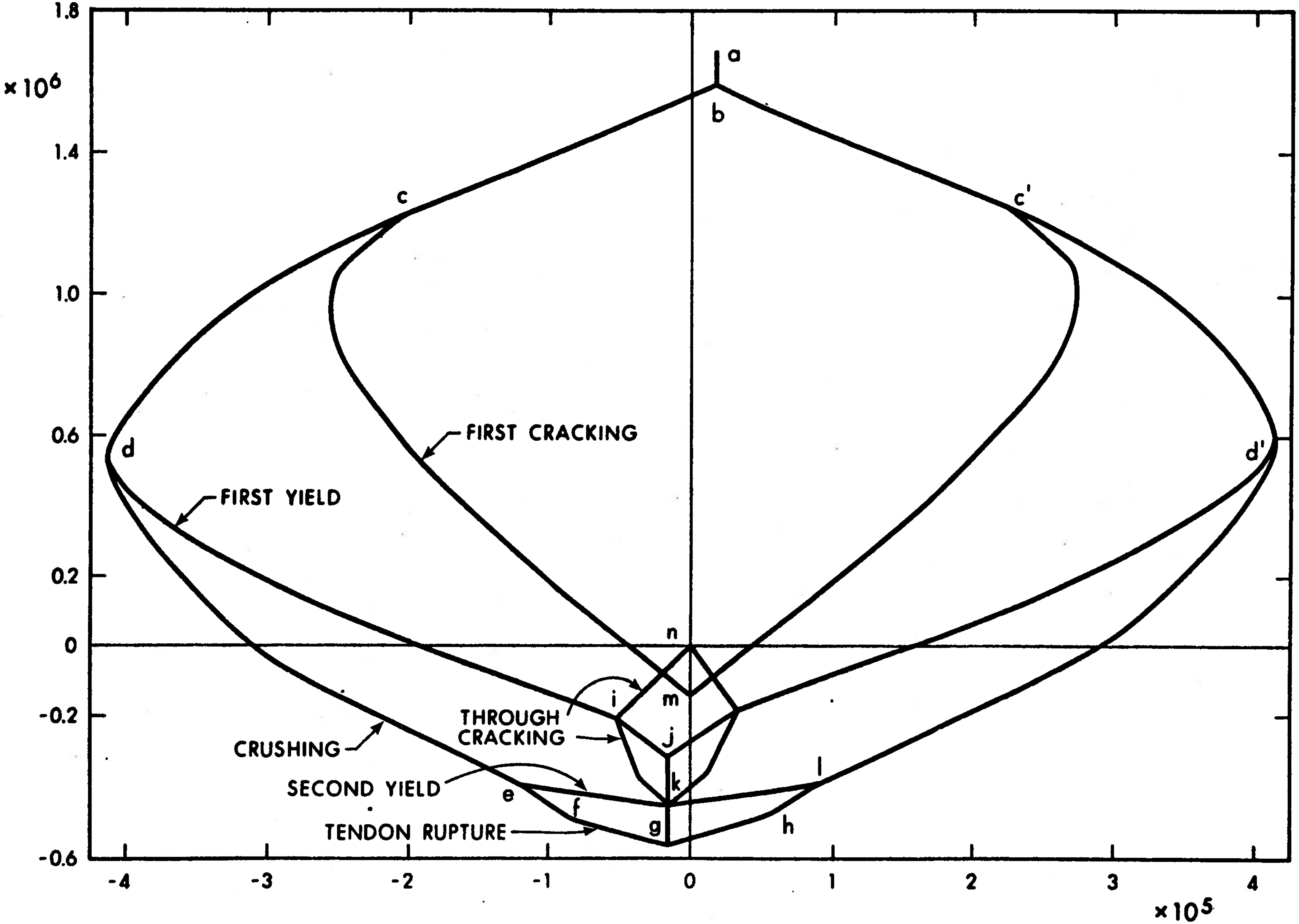

FIGURE 3.10 Typical Interaction Curve

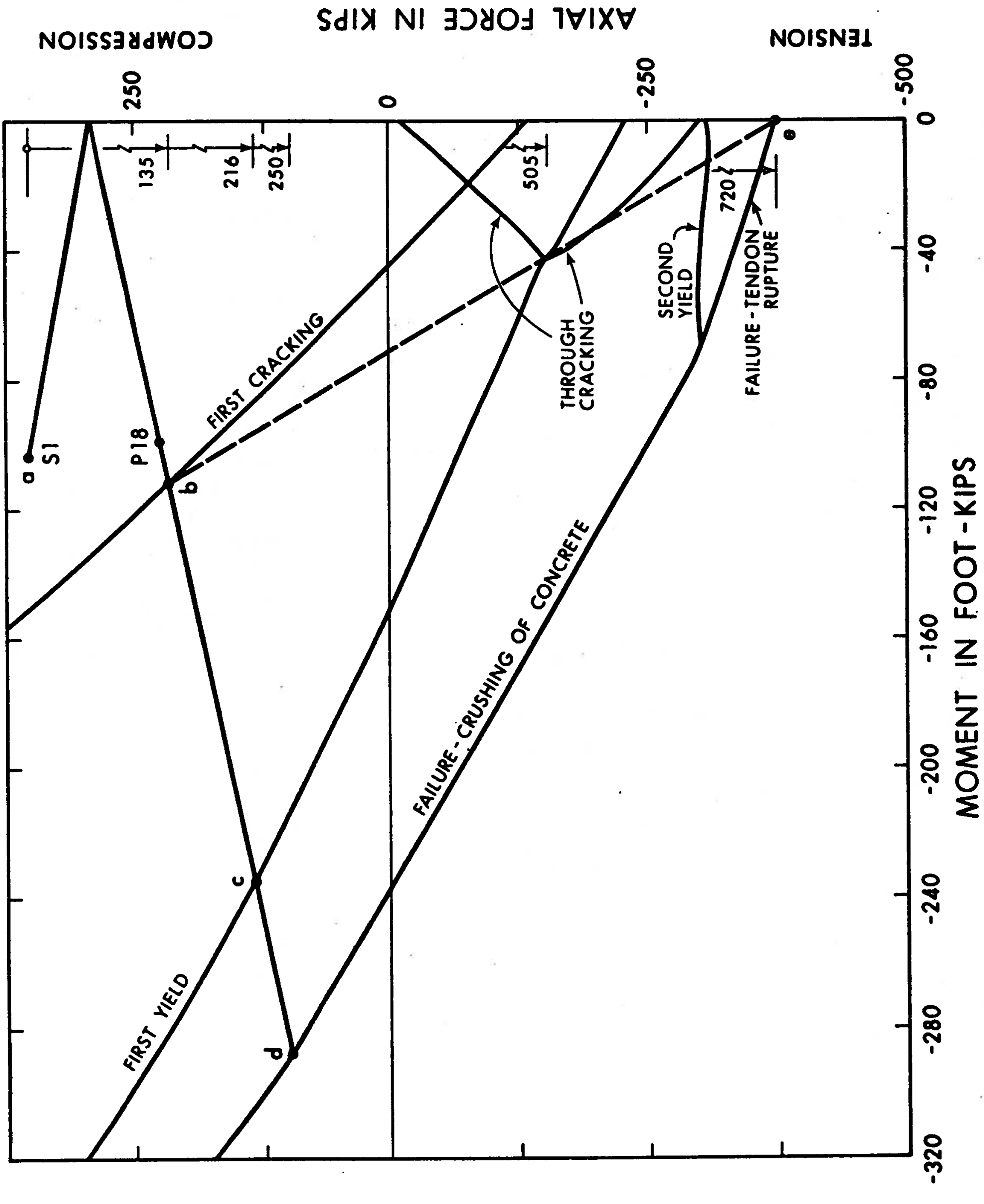

AXIAL FORCE IN KIPS
COMPRESSION
TENSION
250
0
-250
-500
MOMENT IN FOOT-KIPS
0
-40
-80
-120
-160
-200
-240
-280
-320
135
216
250
505
720
a
S1
P18
b
c
d
e
FIRST CRACKING
THROUGH CRACKING
SECOND YIELD
FAILURE-TENDON RUPTURE
FAILURE-CRUSHING OF CONCRETE
FIRST YIELD

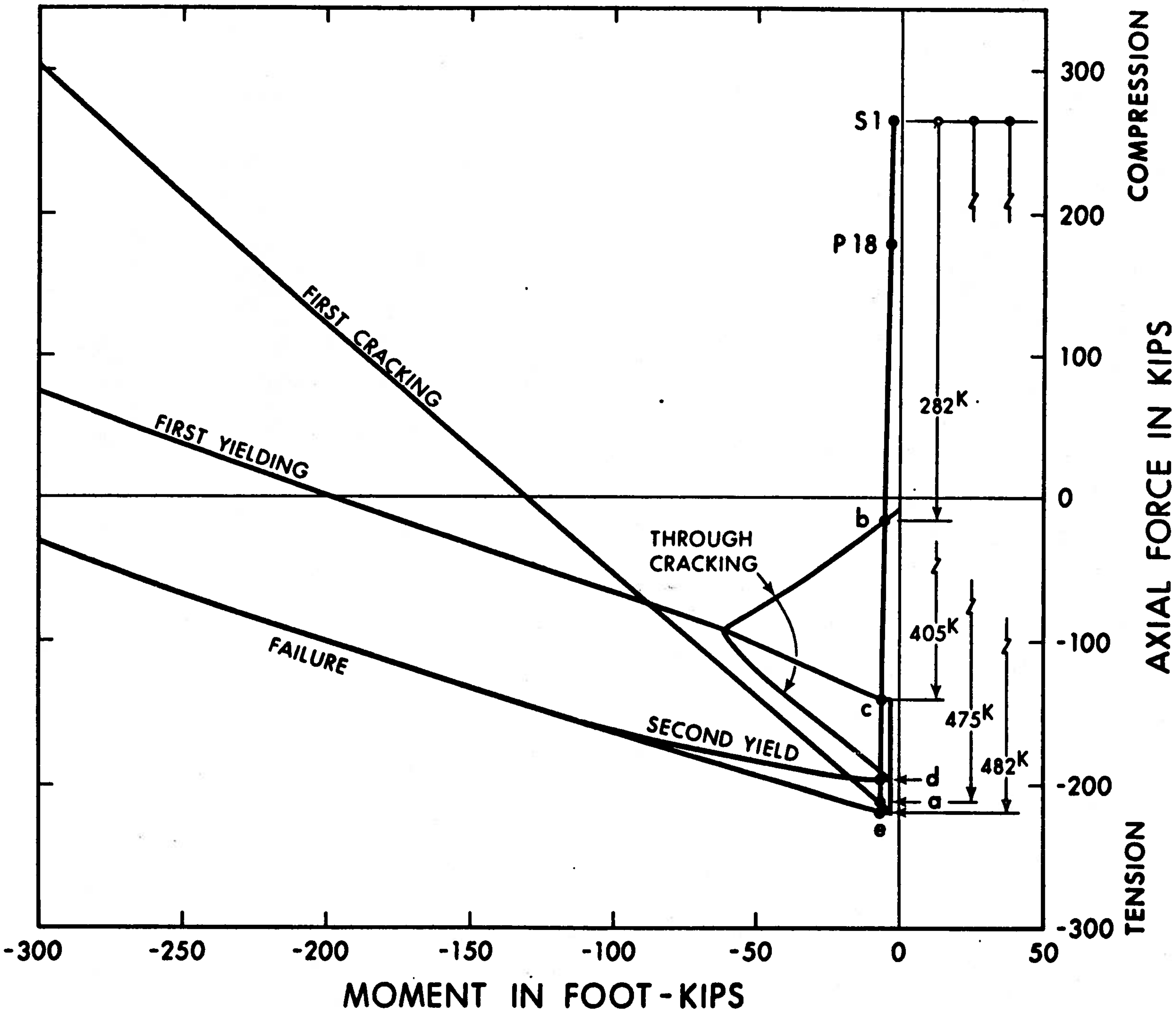

FIGURE 3.12 Loading Path on Interaction Curve for W3H

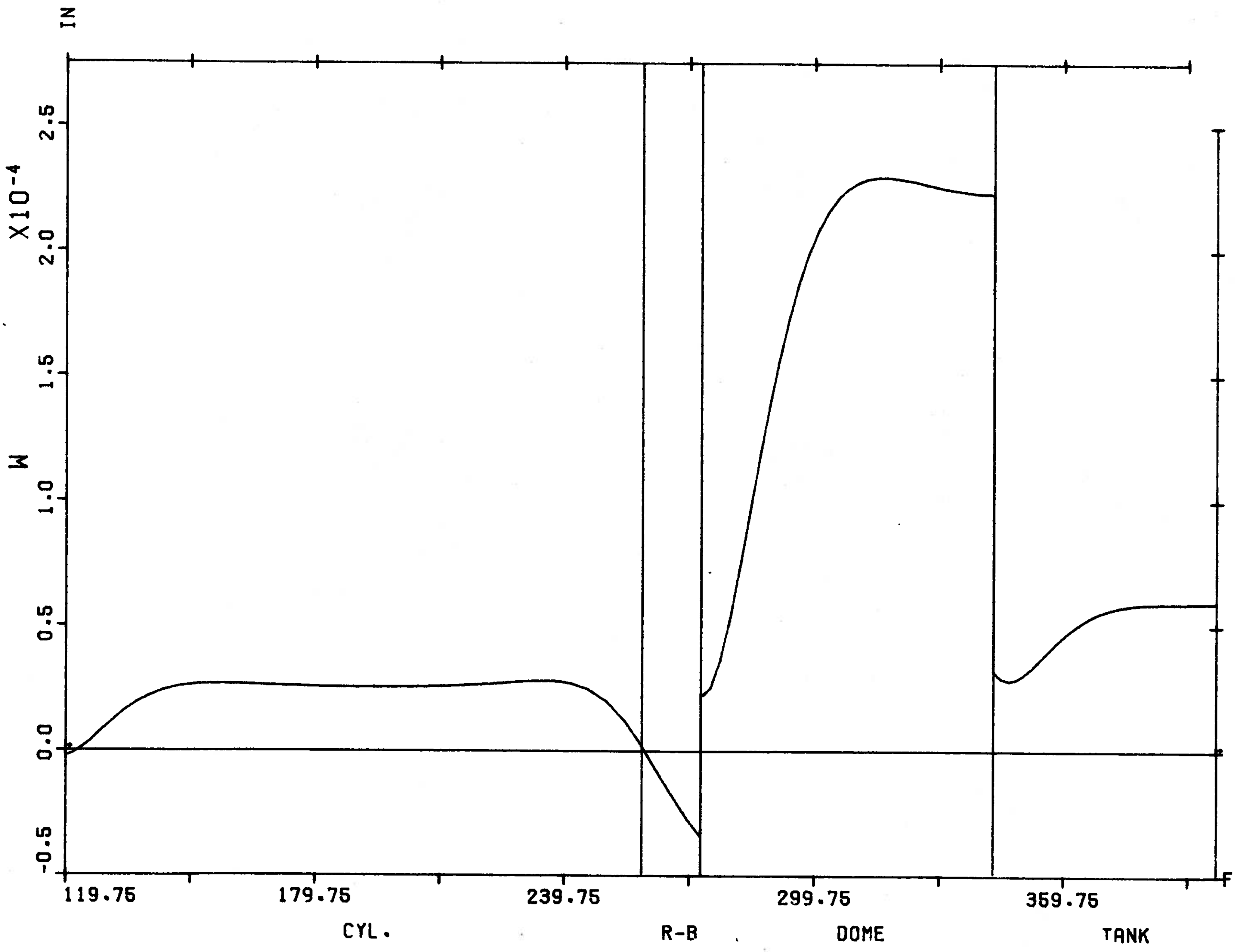

FIGURE 5.1 Local Normal Displacement for C:Cp

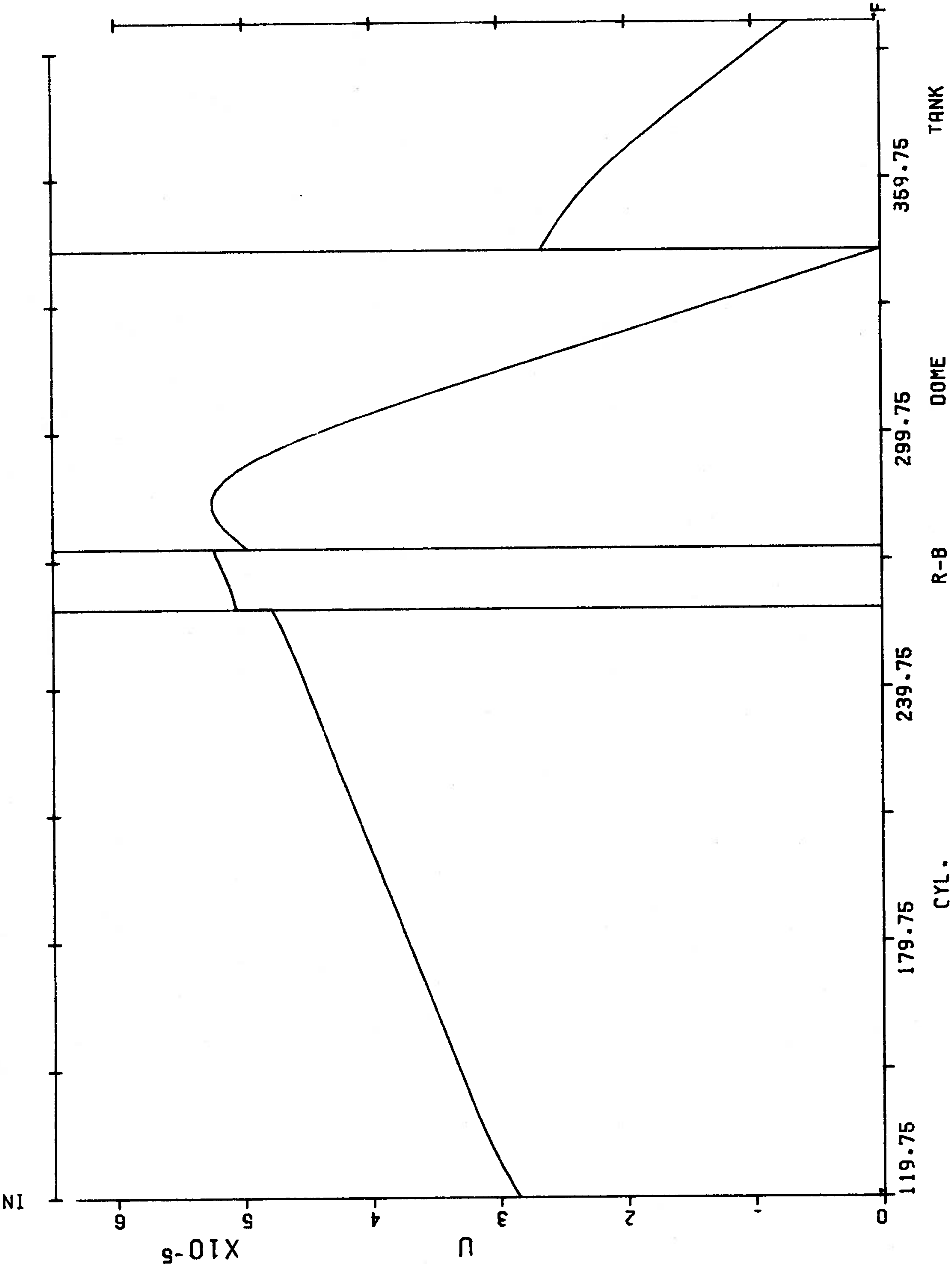

FT
TANK
359.75
DOME
299.75
R-B
239.75
CYL.
179.75
119.75
IN
0
1
2
3
4
5
6
U
X10-5

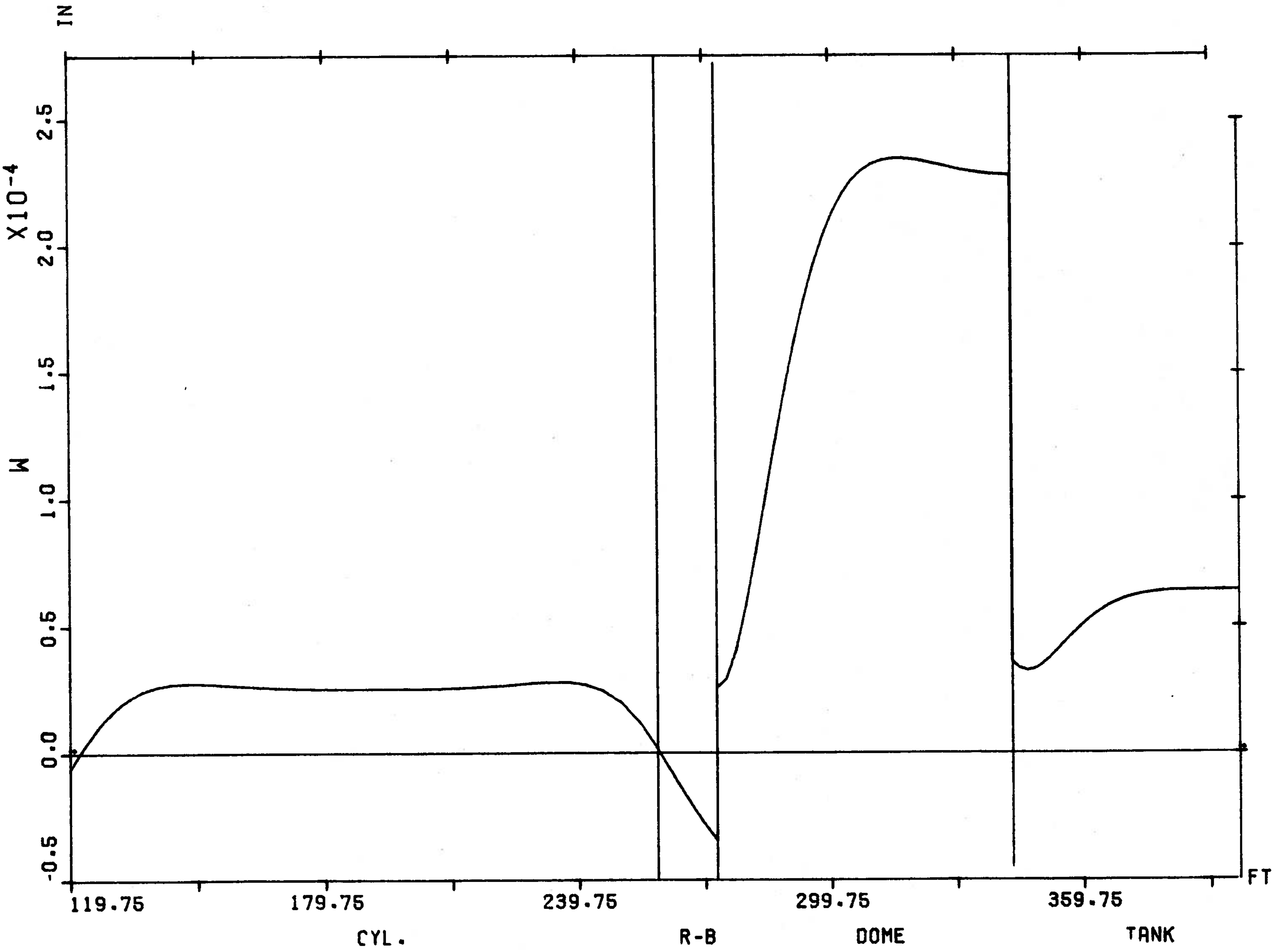

FIGURE 5.3 Local Normal Displacement for CH:Up

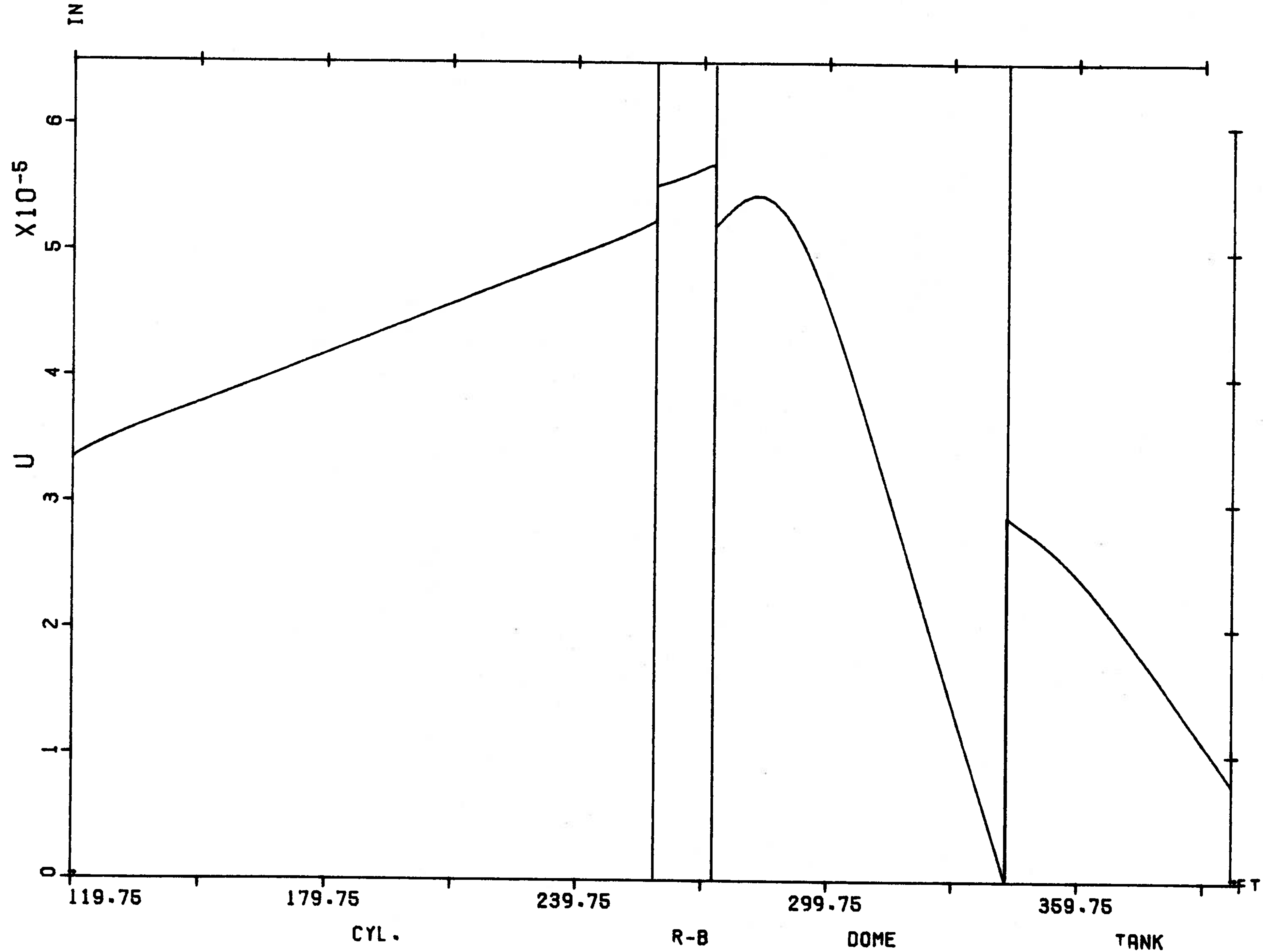

FIGURE 5.4 Local Meridional Displacement for CH:Hp

*

APPENDIX A

Notation

NOTATION

SUBSCRIPTS

0	indicates a reference value
1	indicates location x_1 or 0 on a section (Fig. 3.6)
2	indicates location x_2 or d on a section (Fig. 3.6)
c	indicates cracking
e	indicates effective
f	indicates prestress steel
s	indicates reinforcing steel
u	indicates ultimate

SUPERSCRIPTS

E	indicates elastic
i	indicates initial (i.e. - immediately prior to live load application)
I	indicates inelastic

ALPHABETIC SYMBOLS

A	area
A_T	transformed area
A_{s1}, A_{s2}	areas of steel at locations x_1 and x_2 (Fig. 3.6)
A_f	area of prestressing steel (Fig. 3.6)
b^*	width of section at crack (Fig. 3.6)
b_1	width of section at x=0 (Fig. 3.6)
b_2	width of section at x=d (Fig. 3.6)
d	depth of section (Fig. 3.6)
E	modulus of elasticity
E_e	effective modulus of elasticity $= E/(1-\nu^2)$

f	stress
Δf_c	change in concrete stress
f_c^i	initial concrete stress
f'_c	28 day cylinder strength
f''_c	0.85 f'_c
f_f	stress in prestressing steel
f_{pu}	ultimate strength of prestressing strand
f_t	concrete tensile strength = $k_t\sqrt{f'_c}$
f_{t2}	a pseudo-tensile strength = f_t or f_{c2}^i + $E_e(\phi^*d - \beta\varepsilon_{c2}^T)$
f_y	yield stress of reinforcing steel
k_t	factor to determine f_t from $f_t=k_t\sqrt{f'_c}$
M_1	bending moment from N1 stresses (ft.lb/ft) (Fig. 2.1)
M_2	bending moment from M2 stresses (ft.lb/ft) (Fig. 2.1)
n	modular ratio E(steel)/E(concrete)
N_1	resultant of stress in direction of meridional axis (lb/ft) (Fig. 2.1)
N_2	resultant of stress in tangential direction (lb/ft) (Fig. 2.1)
ΔP	change in membrane force on a section
P	membrane force on a section
P^*	prescribed live load change in membrane force
ΔT	change in temperature
T1, T2, T3	thermal parameters for BOSOR4
x	variable coordinate through thickness (Fig. 3.6)
x_1	depth to reinforcing steel (Fig. 3.6)
x_2	depth to reinforcing steel
x_c	depth to crack (Fig. 3.6)

x_f	depth to prestressing tendon (Fig. 3.6)
v_1	volume of unit stress block = $(2b_1 + b_2)d/6$
v_2	volume of unit stress block = $(2b_2 + b_1)d/6$
v_{1c}	volume of unit stress block = $(2b_1 + b^*)\ x_c/6$
v_{2c}	volume of unit stress block = $(2b^* + b_1)\ x_c/6$
u^*, v^*, w^*	BOSOR displacements (Fig. 2.1)
z	thickness coordinate from centroid (Sect. 3.5.2)
Z	thickness coordinate for BOSOR4

GREEK SYMBOLS

α	coefficient of thermal expansion
β	factor for biaxial thermal stress = $1+\nu$
Δ	change in quantity
ε	total change in strain
ε_o	change in strain at x=0; reference strain in concrete (Fig. 3.3)
ε_c	tensile cracking strain of concrete (Fig. 3.3)
ε_c^T	thermal concrete strain
ε_c^-	strain slightly less than ε_c
ε_c^+	strain slightly greater than ε_c
ε_f	strain in prestressing tendon
ε_r	rupture strain in prestressing tendon (Fig. 3.2)
ε_s	change of strain in steel
ε_s^T	thermal strain in steel
ε_u	ultimate strain of concrete (Fig. 3.3)
ε_y	yield strain of steel
ε^I	change in inelastic strain
ε^E	change in elastic strain
ν	Poisson's ratio of concrete (0.15)

$\Delta\phi$	increment of curvature
ϕ^*	prescribed live load induced change in curvature
σ	stress
σ_u	ultimate stress
χ	rotational displacement in BOSOR4

STRUCTURAL COMPONENT DESIGNATIONS (TAble 2.1)

B	base
W	cylinder wall
LB	lower ring beam
UB	upper ring beam
RB	total ring beam
LD	lower dome
UD	upper dome

STRUCTURE DESIGNATION (Table 2.1)

BW	base and cylinder wall
BD	base to lower dome
C	complete structure
CH	complete structure with base hinge

LOAD SOURCE DESIGNATION (Table 2.1)

f	prestress
d	gravity (dead) load
u	unit uniform strain
g	unit strain gradient
hf	horizontal cylinder prestressing
vf	vertical wall prestressing
p	internal pressure

w	reservoir water
s	snow or shrinkage
t	wind (tornado)

LOADING EFFECTS (Sect. 2.4)

General Form A:Uℓ in which

A =	a structure designation (see above)
U =	a structural component designation (see above)
ℓ =	a load source designation (see above)

REFERENCE STATES (Sect. 2.5)

Rd	a reference state from load source d
Rf	a reference state from load sources d and f
Rs	a reference state from load sources d, f and shrinkage

LOCATIONS (Fig. 2.6)

Wi =	cylinder wall location i
UDi =	upper dome location i
LDi =	lower dome location i

SECTIONS (Sect. 3.5)

WiH =	horizontal section at location Wi
WiV =	vertical section at location Wi

LIMIT STATES (Tables in Chapter 4)

FC	first cracking
FY	first yielding of mild steel
TC	through-cracking
U	ultimate strength

APPENDIX G

Stress Resultants for Reference States

List of Figures for Appendix G

(Note: See Sections 2.4 and 2.5 for load case and reference state designations and Fig. 2.1 for stress resultant notation)

G29	N1	for Reference State Rs1
G30	N2	for Reference State Rs1
G31	M1	for Reference State Rs1
G32	M2	for Reference State Rs1
G33	N1	for Reference State Rf2
G34	N2	for Reference State Rf2
G35	M1	for Reference State Rf2
G36	M2	for Reference State Rf2
G37	N1	for Reference State Rs2
G38	N2	for Reference State Rs2
G39	M1	for Reference State Rs2
G40	M2	for Reference State Rs2

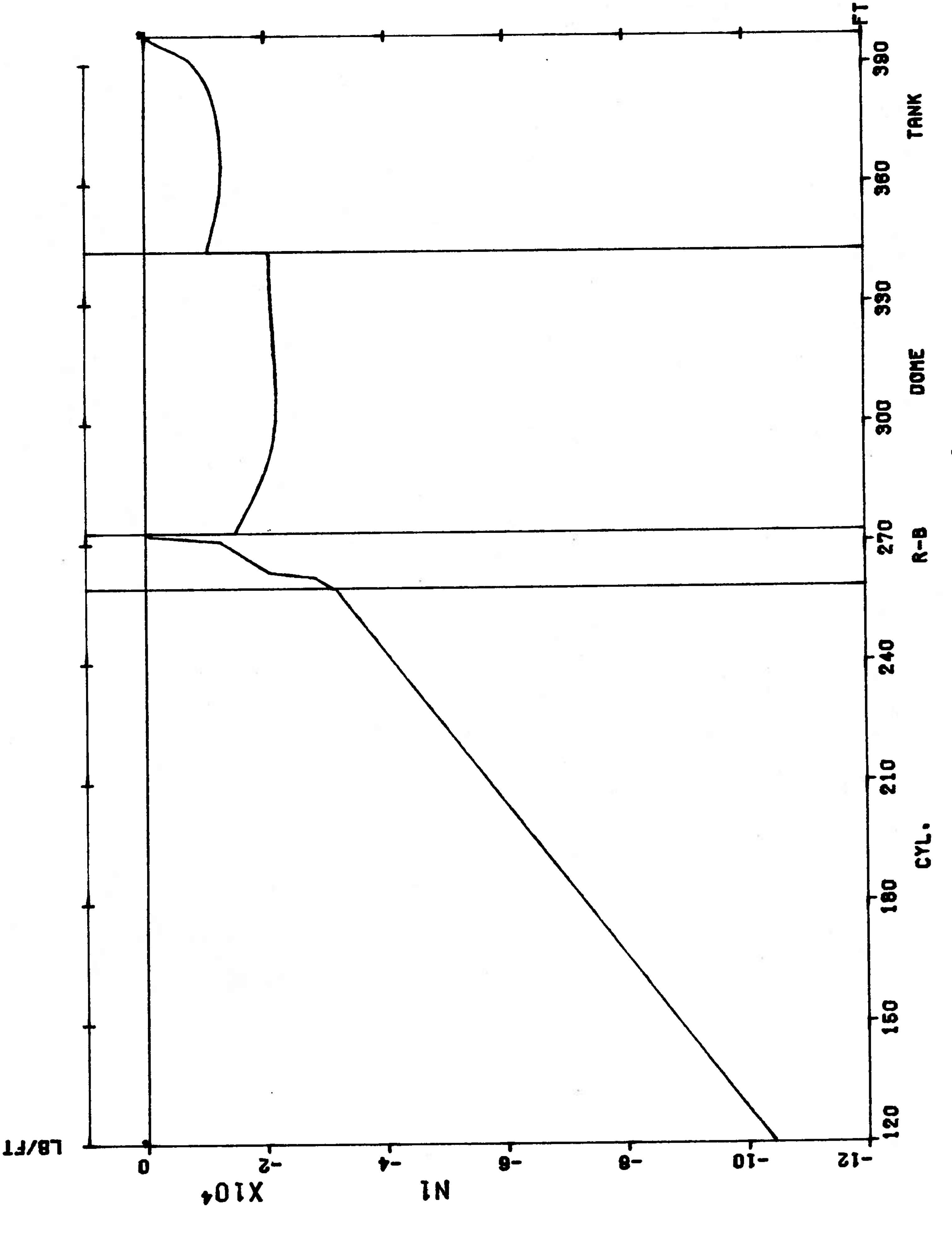
FT
TANK
DOME
R-B
CYL.
120
150
180
210
240
270
300
330
360
390
LB/FT
N1
X10^4
0
-2
-4
-6
-8
-10
-12

G2

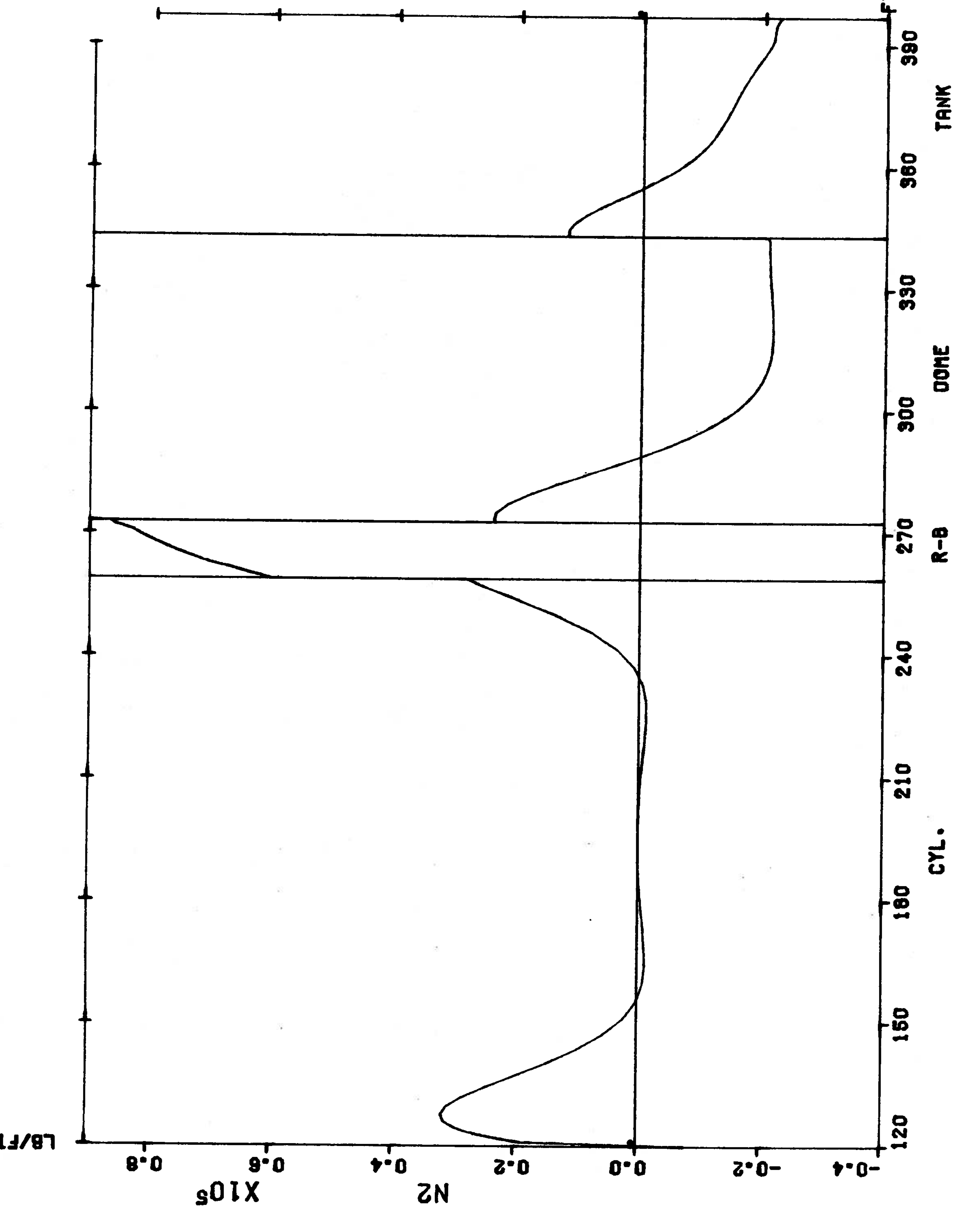

LB/FT
N2
X10^5
0.8
0.6
0.4
0.2
0.0
-0.2
-0.4
120
150
180
210
240
270
300
330
360
390
FT
CYL.
R-B
DOME
TANK

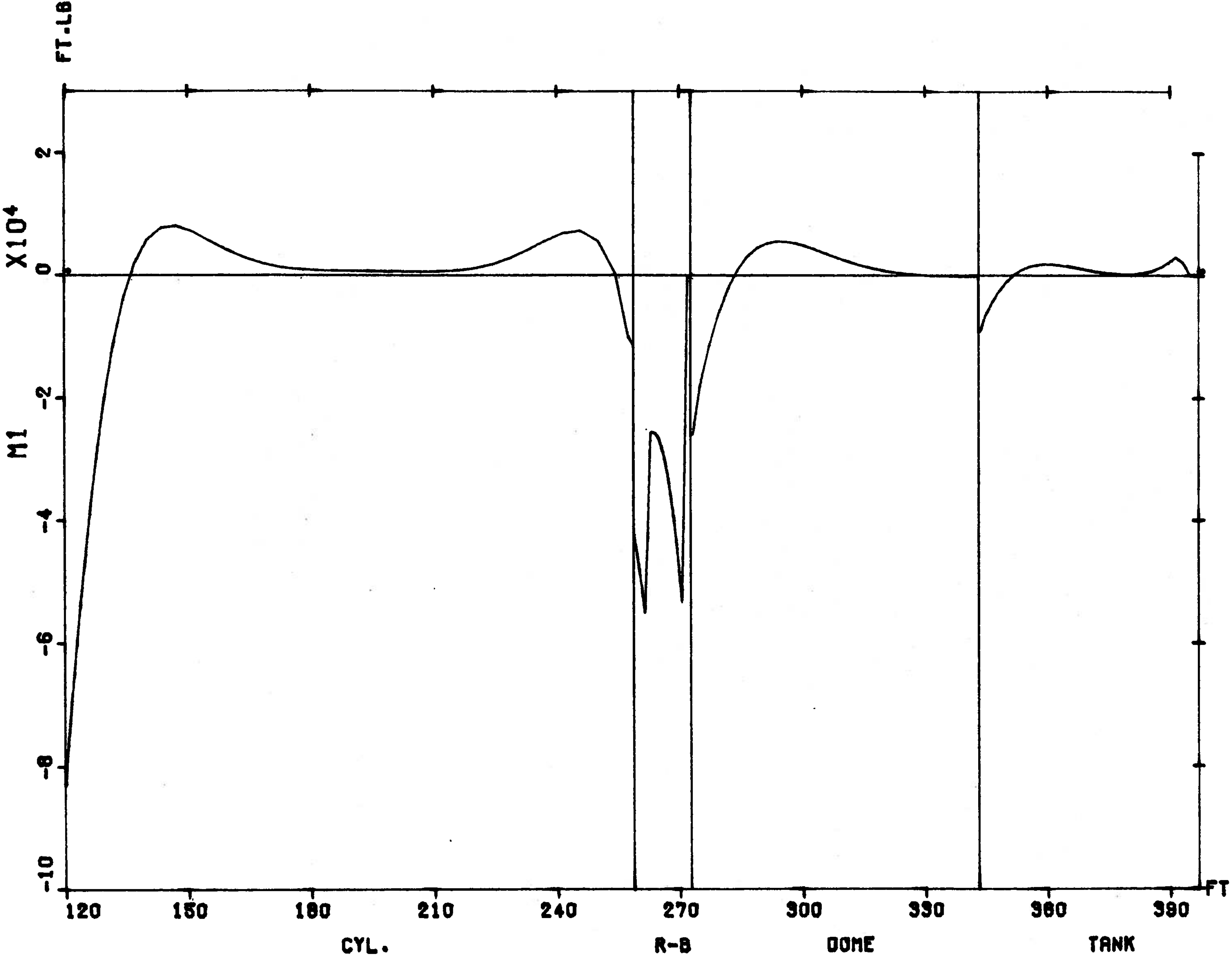

FIGURE G3 M1 for Loading Case C:Cd

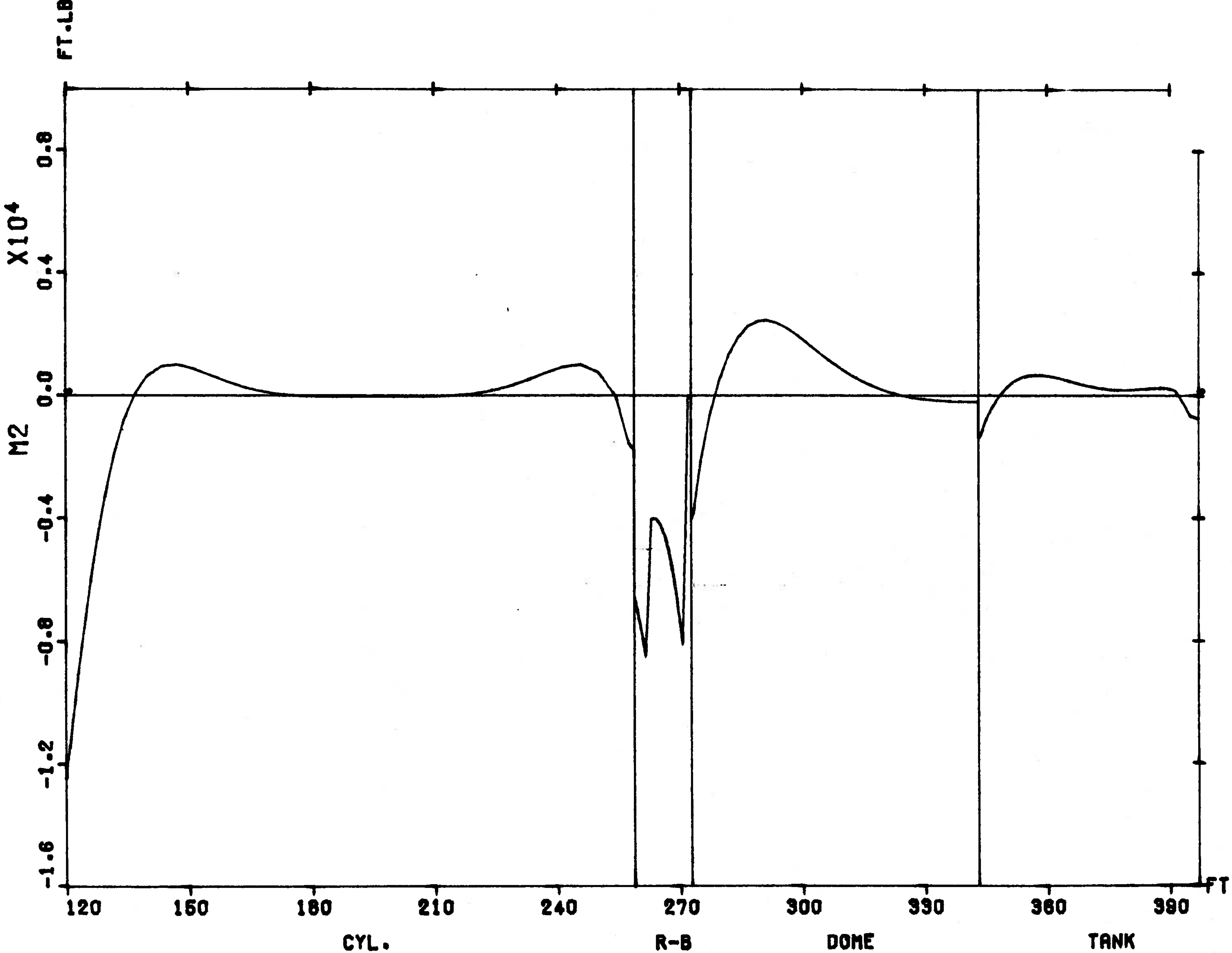

FIGURE G4 M2 for Loading Case C:Cd

G5

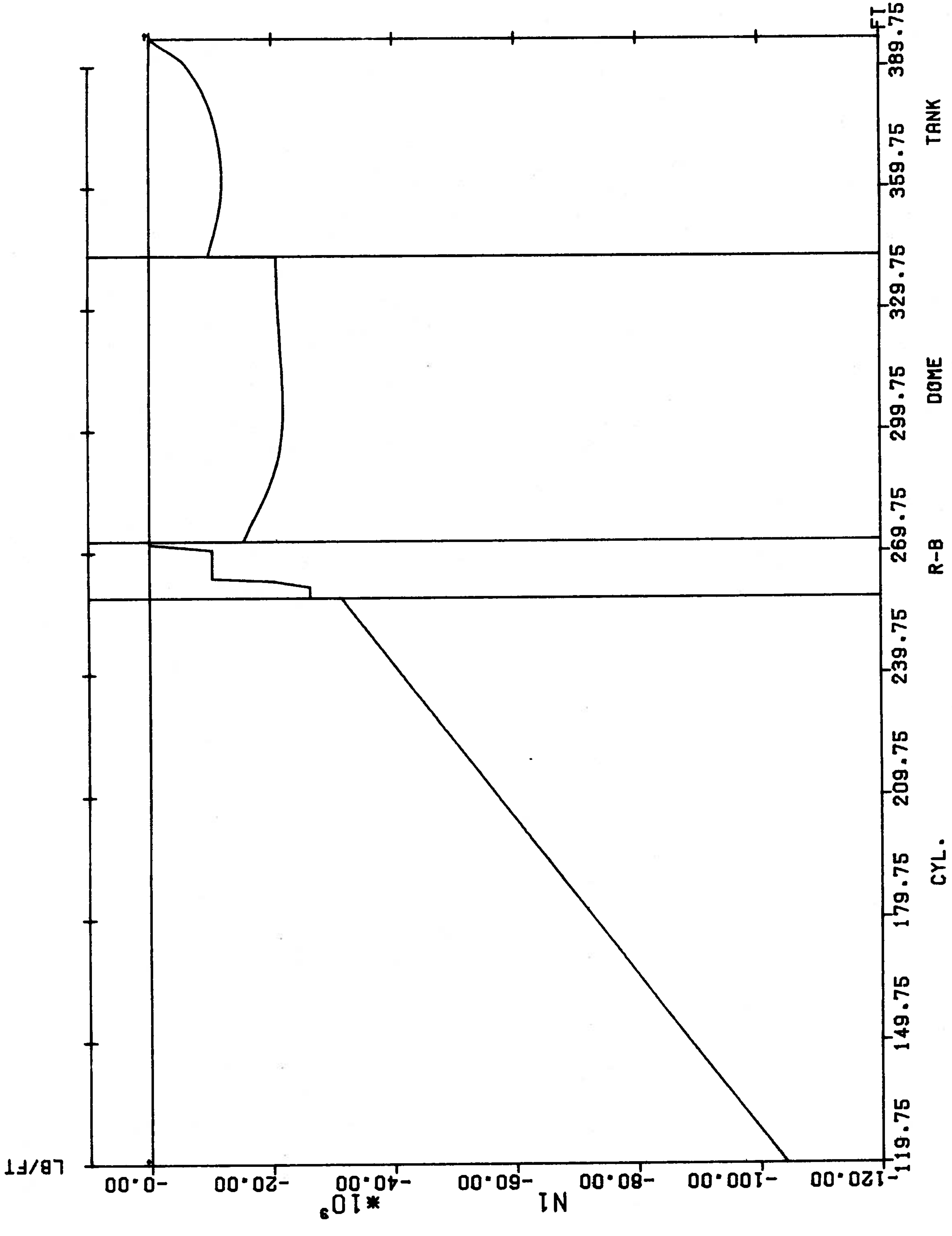
FT
389.75
359.75
329.75
299.75
269.75
239.75
209.75
179.75
149.75
119.75
TANK
DOME
R-B
CYL.
LB/FT
-0.00
-20.00
-40.00
-60.00
-80.00
-100.00
-120.00
N1 *10^3

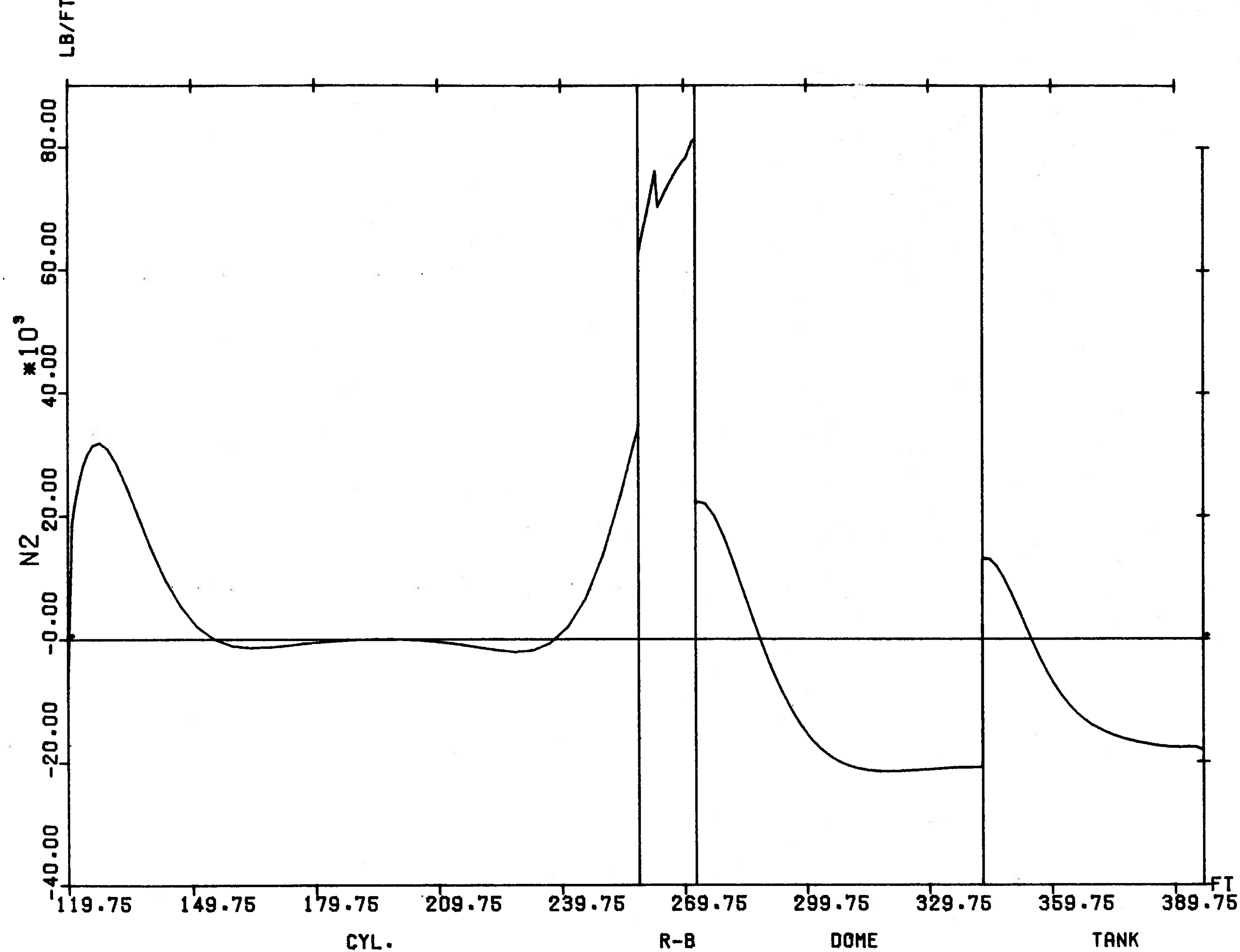

FIGURE G6 N2 for Reference State Rd1

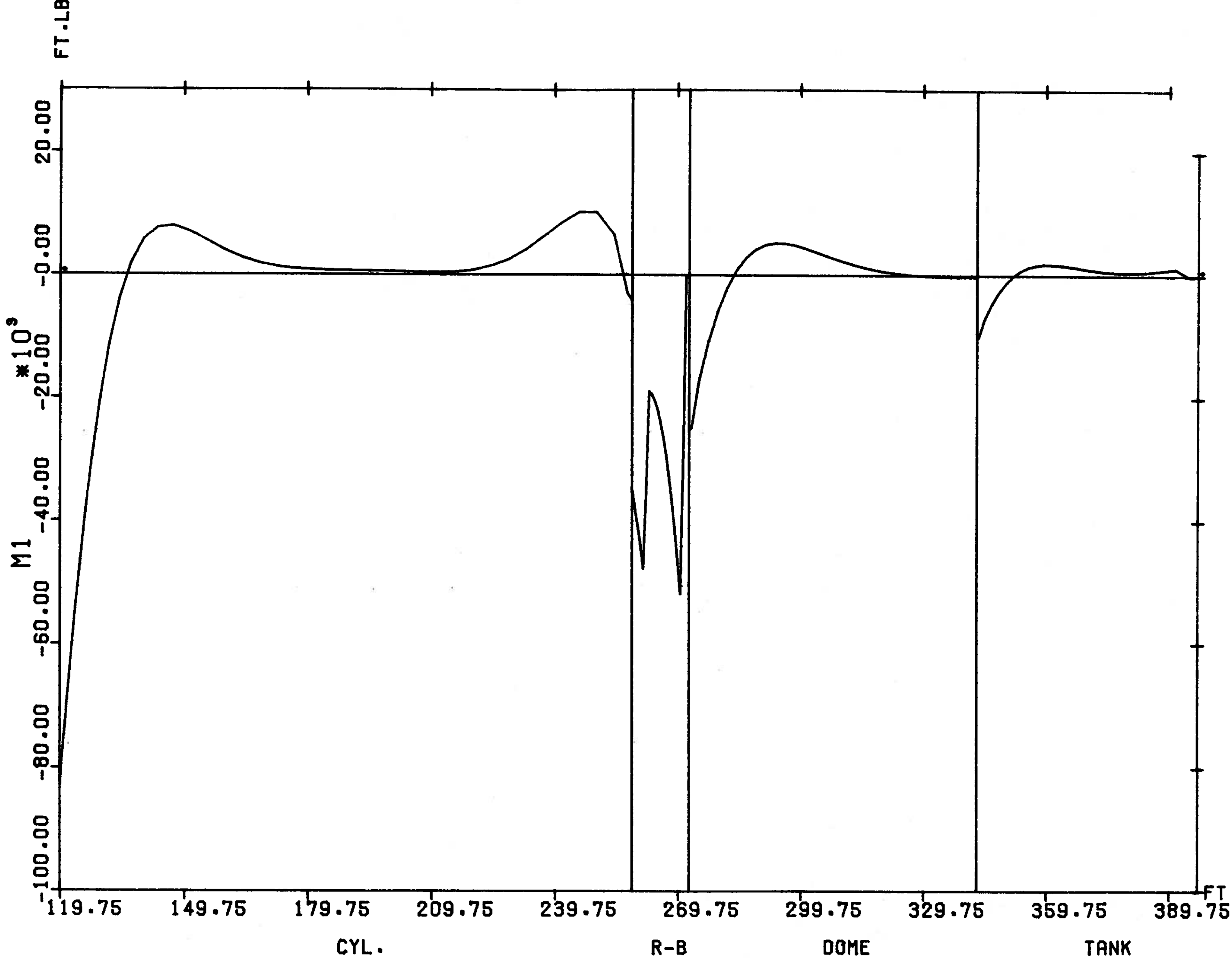

FIGURE G7 M1 for Reference State Rd1

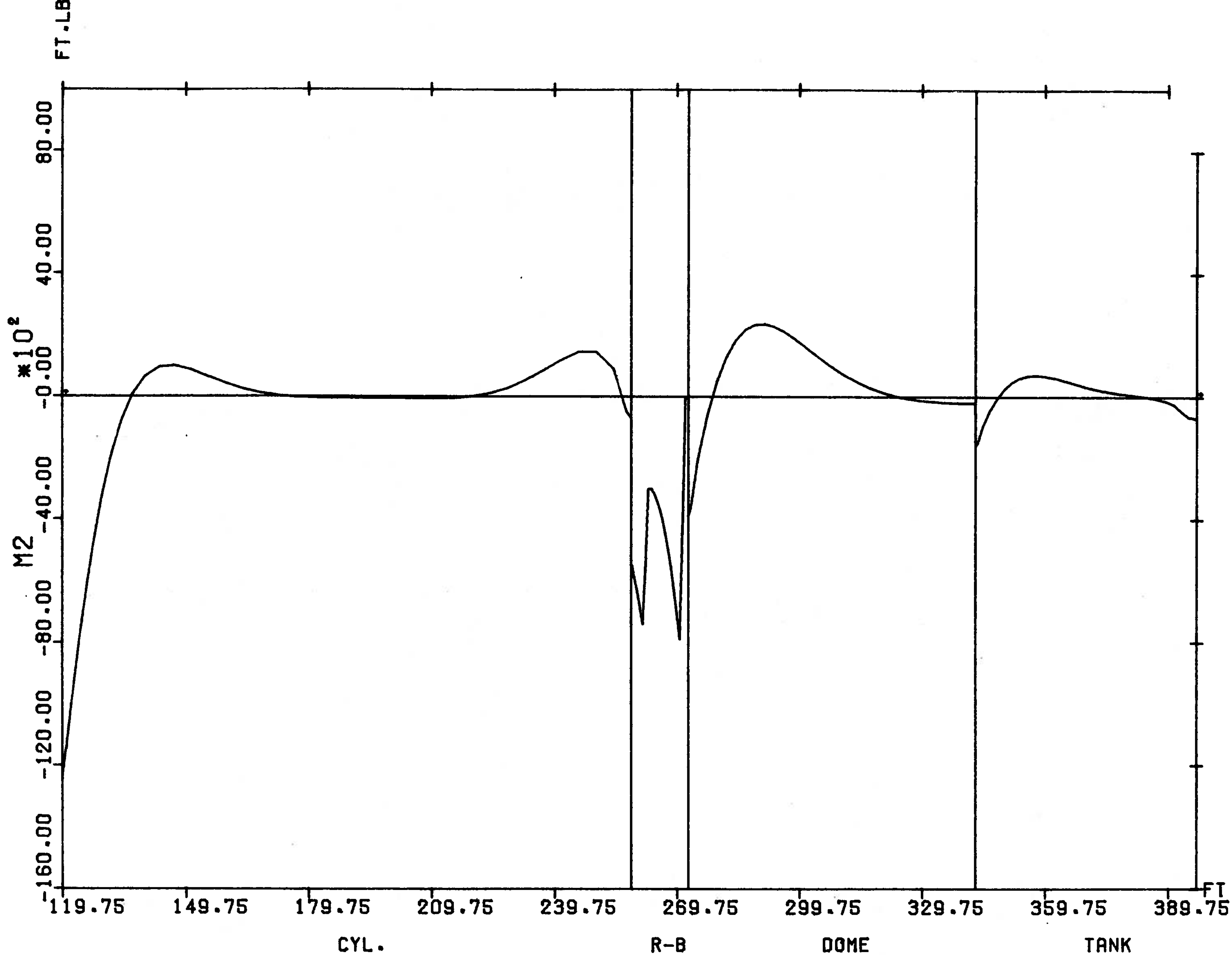

FIGURE G8 M2 for Reference State Rd1

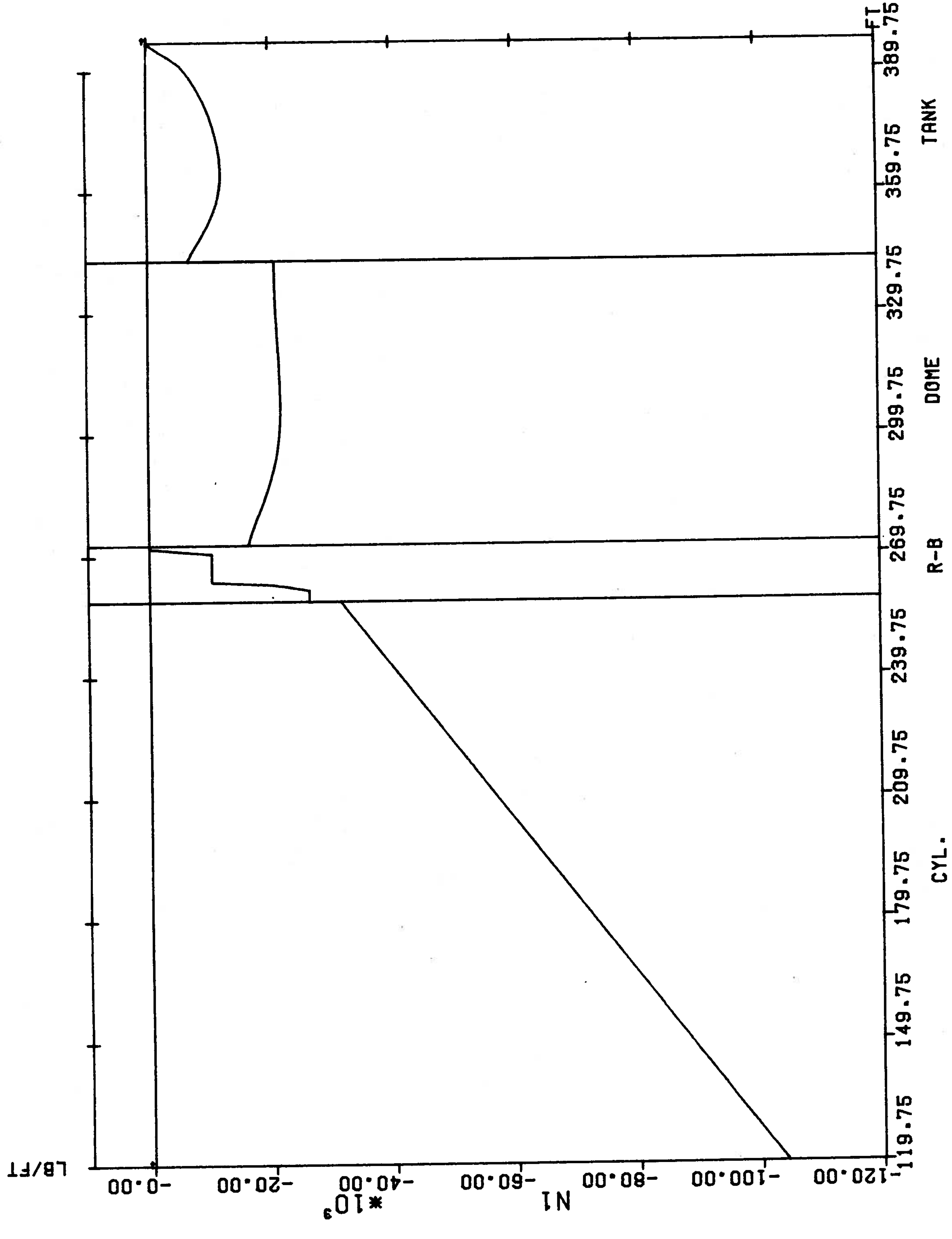

LB/FT
N1
*10³
-0.00
-20.00
-40.00
-60.00
-80.00
-100.00
-120.00
FT
119.75
149.75
179.75
209.75
239.75
269.75
299.75
329.75
359.75
389.75
CYL.
R-B
DOME
TANK

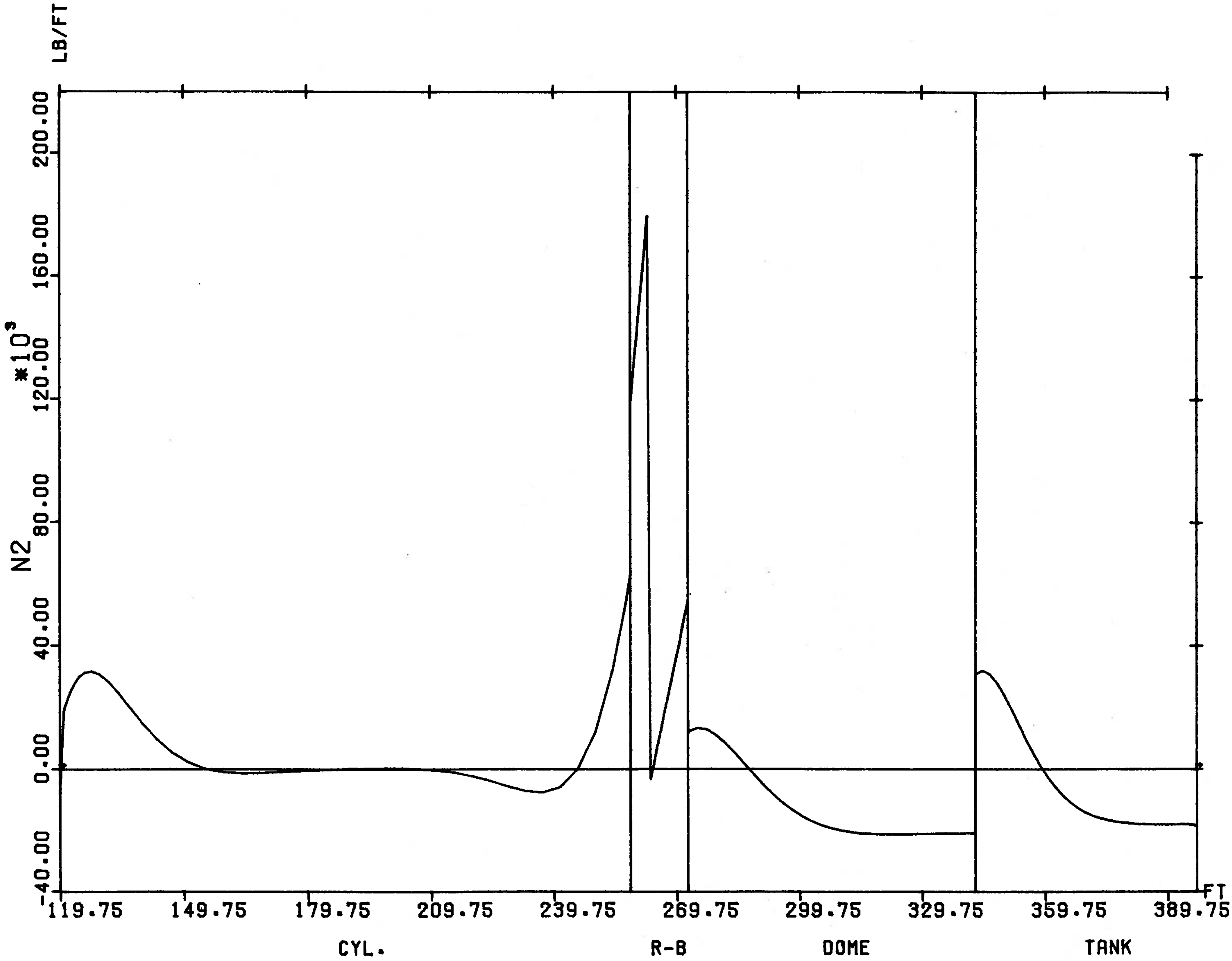
LB/FT
N2
*10³
200.00
160.00
120.00
80.00
40.00
0.00
-40.00
119.75
149.75
179.75
209.75
239.75
269.75
299.75
329.75
359.75
389.75
FT
CYL.
R-B
DOME
TANK

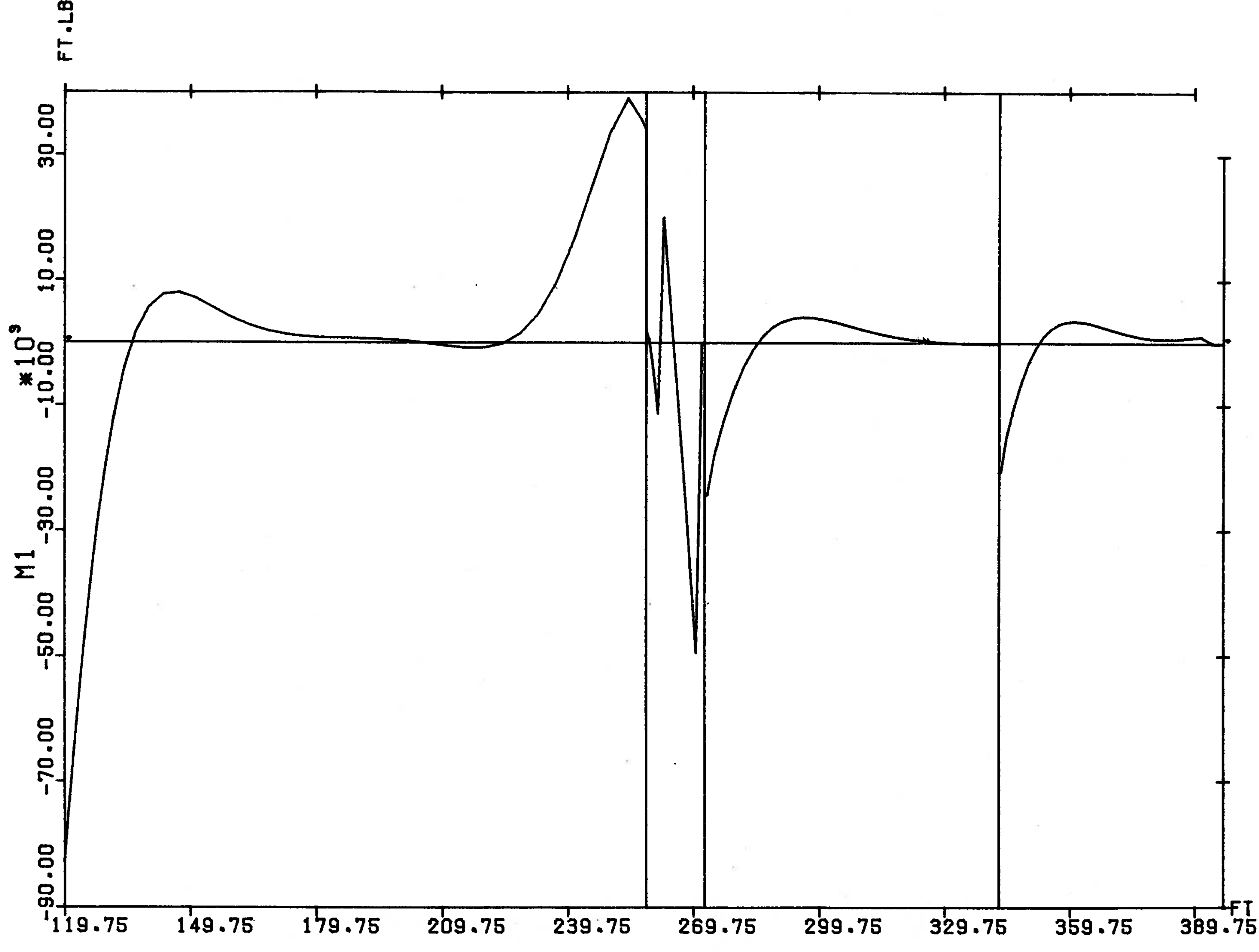

FIGURE G11. M1 for Reference State Rd2

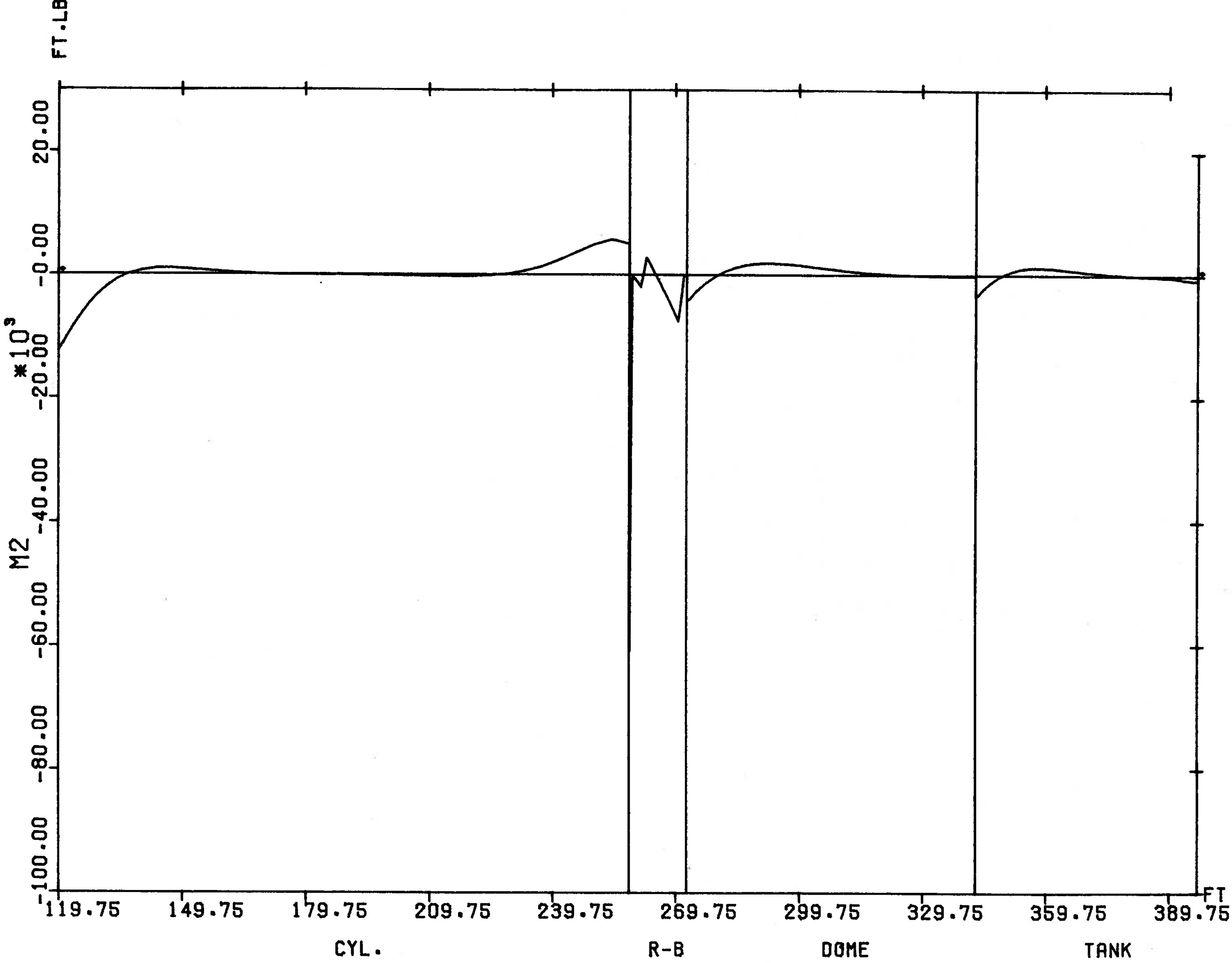
FT.LB
20.00
-0.00
-20.00
-40.00
-60.00
-80.00
-100.00
M2
*10³
119.75
149.75
179.75
209.75
239.75
269.75
299.75
329.75
359.75
389.75
FT
CYL.
R-B
DOME
TANK

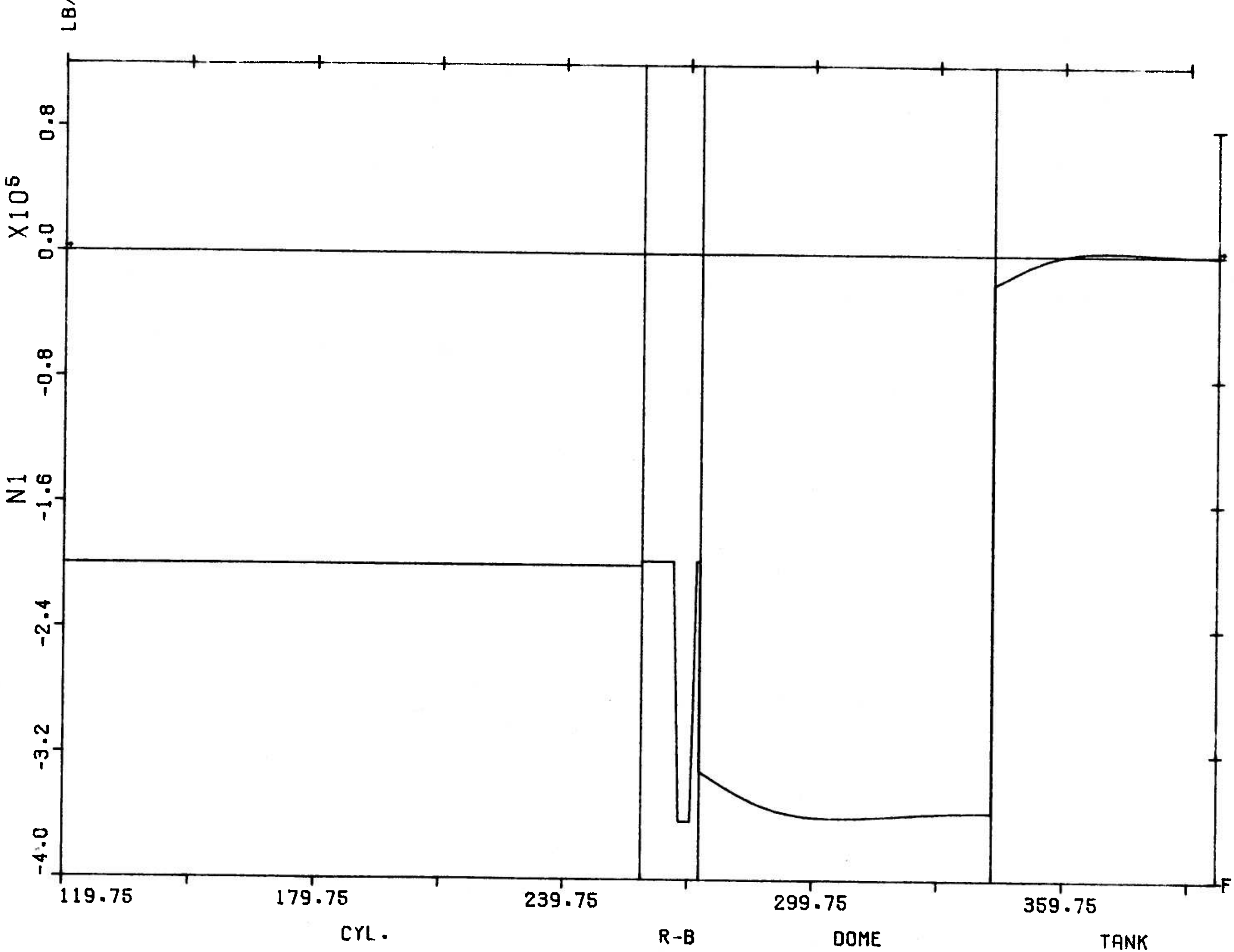

FIGURE G13 N1 for Prestress Load Combination

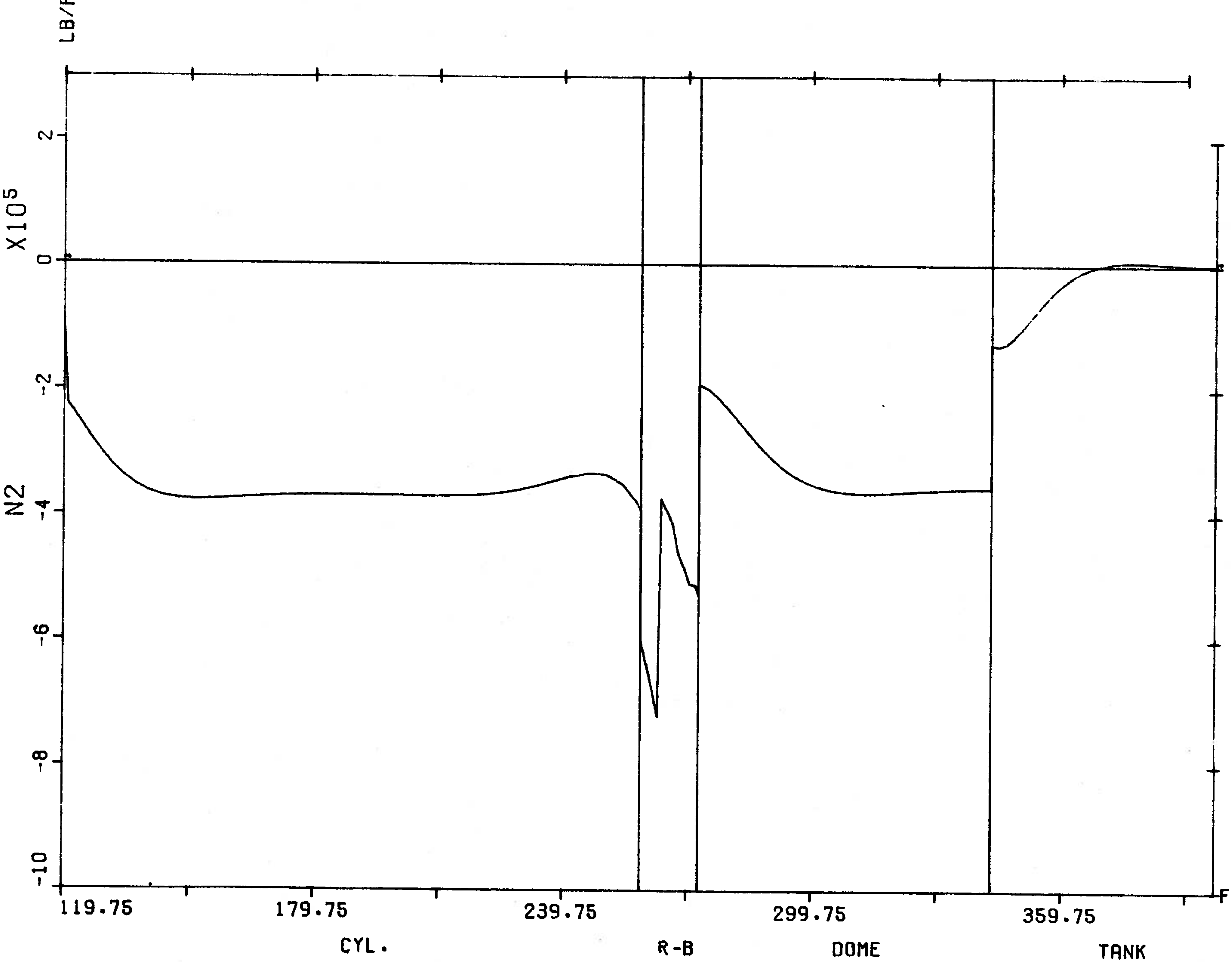

FIGURE G14 N2 for Prestress Load Combination

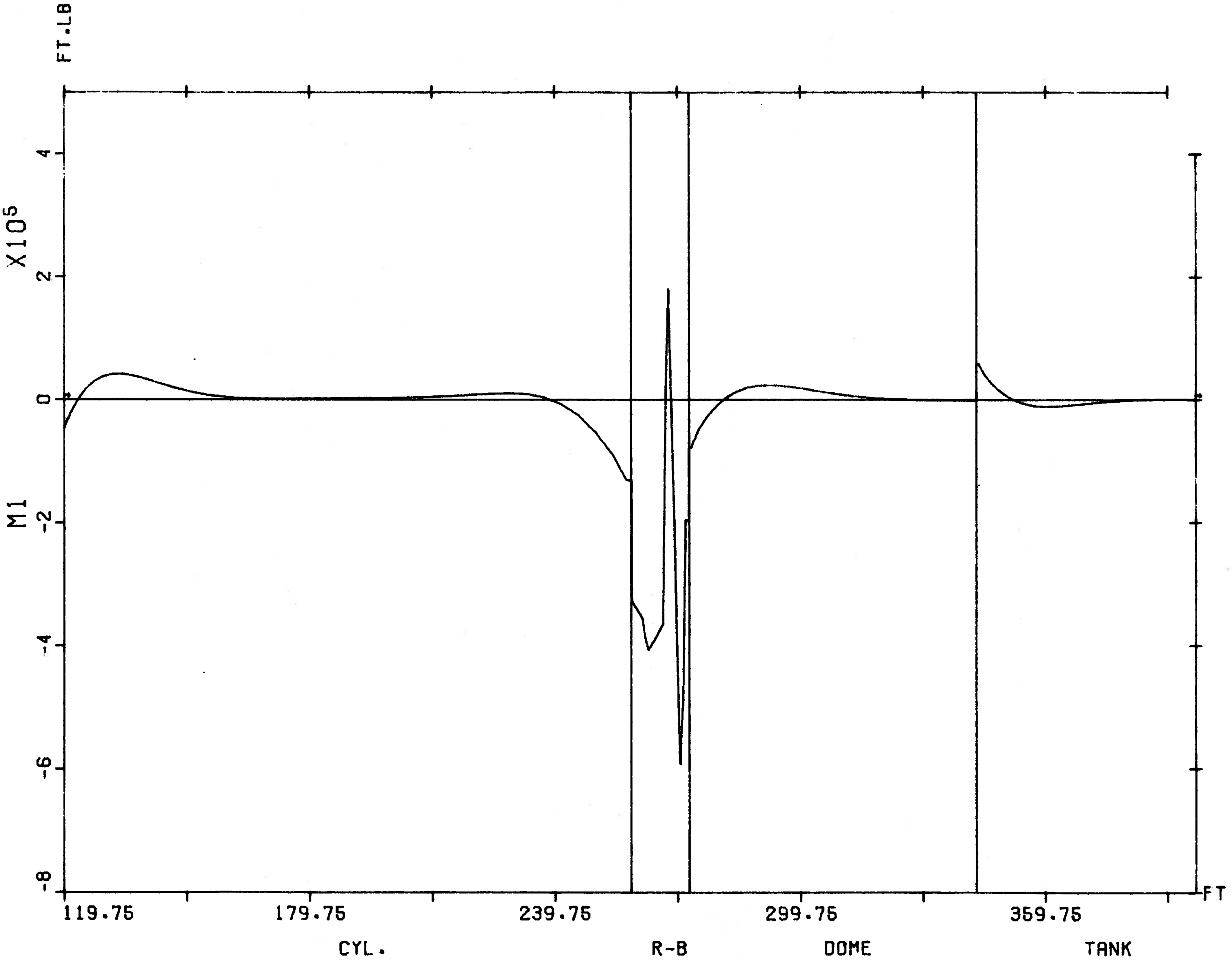

FT.LB
X10^5
M1
4
2
0
-2
-4
-6
-8
119.75
179.75
239.75
299.75
359.75
FT
CYL.
R-B
DOME
TANK

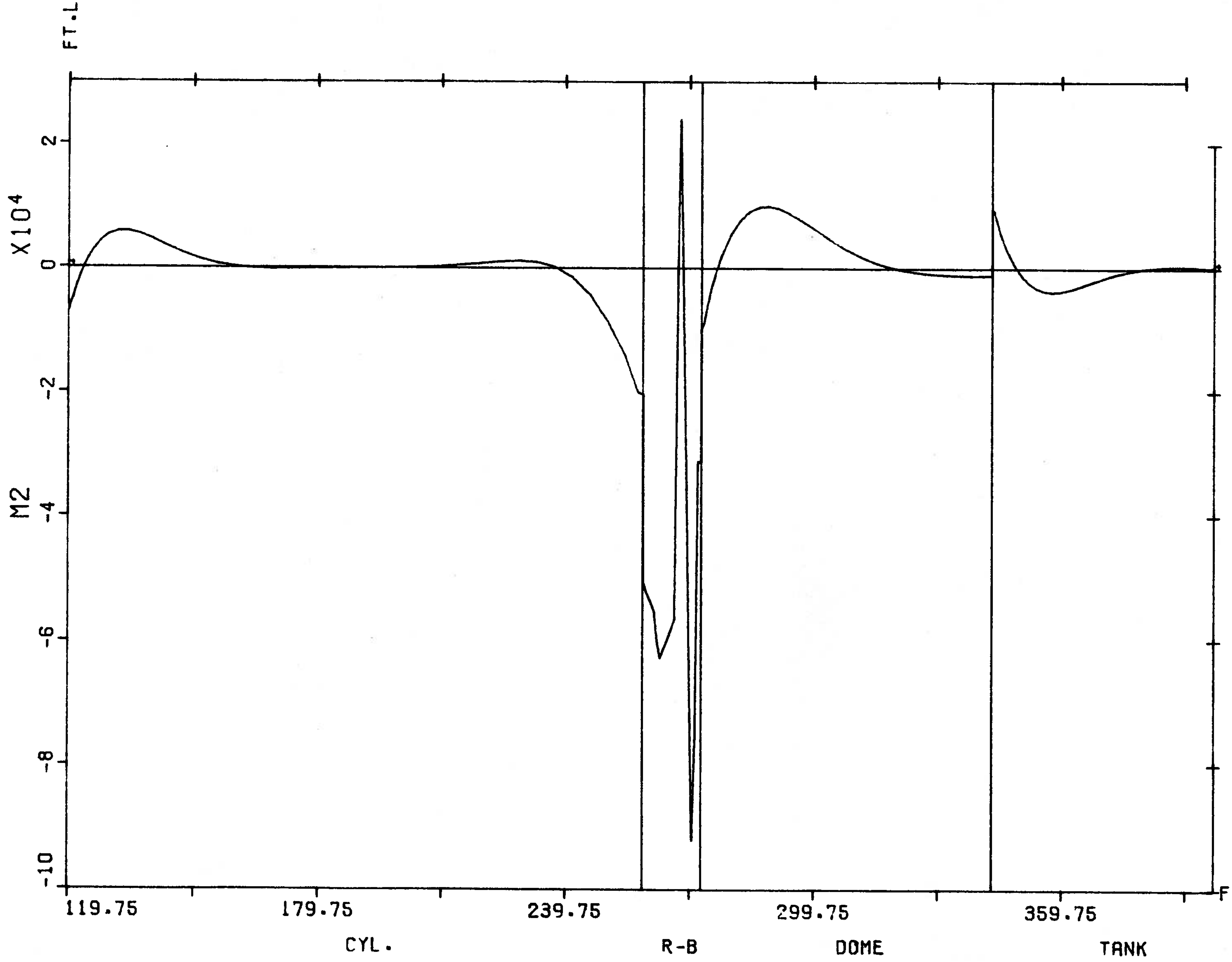

FIGURE G16 M2 for Prestress Load Combination

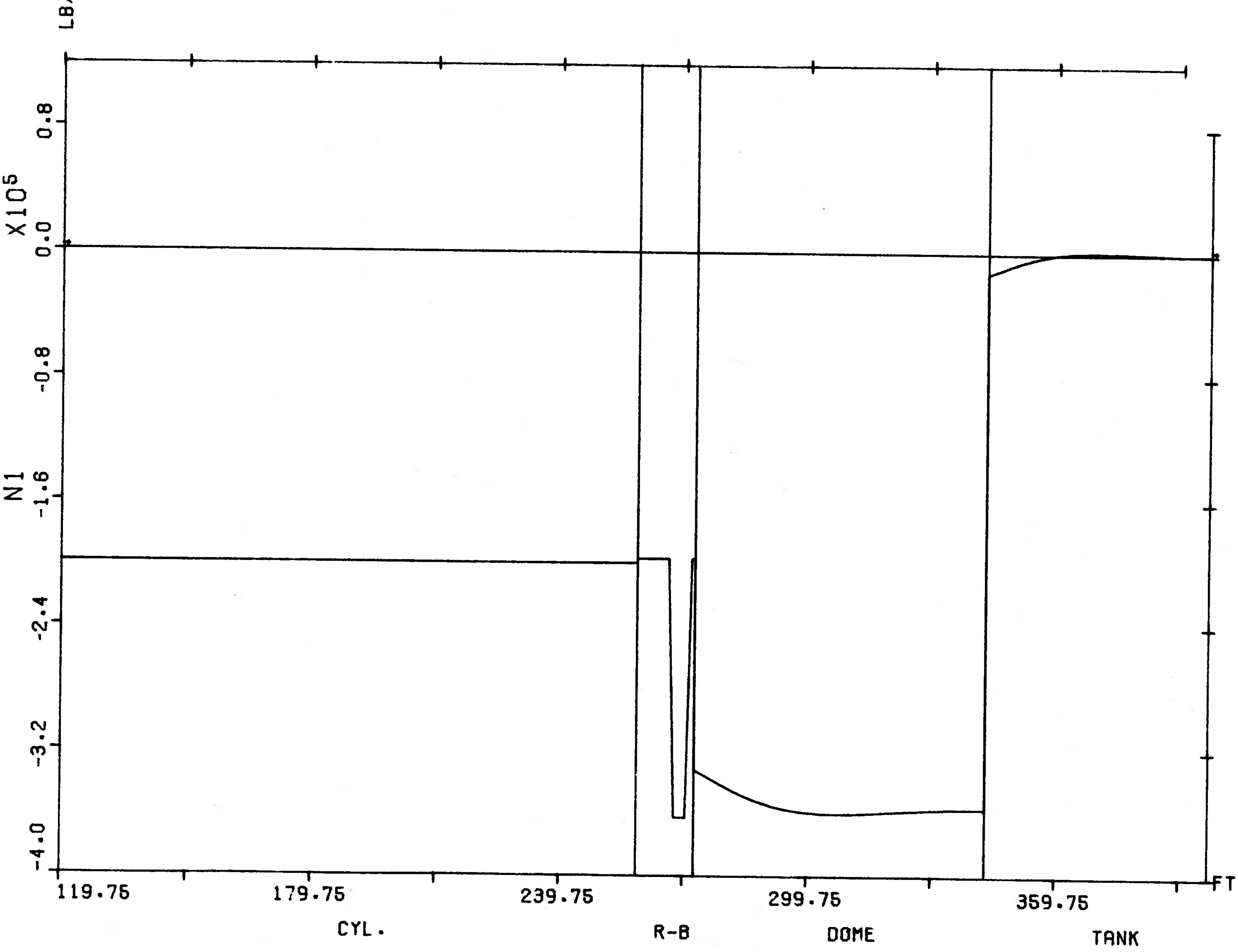

FIGURE G17 N1 for 'Switched-on' Prestressing

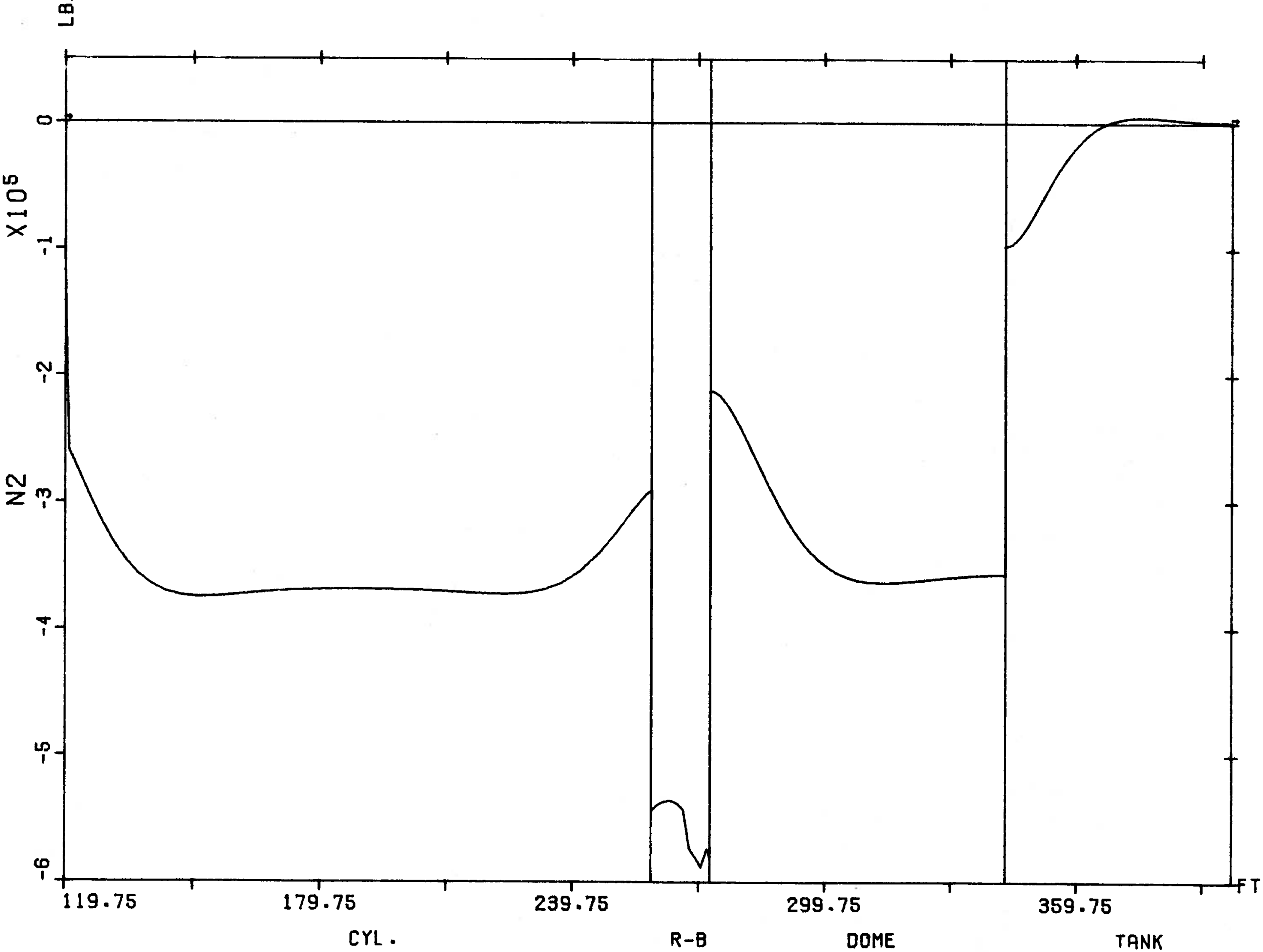

FIGURE G18 N2 for 'Switched-on' Prestressing

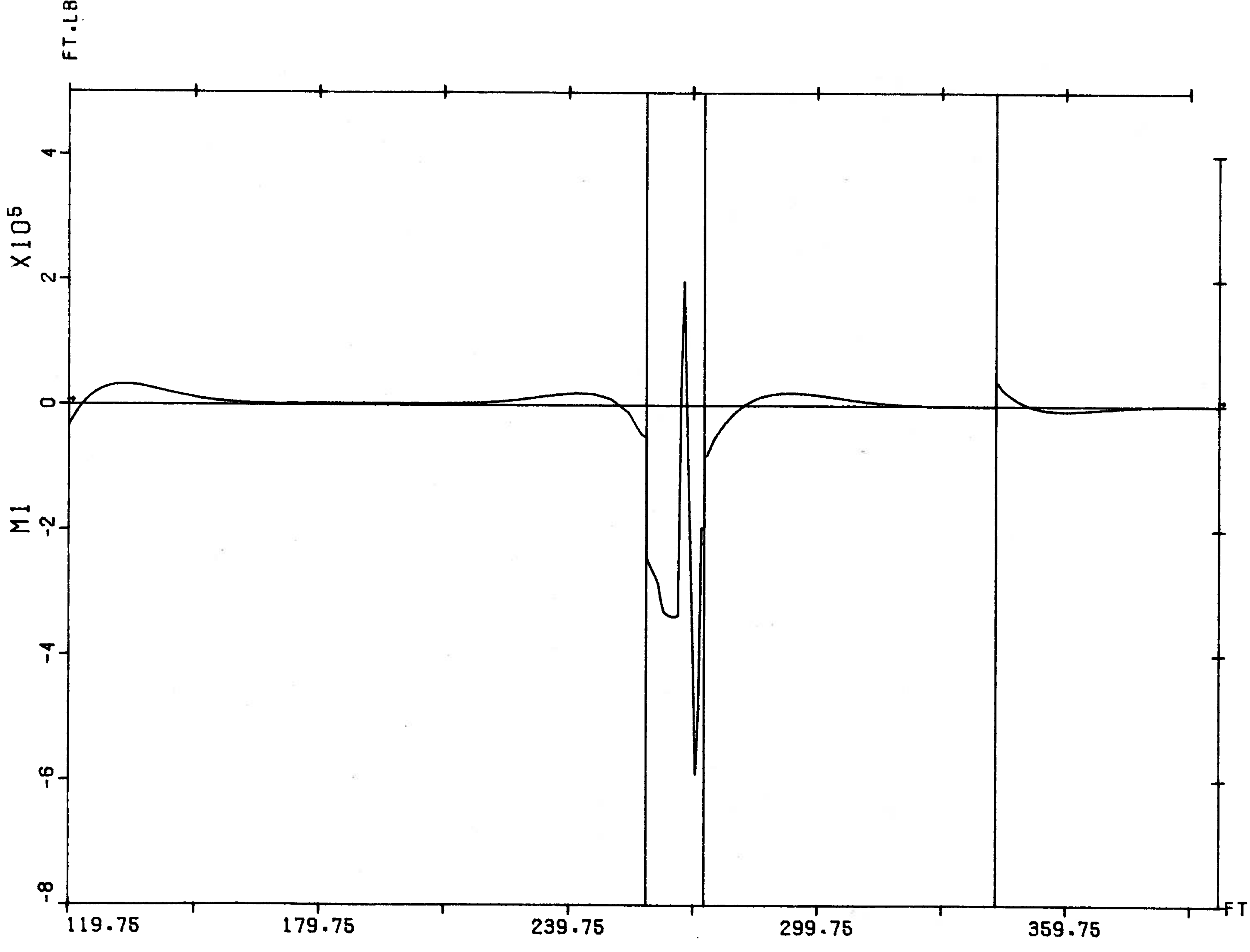

FIGURE G19. M1 for 'Switched-on' Prestressing

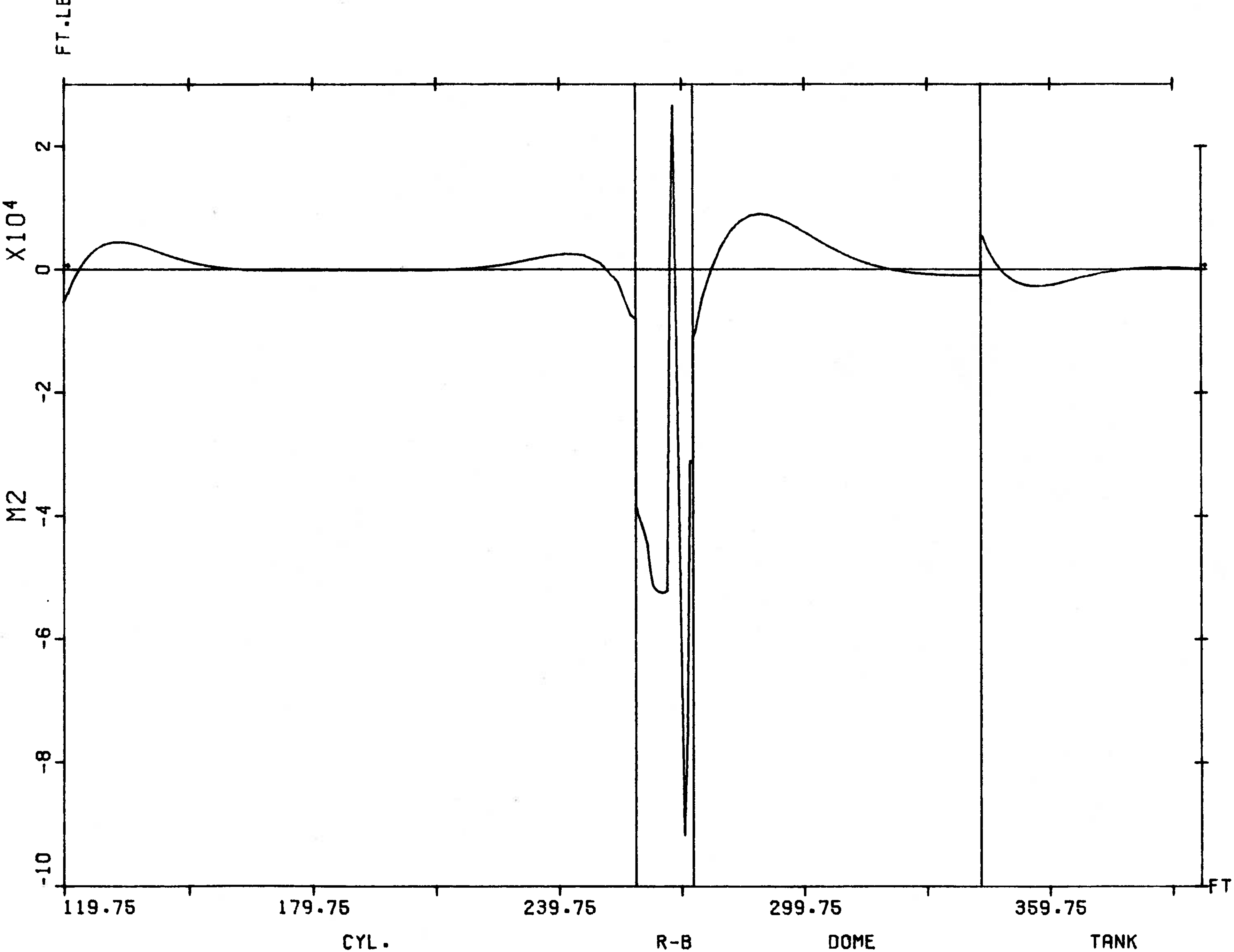

FIGURE G20 M2 for 'Switched-on' Prestressing

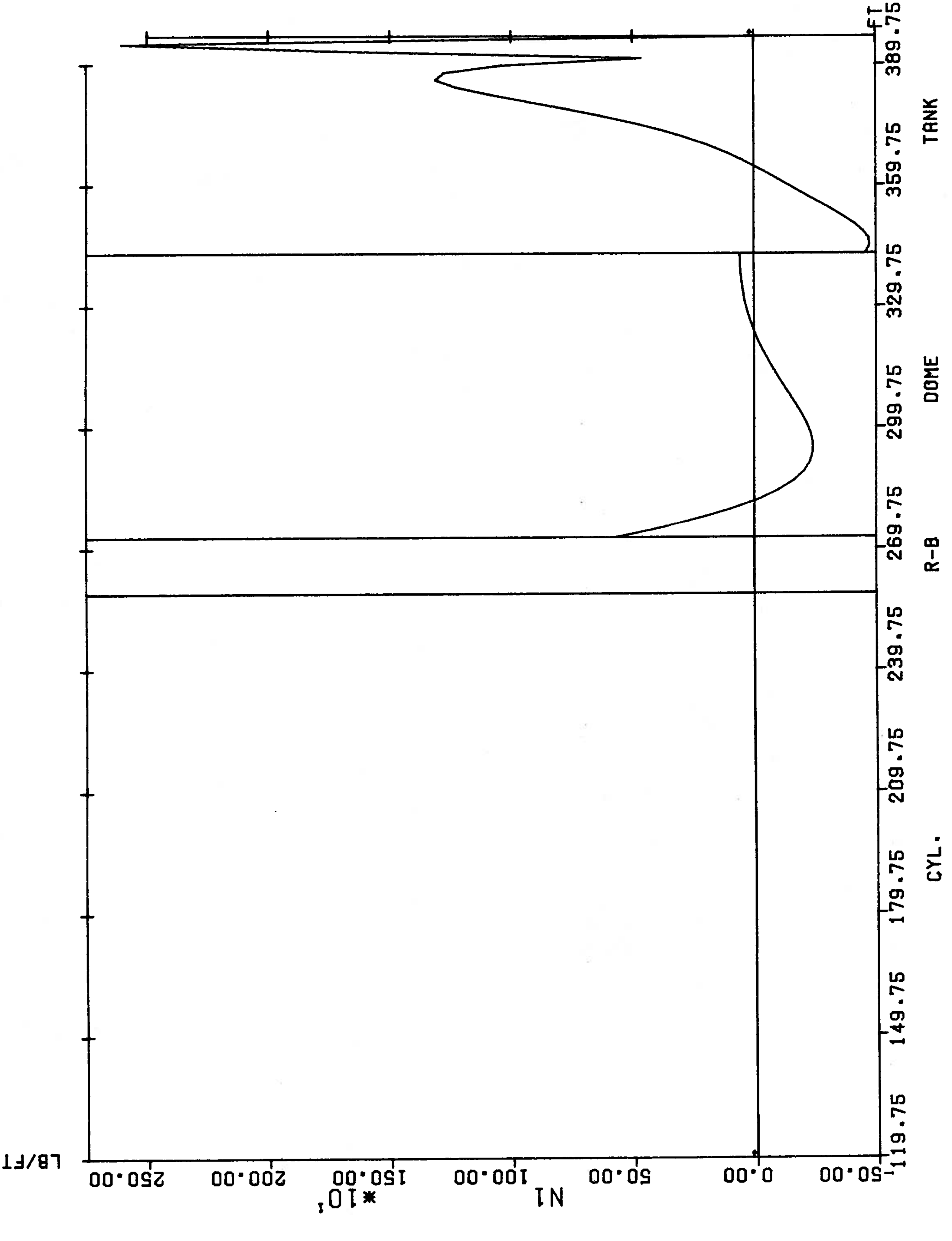

FT
389.75
359.75
329.75
299.75
269.75
239.75
209.75
179.75
149.75
119.75
TANK
DOME
R-B
CYL.
-50.00
0.00
50.00
100.00
150.00
200.00
250.00
N1 *10¹
LB/FT

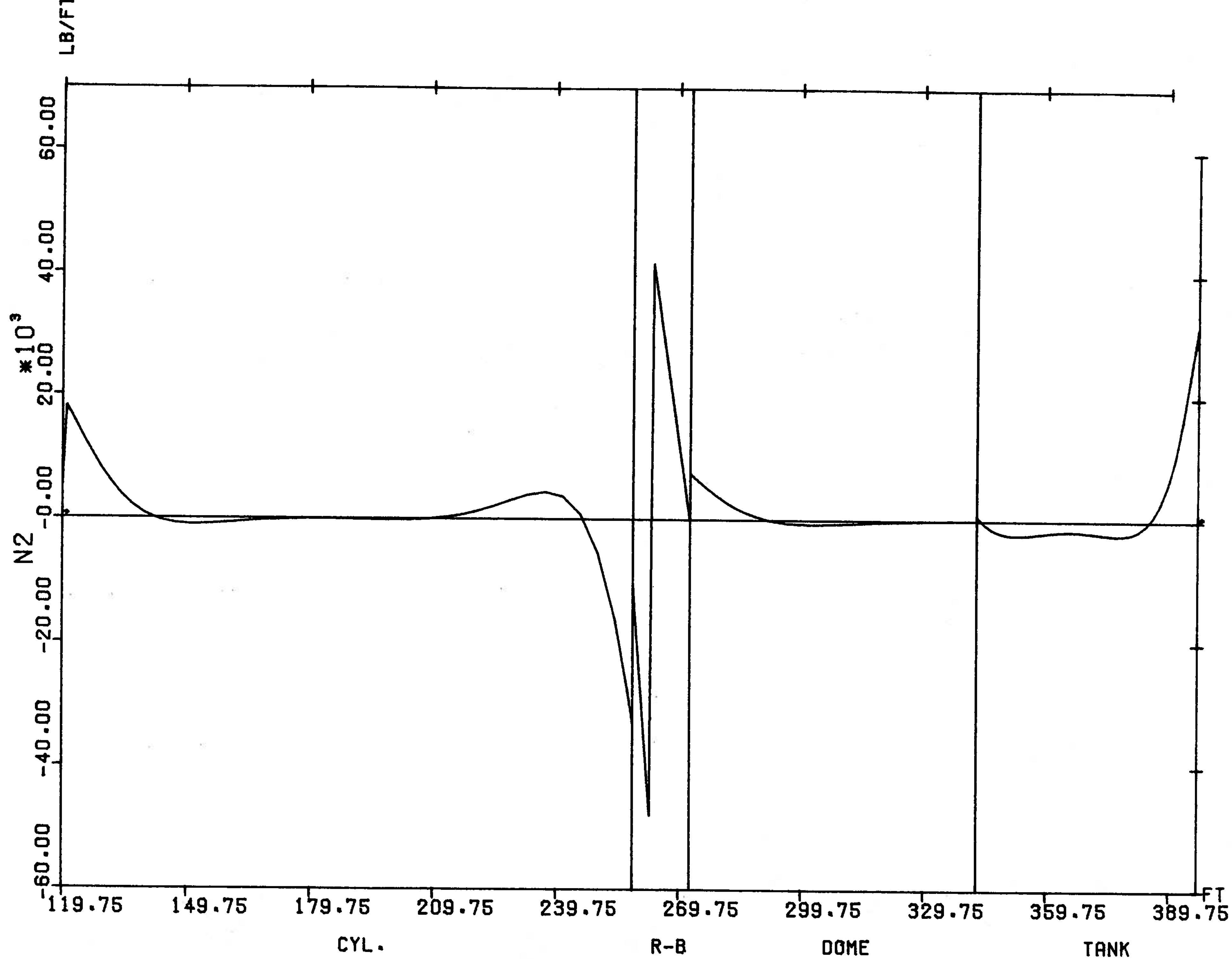

LB/FT
60.00
40.00
20.00
-0.00
-20.00
-40.00
-60.00
N2 *10³
119.75
149.75
179.75
209.75
239.75
269.75
299.75
329.75
359.75
389.75
FT
CYL.
R-B
DOME
TANK

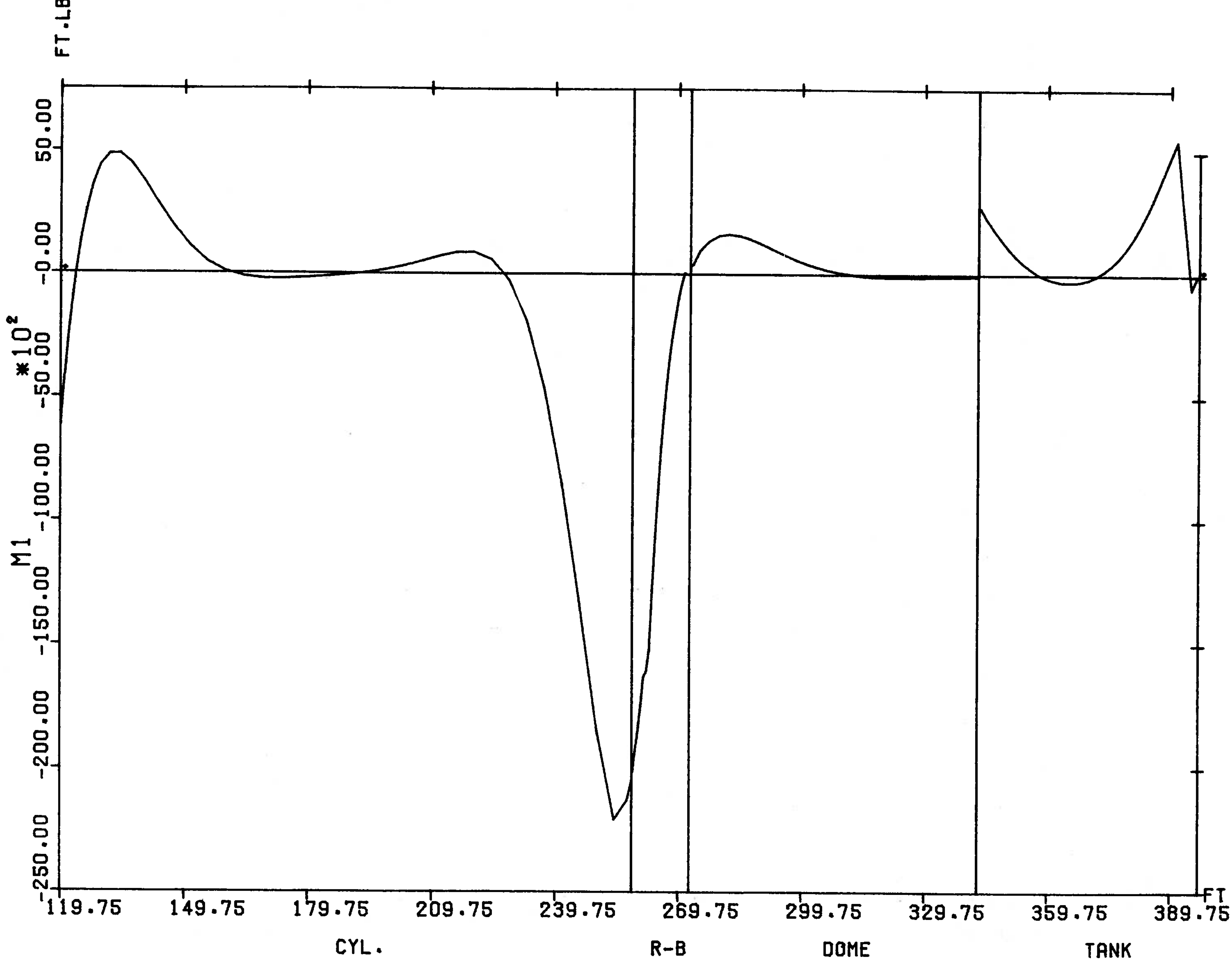

FIGURE G23. M1 for Shrinkage Strains

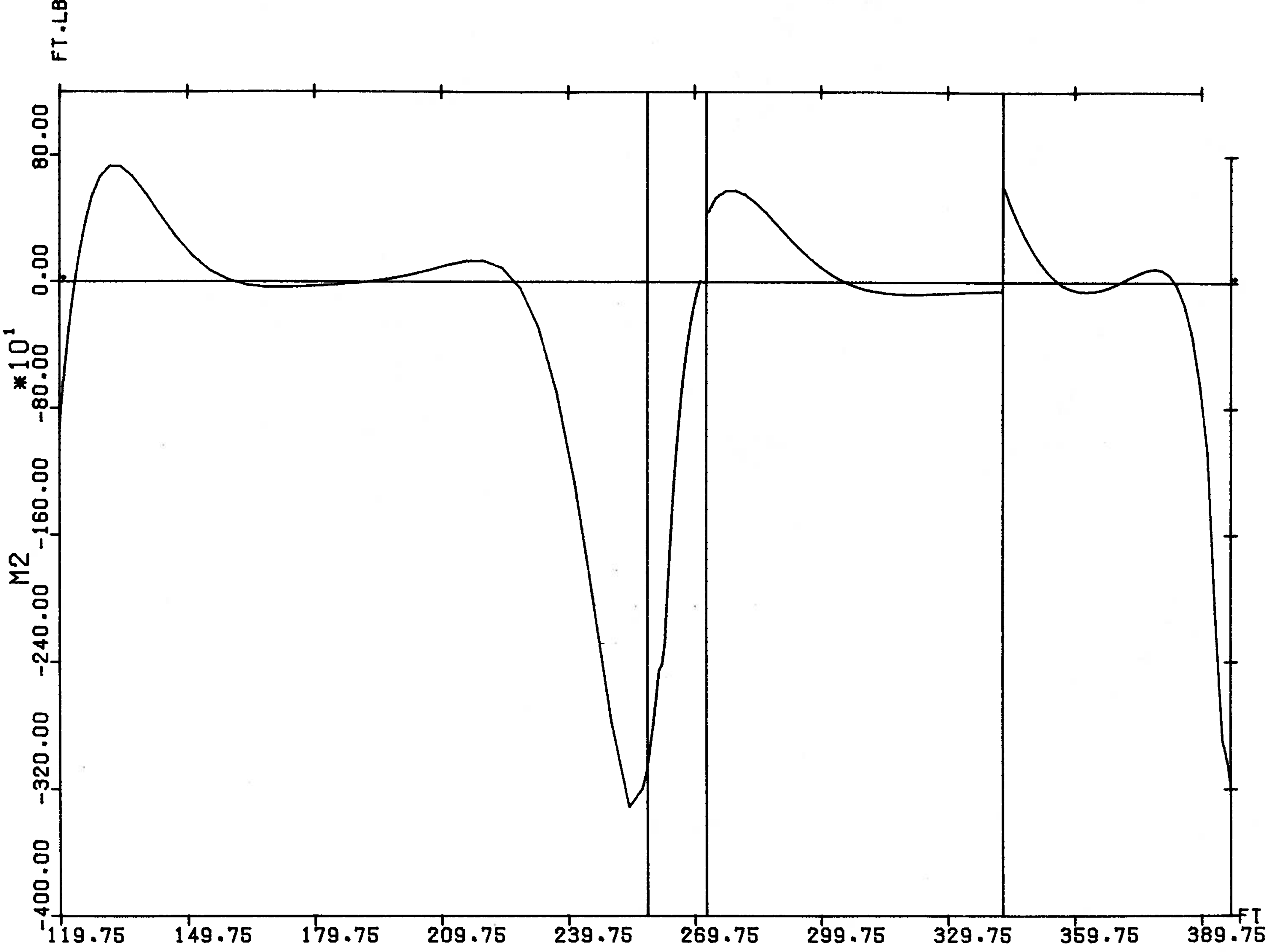

FIGURE G24. M2 for Shrinkage Strains

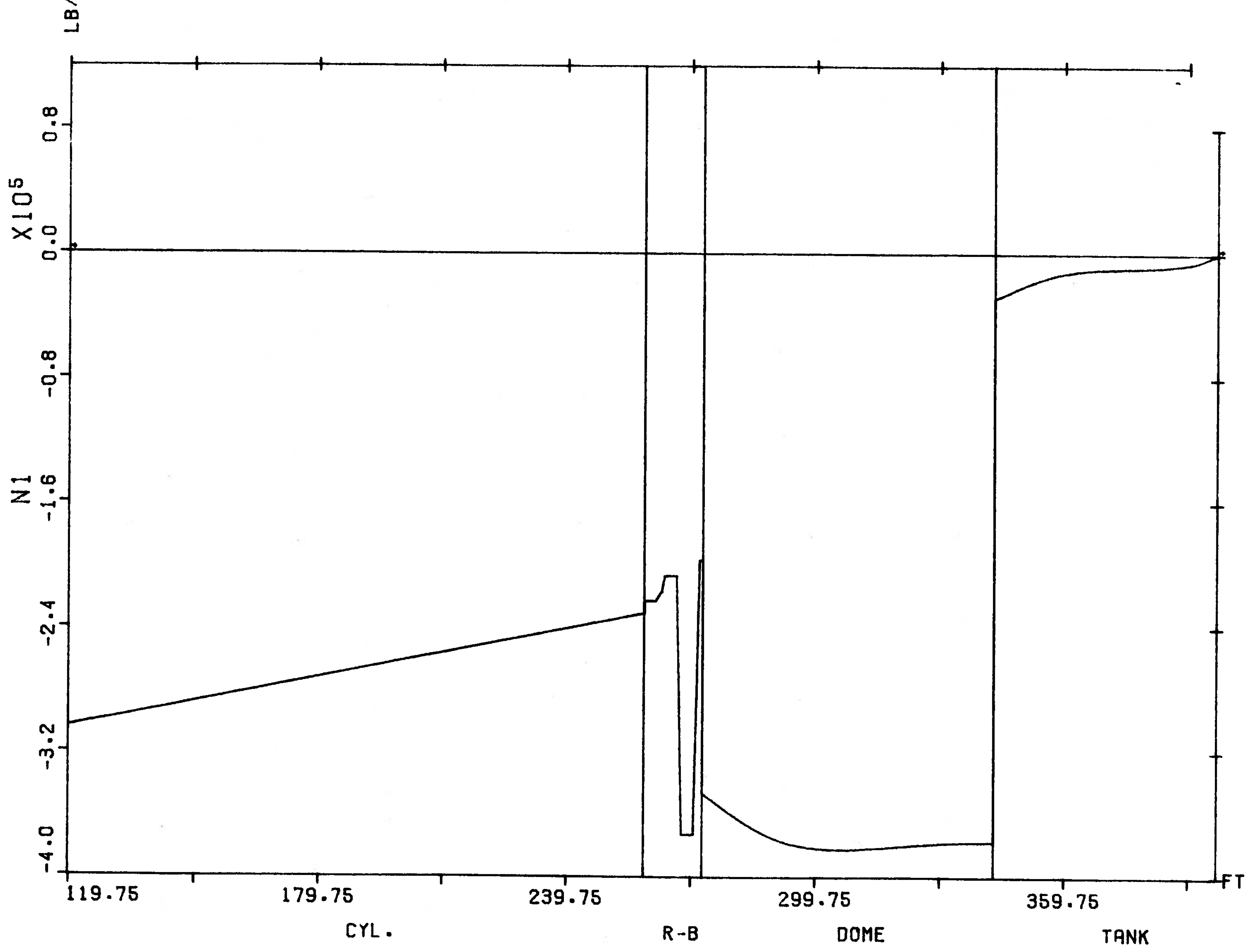

FIGURE G25 N1 for Reference State Rf1

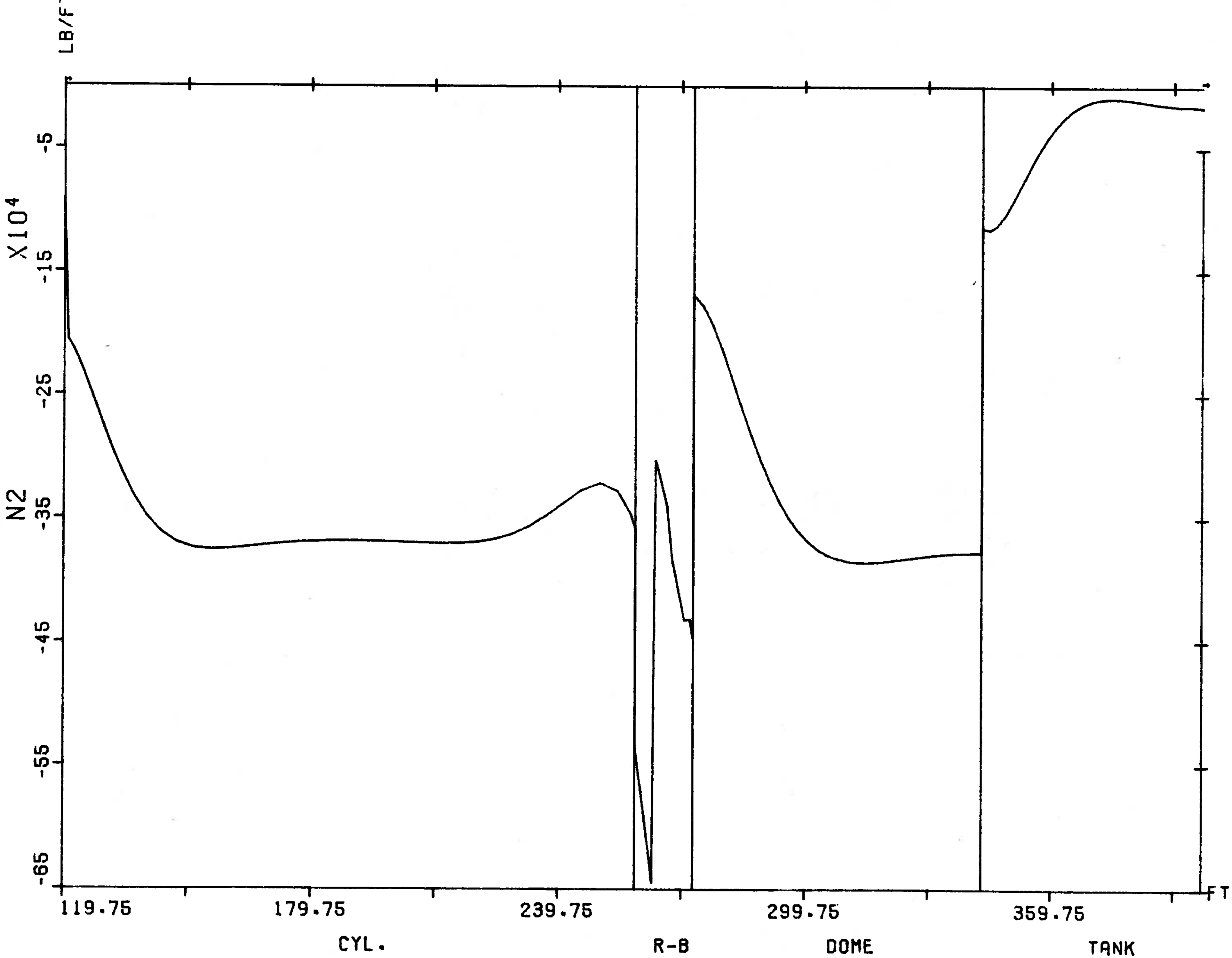

FIGURE G26. N2 for Reference State D51

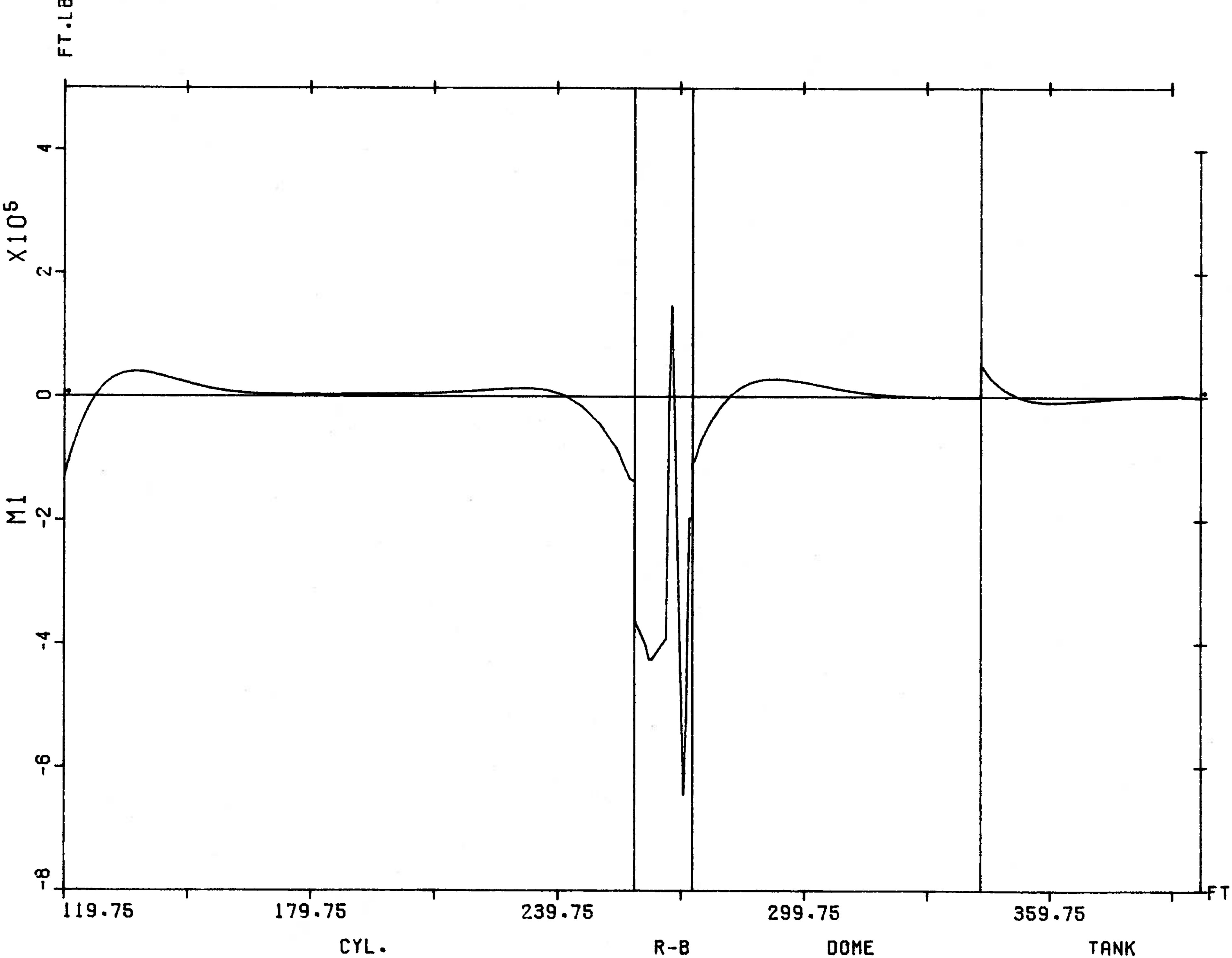

FIGURE G27. M1 for Reference State Rf1

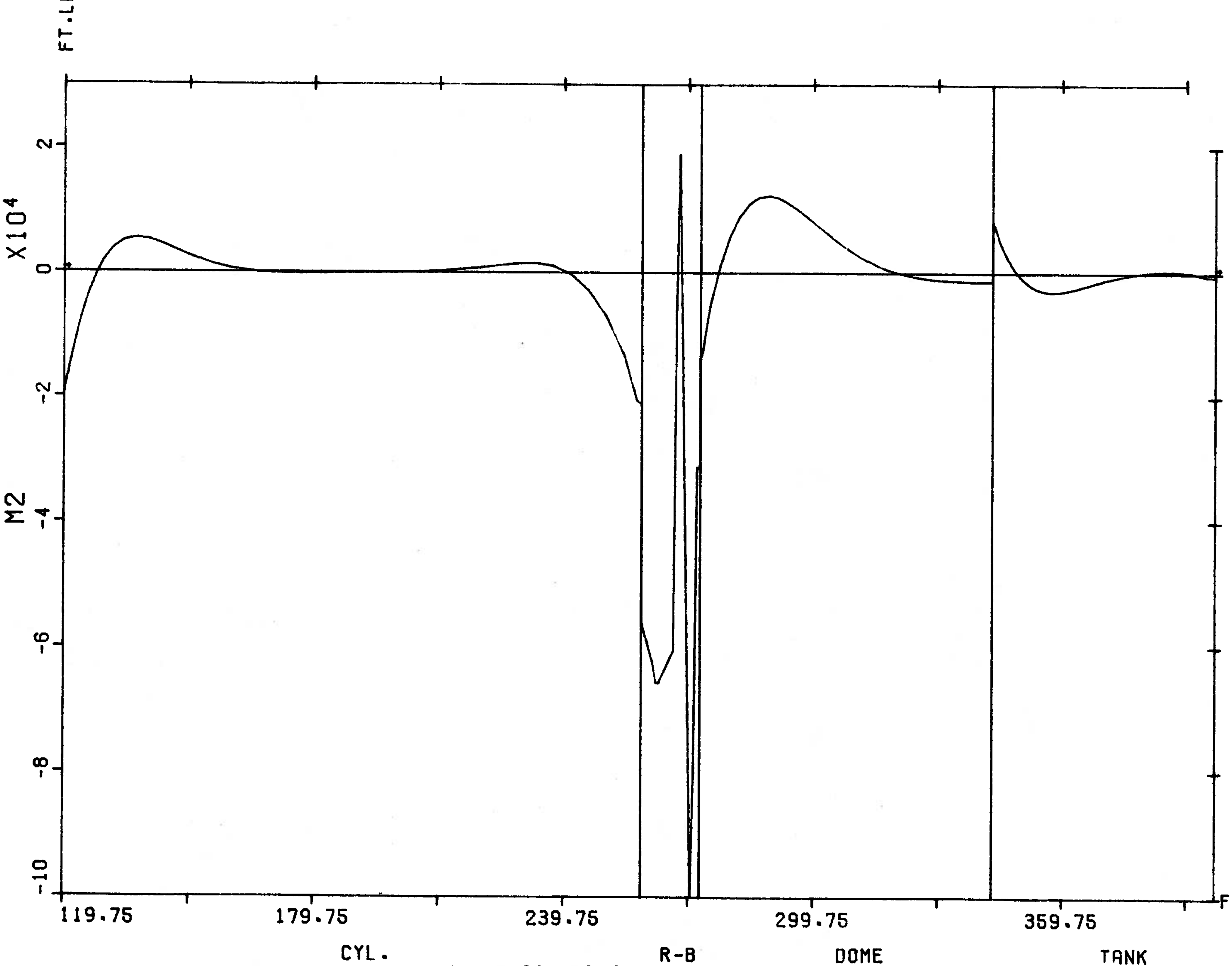

FIGURE G28 M2 for Reference State Rf1

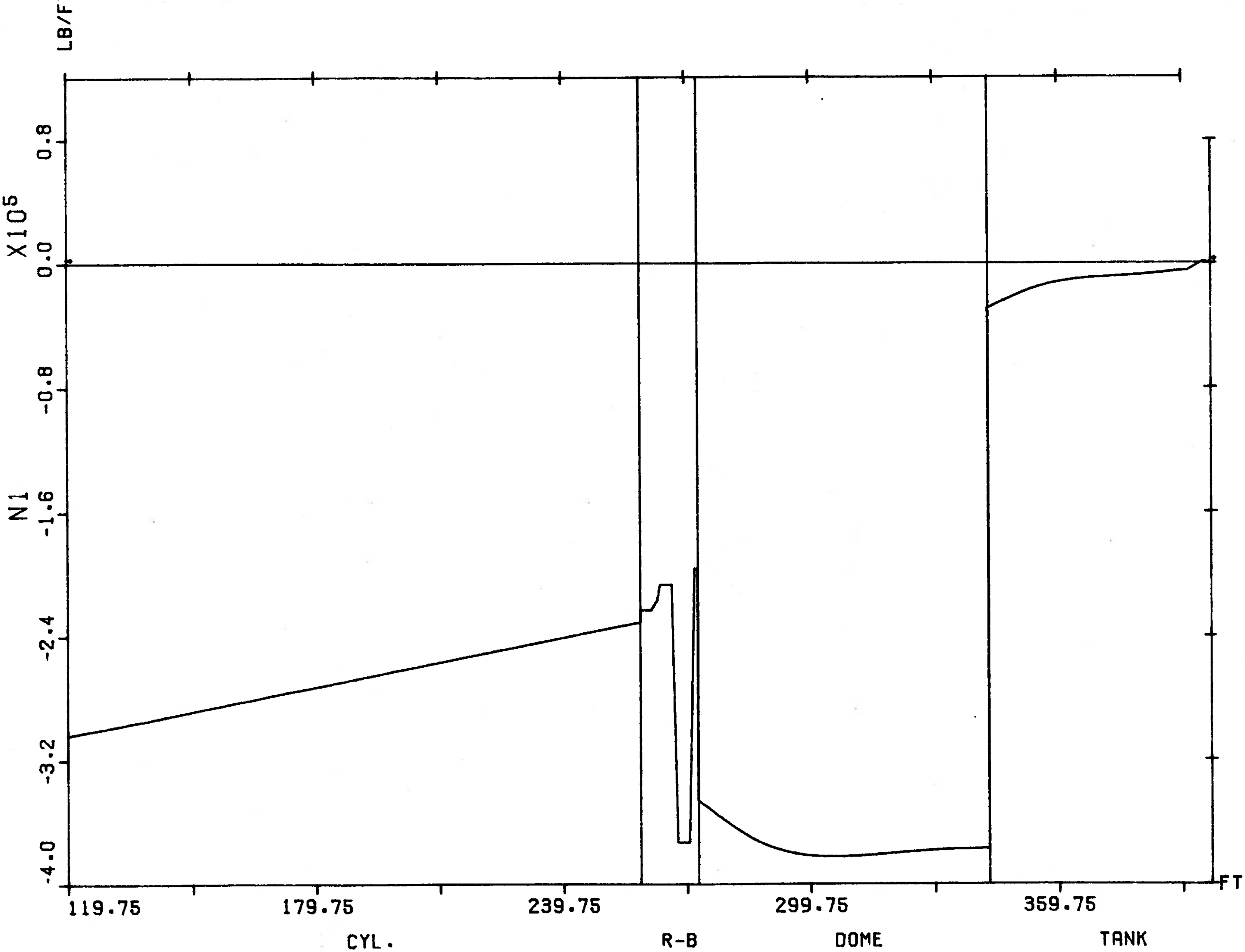

FIGURE G29 N1 for Reference State Rs1

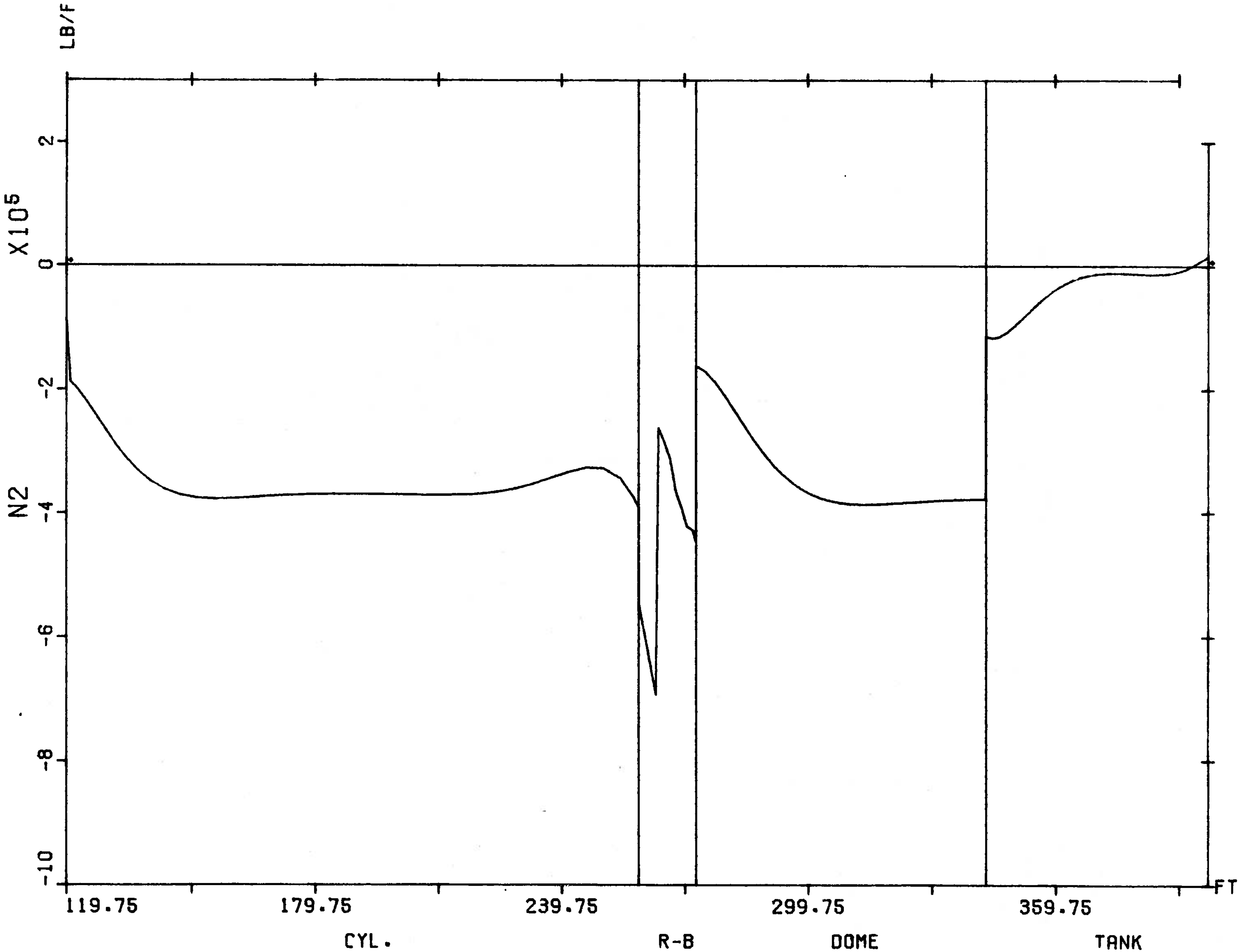

FIGURE G30 N2 for Reference State Rsl

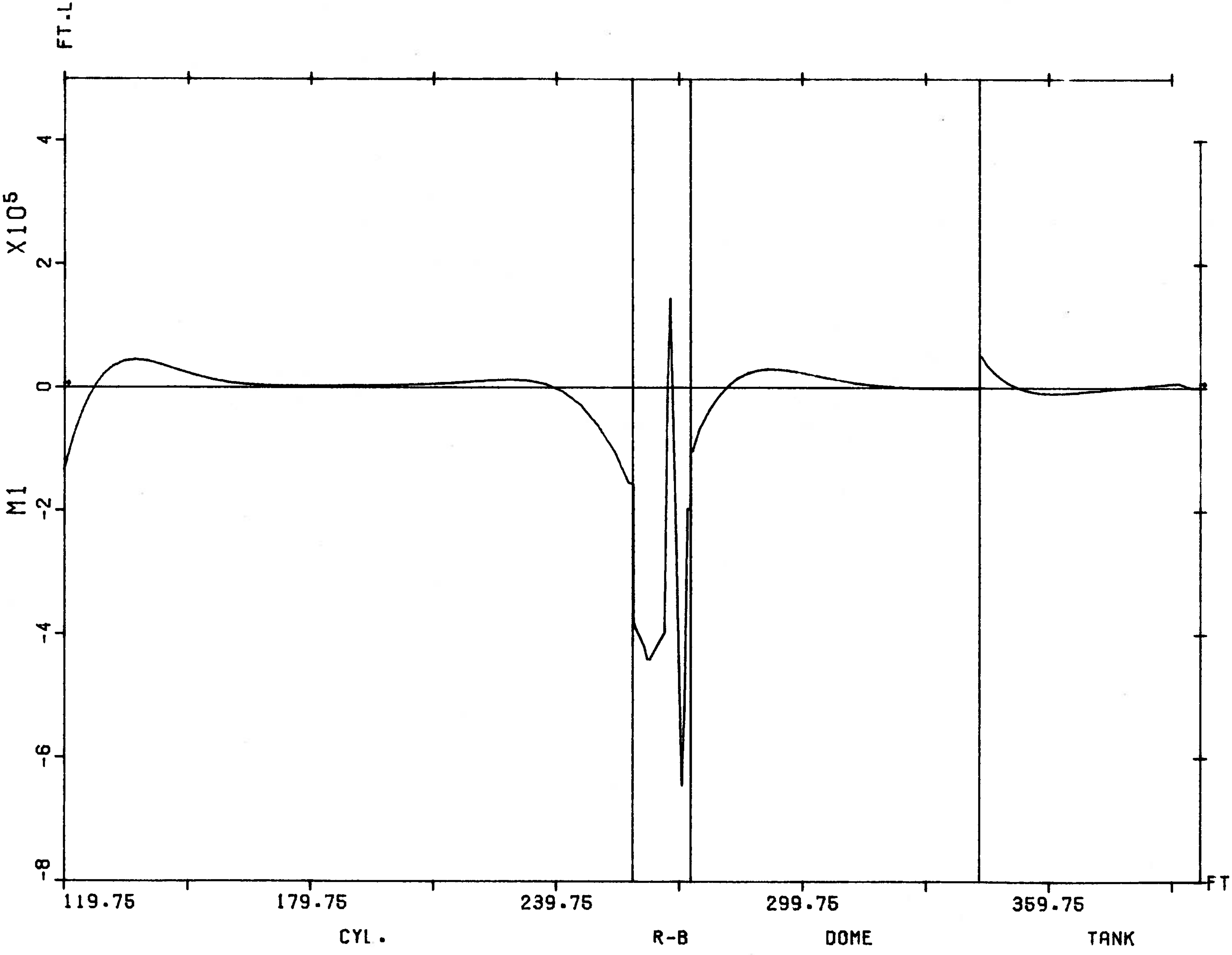

FIGURE G31 M1 for Reference State Rs1

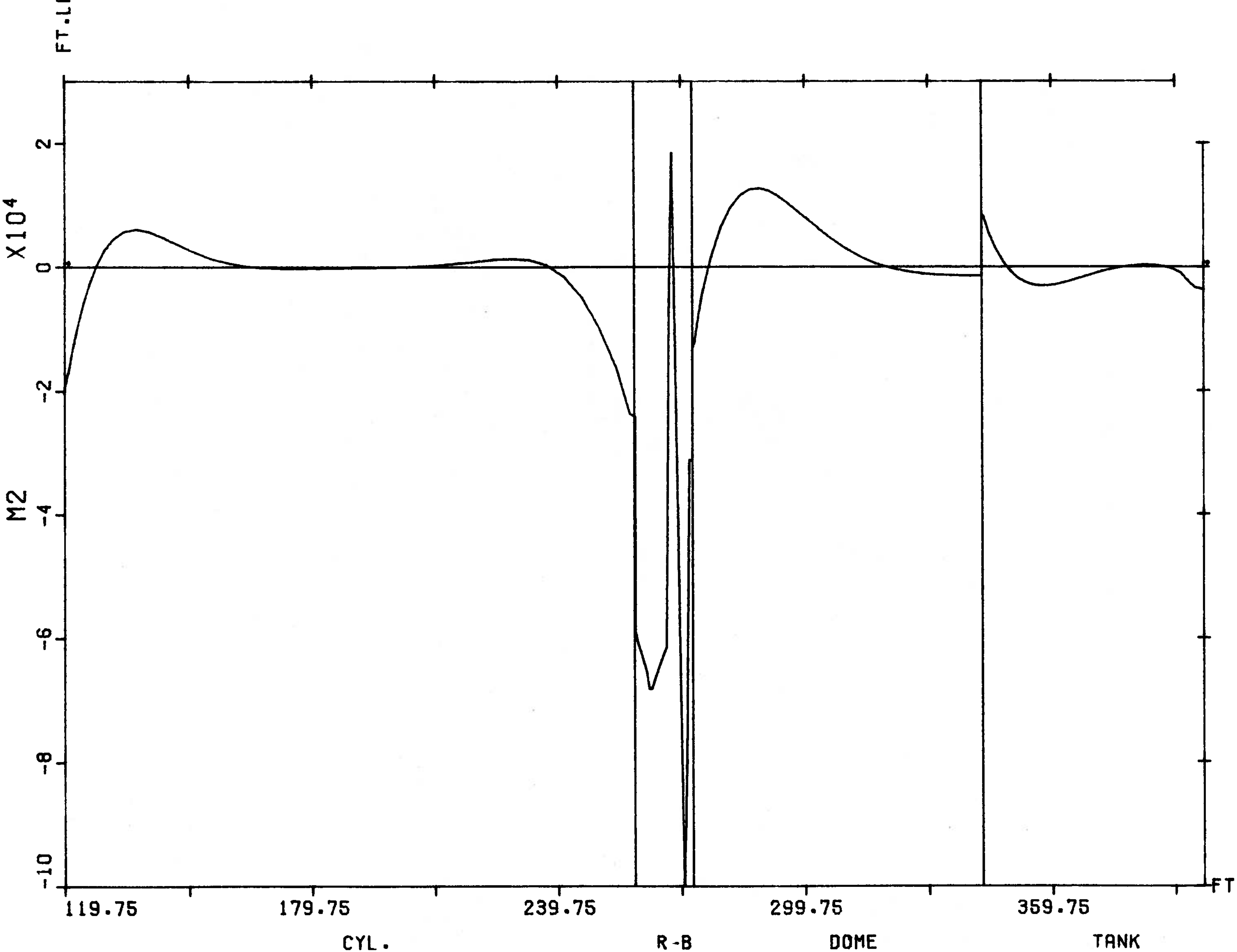

FIGURE G32 M2 for Reference State Rs1

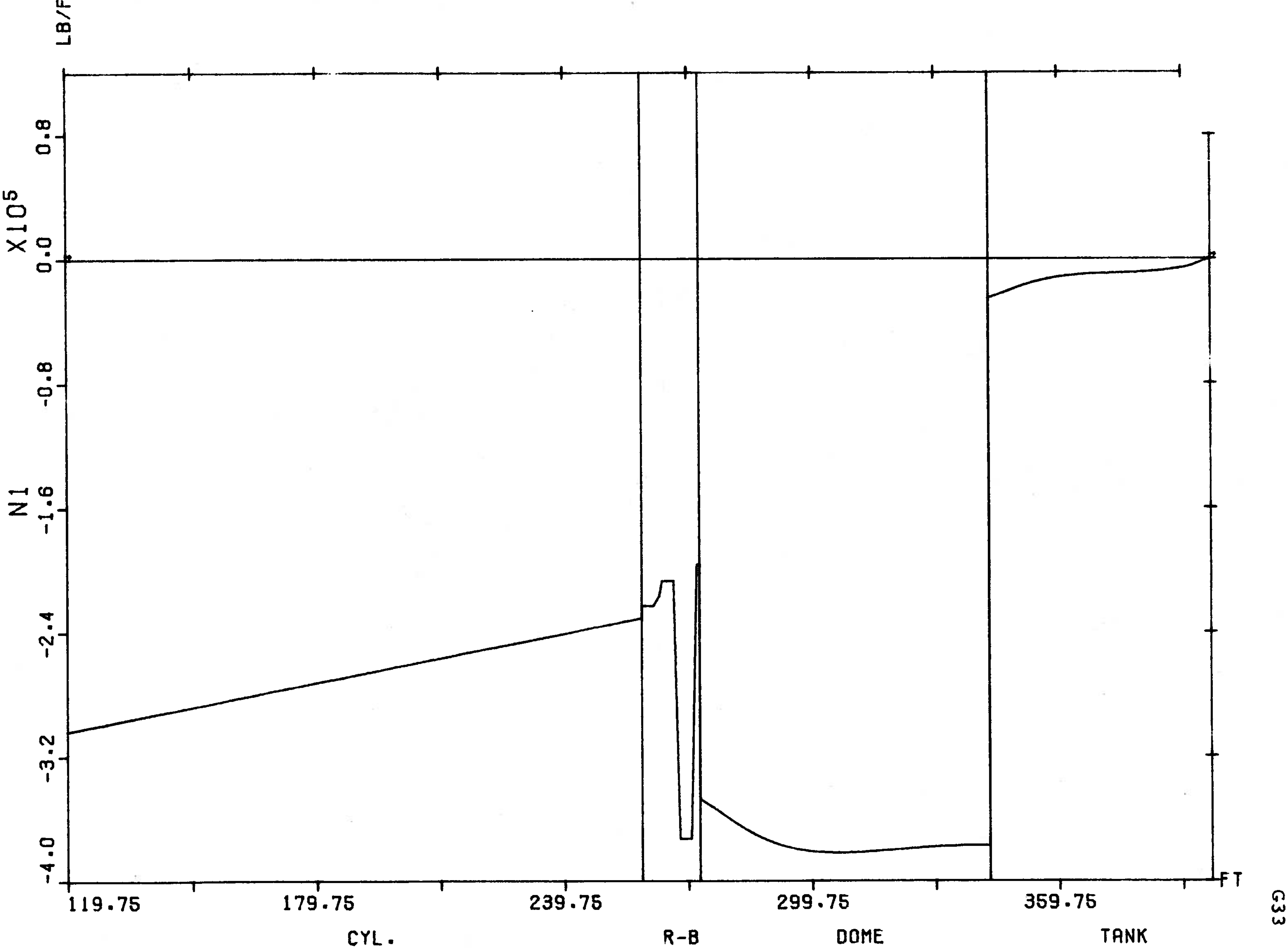

FIGURE G33 N1 for Reference State Rf2

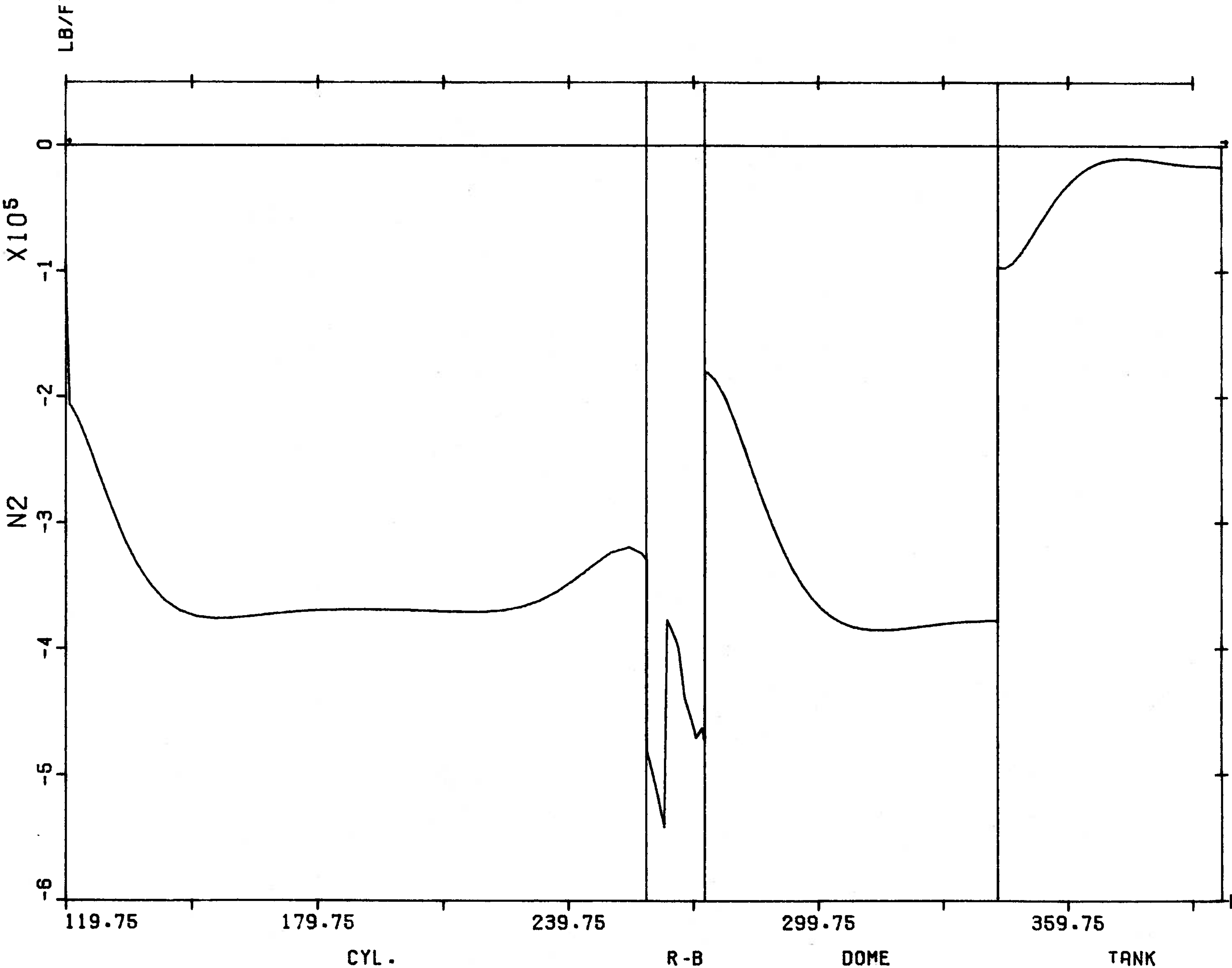

FIGURE G34 N2 for Reference State Rf2

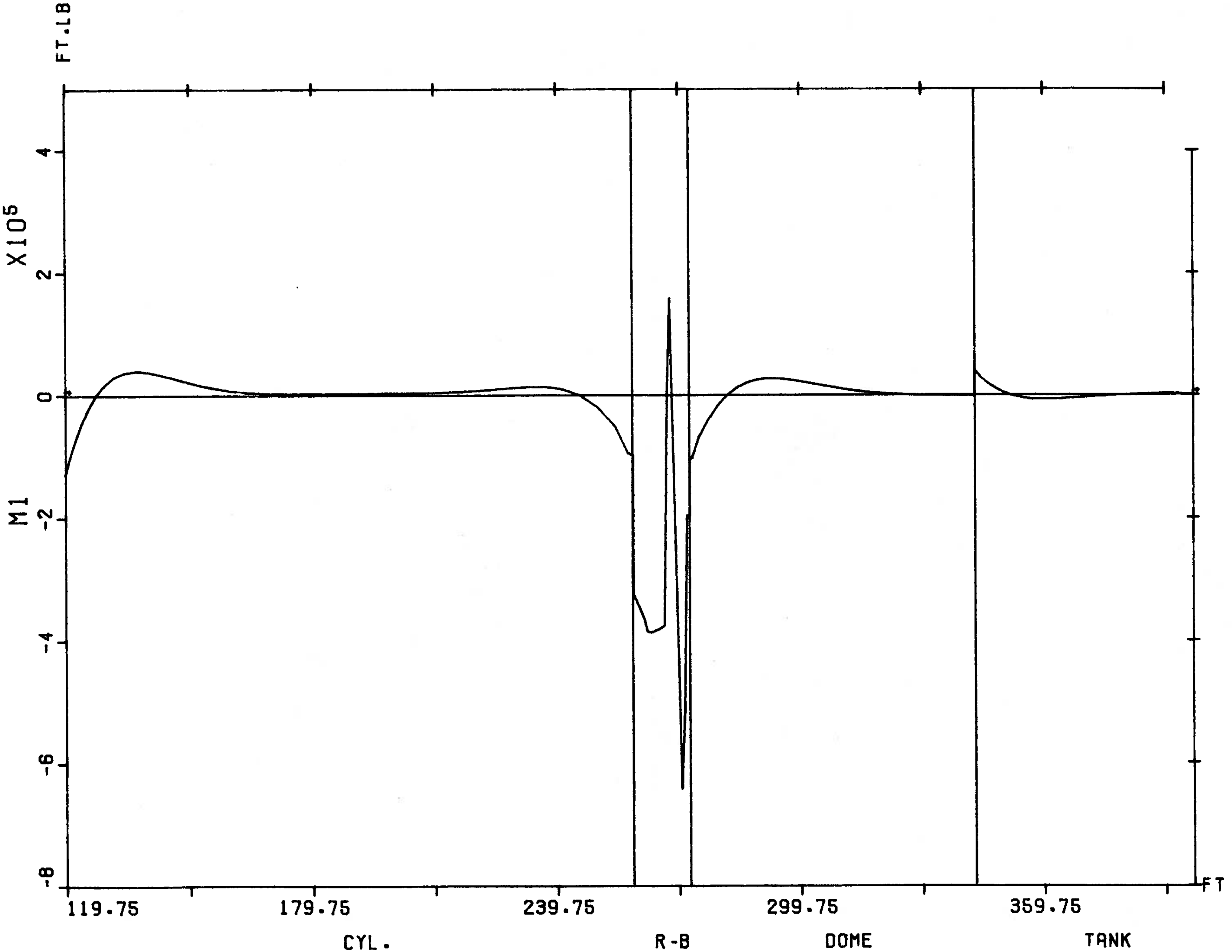

FIGURE G35. M1 for Reference State Rf2

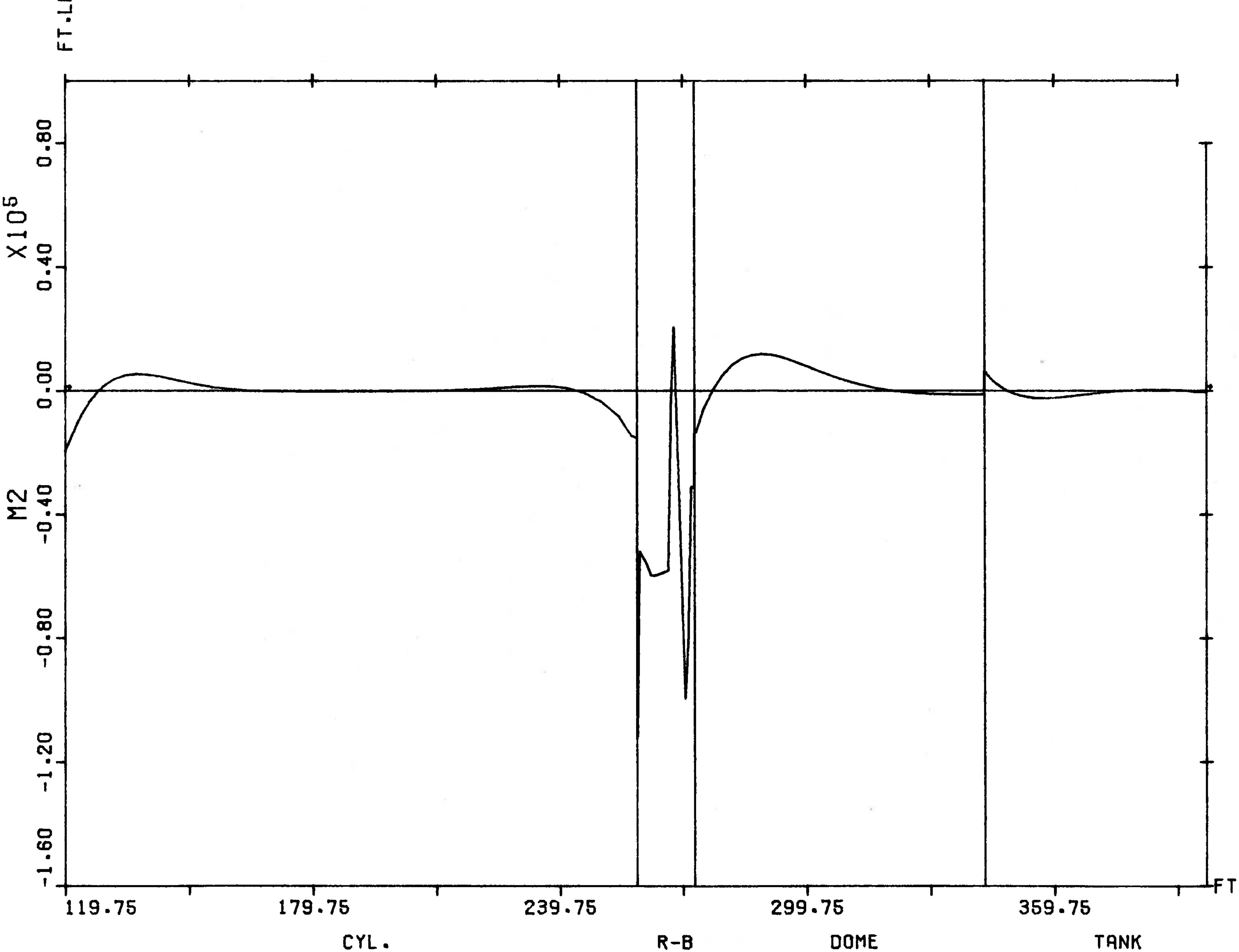

FIGURE G36 M2 for Reference State Rf2

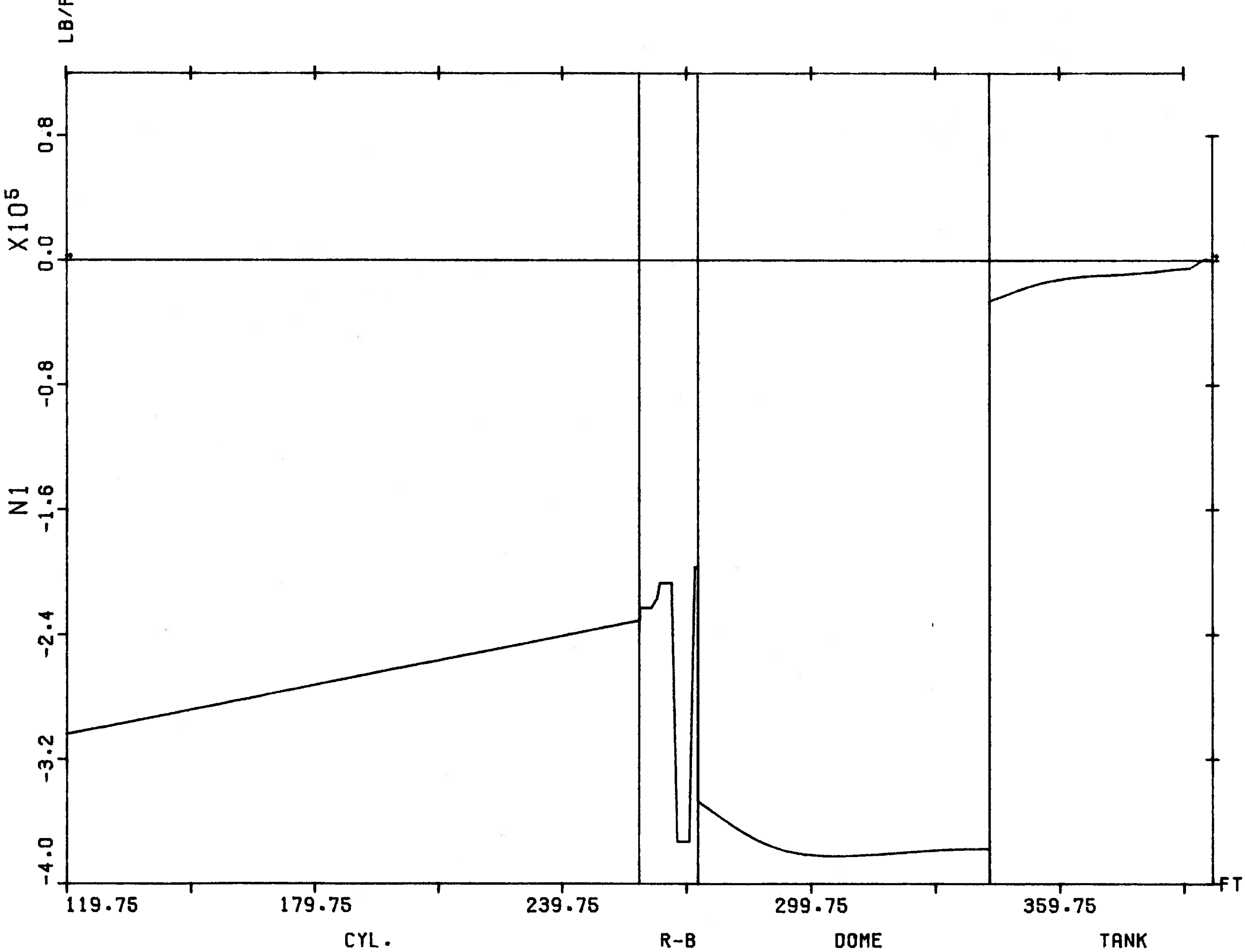

FIGURE G37 N1 for Reference State Rs2

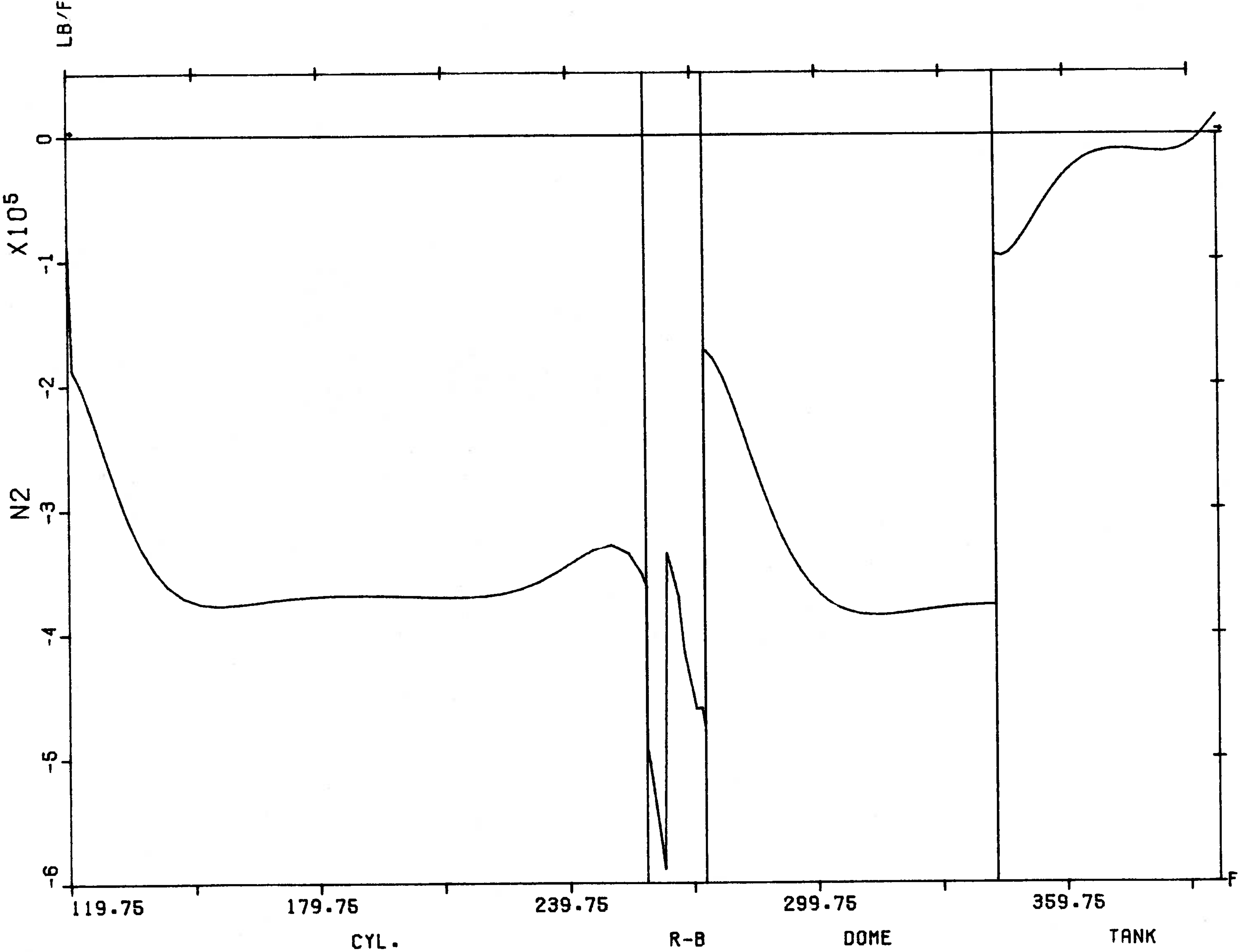

FIGURE G38 N2 for Reference State Rs2

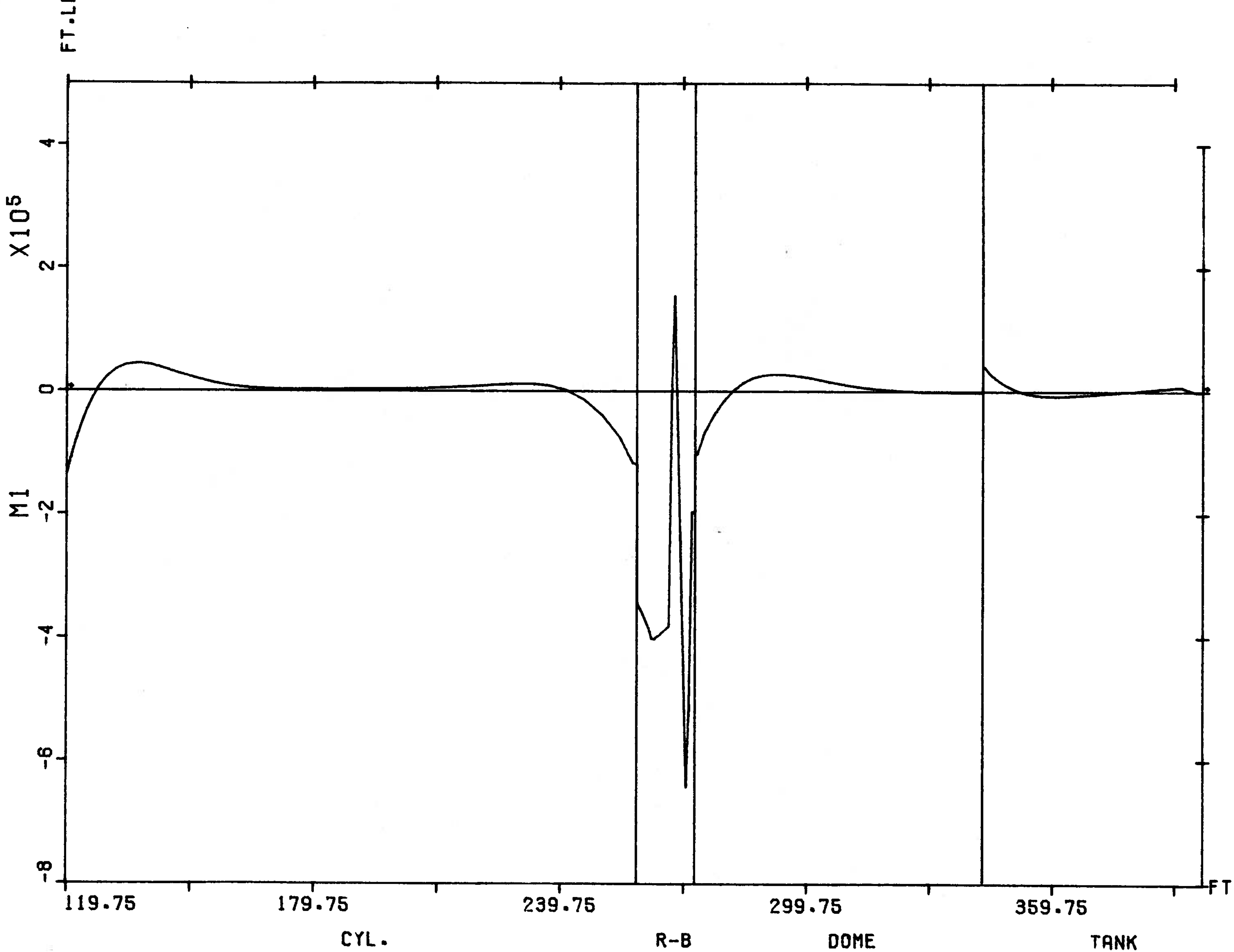

FIGURE G39 M1 for Reference State Ps2

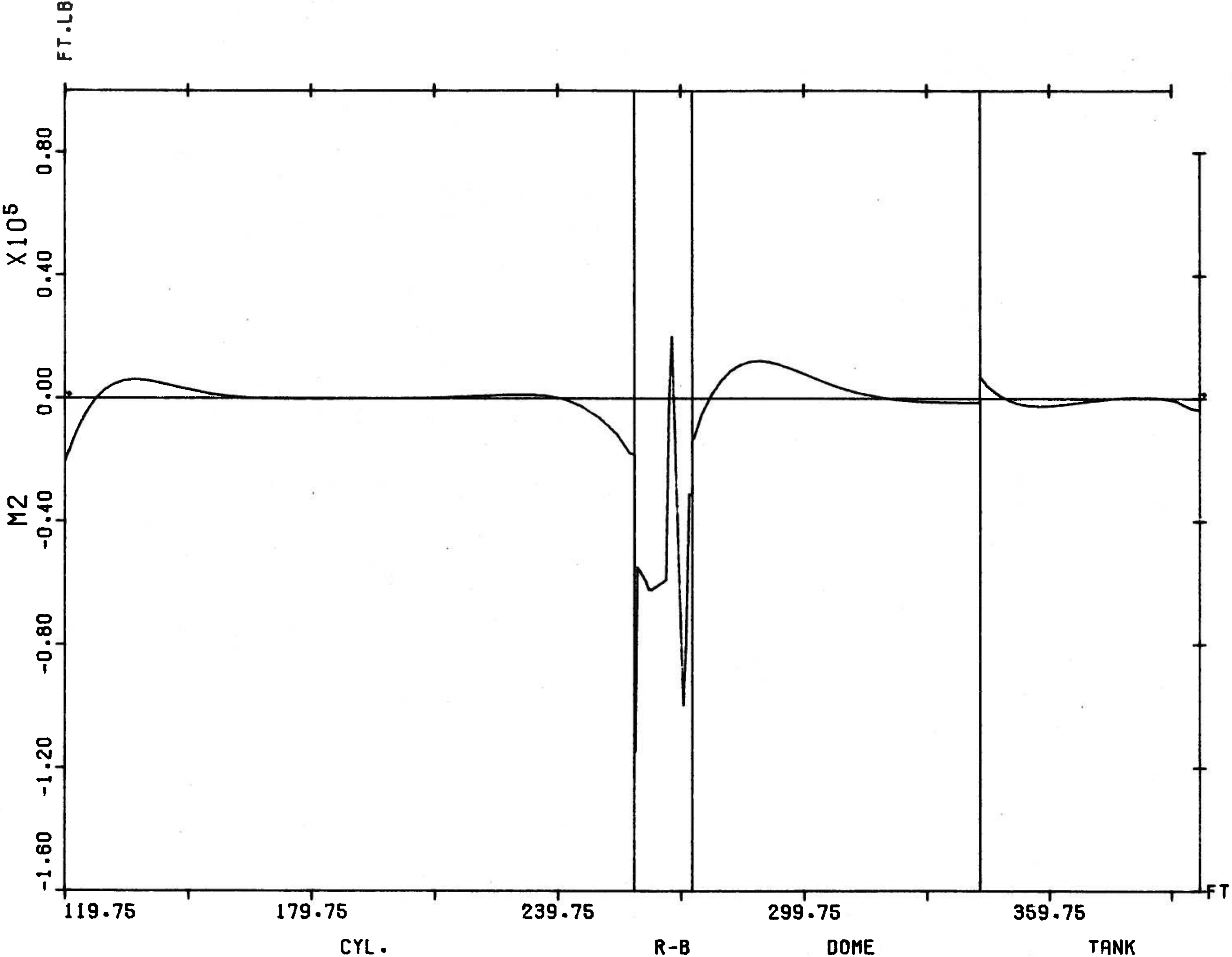

FIGURE G40. M2 for Reference State Rs2

APPENDIX H

Calculation of Shrinkage Strains

APPENDIX H

Calculation of Shrinkage Strains

For Use in Elastic Analysis of Containment Vessel

The calculation of shrinkage strains for use in the BOSOR Analysis of the Gentilly Containment Vessel was based on procedures developed by the European Concrete Committee. They recommend the use of Equation H1 to estimate shrinkage strains:

$$\varepsilon_{cs(t,t_o)} = \varepsilon_{cs\infty}(\beta_{s(t)} - \beta_{s(t_o)}) \tag{H1}$$

The meanings of the various terms in this equation and the assumptions made in calculating each term are outlined below.

t = theoretical age of concrete at end of shrinkage period, days.

t_o = theoretical age of concrete at beginning of period for which shrinkages is to be computed, days.

$\varepsilon_{cs(t,t_o)}$ = shrinkage strain occuring in the interval t_o to t, expressed in terms of average shortening divided by original length.

The "theoretical age" of the concrete, t, is a function of the ambient temperature as given by:

$$t = \frac{\Sigma_o^{t'} [T(t') + 10]\ \Delta t'}{30} \tag{H2}$$

where:

t = theoretical age of concrete

T = average 24 hour temperature of concrete in degrees Celsius

$\Delta t'$ = number of days with average temperature T.

For simplicity in the calculations t was taken equal to the actual elapsed time because the time periods between the placing of the concrete in successive elements in the structure all included more than one season. It was assumed that the base slab of the containment vessel was completed August 1, 1974 (t_1=0), the walls were completed December 15, 1974 (t_2=136 days), the lower ring beam and lower dome were completed September 1, 1975 (t_3=396 days) and the upper ring beam and dome were completed March 15, 1976 (t_4=592 days). These were rounded off to 0, 140, 400 and 600 days respectively. The assumed values of t for the concrete at various stages in construction are given in Table H1.

$\varepsilon_{cs\infty}$ = Shrinkage strain which would occur in an infinite period of time for a member of the same thickness as the one under consideration, composed of the type of concrete involved and cured under the same relative humidity. The value of $\varepsilon_{cs\infty}$ is given by Equation H3:

$$\varepsilon_{cs\infty} = \beta_{1s}\ \beta_{2s} \tag{H3}$$

β_{1s} = the final amount of shrinkage which would occur in a 12 cm (4.7 inch) thick concrete wall exposed to air on two faces.

The term β_{1s} is given in Reference 17 as a function of the relative humidity of the ambient air and the consistency (slump) of the concrete. For concrete outdoors in a relative humidity of 70 percent, $\beta_{1s} = -20 \times 10^{-5}$. For slumps less than 1 inch or more than 2 inches this is multiplied by 0.75 and 1.25 respectively. Based on discussions with site engineers the slump was assumed to be 1 inch or less and β_{1s} was taken as $\beta_{1s} = -15 \times 10^{-5}$ in/in.

β_{2s} = a number varying from 1.2 to 0.7 as the thickness increases to account for the reduced shrinkage in thicker members.

Throughout these calculations the thickness is expressed in terms of a "theoretical thickness" which is the thickness of any equivalent long wall exposed to the air on two sides. The theoretical thickness, h_{th}, is defined as:

$$h_{th} = \frac{\lambda \ 2A_c}{u}$$

where λ = 1.0 for a 40 percent relative humidity, increasing to 1.5 for a 70 percent relative humidity and 5 for a 90 percent relative humidity.

A_c = area of the concrete

u = perimeter exposed to air.

The theoretical thickness of the base slab was computed assuming it was exposed to air on the upper surface only. The theoretical thickness of the ring beam was evaluated from the dimensions given on the drawings including an allowance for the two stage construction of the ring beam.

The remaining terms in Equation H1 are:

$\beta_{s(t)}$ and $\beta_{s(t_o)}$ = the fraction of $\varepsilon_{cs\infty}$ which will have occurred at times t and t_o. Graphs are presented in Reference 17 in terms of the effective thickness of the wall.

Using this procedure, shrinkage strains were computed for each element (base, wall, etc.) for the time intervals given in Table H1 and were incorporated in the corresponding stage in the analysis. The resulting shrinkage strains are summarized in Table 2.2.

In addition, an estimate of the effect of differential shrinkage through the wall was obtained by arbitrarily assuming the shrinkage of the outer 5 cm. of the wall was equal to that of a wall of theoretical thickness 10 cm. The remainder of the wall was assumed to have shrinkage strains equal to those computed for the entire wall.

Table H1

Age of Concrete at Various Stages of Construction

Date	Stage	Base Concrete	Wall Concrete	Lower Dome Concrete	Upper Dome Concrete
August 1/74	Base Completed	t_o=0 days	-	-	-
December 15/74	Walls Completed	t=140	t_o=0	-	-
September 1/75	Lower Dome Completed	t=400	t=260	t_o=0	-
March 15/76	Upper Dome Completed	t=600	t=460	t=200	t_o=0
-----	Life of Structure	t=∞	t=∞	t=∞	t=∞

APPENDIX I

Computer Program for Section Cracking Analysis

APPENDIX I

The program is based on the theory presented in Section 3.4. For a given trapezoidal section with up to 5 layers of mild steel bars and up to 5 layers of prestressing strands, the program generates the ΔP, ε and x_c, ε arrays for a specified range of loading, temperature and geometrical constraint. (These arrays are stored in disk files from where they are retrieved later by a plotting routine which produces the graphs). The program stops automatically when rupture of a prestressing strand is reached.

Although the program was written taking advantage of some interactive features of MTS (Michigan Terminal System, the system used at the U. of A. computing centre), it can be adapted easily for use in any other system with a Fortran compiler. The only changes will involve input/output statements (where consideration has to be given to the file manipulation technique peculiar to the system).

The program is straightforward and Fortran variable names have been chosen so as to resemble as closely as possible the corresponding variable names of Section 3.4.

<u>Description of input variables</u> (units are pounds, inches, °F, except when noted otherwise).

B1 : "inside" width of cross section

B2 : "outside" width of cross section

D : height

NMS : number of mild-steel layers

XMS(I) : location of I-th layer measured from inside

AMS(I) : area of I-th layer

NF : number of prestressing strands

XF(I) : location of the I-th strand

AF(I) : area of the I-th strand

FY : yielding stress of mild steel

FC : f'_c (ultimate strength of concrete)

XK : k (constant to calculate tensile strength of concrete)

PR : Poisson's ratio of concrete

ALFAC,ALFAS: thermal expansion coefficients of concrete and steel, respectively.

DELAY : factor for delayed effects in concrete (usually 2.5)

XNI,XMI : initial force (lb/ft) and moment (lb-ft/ft)

XSK(I) : factor for initial value of prestressing of I-th strand (XSK(I)* 255000)

XNP,XMP : force (lb/ft) and moment (lb-ft/ft) due to live load (any value)

TDPO,TDP : initial and total increment of external force (ΔP)

NINC : number of increments between TDPO and TDP

DTC1I,DTC2I: initial temperature increments on inside, outside faces

DELTC1,DELTC2: additional temperature increments on inside, outside faces.

```
C      PROGRAM TO GENERATE SECTION BEHAVIOR ARRAYS
      IMPLICIT REAL*8(A-H,O-Z)
      DIMENSION A(100,21),DU(21),B(100,30)
      DIMENSION XSK(5)
      DIMENSION DPMS(5)
      DIMENSION FIMS(5),DFMS(5),FMS(5),DETMS(5)
      DIMENSION FIF(5),DFF(5),FF(5),DETF(5)
      DIMENSION XMS(5),XF(5)
      DIMENSION AMS(5),AF(5)
      EQUIVALENCE (DU(1),DP) ,(DU(2),FI) ,(DU(3),EPSC), (DU(4),XC) ,
     *  (DU(5),FIC1) ,(DU(6),DELFC1),(DU(7),FC1)   ,
     *  (DU(8),FIC2),(DU(9),DELFC2),(DU(10),FC2) ,(DU(11),PI)    ,
     *  (DU(12),DELTAP),(DU(13),P)   ,(DU(14),XMI) ,(DU(15),DELTAM),
     *  (DU(16),XM)   ,(DU(17),XMIL) ,(DU(18),DML),(DU(19),XML),
     *  (DU(20),DTC1) ,(DU(21),DTC2)
C
       IN=7
      IP=8
      READ(IN,1000) B1,B2,D
      READ(IN,1000) NMS,(XMS(I),AMS(I),I=1,NMS)
      READ(IN,1000)  NF,(XF(I),AF(I),I=1,NF)
      READ(IN,1000) FY
      READ(IN,1000) FC,XK,PR
      FT=XK*DSQRT(FC)
      E=57000.*DSQRT(FC)/(1.-PR**2)
      CT=1.+PR
      ET=CT*E
      XN=29.6E06/E
      READ(IN,1000)  ALFAC,ALFAS
C READ MAGNIF. FACTOR TO TAKE INTO ACCOUNT CREEP, ETC. IN INITIAL STRESS
      READ(IN,1000)  DELAY
C  INITIAL FORCE AND MOMENT
C  FORCE IS + IF TENSILE; MOMENT IS + IF PRODUCES TENSION INSIDE
      READ(IN,1000)  XNI,XMI
C TRANSFORM UNITS
      XMI=XMI*12.
C  CALCULATE PROPERTIES OF TRANSF. SECTION (WITH AND WITHOUT DELAYED EFFECTS)
      CG=(B1+2.*B2)*D/(3.*(B1+B2))
      AMSTOT=0.
      AMS2=0.
      AMS1=0.
      DO 11 I=1,NMS
      AMSTOT=AMSTOT+AMS(I)
      AMS1=AMS1+AMS(I)*XMS(I)
   11 CONTINUE
      AFTOT=0.
      DO 12 I=1,NF
   12 AFTOT=AFTOT+AF(I)
      AL=0.5*(B1+B2)*D+(AMSTOT)*DELAY*XN
      CG=(CG*0.5*(B1+B2)*D+AMS1*DELAY*XN)/AL
      DO 13 I=1,NMS
   13 AMS2=AMS2+AMS(I)*(XMS(I)-CG)**2
      XIC=B2*D**3/12.+B2*D*(0.5*D-CG)**2+(B1-B2)*D**3/36. +
     1          0.5*(B1-B2)*D*(D/3.-CG)**2
      XIL=XIC+(AMS2)*DELAY*XN
      AS=0.5*(B1+B2)*D+(AMSTOT)*XN
      XIS=XIC+(AMS2)*XN
C  NOTE THAT GIVEN MOMENT IS W.R.T. CENTERLINE
      XMIG=XMI-XNI*(D/2.-CG)
 1000 FORMAT(8G10.0)
```

```
C CALCULATE INITIAL STRESSES
      FIC1=XMIG*CG/XIL+XNI/AL
      FIC2=XMIG*(CG-D)/XIL+XNI/AL
      DO 2 I=1,NMS
      FIMS(I)=DELAY*XN*(XMIG*(CG-XMS(I))/XIL+XNI/AL)
    2 CONTINUE
C READ FACTORS FOR PRESTRESSING AFTER ALL LOSES
C    (ONE FOR EACH PRESTRESSING STRAND)
      READ(IN,1000)  (XSK(I),I=1,NF)
      DO 3  I=1,NF
      FIF(I)=255000.*XSK(I)
    3 CONTINUE
C
C  EXTERNAL FORCE AND GEOMETRIC CONSTRAINT
C
      WRITE(6,1504)
 1504 FORMAT(1H0,'NP AND MP FROM BOSCR')
      READ(5,1000) XNP,XMP
      WRITE(6,1505)
 1505 FORMAT (1H0,'TDP,NINC,TDPO')
      READ(5,1000) TDP,NINC,TDPO
      TDFIO=-12.*(XMP/XNP)*TDPO/(E*XIS)
      TDFI=-12.*(XMP/XNP)*TDP/(E*XIS)
      WRITE(6,1506)
1506  FORMAT(1H0,'DTC1I, DTC2I, DELTC1, DELTC2')
      READ(5,1000) DTC1I,DTC2I,DELTC1,DELTC2
C
      C6=1./6.
      V1=(2.*B1+B2)*D*C6
      V2=(2.*B2+B1)*D*C6
      WRITE(IF,2000)
 2000 FORMAT(1H1,20X,'LINEAR CRACKING ANALYSIS',///,2X,'DATA',/,8X,
     1  '(FOR NOTATION REFER TO AECB REPORT)',//,12X,
     2  'UNITS ARE POUNDS,INCHES, DEG. FAHRENHEIT')
      WRITE(IF,2001) B1,B2,D,FY,FC,XK,PR,FT,
     1   E,XN,ALFAC,ALFAS,FIC1,FIC2
 2001 FORMAT(1H0,5X,'B1=',E23.7,/,6X,'B2=',E23.7,/,6X,'D=',E24.7,
     1/,6X,
     2                                                  'FY=',E23.7,
     * /,6X,'F''C=',
     3E22.7,/,6X,'K=',E24.7,/,6X,'PR=',E23.7,/,6X,'FT=',E23.7,2X,
     * '(=K*DSQRT(F''C))'
     4,/,6X,'E=',E24.7,2X,'(=57000.*DSQRT(F''C))',/,6X,'N=',E24.7,2X,
     5'(=29600000./E)',/,6X,'ALFAC=',E20.7,/,6X,'ALFAS=',E20.7,/,6X,
     7   'FIC1=',E21.7,/,6X,'FIC2=',E21.7,//)
      WRITE(IF,2010)   (I,XMS(I),AMS(I),FIMS(I),I=1,NMS)
 2010 FORMAT(1H0,5X,'BAR TYPE NO.',3X,'LOCATION',10X,'AREA',
     1    6X,'INITIAL STRESS',//,(10X,'MILD',I3,3E14.3,/))
      WRITE(IF,2011)   (I,XF(I),AF(I),FIF(I),I=1,NF)
 2011 FORMAT(8X,'PRESTR.',I2,3E14.3,/)
      WRITE(IF,2300) NINC,TDP,TDFI,TDPO,TDFIO,DTC1I,DTC2I,
     *  DELTC1,DELTC2
2300  FORMAT(1H0,5X,' *** LOADING SPECIFICATIONS ***'/
     *  5X,'NUMBER OF INCREMENTS                         =',I3/
     *  5X,'MAXIMUM APPLIED MEMBRANE FORCE               =',E13.6/
     *  5X,'MAXIMUM IMPOSED CURVATURE                    =',E13.6/
     *  5X,'MINIMUM APPLIED MEMBRANE FORCE               =',E13.6/
     *  5X,'MINIMUM IMPOSED CURVATURE                    =',E13.6/
     *  5X,'INITIAL TEMPERATURE INCREMENT (FACE 1)=',E13.6/
     *  5X,'INITIAL TEMPERATURE INCREMENT (FACE 2)=',E13.6/
```

```
     *  5X,'ADDITICNAL TEMPERATURE INCRMT (FACE 1)=',E13.6/
     *  5X,'ADDITICNAL TEMPERATURE INCRMT (FACE 2)=',E13.6)
      WRITE(9,2400)
2400  FORMAT(1H1,10X,'*** TRACE OF ITERATICNS ***'//)
C
C  START LOOP TO SELECT LCADS AND STCRE RESULTS
C
C   MOVE ORIGIN CF PRESTRESS TO ZERO
      DO 7 I=1,NF
    7 FIF(I)=0.
C
      DELP=(TDP-TDPO)/FLOAT(NINC)
      DELF=(TDFI-TDFIC)/FLOAT(NINC)
      DELT1=DELTC1/FLOAT(NINC)
      DELT2=DELTC2/FLOAT(NINC)
      NINC=NINC+1
      DP=TDPO-DELP
      FI=TDFIO-DELF
      DTC1=DTC1I-DELT1
      DTC2=DTC2I-DELT2
CC
      KINC=0
      DO 500 N=1,NINC
      DP=DP+DELP
      FI=FI+DELF
      DTC1=DTC1+DELT1
      DTC2=DTC2+DELT2
      IF(N.EQ.1) XC=0.0
      EPSOLD=-1.0
      IT=0
      NIT=30
      DO 8 I=1,NMS
    8 DPMS(I)=0.
      DETC1=ALFAC*DTC1
      DETC2=ALFAC*DTC2
      DO 4 I=1,NMS
      DETMS(I)=ALFAS*(DTC1+(DTC2-DTC1)*XMS(I)/D)
    4 CONTINUE
      DO 5 I=1,NF
       DETF(I)=ALFAS*(DTC1+(DTC2-DTC1)*XF(I)/D)
    5 CONTINUE
      WRITE(9,2500) DP,FI,DTC1,DTC2
2500  FORMAT(1H0,' CONVERGENCE TRACE FOR '/2X,' DP=',E12.5,
     * 2X,' FI=',E12.5,2X,' DTC1=',E12.5,2X,' DTC2=',E12.5)
C
C  ITERATIVE LCOP CN CRACKING STARTS HERE
   10 G=0.0
      FT2=FT
      IF(XC.LT.0.0) XC=0.0
      IF(XC.LE.D) GO TO 15
      XC=0.0
      FTEMP=FIC2+E*(FI*D-CT*DETC2)
      IF (EEPS+FTEMP.LT.FT) GO TO 15
      XC=D
      FT2=FTEMP
      G=1.0
   15 BC=B1+(B2-B1)*XC/D
      VC1=XC*(2.*B1+BC)*C6
      VC2=XC*(2.*BC+B1)*C6
      DEN=V1+V2+XN*(AMSTOT+AFTOT)-VC1-VC2*G
```

```
      AUX1=0.
      DO 16 I=1,NMS
   16 AUX1=AUX1+(DETMS(I)-FI*XMS(I))*AMS(I)
      AUX2=0.
      DO 17 I=1,NF
   17 AUX2=AUX2+(DETF(I)-FI*XF(I))*AF(I)
      DPTOT=0.
      DO 18 I=1,NMS
   18 DPTOT=DPTOT+DPMS(I)
      EEPS=DP+ET*(V1*DETC1+V2*DETC2)-E*FI*D*V2+E*XN*(    AUX1    +
     *        AUX2       )+VC1*(FIC1-ET*DETC1)+FT2*VC2
     * +DPTOT
      EEPS=EEPS/DEN
      IF(EEPS+FI*D*E-ET*DETC2-FT+FIC2.GT.0.0.AND.EEPS-FT+FIC1
     * -ET*DETC1.LT.0.0)  GO TO 999
      EPS=EEPS/E
      EPSC=EPS+0.5*D*FI
C
      DEN=FIC1-FIC2+ET*(DETC2-DETC1)-E*FI*D
      IF(DABS(DEN).GT.1.0E-10) GO TO 50
      XCNEW=0.0
      IF(EEPS.GT.(FT-FIC1))   XCNEW=D
      GO TO 60
   50 XCNEW=(EEPS-ET*DETC1+FIC1-FT)*D/DEN
   60 IF(DABS(EPSOLD-EPSC).LT.1.0E-10)   GO TO 100
      EPSOLD=EPSC
      WRITE(9,3500)   EPSC,FI,XC,XCNEW
 3500 FORMAT(1H ,'EPSC=',E12.5,2X,'FI=',E11.4,2X,'OLD XC =',E11.4,
     1   4X,'NEW XC =',E11.4)
      DO 69 I=1,NMS
      FMS(I)=FIMS(I)+E*XN*(EPS+FI*XMS(I)-DETMS(I))
      IF(FMS(I).LT.FY)   GO TO 69
      DPMS(I)=AMS(I)*(FMS(I)-FY)
   69 CONTINUE
   70 IT=IT+1
      IF(IT.LT.NIT) GO TO 75
      WRITE(IF,4500) IT,N
 4500 FORMAT(' *** SOLUTION DID NOT CONVERGE AFTER',I4,'  ITERATES',
     *  ',FOR LOAD INCREMENT',I4)
      GO TO 100
   75 XC=XCNEW
      GO TO 10
C
  100 CONTINUE
C
C  COMPUTATION OF STRESS RESULTANTS
      DFC1=EEPS-ET*DETC1
      DELFC1=DFC1
      IF(XC.GE.0.0001) DELFC1=-FIC1
      DO 118 I=1,NMS
  118 DFMS(I)=XN*(EEPS+E*FI*XMS(I)-E*DETMS(I))
      DO 119  I=1,NF
  119 DFF(I)=XN*(EEPS+E*FI*XF(I)-E*DETF(I))
      DFC2=EEPS+E*FI*D-ET*DETC2
      DELFC2=DFC2
      IF(XC.GT.D-0.0001) DELFC2=-FIC2
      FC1=FIC1+DELFC1
      DO 120 I=1,NMS
      FMS(I)=FIMS(I)+DFMS(I)
      IF(FMS(I).LT.FY)  GO TO 120
```

```
      FMS(I)=FY
      DFMS(I)=FY-FIMS(I)
  120 CONTINUE
      DO 124 I=1,NF
  124 FF(I)=FIF(I)+DFF(I)
  140 FC2=FIC2+DELFC2
      D12=D*D/12.
      DC12=XC*XC/12.
      AUX3=0.
      DO 146 I=1,NMS
  146 AUX3=AUX3+FIMS(I)*AMS(I)
      AUX4=0.
      DO 147 I=1,NF
  147 AUX4=AUX4+FIF(I)*AF(I)
      PI=FIC1*V1+FIC2*V2+AUX3+AUX4
      AUX5=0.
      DO 148 I=1,NMS
  148 AUX5=AUX5+FIMS(I)*AMS(I)*XMS(I)
      AUX6=0.
      DO 149 I=1,NF
 149  AUX6=AUX6+FIF(I)*AF(I)*XF(I)
      XMI=(FIC1*(B1+B2)*D12+FIC2*(3.*B2+B1)*D12+
     1                   AUX5+AUX6)/12.
      XMIL=XMI-PI*D/24.
      IF(DFC2+FIC2.GT.FT) FT2=FT2+FEPS
      AUX9=0.
      AUX7=0.
      DO 151  I=1,NMS
      AUX7=AUX7+DFMS(I)*AMS(I)
      AUX9=AUX9+DFMS(I)*AMS(I)*XMS(I)
  151 CONTINUE
      AUX8=0.
      AUX10=0.
      DO 152 I=1,NF
      AUX8=AUX8+DFF(I)*AF(I)
      AUX10=AUX10+DFF(I)*AF(I)*XF(I)
  152 CONTINUE
      DELTAP=DFC1*V1+DFC2*V2-(FIC1+DFC1)*VC1-FT2*VC2+AUX7
     *      +AUX8
      DELTAM=(DFC1*D12*(B1+B2) +DFC2*D12*(3.*B2+B1)
     *  -(FIC1+DFC1)*DC12*(B1+BC) -FT2*DC12*(3.*BC+B1)
     *   +AUX9+AUX10)/12.
      P=PI+DELTAP
      DML=DELTAM-DELTAP*D/24.
      XM=XMI+DELTAM
      XML=XMIL+DML
C
      DO 398 I=1,NMS
      B(N,I)=FIMS(I)
      B(N,5+I)=DFMS(I)
      B(N,10+I)=FMS(I)
  398 CONTINUE
      DO 399 I=1,NF
      B(N,15+I)=25500.*XSK(I)
      B(N,20+I)=DFF(I)
      B(N,25+I)=B(N,15+I)+DFF(I)
C FOR PRINTING PURPOSES, ORIGIN OF PRESTRESS HAS BEEN RESTORED
  399 CONTINUE
      DO 400 I=1,21
  400 A(N,I)=DU(I)
```

```
      DO 410 I=1,NF
      IF(FF(I).GE.255000.*(1.-XSK(I)))  GO TO 549
  410 CONTINUE
      KINC=KINC+1
C
500   CONTINUE
C
      KINC=KINC-1
  549 WRITE(10'1000,3333) KINC
      WRITE(11'1000,3333) KINC
 3333 FORMAT(8G20.7)
      KINC1=KINC+1
550   DO 600 N=1,KINC1
      WRITE(IF,3000) A(N,1),A(N,2),A(N,20),A(N,21),(A(N,J),J=3,19)
      WRITE(IF,3001) (I,B(N,I),B(N,I+5),B(N,I+10),I=1,NMS)
      WRITE(IF,3002)  (I,B(N,I+15),B(N,I+20),B(N,I+25),I=1,NF)
 3001 FORMAT(/,' M-S',I2,1X,3E20.7)
 3002 FORMAT(/,' PRS',I2,1X,3E20.7)
      NNN=1000*(N+1)
      EPSPLT=A(N,3)-A(1,3)
      XCREL=A(N,4)/D
      WRITE(10'NNN,3333) EPSPLT,A(N,1)
      WRITE(11'NNN,3333) XCREL,A(N,1)
600   CONTINUE
C
      STOP
999   NINC=N-1
      WRITE(IF,4000) NINC
4000  FORMAT(//' *** SECTICN CRACKED ON WRCNG SIDE FCR',
     * ' LOAD INCREMENT',I4)
      GO TO 550
C
3000  FORMAT(//5X,'OUTPUT FOR SECTION ANALYSIS WITH'/
     * 5X,' DP =',E13.5,5X,' FI =',E13.5,5X,'DTC1=',E13.5,
     * 5X,'DTC2=',E13.5,/5X,' FOR WHICH THE FOLLOWING VALUES APPLY'/
     * 5X,' EPSC=',E13.5,/5X,' XC =',E13.5,/
     * 5X,' (NOTE:STRESSES IN PSI; FCRCES IN LBS; MCMENTS IN FT-LB;'
     * ,' XC IN INCHES'//14X,'INITIAL',13X,'DELTA',15X,'FINAL'/
     * ' FC1',3X,3E20.7,/,
     *                         ' FC2',3X,3E20.7,/,' P  ',3X,3E20.7,/
     * ' M  ',3X,3E20.7,/,' ML ',3X,3E20.7)
      END
```

APPENDIX J

Computer Program for Interaction Curves

APPENDIX J

The program is based on the theory described in Section 3.6.

The cross section has to be rectangular and up to 5 layers of mild steel bars and 5 layers of prestressing are allowed. The constitutive equations are nonlinear, as shown in Figs. 3.1, 3.2 and 3.3.

The same general remarks as for Appendix I are valid in the present case.

Description of input variables (units are pounds, inches, except where noted otherwise)

- H : height of cross section
- FC : f'_c (ultimate strength of concrete)
- XK : k (constant to calculate tensile strength of concrete)
- EO,EU : ε_o and ε_u, respectively (see Fig. 3.3)
- SY : yielding stress of mild steel
- SU : ultimate strength of prestressing steel
- SK : factor for initial value of prestressing strand (SK*SU)
- NMS : number of mild steel layers
- XMS(I) : location of I-th layer measured from inside
- AMS(I) : area of I-th layer
- NF : number of prestressing strands
- XF(I) : location of the I-th strand
- AF(I) : area of the I-th strand

N	:	number of control strain intervals
X1,X2	:	location of pivot, control points respectively (measured from inside face)
EX1	:	pivot strain
EX21,EX22	:	extreme control strains (EX22-EX21 is divided into N equal parts).
TITLE	:	literal data (up to 80 characters)

All other data remaining fixed the program keeps reading new values of X1, X2, EX1, EX21 and EX22. Execution stops when X1=X2 (for instance, a blank record).

```
C MAIN PROGRAM FOR INTERACTION CURVES
      IMPLICIT REAL*8(A-H,O-Z)
C         FOR A RECTANGLE WITH B=12. INCHES
C          UNITS ARE POUNDS, INCHES
      COMMON/CNSTEQ/AA(5),BB(5),CC(5)
      DIMENSION E(4)
      DIMENSION TITLE(20)
      DIMENSION PS(5),PF(5)
      DIMENSION EST(5),EF(5)
      DIMENSION XMS(5),XF(5),AMS(5),AF(5)
      DIMENSION SK(5)
      READ(5,4321) TITLE
 4321 FORMAT(20A4)
C    ****   INPUT   ****
C  HEIGHT
      READ(5,1000) H
C  CONCRETE STRENGTH (ALL POSITIVE)
      READ(5,1000) FC,XK,E0,EU
C  MILD STEEL AND PRESTRESSING STEEL STRENGTHS
      READ(5,1000)   SY,SU
C  STEEL AREAS (SQIN/FT) AND LOCATIONS(IN)
      READ(5,1000) NMS,(XMS(I),AMS(I),I=1,NMS)
      READ(5,1000) NF,(XF(I),AF(I),I=1,NF)
C  COEFFICIENTS FOR INITIAL STRESS IN PRESTRESSING STRANDS
      READ(5,1000)   (SK(I),I=1,NF)
C  TRANSFORM STEEL AREAS TO SQIN/IN
      DO 710 I=1,NMS
  710 AMS(I)=AMS(I)/12.
      DO 720 I=1,NF
  720 AF(I)=AF(I)/12.
C  NUMBER OF CONTROL STRAIN INTERVALS
      READ(5,1001)   N
      IR=1000
    1 CONTINUE
      WRITE(10'IR,3333) N
      IR=IR+1000
C  PIVOT POINT AND CONTROL POINT
      READ(5,1000)   X1,X2
      IF(X1.NE.X2) GO TO 55
      IZERO=0
      WRITE(10'IR-1000,3333) IZERO
      STOP
   55 CONTINUE
C  PIVOT STRAIN, EXTREME CONTROL STRAINS
      READ(5,1000) EX1,EX21,EX22
 1000 FORMAT(8G10.0)
 1001 FORMAT(I8)
      WRITE(6,1499) TITLE
 1499 FORMAT(1H0,20A4,/)
      WRITE(6,1500) H,FC,XK,E0,EU,SY,SU,
     1                             X1,X2,EX1,EX21,EX22
 1500 FORMAT(1H1,20X,'DATA',//,6X,'H=',E23.7,/,6X,'F''C=',E21.7,/,
     1   6X,'K=',E23.7,/,6X,'E0=',E22.7,/,6X,'EU=',E22.7,/,6X,
     2   'SY=',E22.7,/,6X,'SU=',E22.7,/,6X,
     5   'XPIVOT=',E18.7,/,6X,'XCONTROL=',E16.7,/,6X,'EXP=',
     6   E21.7,/,6X,'EXC1=',E20.7,/,6X,'EXC2=',E20.7)
      WRITE(6,1501)  (I,XMS(I),AMS(I),I=1,NMS)
 1501 FORMAT(1H0,5X,'BAR TYPE NO.',3X,'LOCATION',10X,'AREA',
     1  2X,'PRESTR. COEF.',//,(10X,'MILD',I3,2E14.3))
      WRITE(6,1502)  (I,XF(I),AF(I),SK(I),I=1,NF)
```

```
 1502 FORMAT(8X,'PRESTR.',I2,3E14.3)
C  BUILD CONCRETE CONSTITUTIVE EQUATIONS
      FT=XK*DSQRT(FC)
      EC=57000.*DSQRT(FC)
      E(1)=E0*(-1.+DSQRT(1.-FT/(.85*FC)))
      E(2)=0.
      E(3)=E0
      E(4)=EU
      AA(1)=0.
      BB(1)=0.
      CC(1)=0.
      AA(2)=.85*FC/(E0*E0)
      BB(2)=1.7*FC/E0
      CC(2)=0.
      AA(3)=-.85*FC/(E0*E0)
      BB(3)=1.7*FC/E0
      CC(3)=0.
      AA(4)=0.
C     BB(4)=-0.15*0.85*FC/(EU-E0)
      BB(4)=0.
C     CC(4)=(+1.+0.15*E0/(EU-E0))*0.85*FC
      CC(4)=0.85*FC
      AA(5)=0.
      BB(5)=0.
      CC(5)=0.
      N1=N+1
      WRITE(6,1700)
 1700 FORMAT(1H0,///,20X,'RESULTS',//,7X,'P',14X,'M',13X,'EC1',
     1   12X,'EC2',13X,'FI',/,22X,'MILD STEEL STRAINS',40X,
     2    'PRESTR. BARS STRAINS',//)
      DO 100 I=1,N1
      EX2=EX21+(I-1)*(EX22-EX21)/N
      ECA=EX1-(EX2-EX1)*X1/(X2-X1)
      ECB=EX1+(EX2-EX1)*(H-X1)/(X2-X1)
      DO 730 J=1,NMS
  730 EST(J)=EX1+(EX2-EX1)*(XMS(J)-X1)/(X2-X1)
      DO 740 J=1,NF
  740 EF(J)=EX1+(EX2-EX1)*(XF(J)-X1)/(X2-X1)
      CALL CNCRT(ECB,ECA,H,E,BMOM,P)
      DO 750 J=1,NMS
  750 PS(J)=SIGMAS(SY,EST(J))
      DO 760 J=1,NF
  760 PF(J)=SIGMAF(SU,SK(J),EF(J))
      PSTOT=0.
      PSMOM=0.
      DO 770 J=1,NMS
      PSTOT=PSTOT+PS(J)*AMS(J)
  770 PSMOM=PSMOM+PS(J)*AMS(J)*(XMS(J)-H/2.)
      PFTOT=0.
      PFMOM=0.
      DO 780 J=1,NF
      PFTOT=PFTOT+PF(J)*AF(J)
  780 PFMOM=PFMOM+PF(J)*AF(J)*(XF(J)-H/2.)
      PT=P+PSTOT+PFTOT
      BMOMT=BMOM+PSMOM+PFMOM
C TRANSFORM BACK TO 12 IN WIDTH
      PT=12.*PT
      FI=(ECB-ECA)/H
      WRITE(6,2000) PT,BMOMT,ECA,ECB,FI
      WRITE(6,2001)   (EST(J),J=1,NMS)
```

```
      WRITE(6,2002)   (EF(J),J=1,NF)
 2001 FORMAT(5E12.4)
 2002 FORMAT(1H+,59X,5E12.4)
      WRITE(10'IR,3333) BMOMT,PT
 3333 FORMAT(8G20.7)
      IR=IR+1000
  100 CONTINUE
 2000 FORMAT(8E15.4)
      GO TO 1
      END
      FUNCTION SIGMAB(EA,E)
      IMPLICIT REAL*8(A-H,O-Z)
      DIMENSION E(4)
      COMMON/CNSTEQ/AA(5),BB(5),CC(5)
      IND=1
      DO 10 I=1,4
   10 IF(EA.GT.E(I)*1.000001)    IND=IND+1
      SIGMAB=AA(IND)*EA*EA + BB(IND)*EA + CC(IND)
      RETURN
      END
      FUNCTION SINT(IND,Z1,Z2,EA,EB,H)
      IMPLICIT REAL*8(A-H,O-Z)
      COMMON/CNSTEQ/AA(5),BB(5),CC(5)
      A=(EA-EB)*Z1/H+(EA+EB)/2.
      B=(EA-EB)*Z2/H+(EA+EB)/2.
      SINT=AA(IND)*(B**3-A**3)/3. + BB(IND)*(B*B-A*A)/2. +
     1      CC(IND)*(B-A)
      SINT=SINT*H/(EA-EB)
      RETURN
      END
      FUNCTION SZINT(IND,Z1,Z2,EA,EB,H)
      IMPLICIT REAL*8(A-H,O-Z)
      COMMON/CNSTEQ/AA(5),BB(5),CC(5)
      A=(EA-EB)*Z1/H+(EA+EB)/2.
      B=(EA-EB)*Z2/H+(EA+EB)/2.
      SZINT=AA(IND)*(B**4-A**4)/4. + BB(IND)*(B**3-A**3)/3. +
     1      CC(IND)*(B*B-A*A)/2.
      SZINT=SZINT*(H/(EA-EB))**2 - (EA+EB)*0.5*H*SINT(IND,Z1,Z2,
     1      EA,EB,H)/(EA-EB)
      RETURN
      END
      SUBROUTINE CNCRT(EEA,EEB,H,E,BMOM,P)
      IMPLICIT REAL*8(A-H,O-Z)
      DIMENSION E(4),ZE(4)
      EA=DMAX1(EEA,EEB)
      EB=DMIN1(EEA,EEB)
      IF(DABS(EA-EB).GT.1.0 D-06)   GO TO 100
   10 BMOM=0.
      P=SIGMAB(EA,E)*H
      RETURN
  100 DO 105 I=1,4
  105 ZE(I)=(E(I)-0.5*(EA+EB))*H/(EA-EB)
      A=-0.5*H
      BMOM=0.
      P=0.
      IND=1
      DO 110  I=1,4
      IF(A.GE.ZE(I))   GO TO 109
      IF(ZE(I).GE.H/2.)   GO TO 120
      P=P+SINT(IND,A,ZE(I),EA,EB,H)
```

```
      BMOM=BMOM+SZINT(IND,A,ZE(I),EA,EB,H)
      A=ZE(I)
  109 IND=IND+1
  110 CONTINUE
  120 P=P+SINT(IND,A,H/2.,EA,EB,H)
      BMOM=BMOM+SZINT(IND,A,H/2.,EA,EB,H)
      IF(EEA.LT.EEB) BMOM=-BMOM
      RETURN
      END
      FUNCTION SIGMAS(SY,E)
      IMPLICIT REAL*8(A-H,O-Z)
      SIGMAS=0.
      IF(E.EQ.0.0) RETURN
      SIGMAS=SY*E/DABS(E)
      IF(DABS(E).LT.SY/29.6 E06) SIGMAS=29.6 E06*E
      RETURN
      END
      FUNCTION SIGMAF(SU,SK,EP)
      IMPLICIT REAL*8(A-H,O-Z)
      EK=SK*SU/29.6 E06
      IF(SK.GT.0.7)  EK=EK+0.2*(SK-0.7)**2
      E=EP-EK
      SIGMAF=29.6 E06*E
      IF(DABS(E).GT.0.7*SU/29.6 E06) SIGMAF=SU*(.6784+
     1          DSQRT(5.*DABS(E)-.02978))*E/DABS(E)
      SIGMAF=SIGMAF+SK*SU
      IF(DABS(SIGMAF).GT.SU*1.000001)  SIGMAF=0.
      RETURN
      END
```

APPENDIX K

Interaction Curves at Selected Locations

List of Figures for Appendix K

(Note: See Sect. 3.5 for section designations)

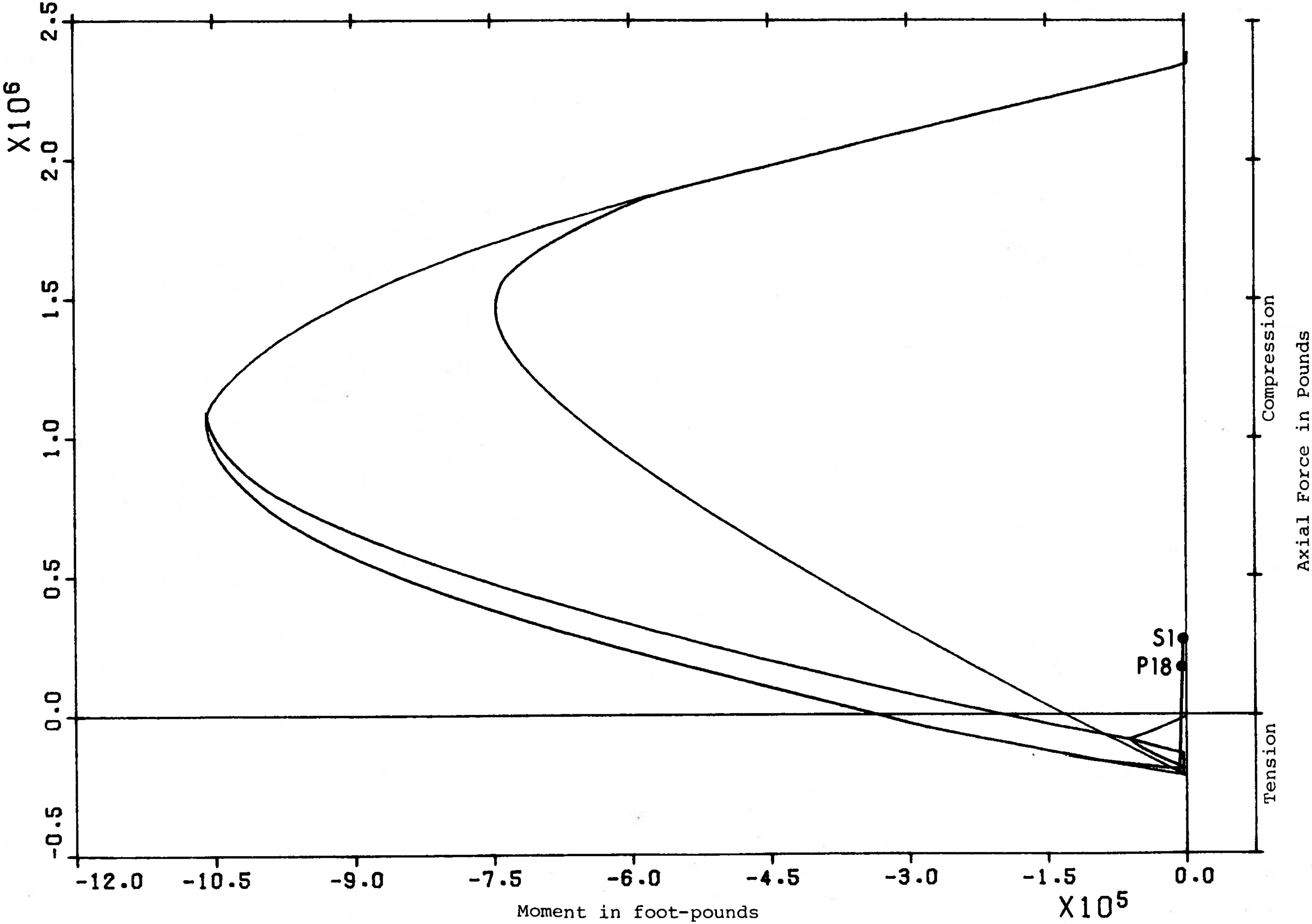

FIGURE K1 Interaction Curve for Section W3H

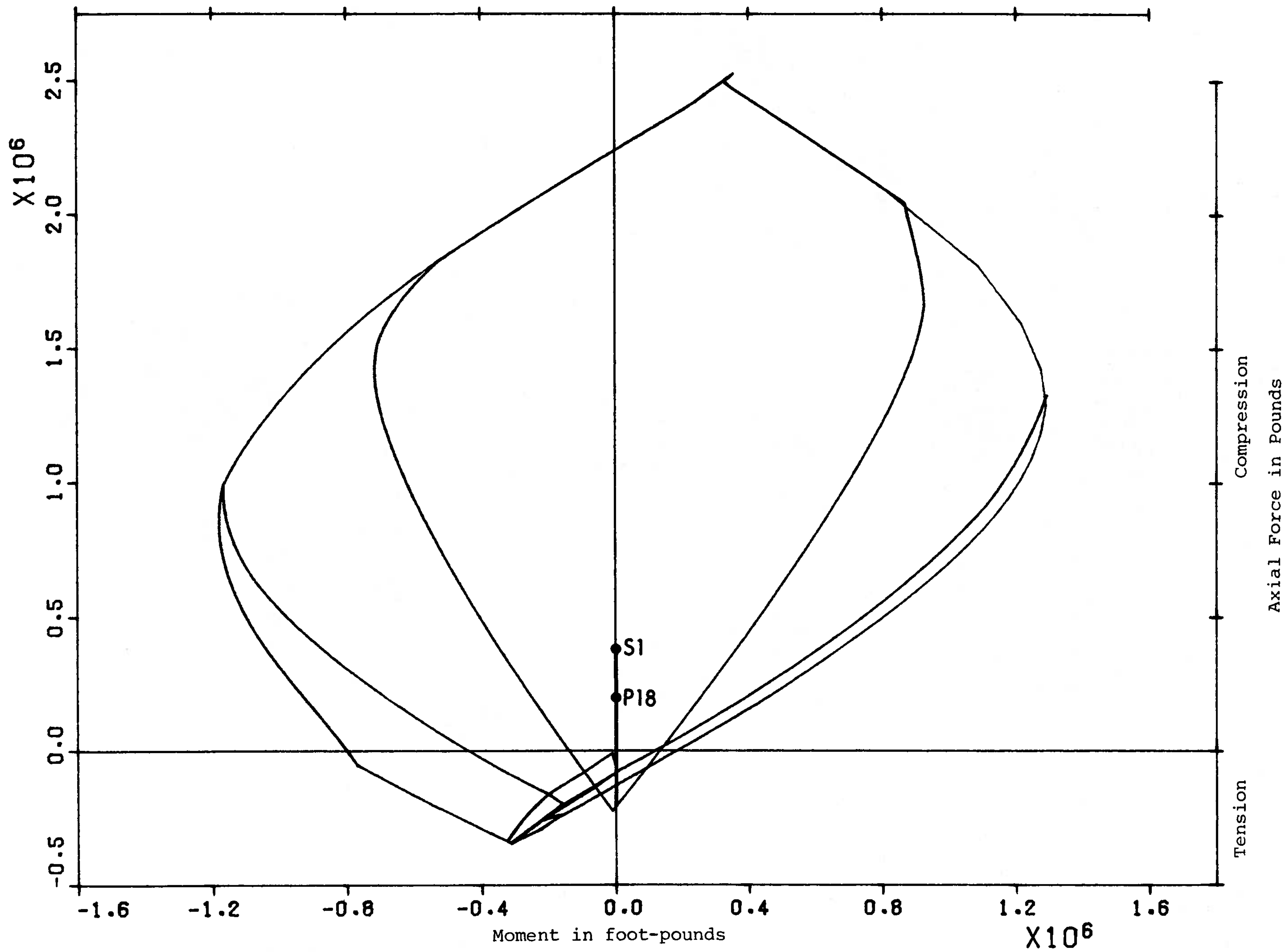

FIGURE K2. Interaction Curve for Section W3V

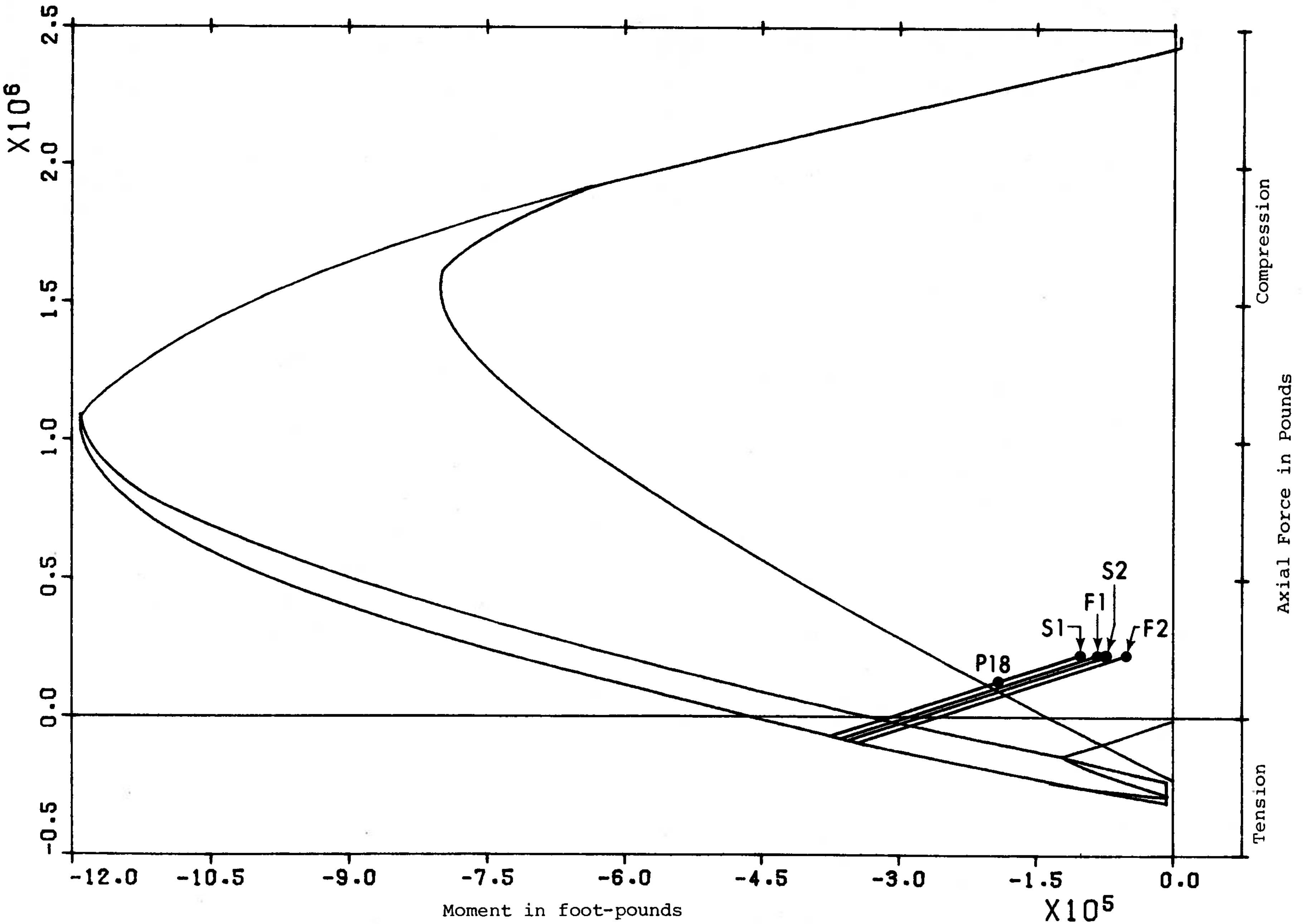

FIGURE K3 Interaction Curve for Section W5H

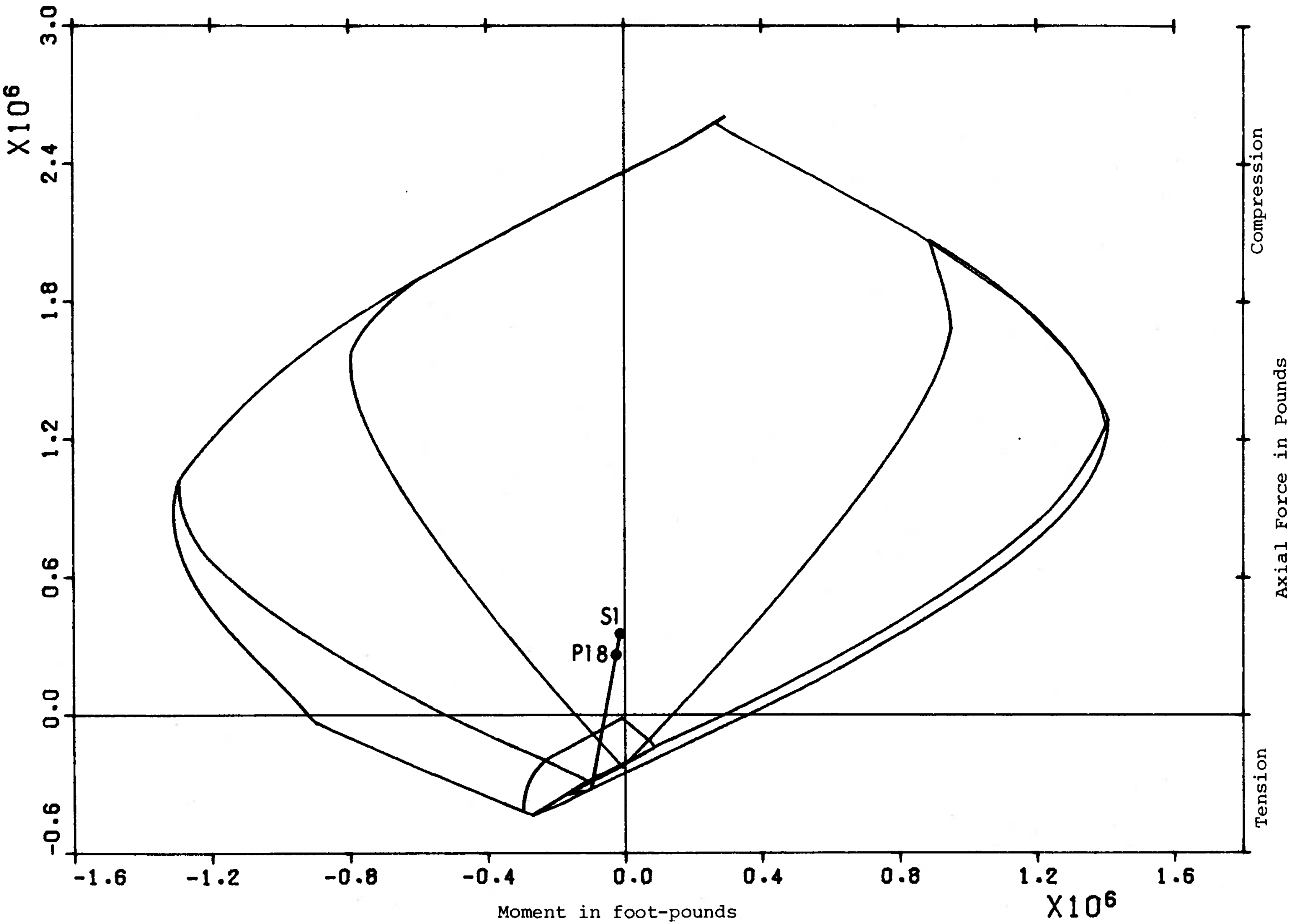

FIGURE K4 Interaction Curve for Section W5H

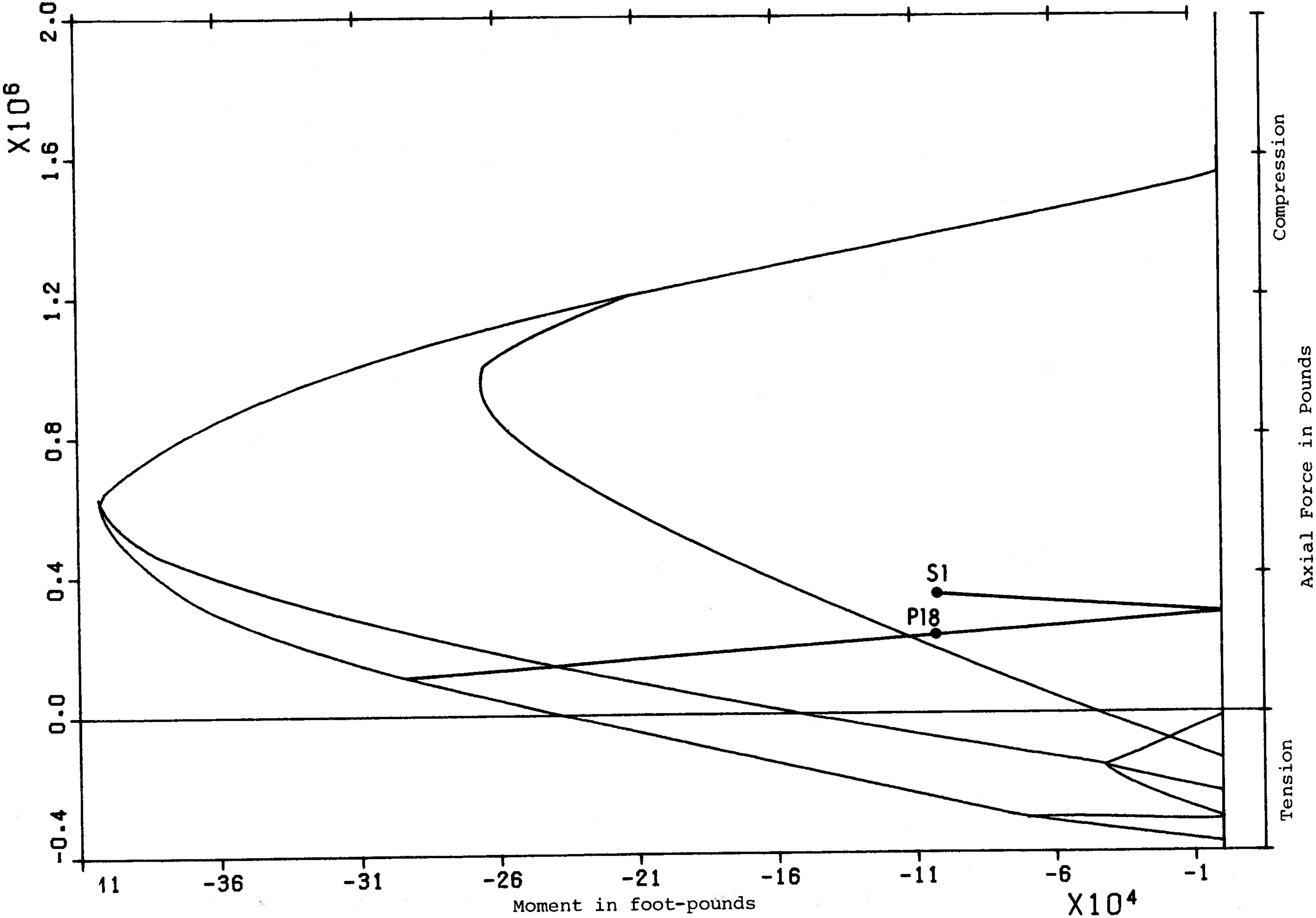

FIGURE K5 Interaction Curve for Section UD1H

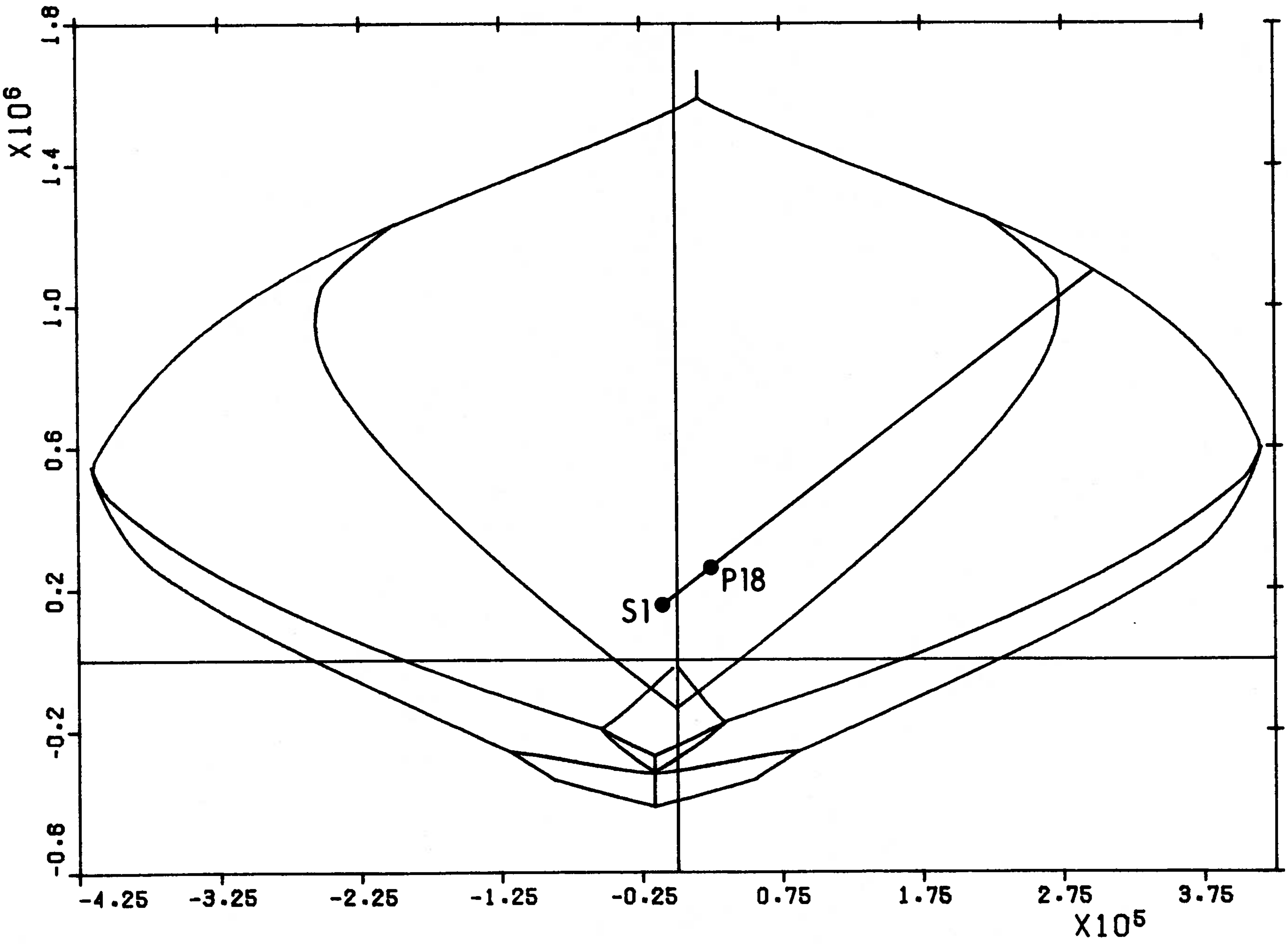

FIGURE K6 Interaction Curve for Section UDIV

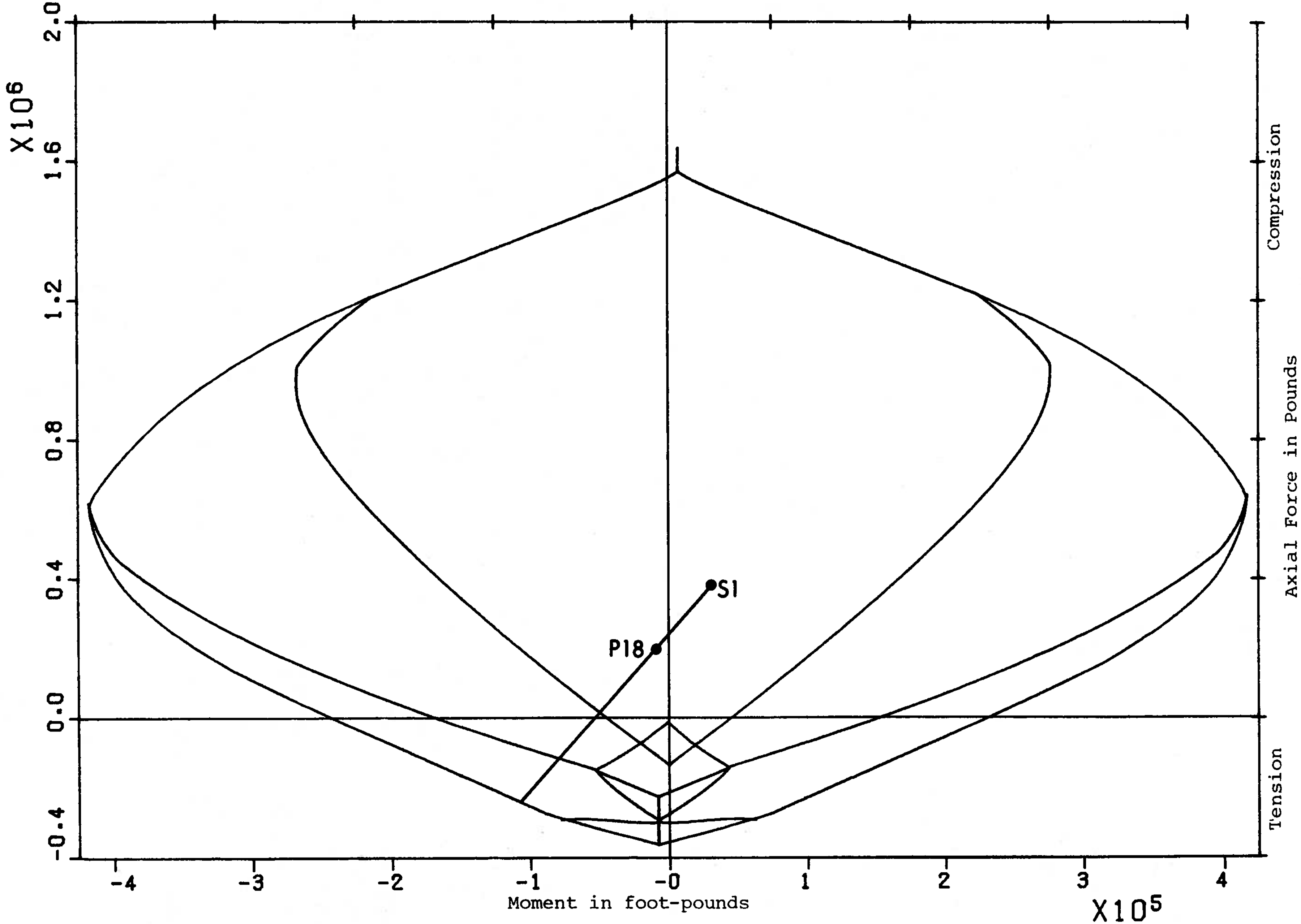

FIGURE K7 Interaction Curve for Section UD2H

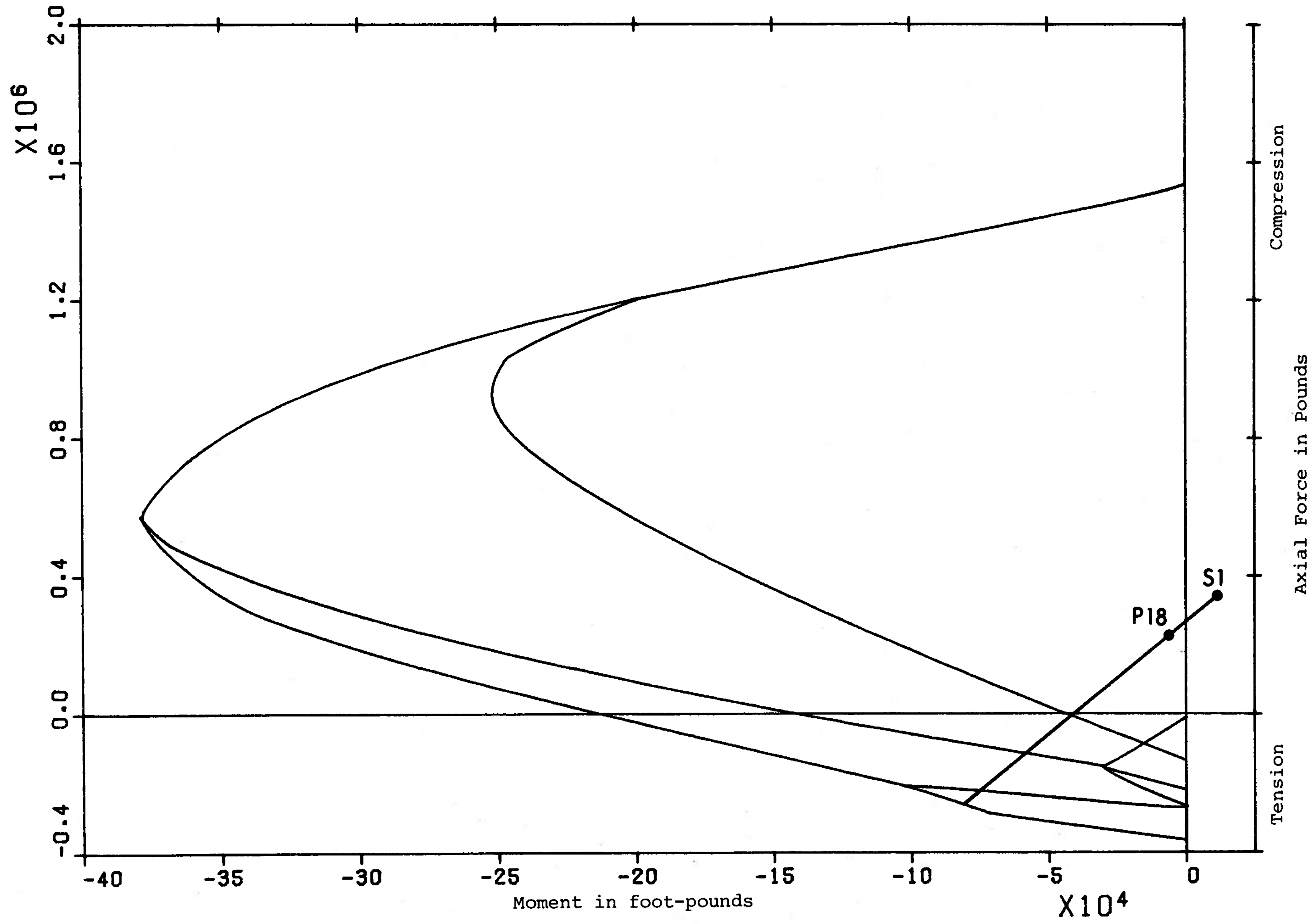

FIGURE K8 Interaction Curve for Section UD2V

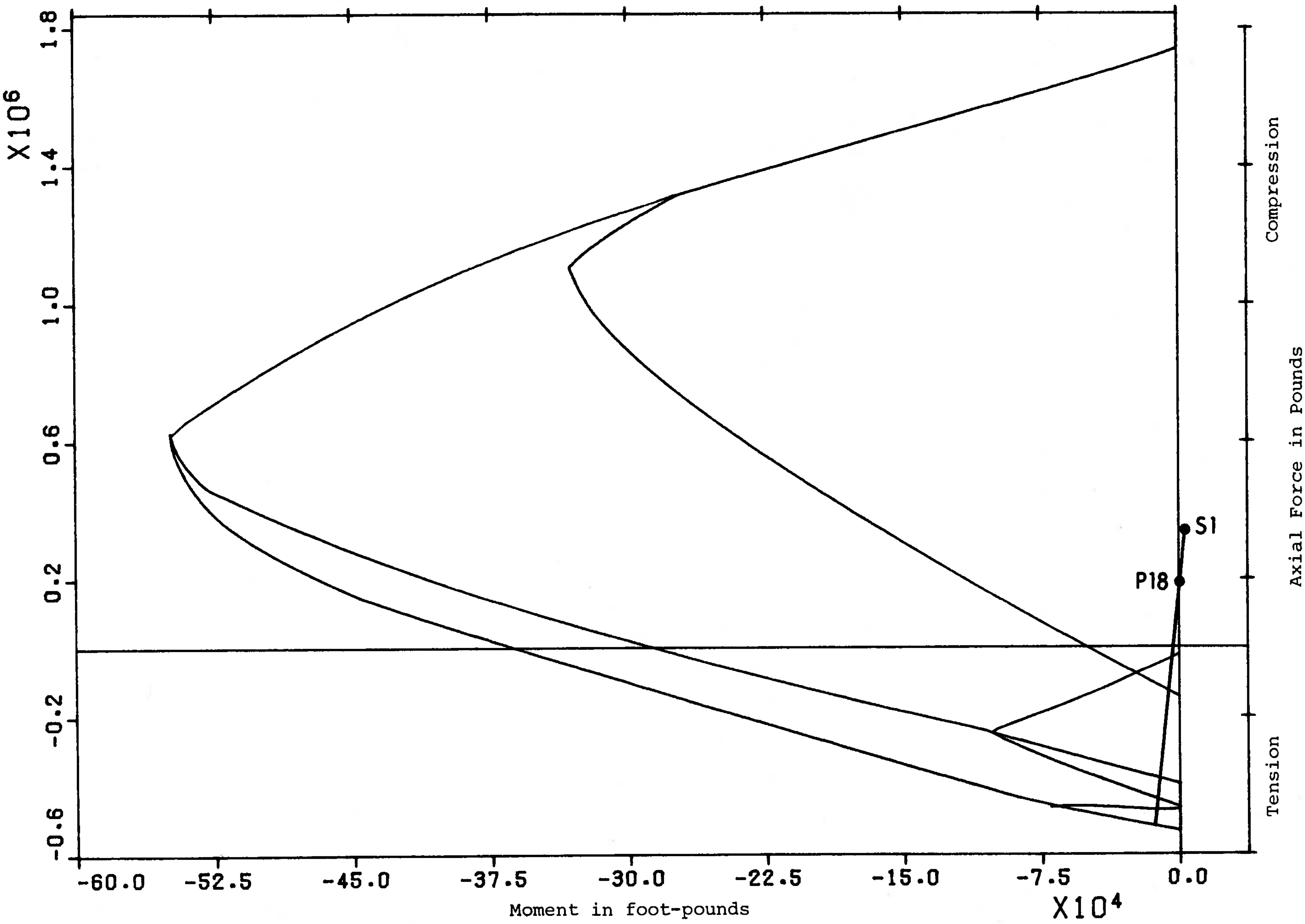

FIGURE K9 Interaction Curve for Section UD3H

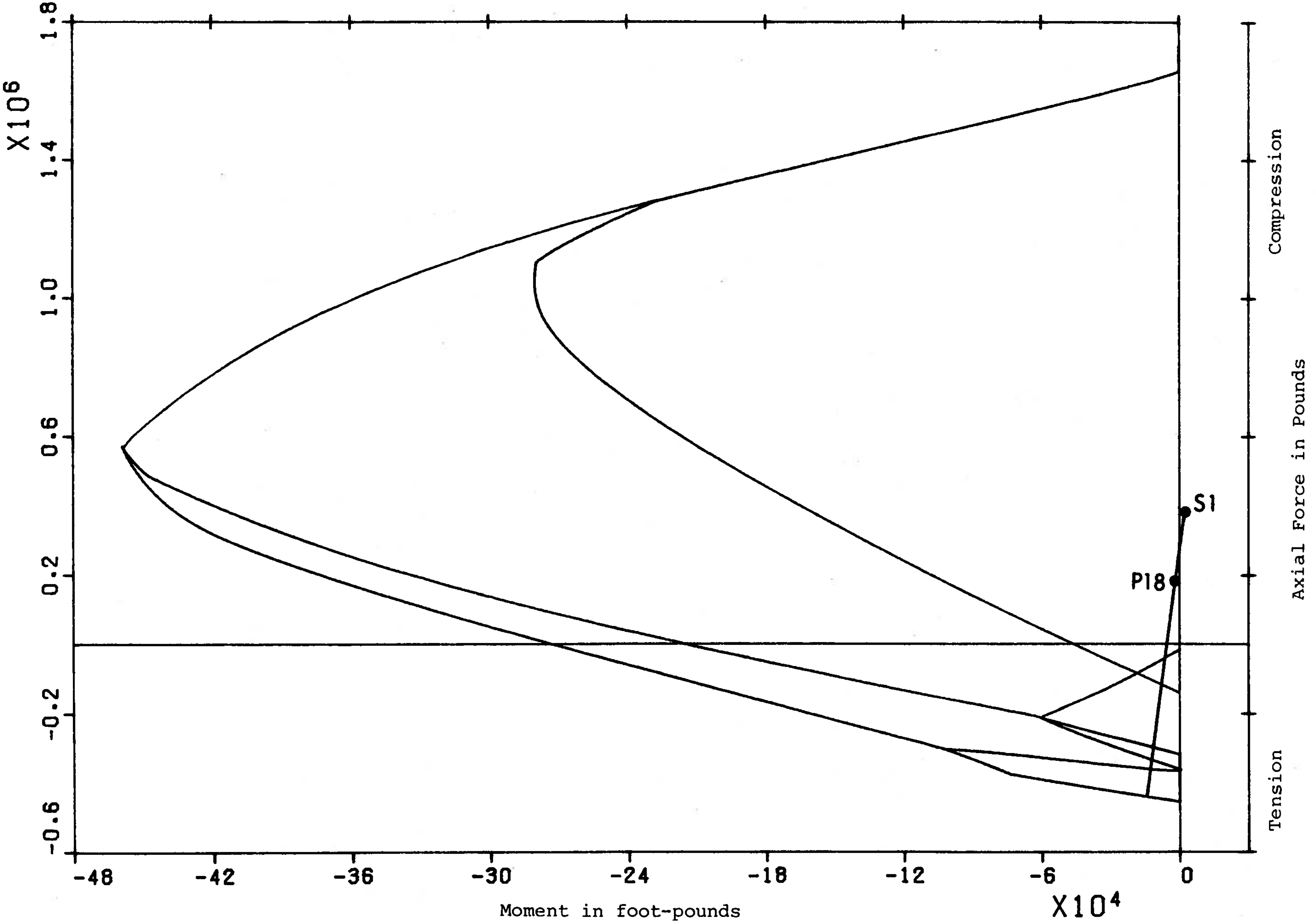

FIGURE K10 Interaction Curve for Section UD3V

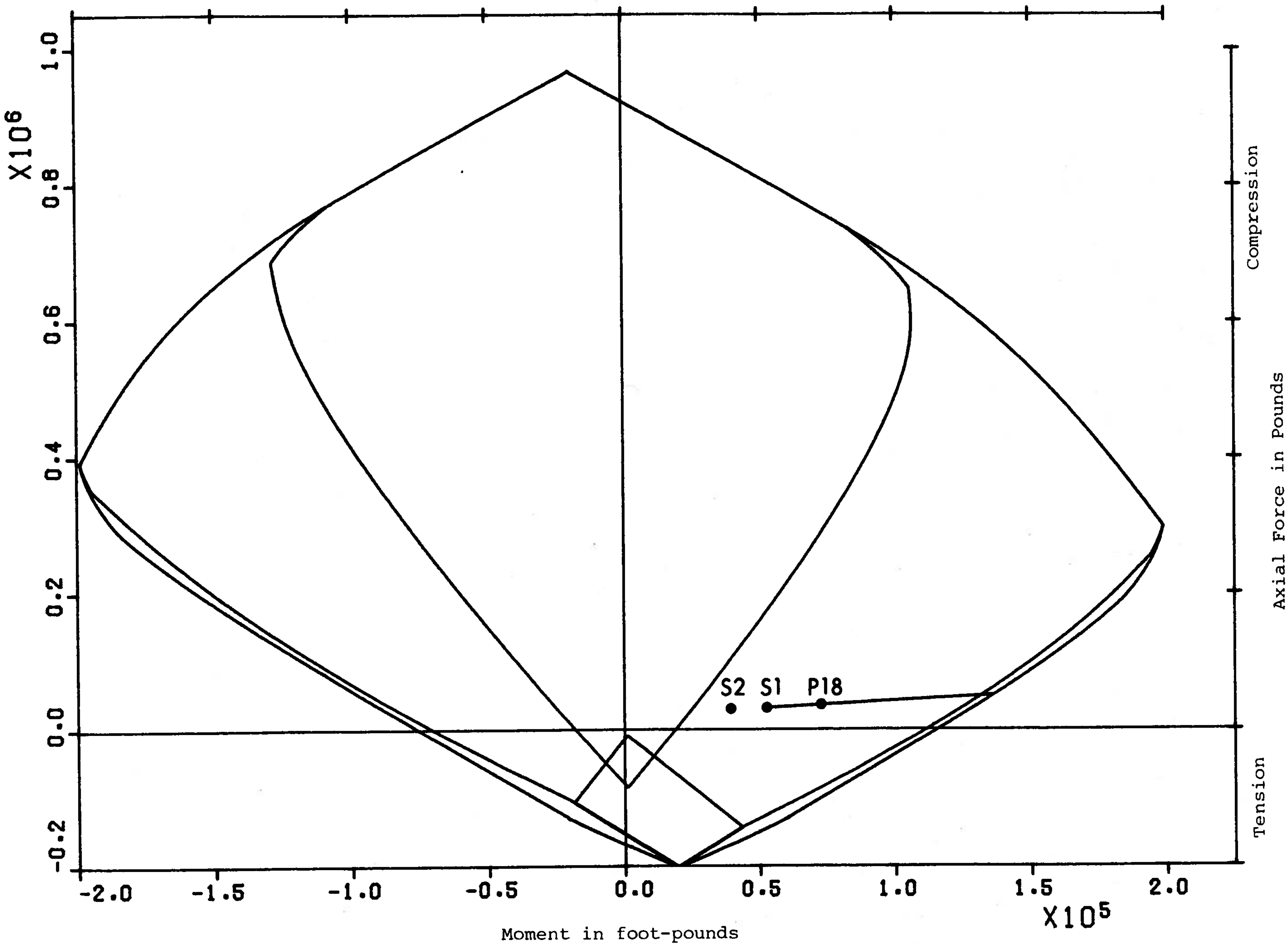

FIGURE K11 Interaction Curve for Section LD1H

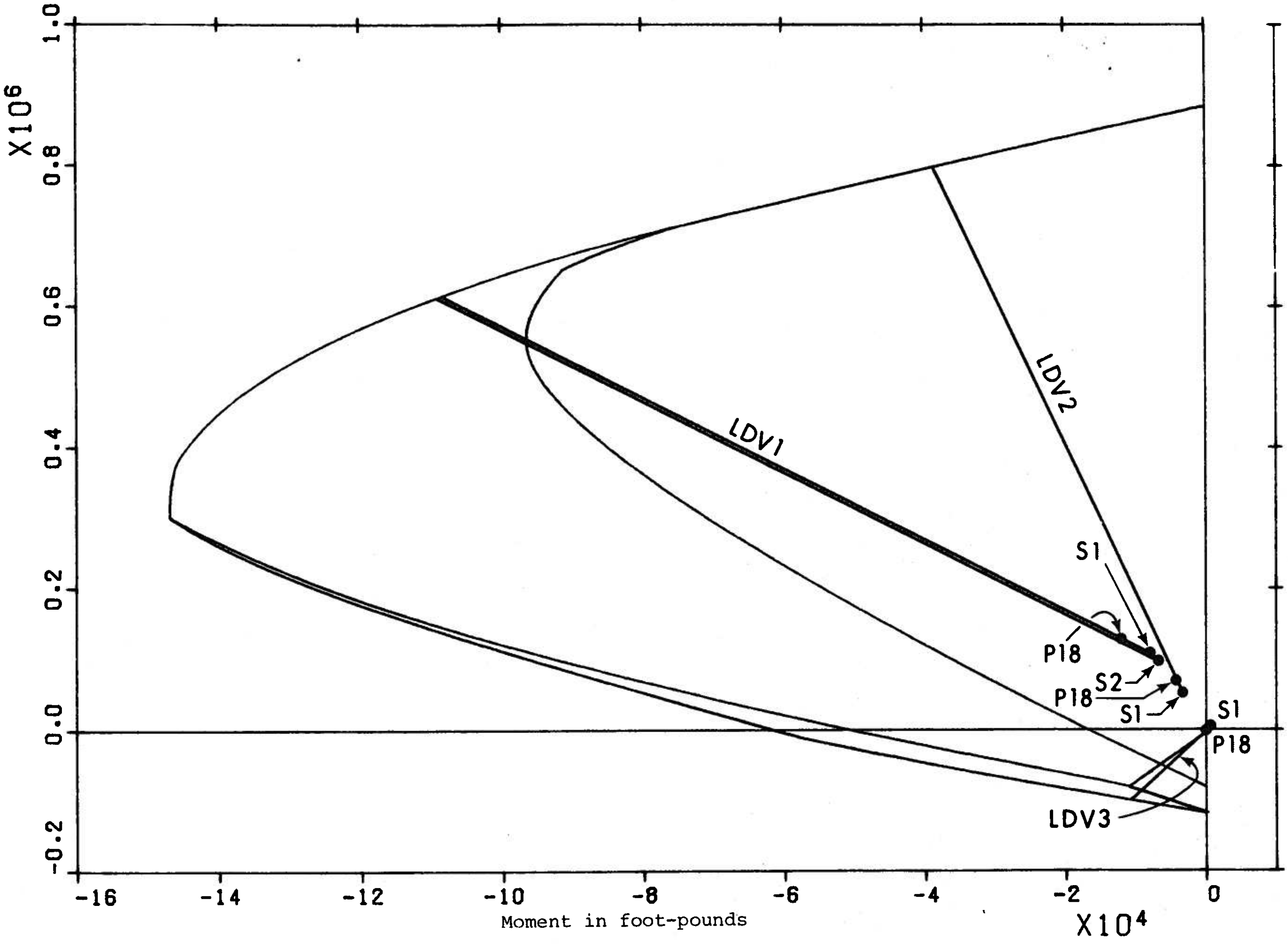

FIGURE K12 Interaction Curve for LDV Sections

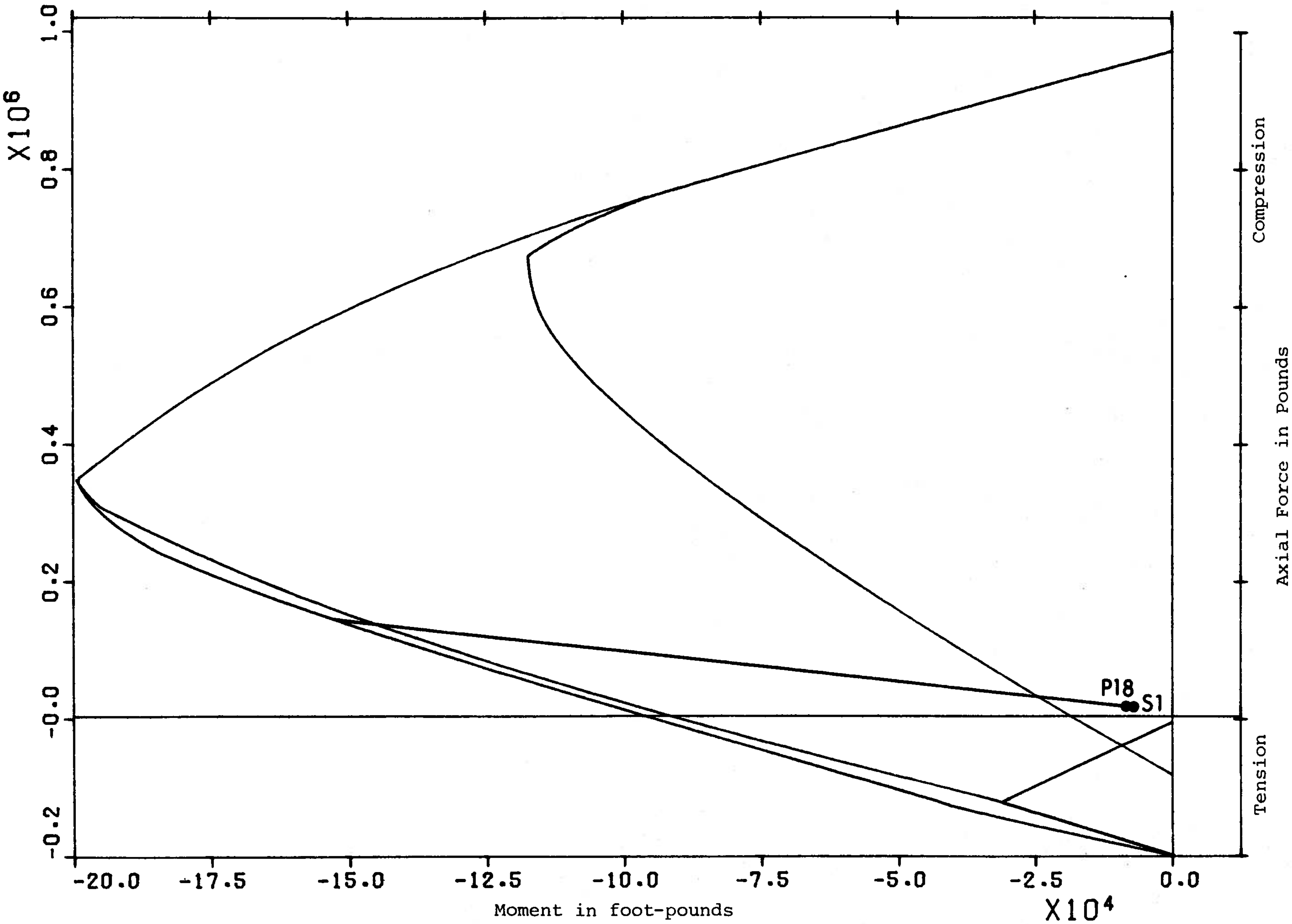

FIGURE K13 Interaction Curve for Section LD2H

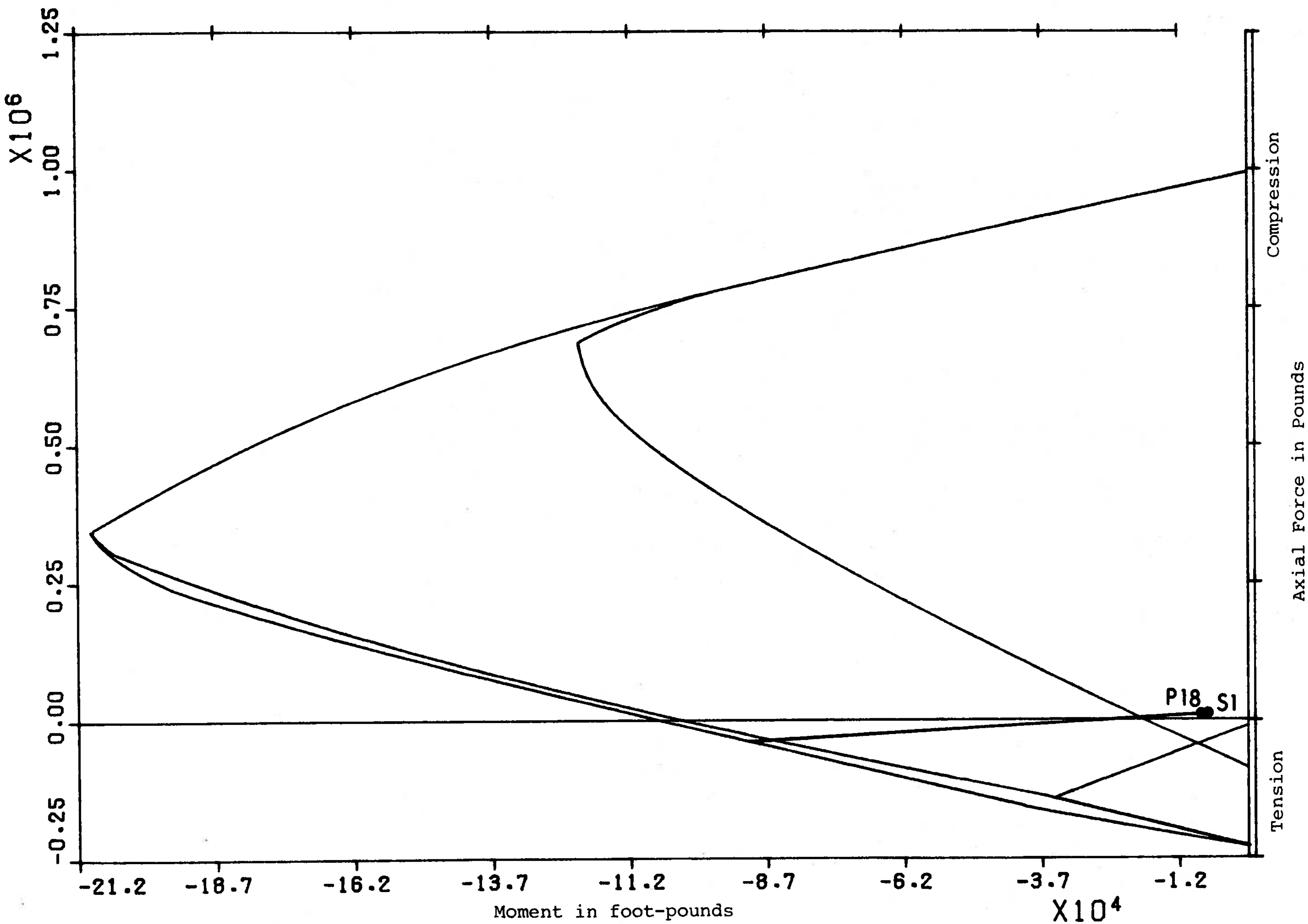

FIGURE K14 Interaction Curve for Section LD3H

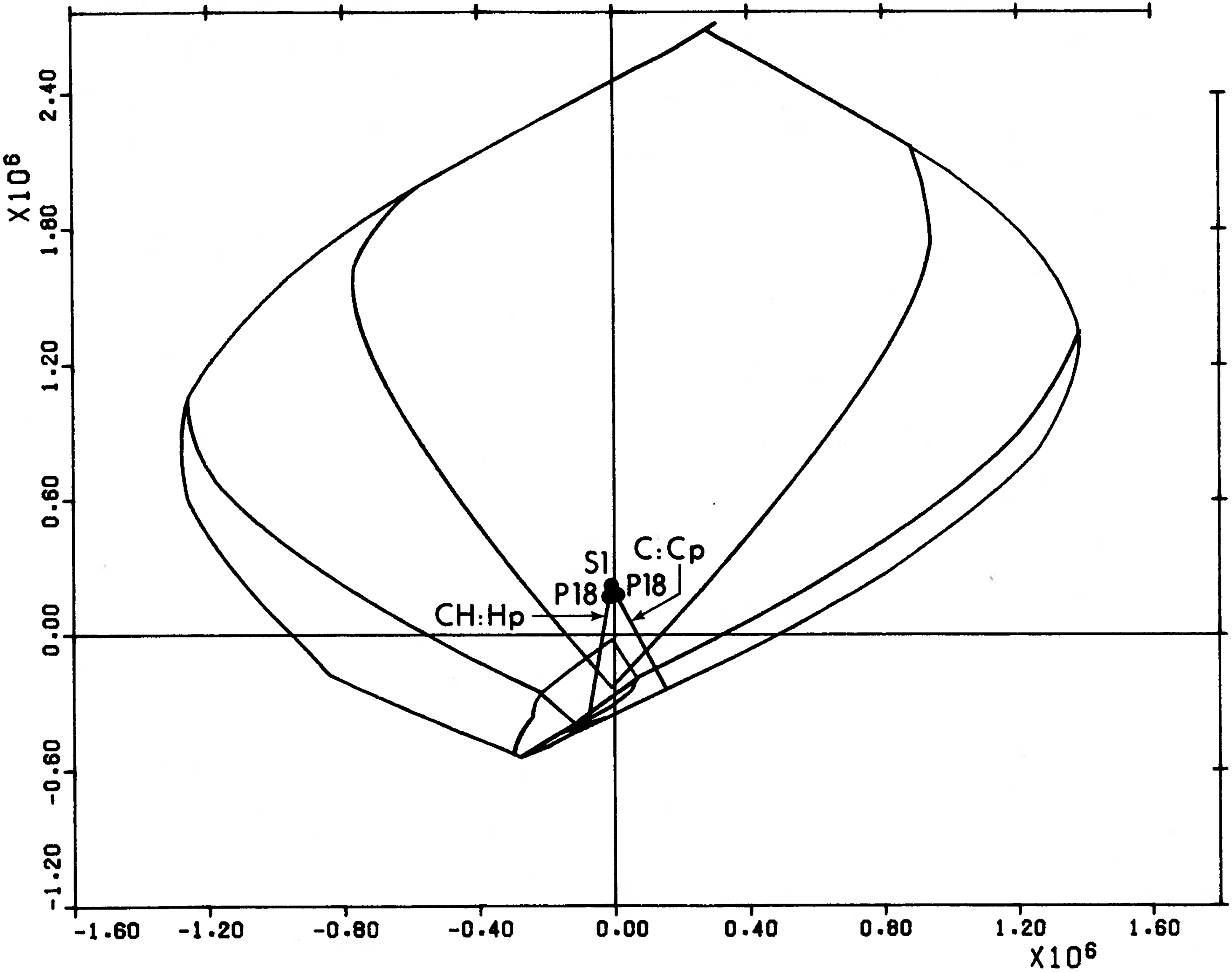

FIGURE K15 Interaction Curve for Section W2V

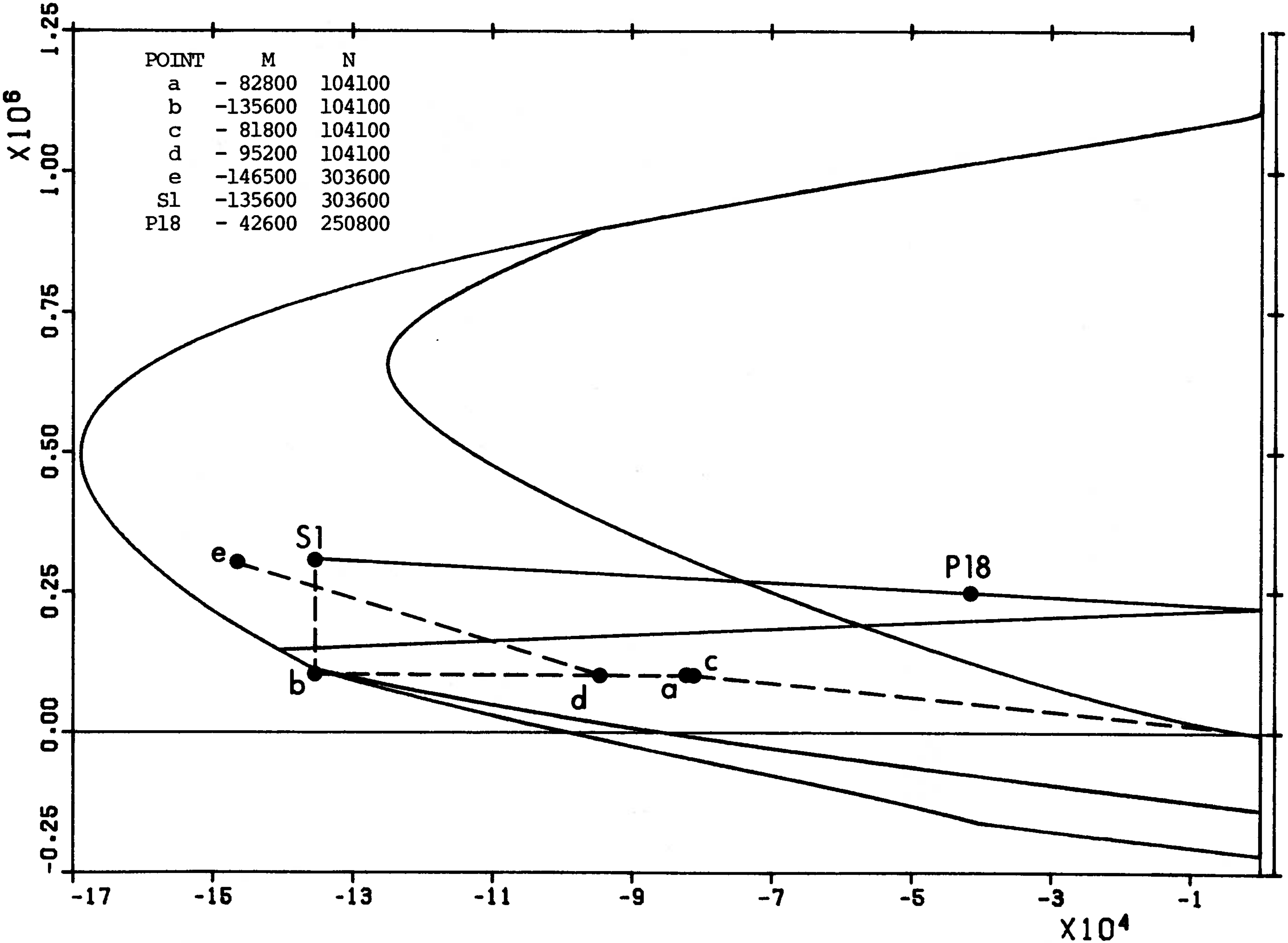

FIGURE K16 Interaction Curve for Section W1H

APPENDIX L

Results of Cracking Analysis at Selected Locations

List of Figures for Appendix L

(Note: See Sect. 3.5 for section designations)

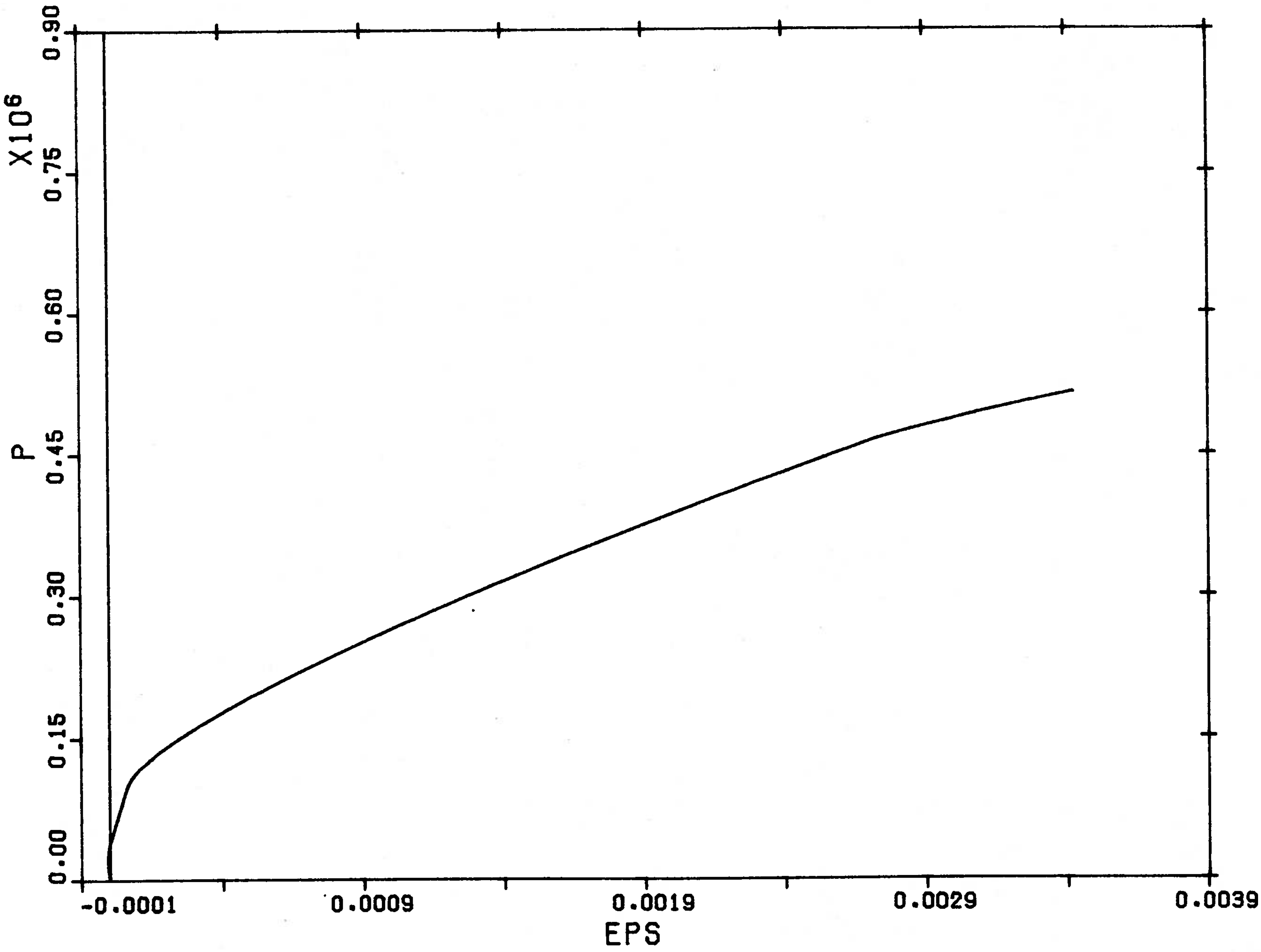

FIGURE L1 P vs ε for Section W1h

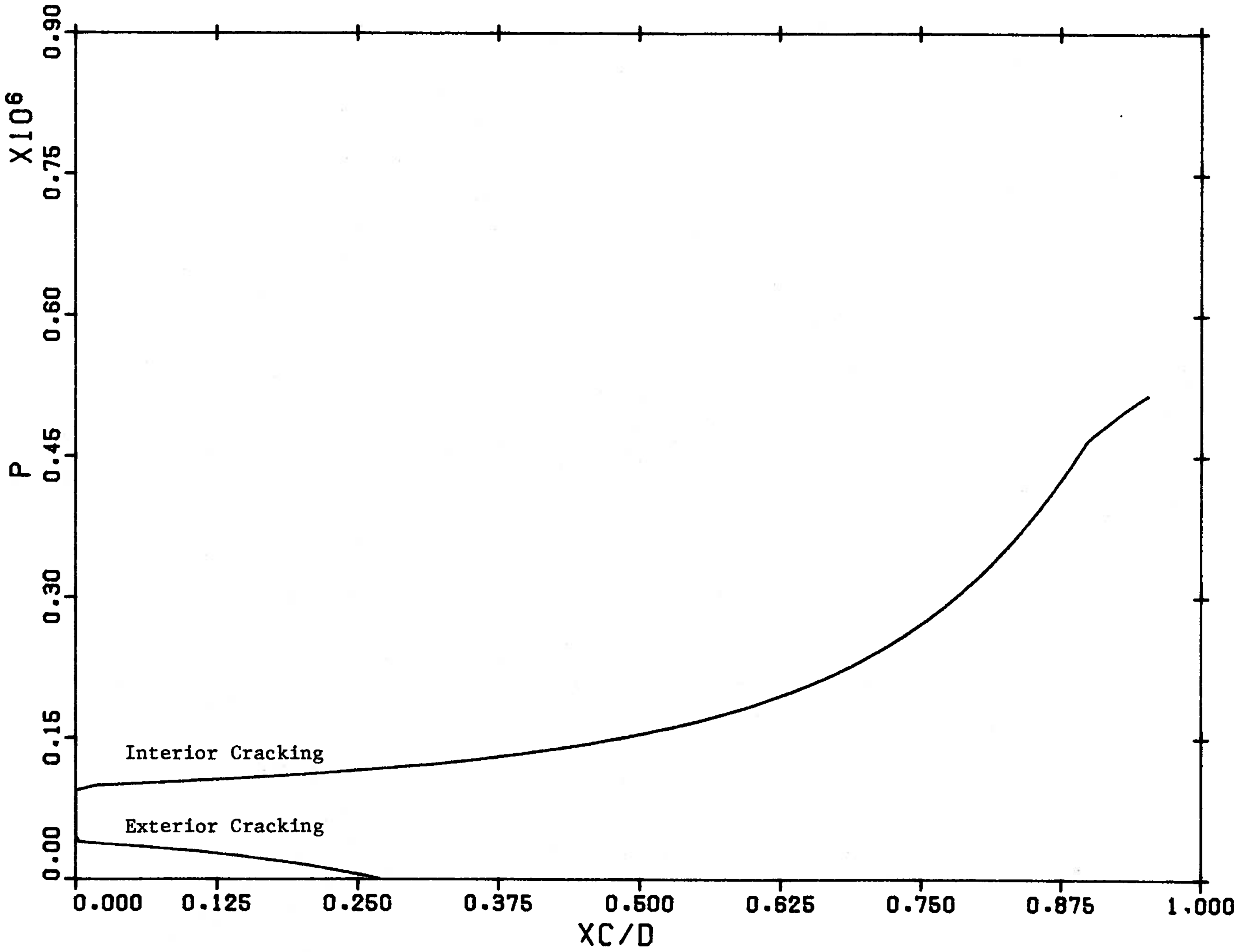

FIGURE L2 x_c/d for Section W1H

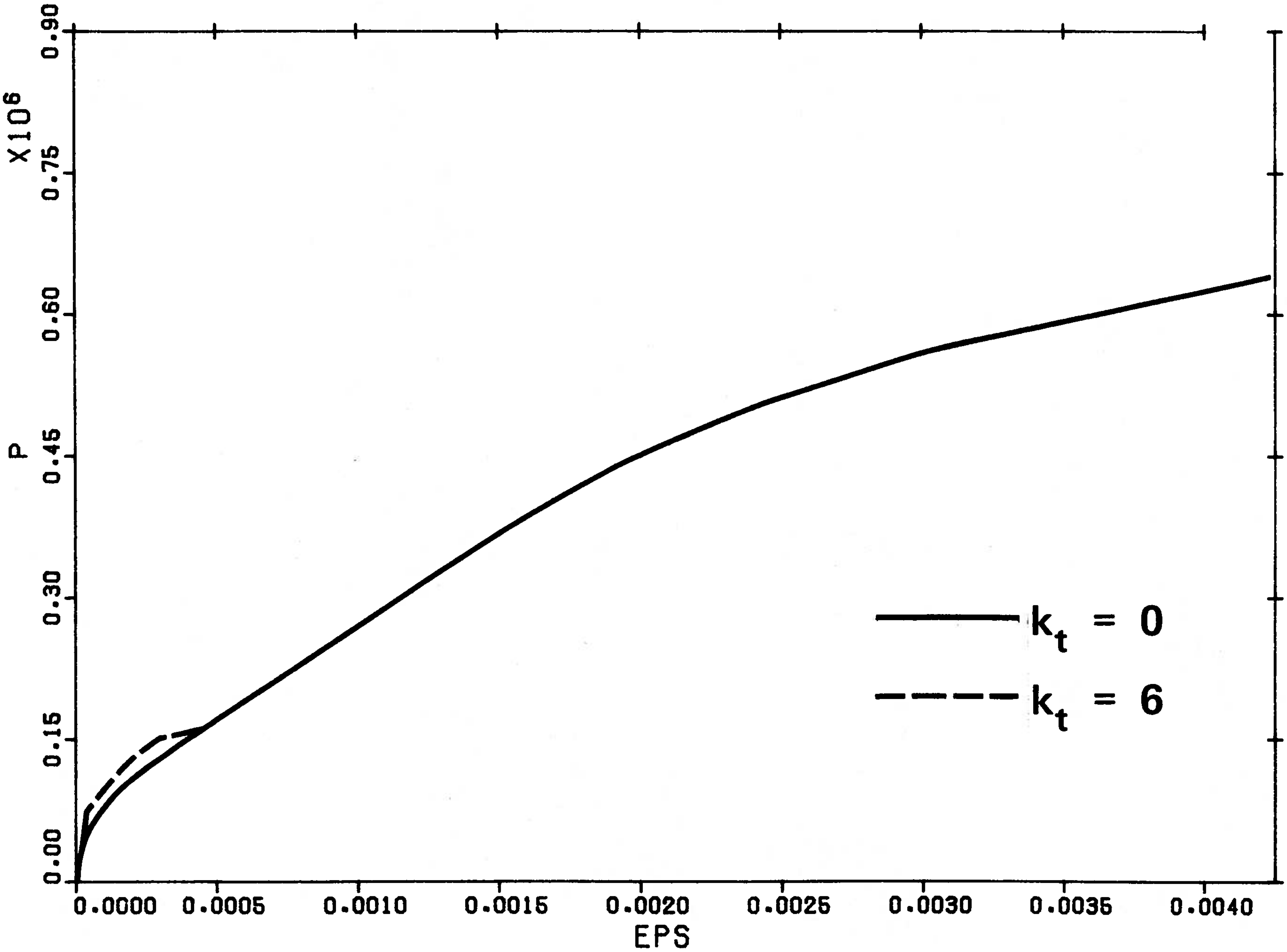

FIGURE L3 P vs ε for Section W1V

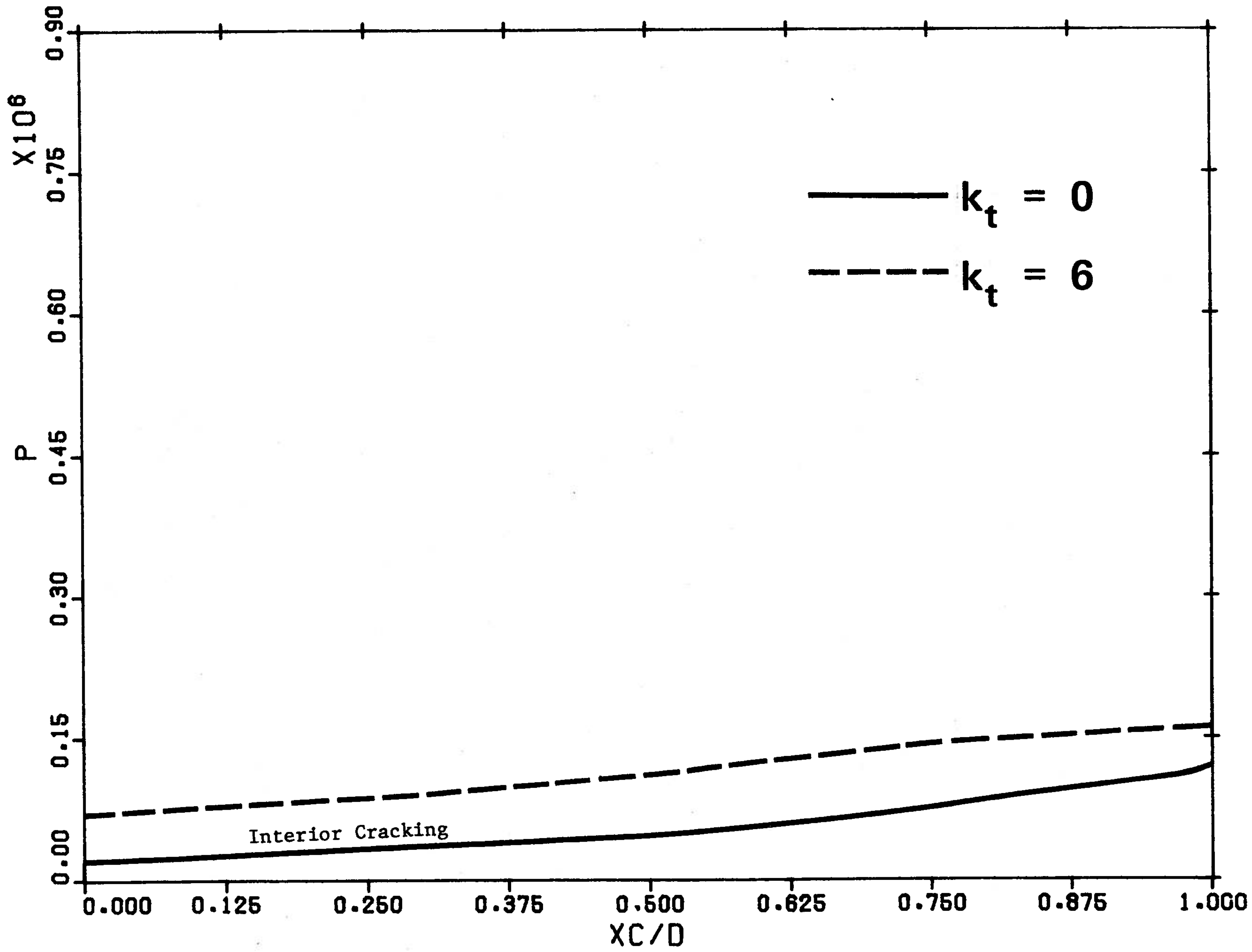

FIGURE L4 x_c/d for Section W1V

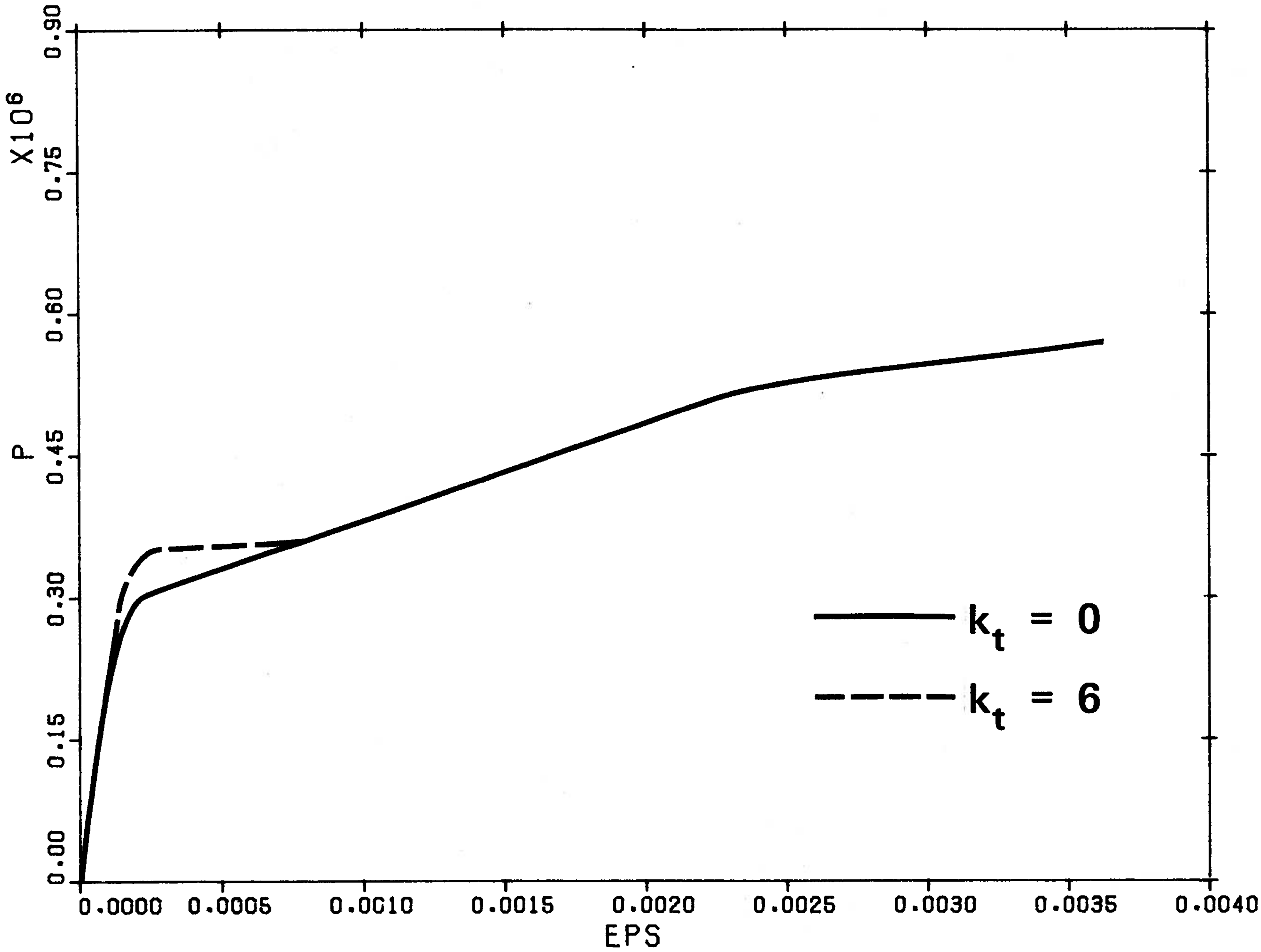

FIGURE L5 P vs ε for Section W2H

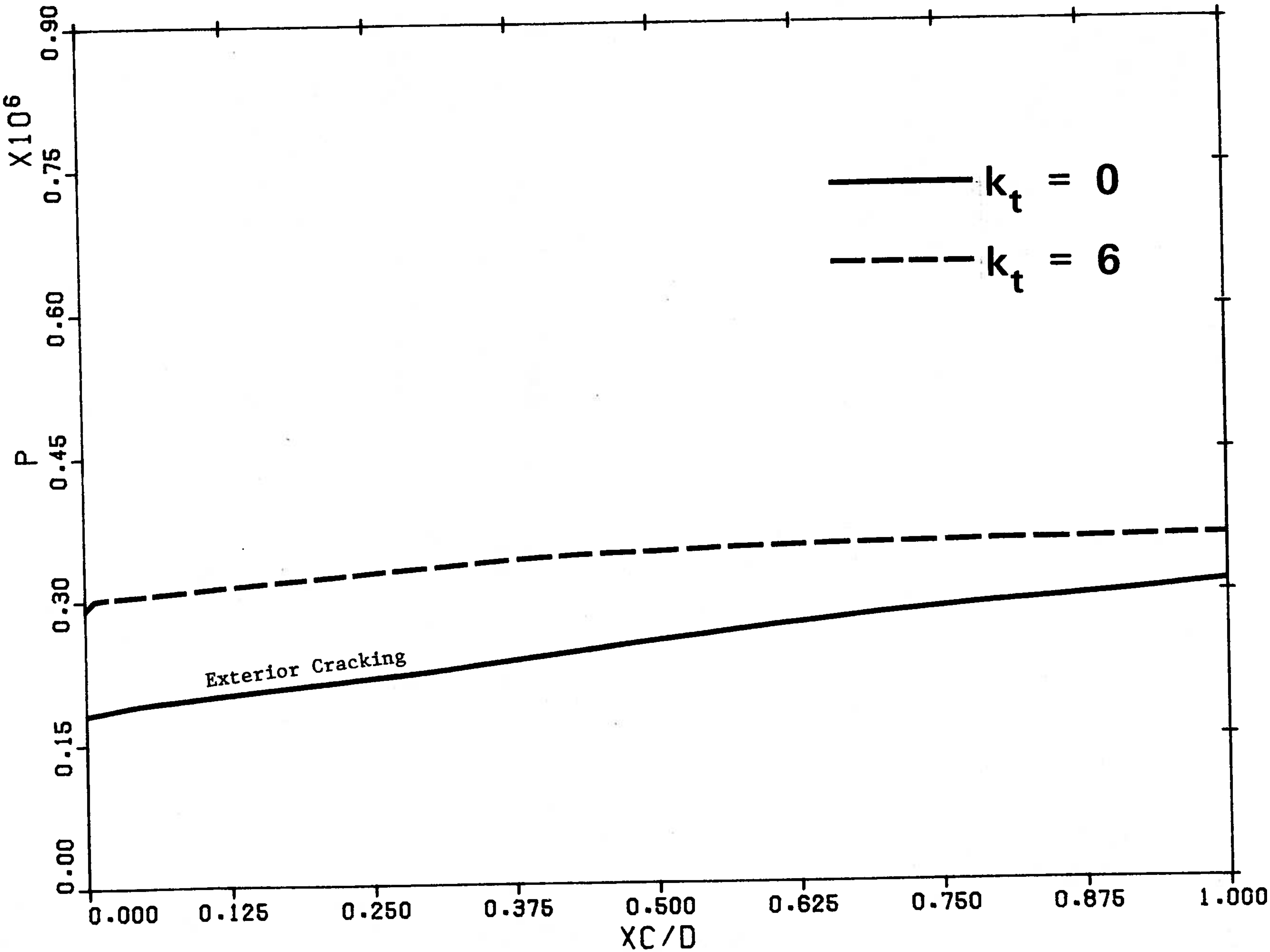

FIGURE L6 x_c/d for Section W2H

*

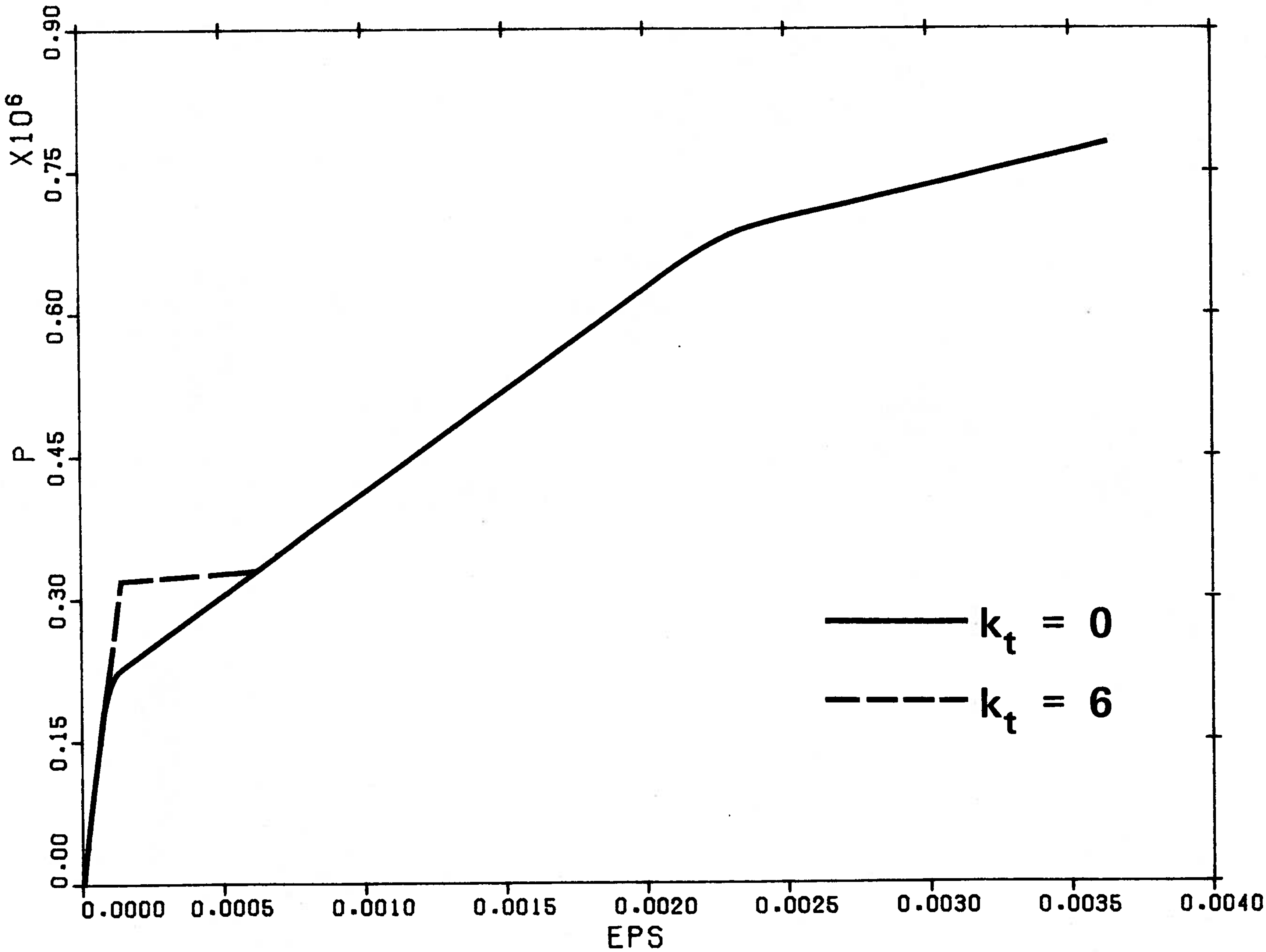

FIGURE L7 P vs ε for Section W2V

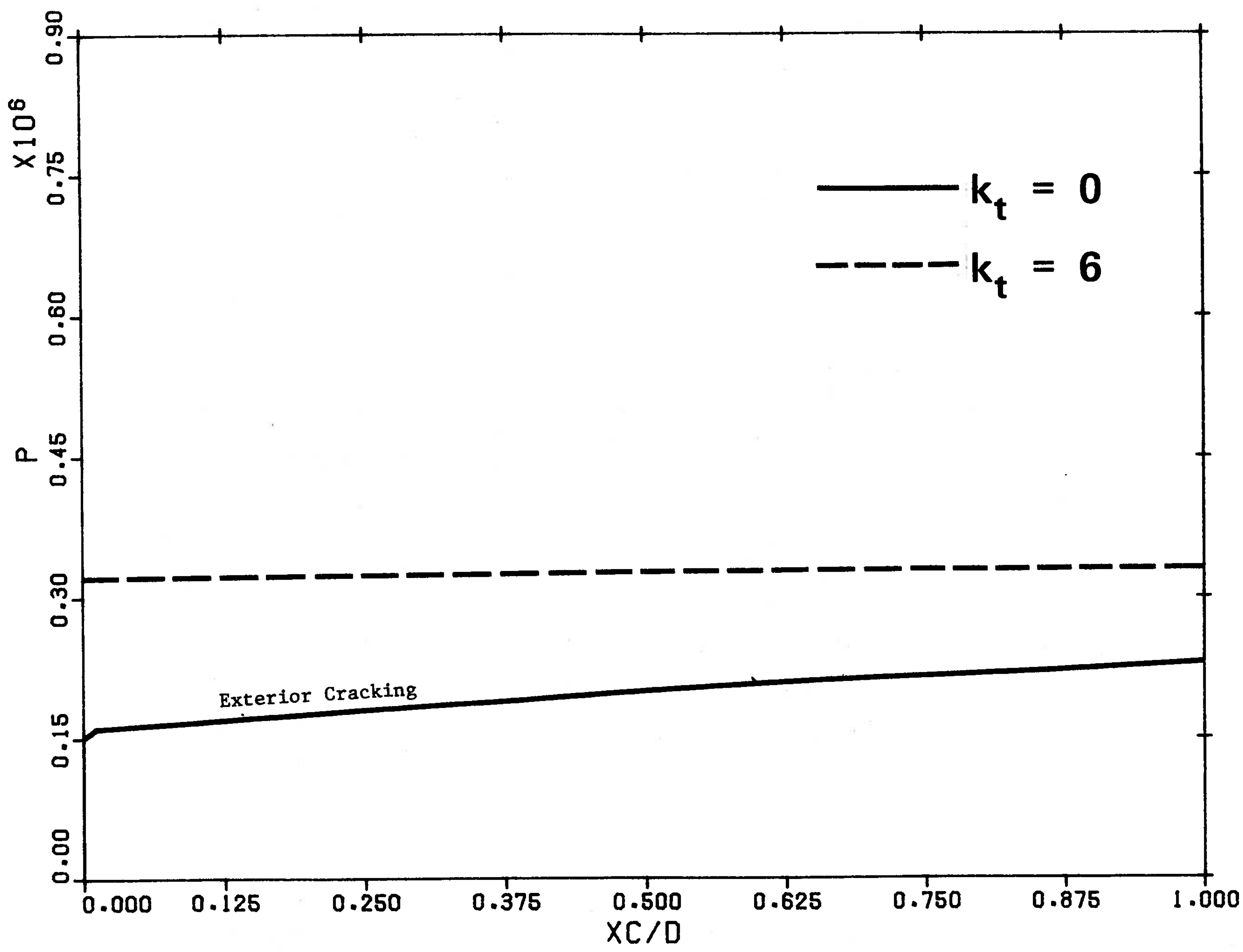

FIGURE L3 x_c/d for Section W2V

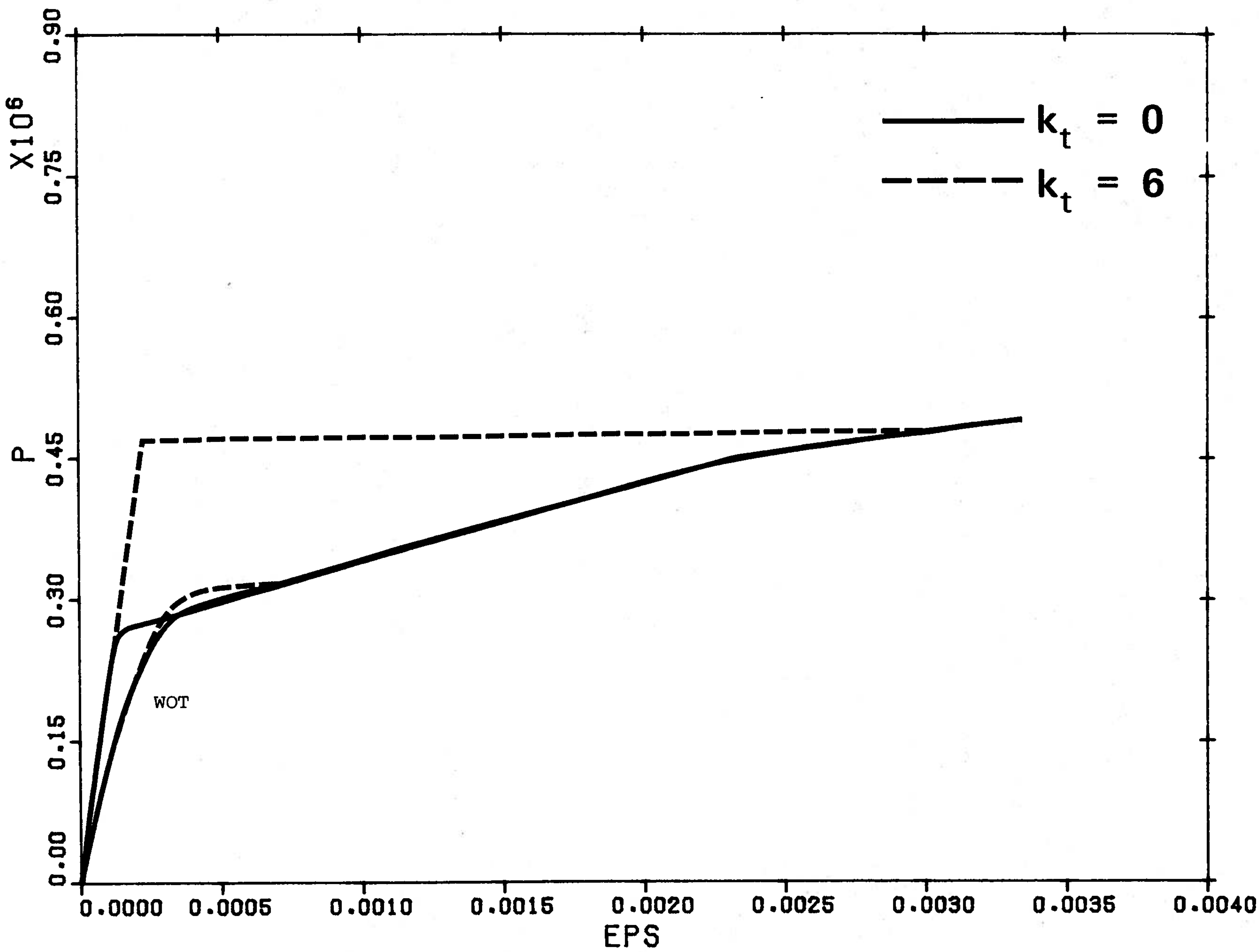

FIGURE L9 P vs ε for Section W3H

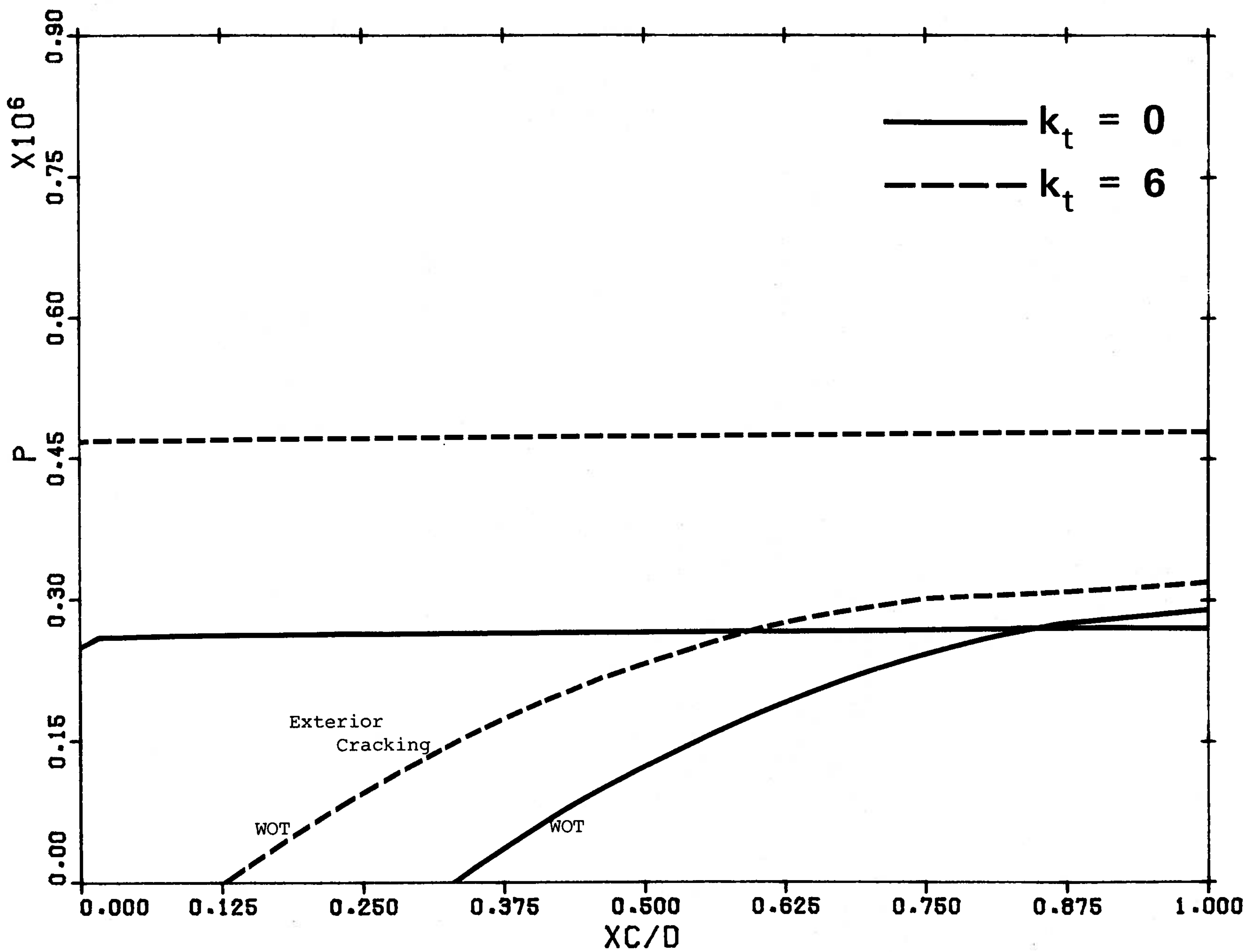

FIGURE L10 x_c/d for Section W3H

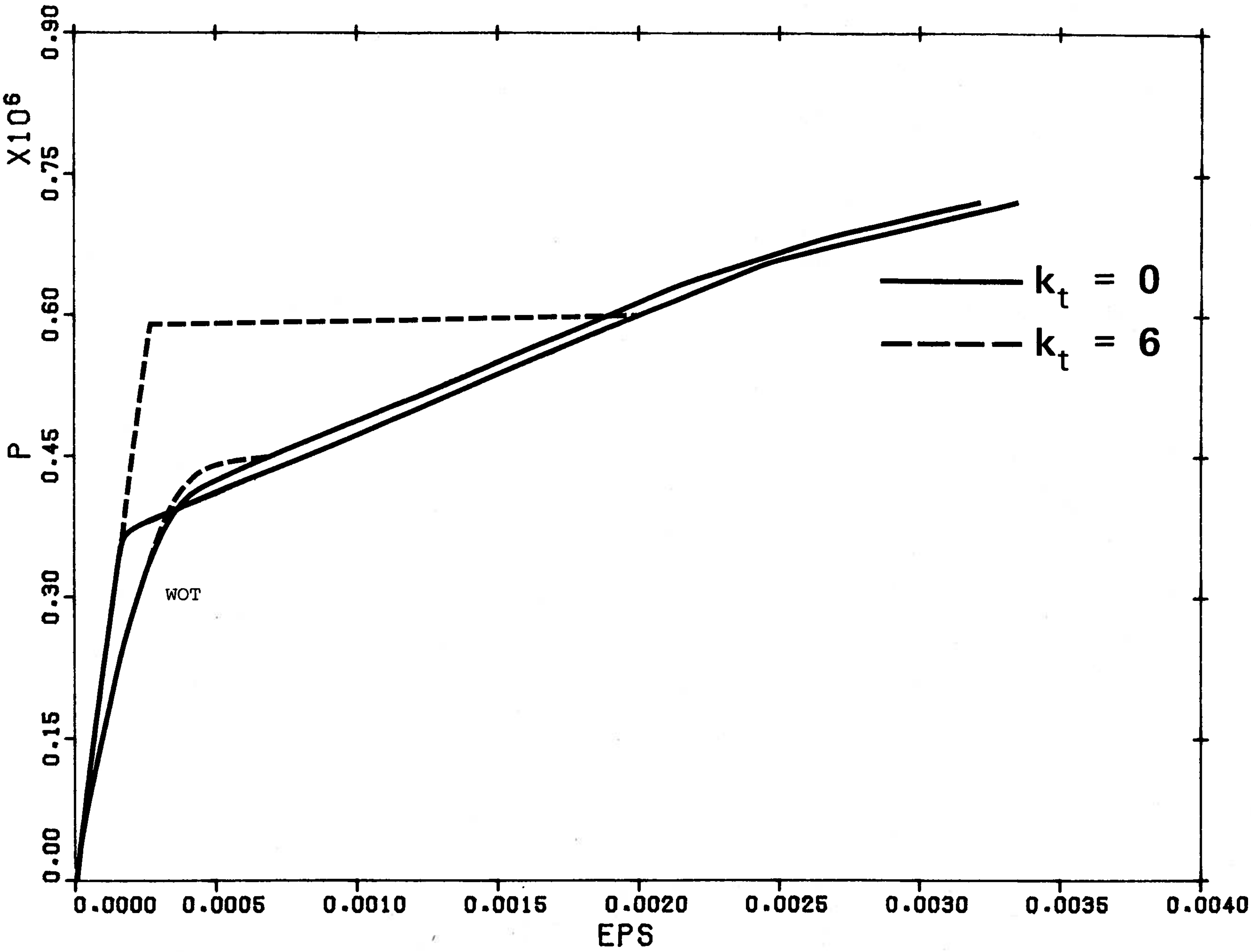

FIGURE L11 P vs ε for Section W3V

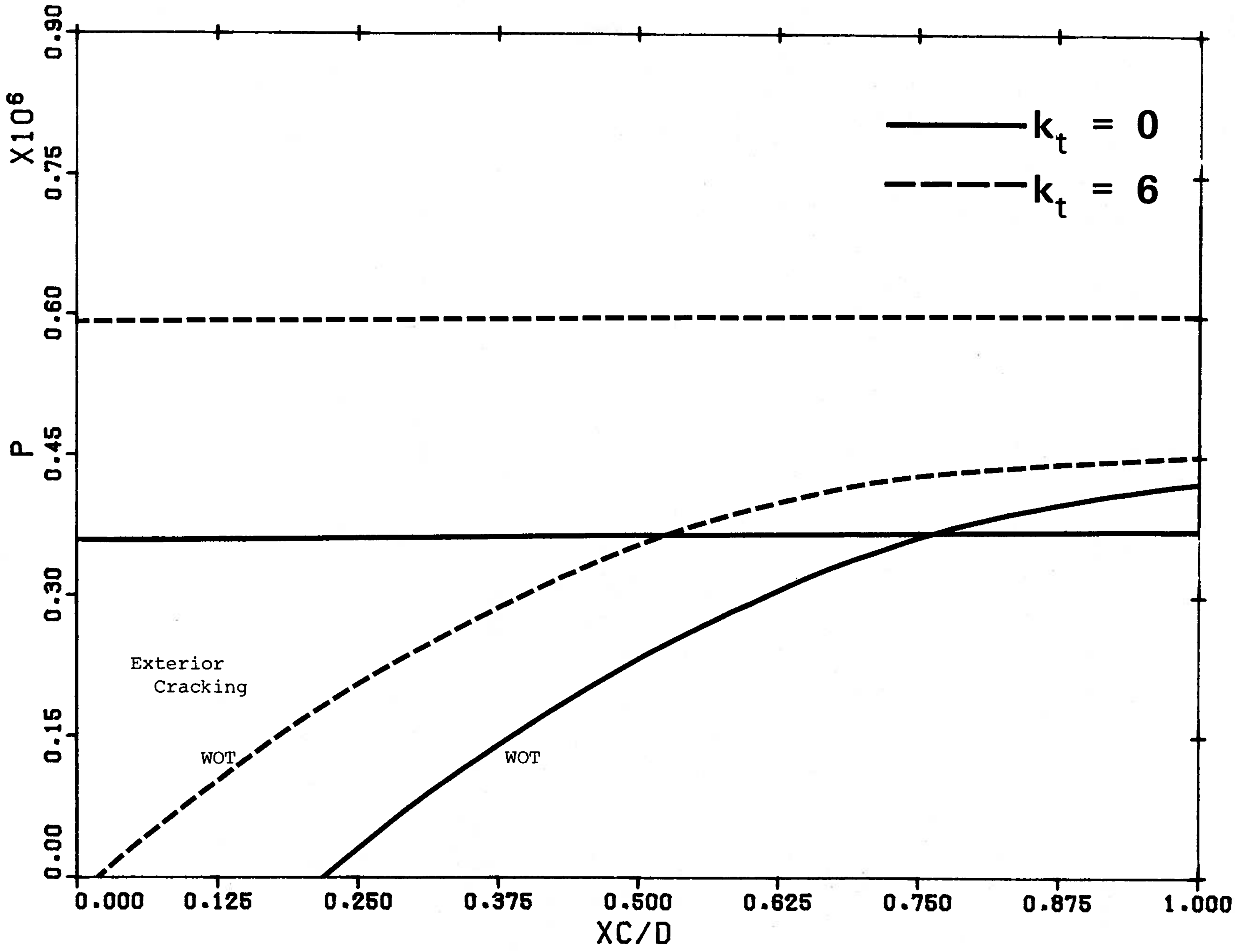

FIGURE L12 x_c/d for Section W3V

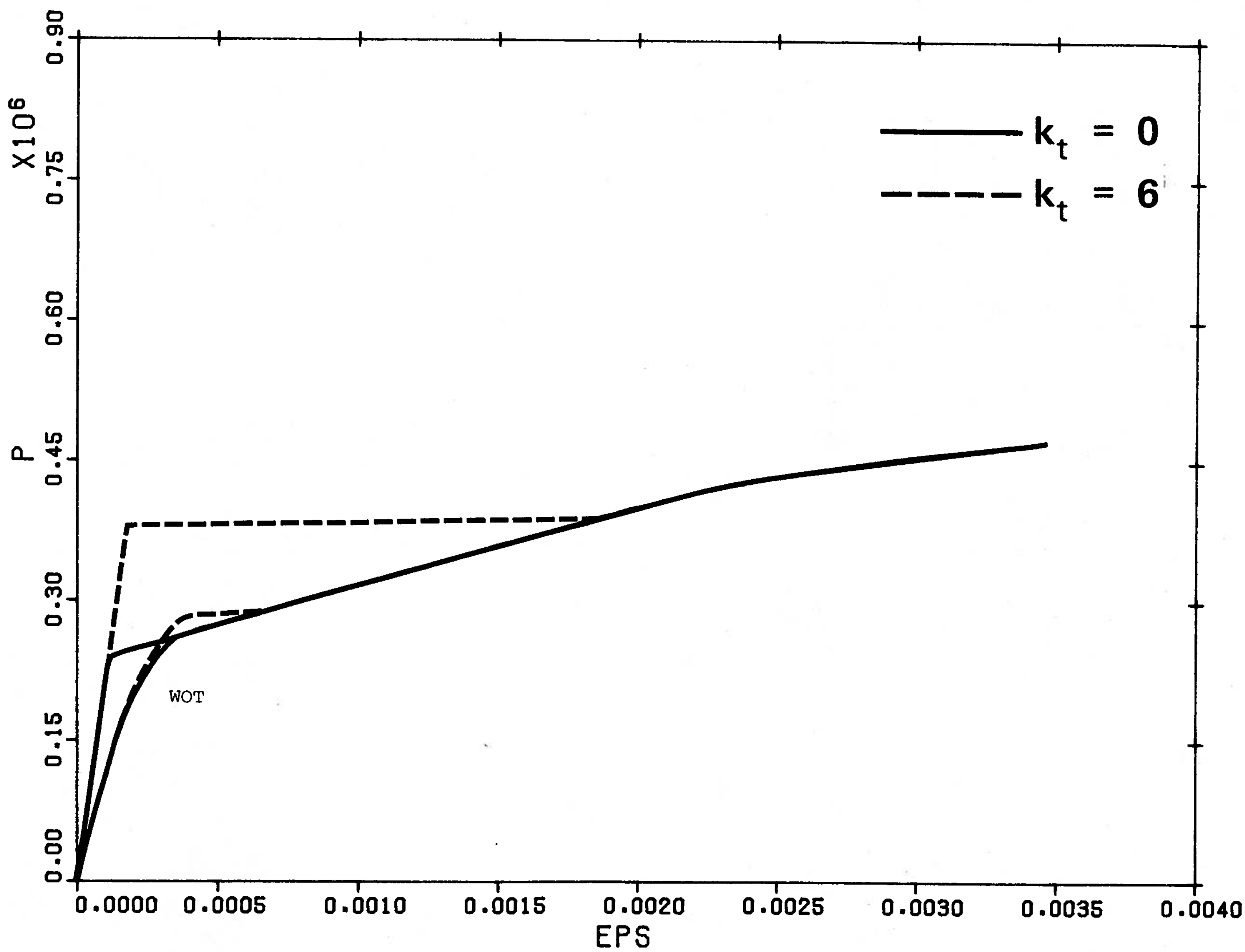

FIGURE L13 P vs ε for Section W4H

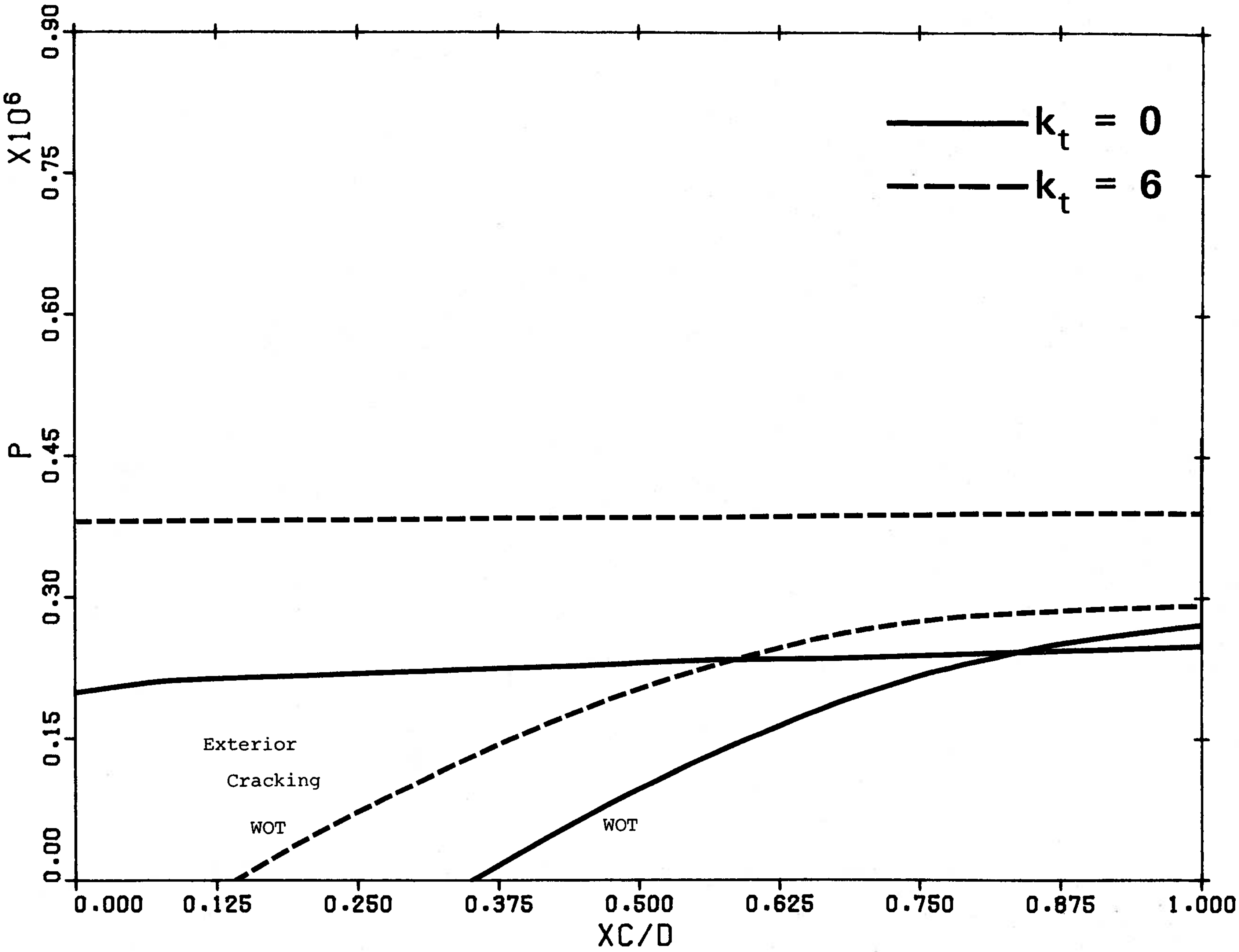

FIGURE L14 x_c/d for Section W4H

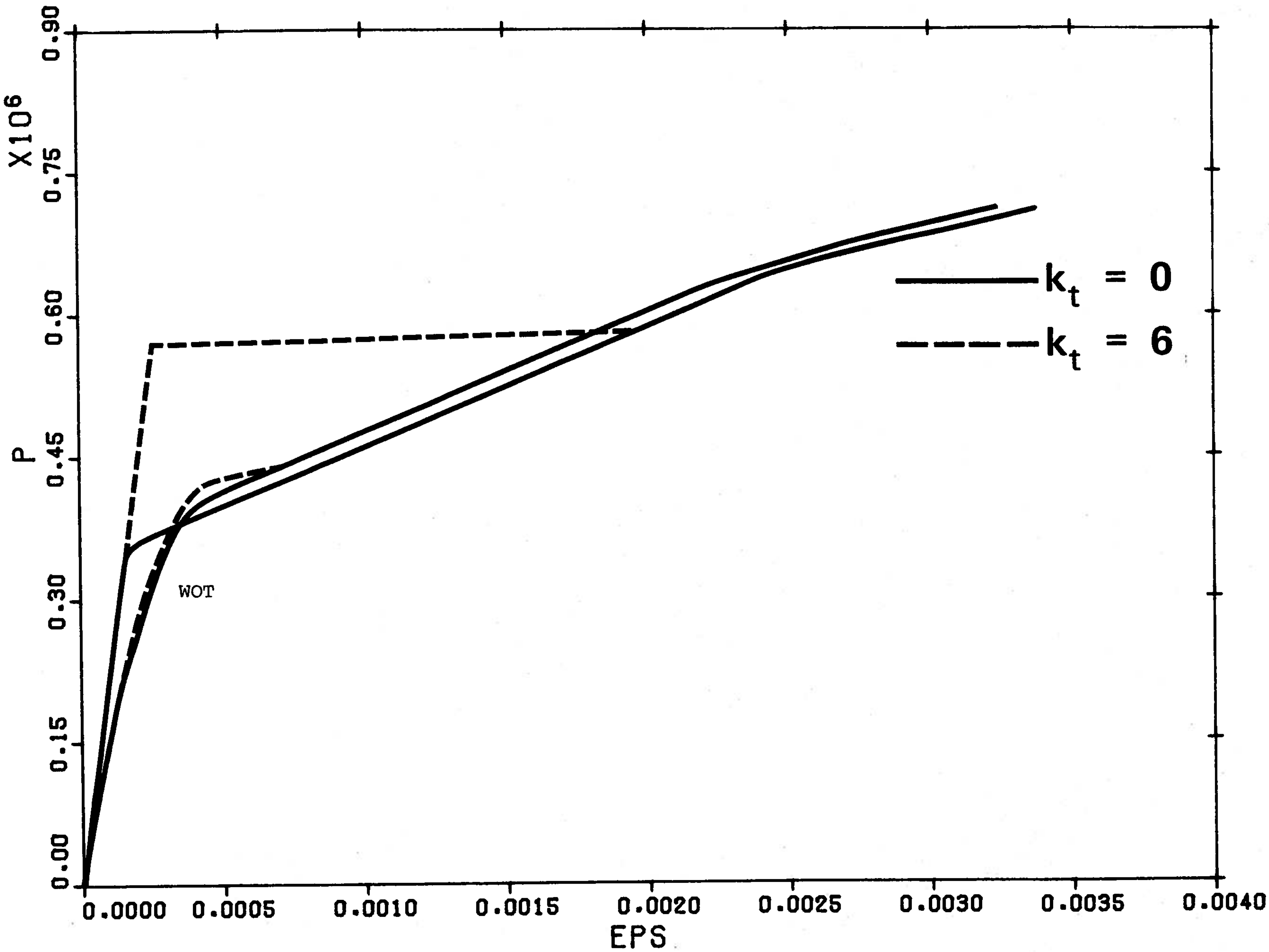

FIGURE L15 P vs ε for Section W4V

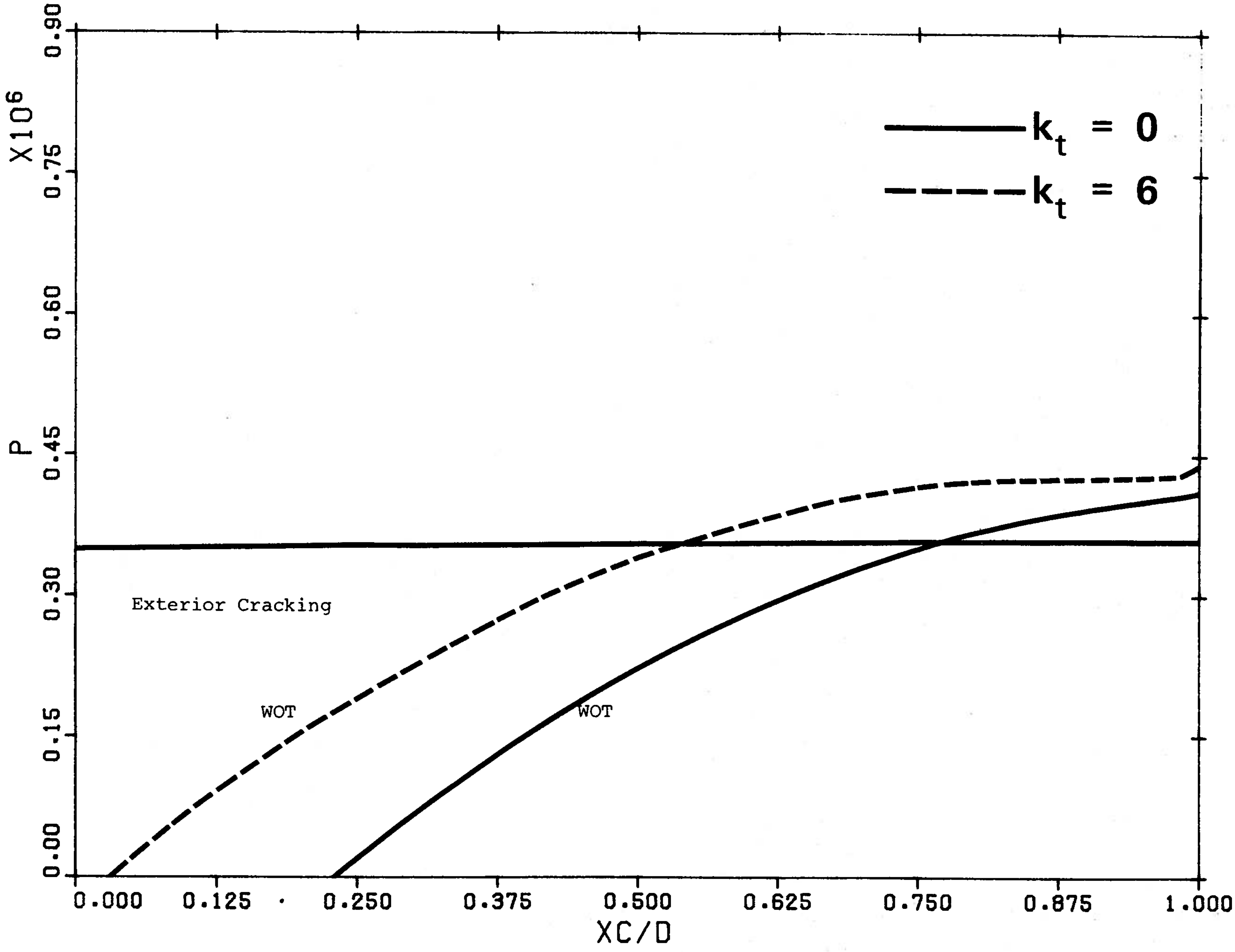

FIGURE L16 x_c/d for Section W4V

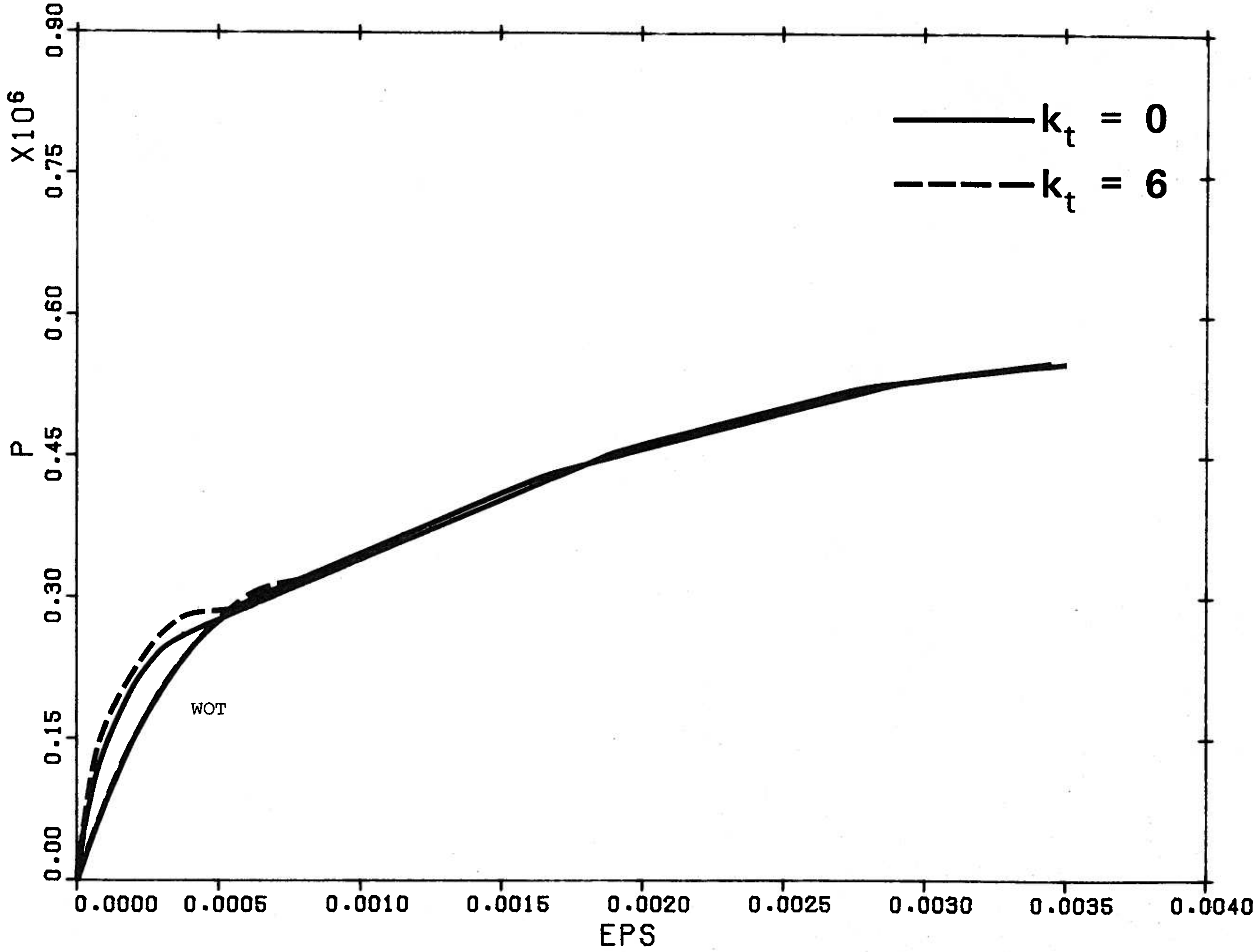

FIGURE L17 P vs ε for Section W5H

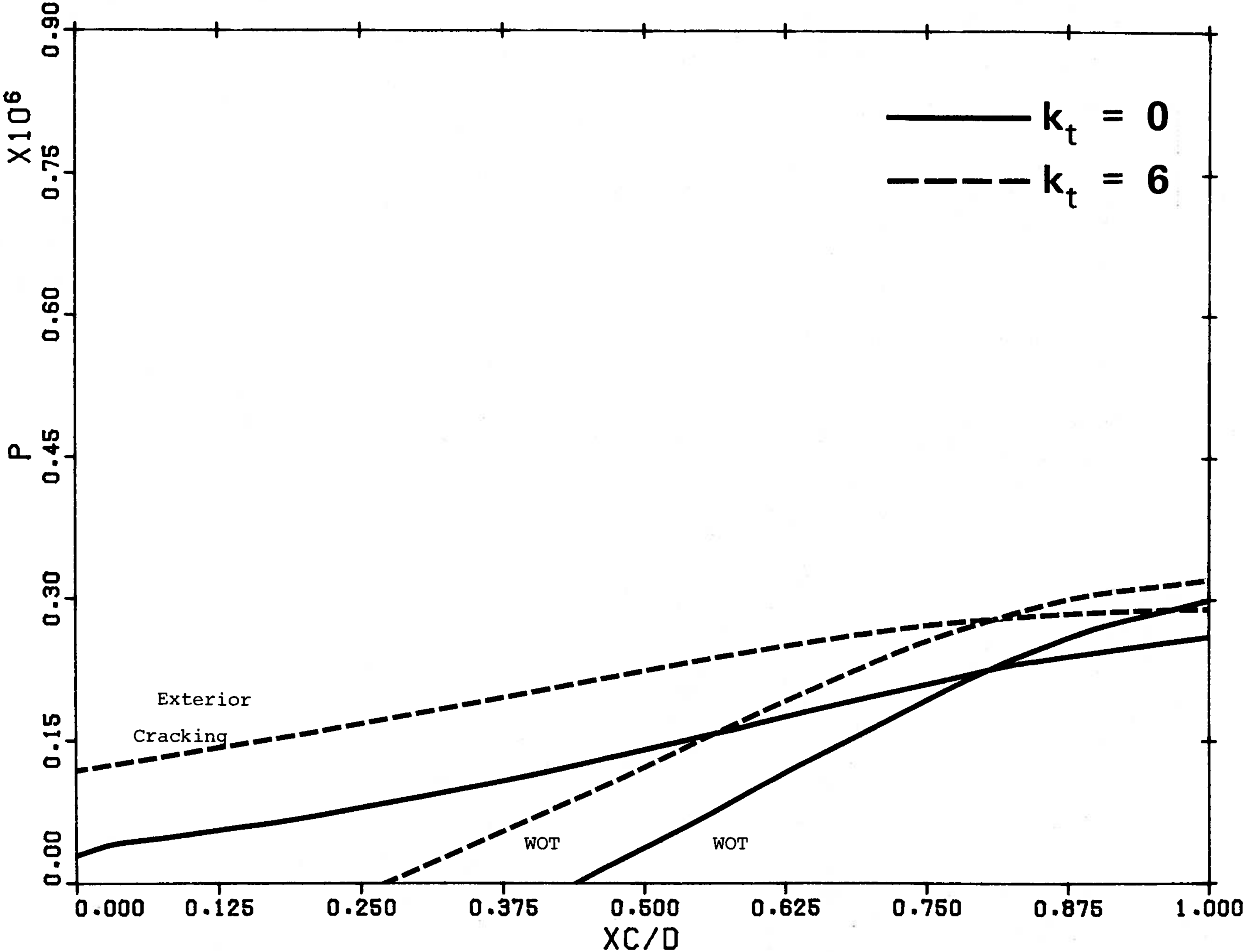

FIGURE L18 x_c/d for Section W5H

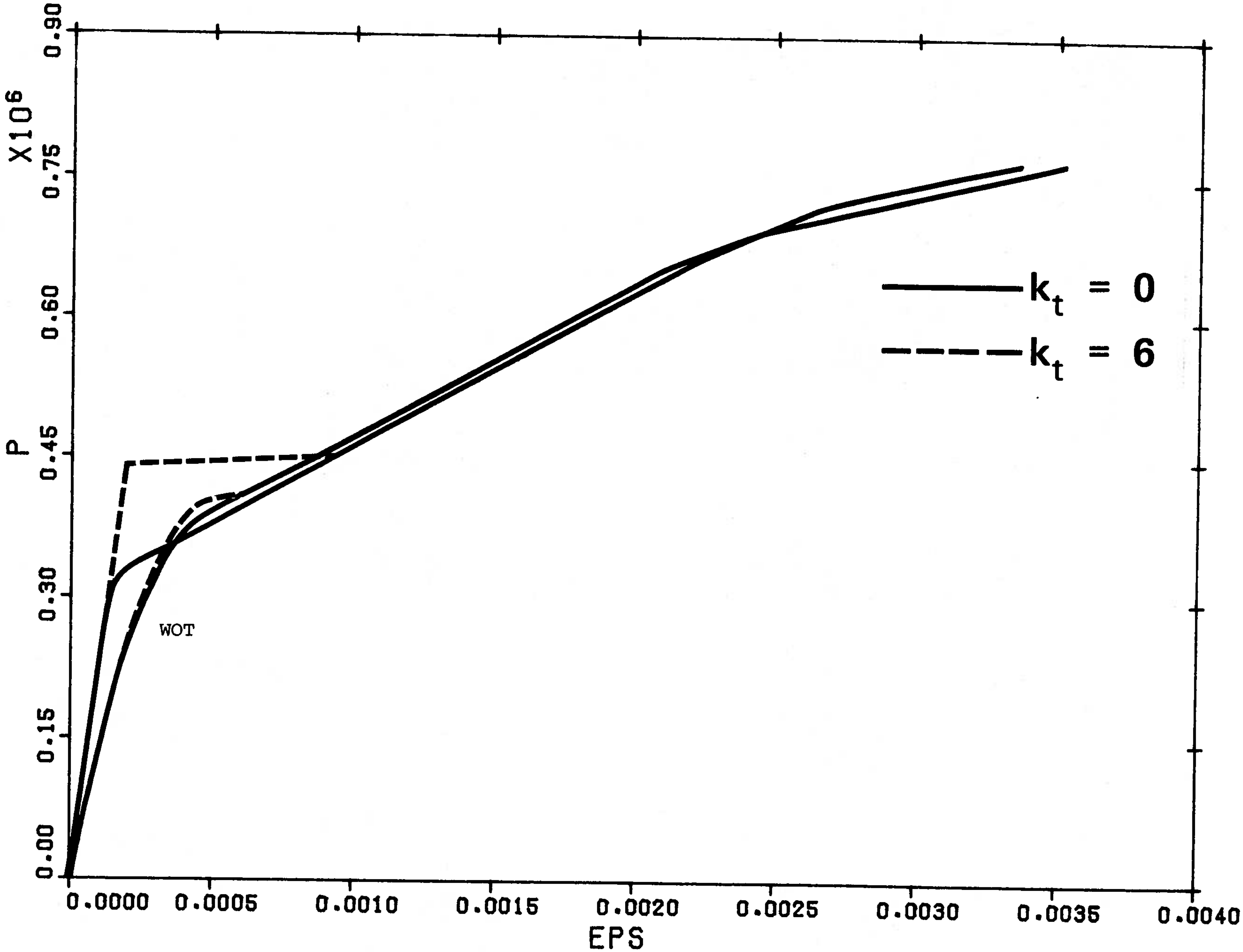

FIGURE L19 P vs ε for Section W5V

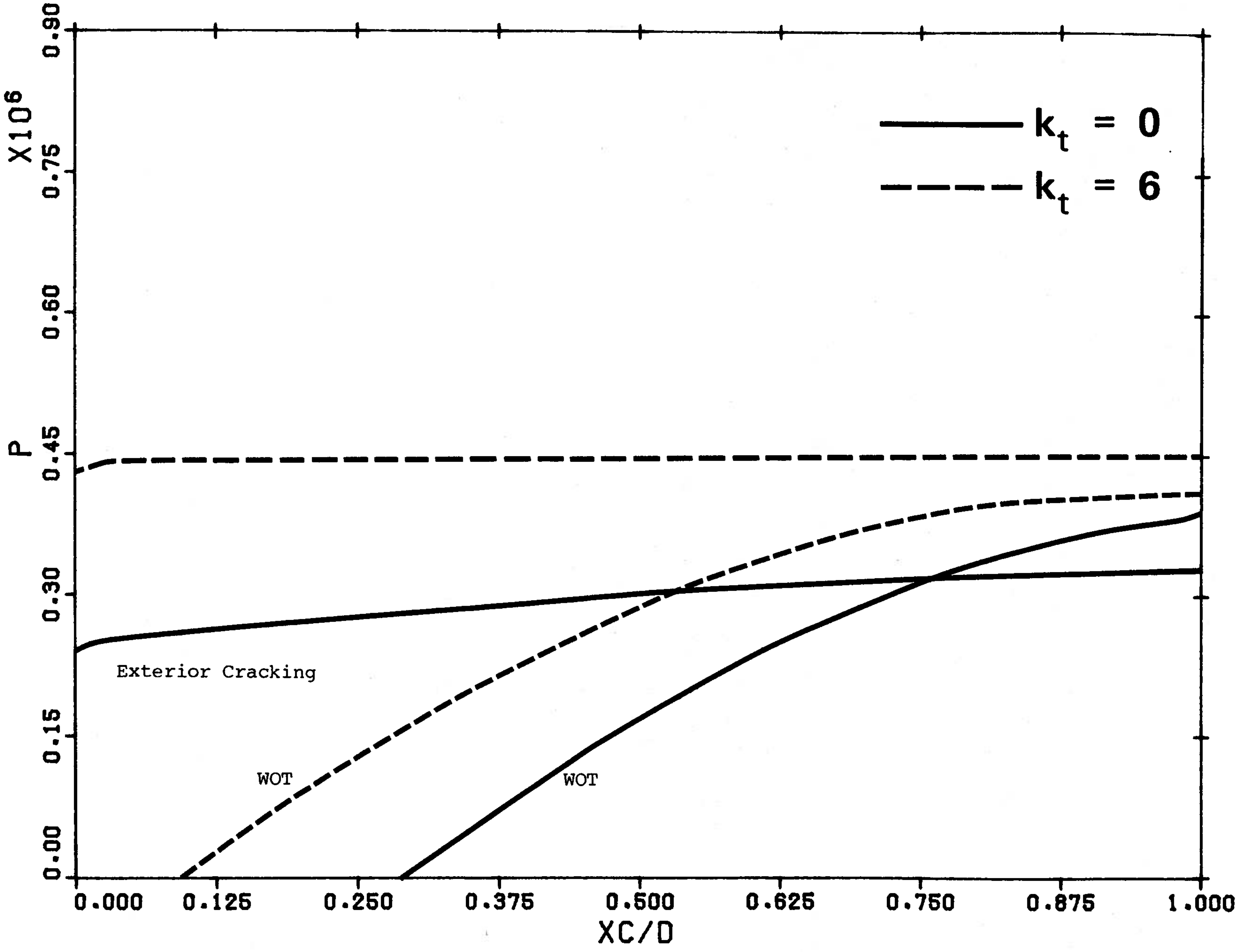

FIGURE L20 x_c/d for Section W5V

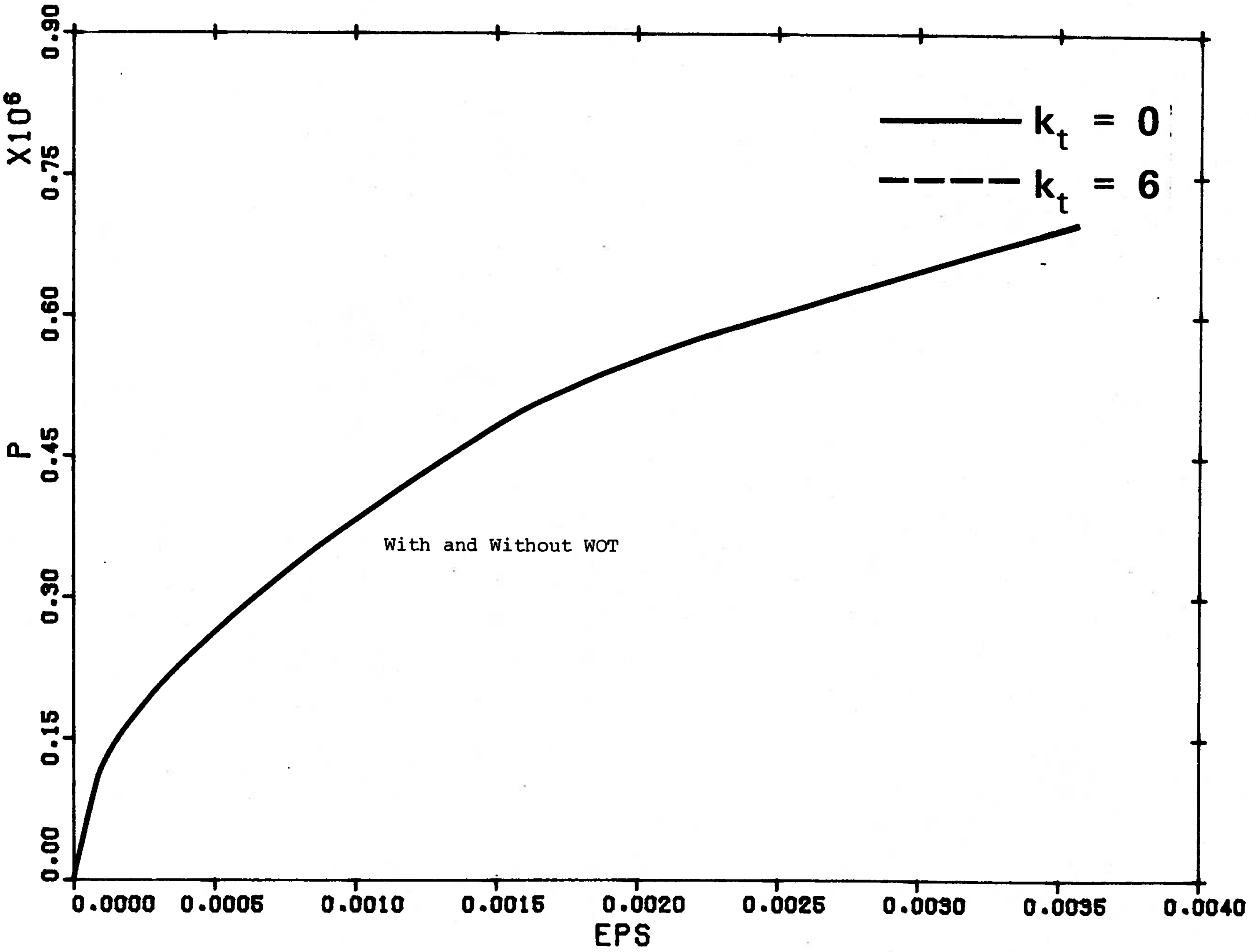

FIGURE L21 P vs ε for Section UD1H

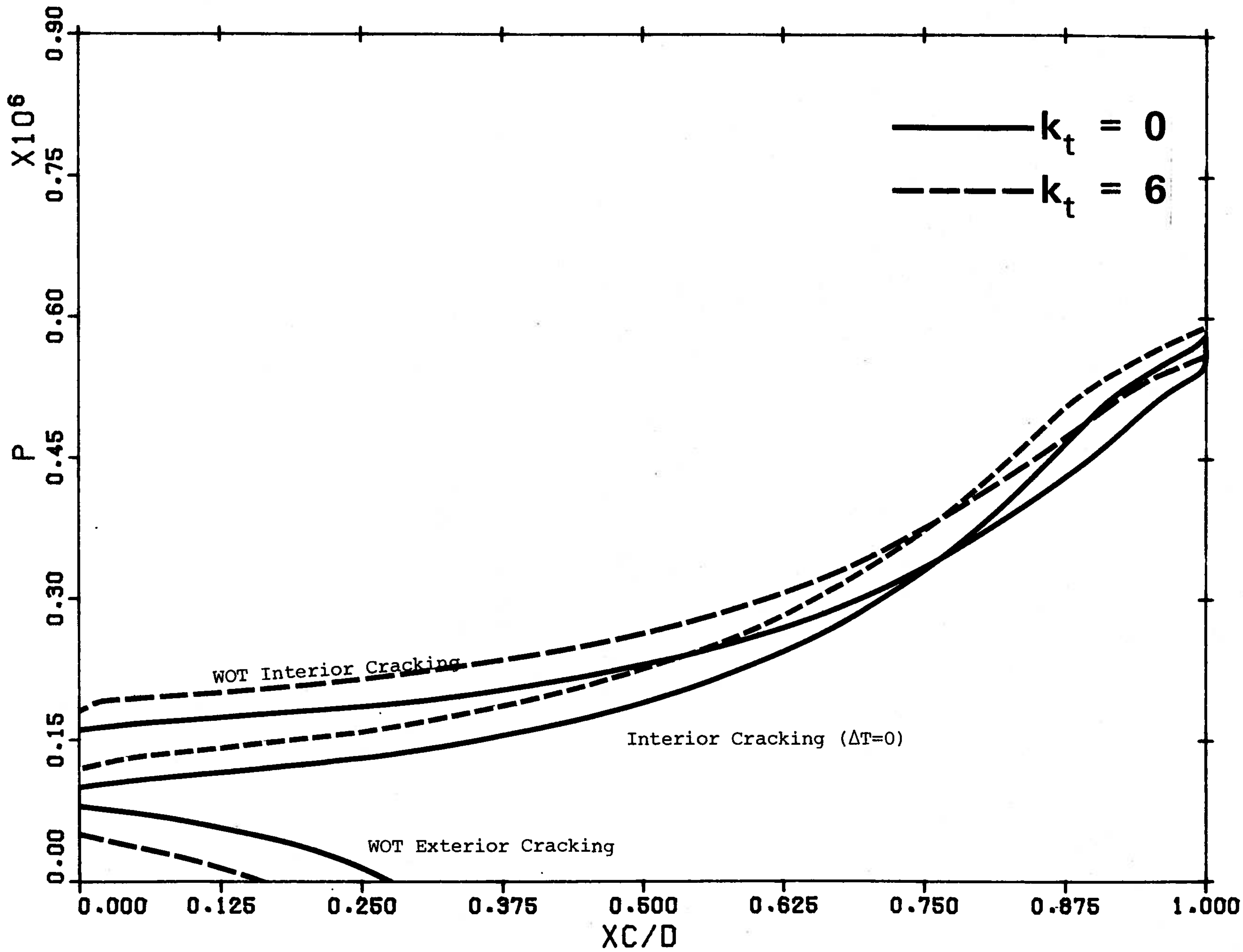

FIGURE L22 x_c/d for Section UD1H

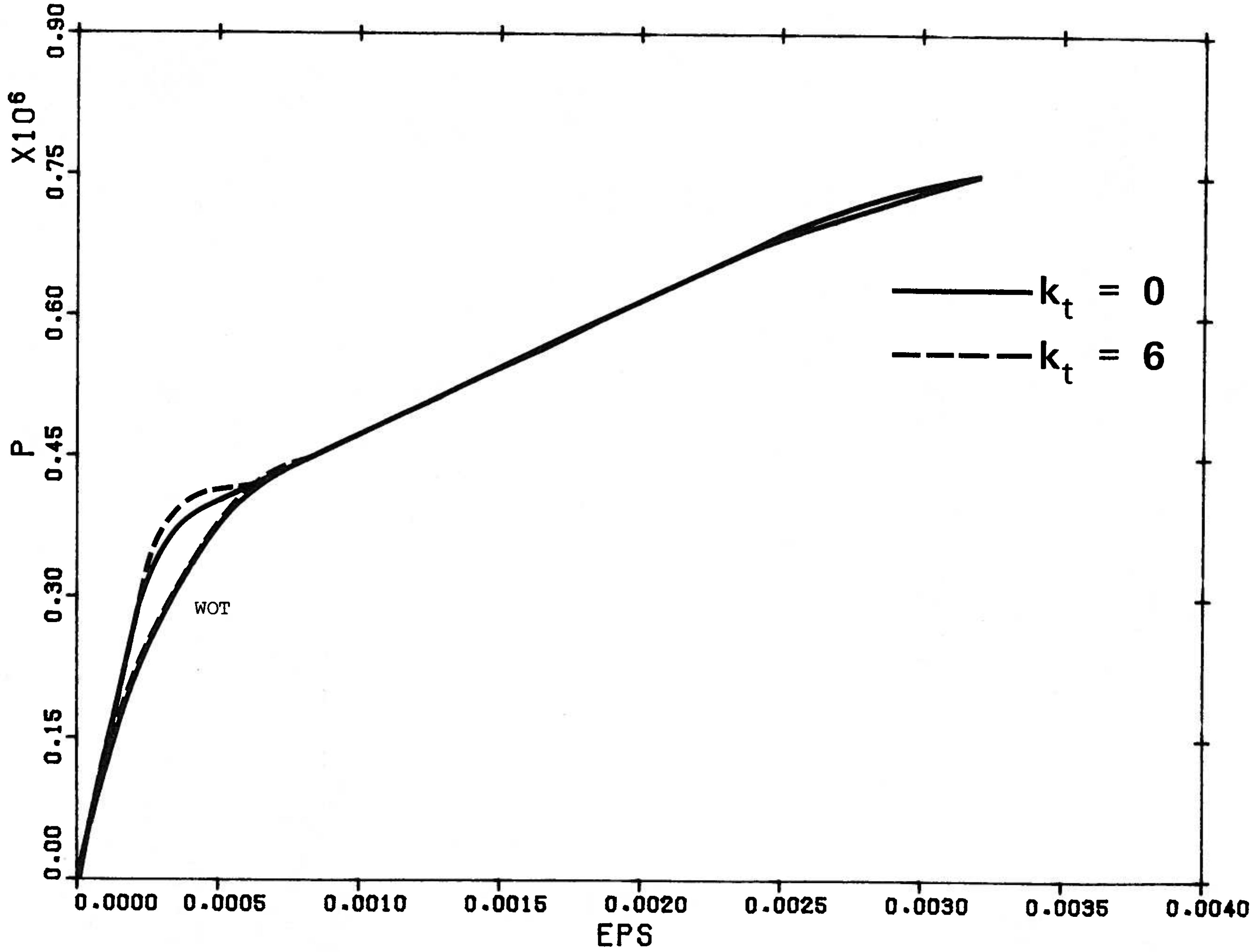

FIGURE L23 P vs ε for Section UD2H

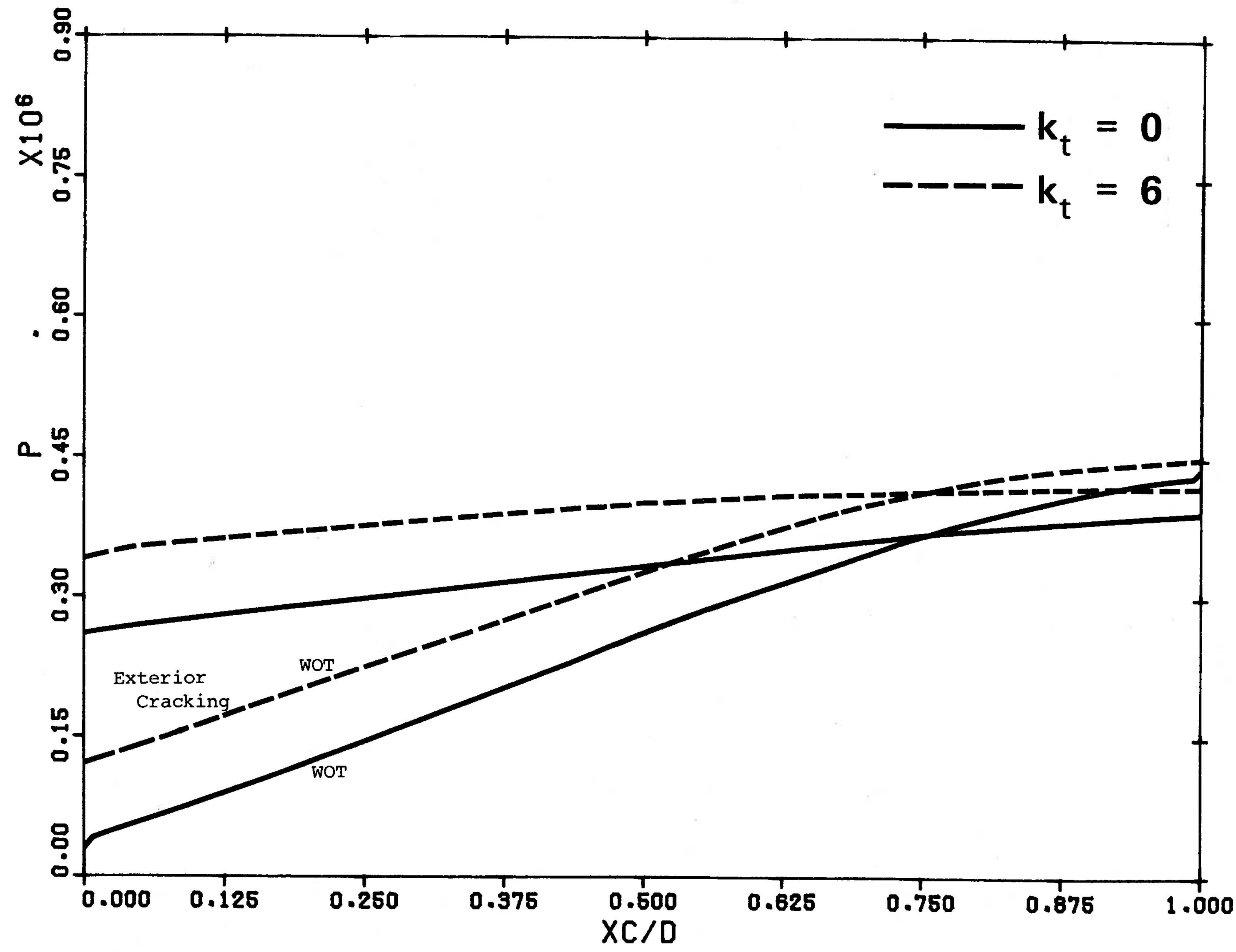

FIGURE L24 x_c/d for Section UD2H

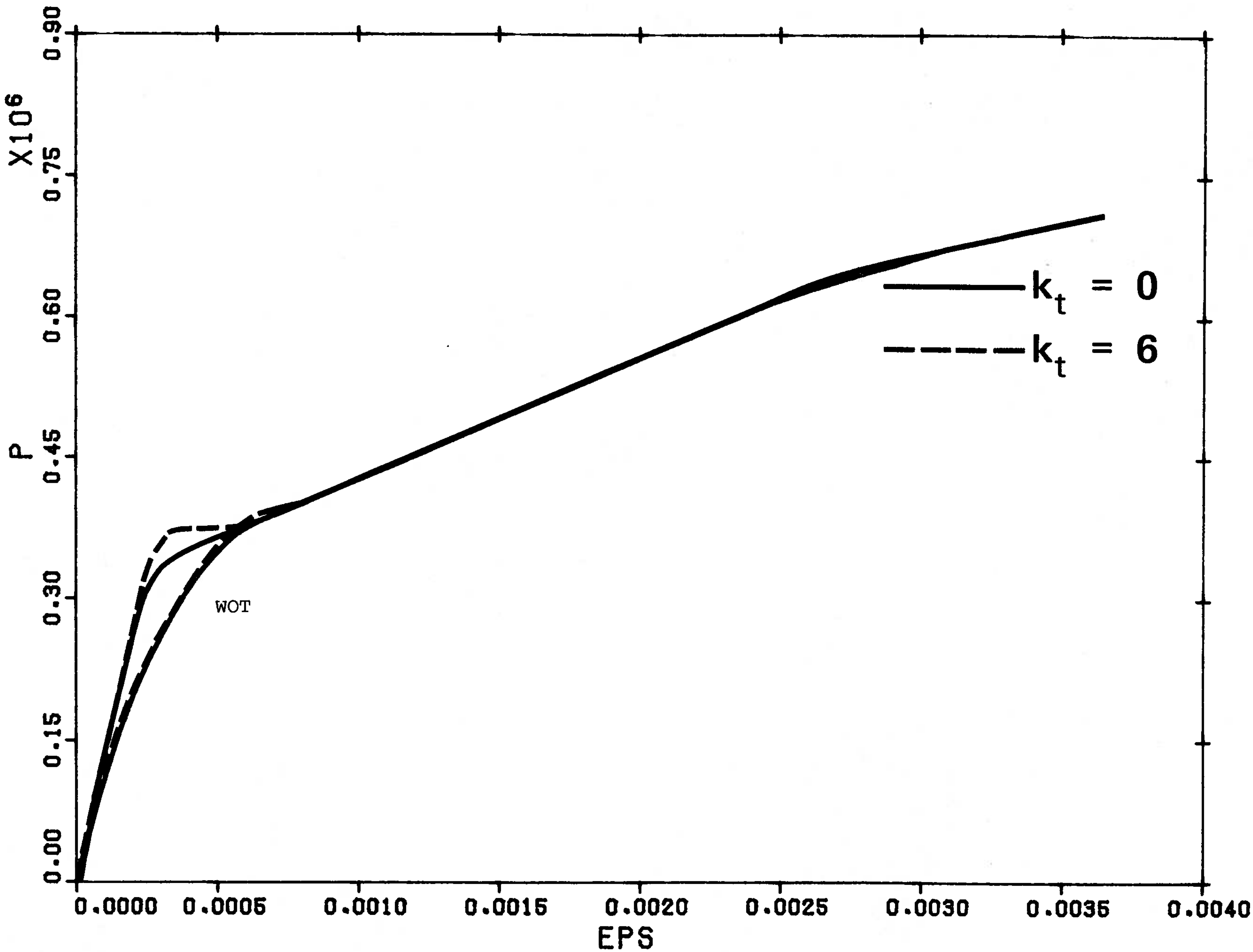

FIGURE L25 P vs ε for Section UD2V

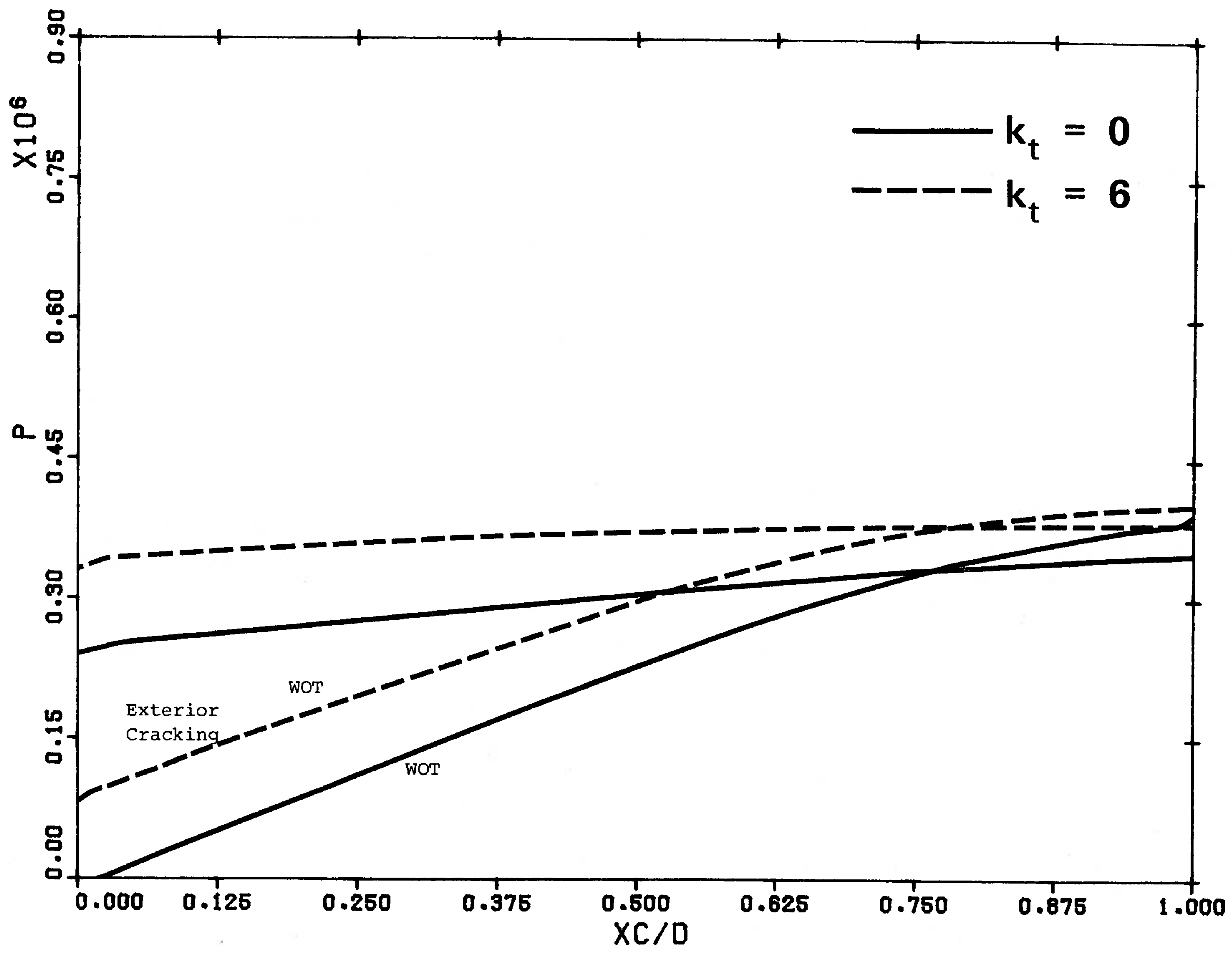

FIGURE L26 x_c/d for Section UD2V

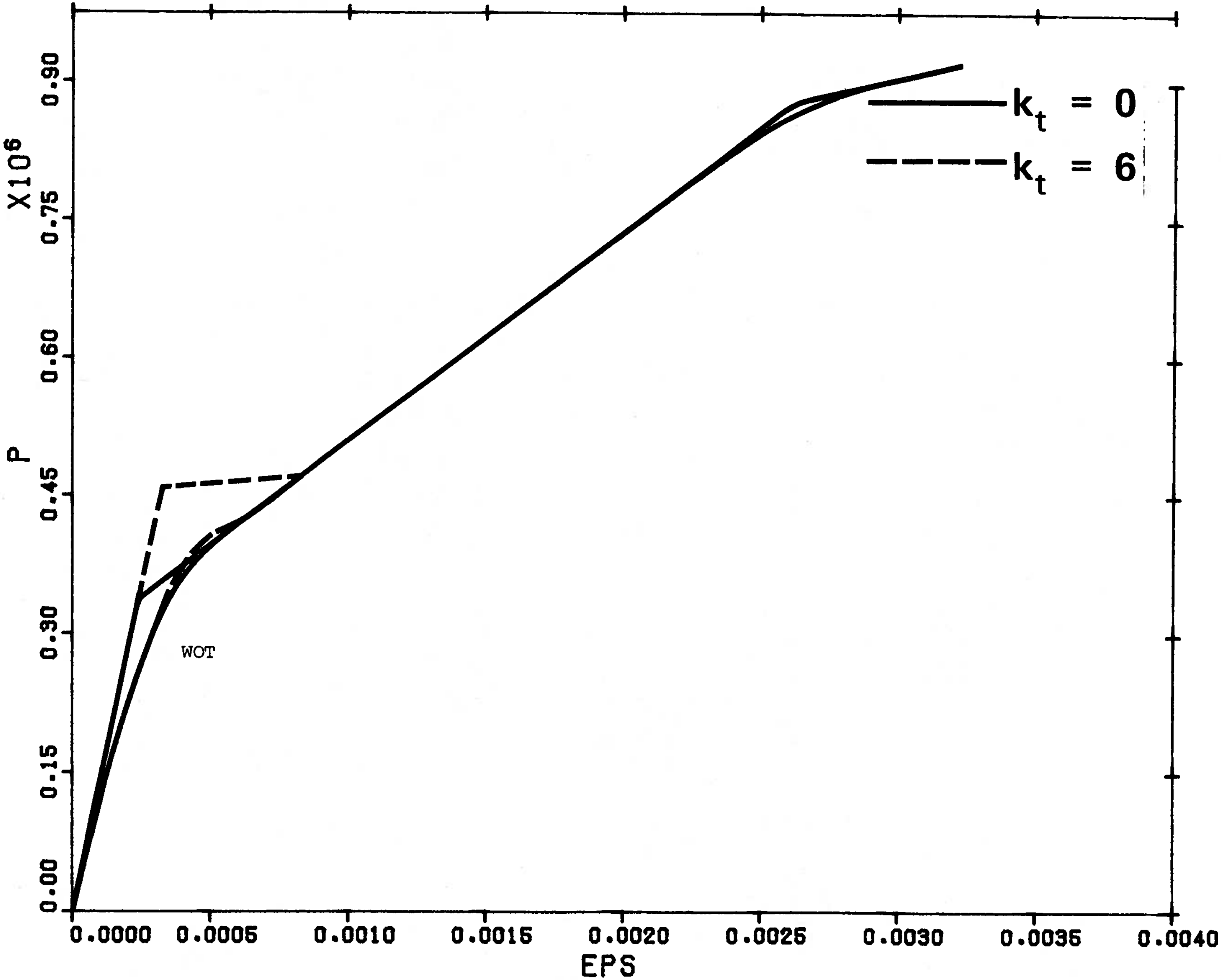

FIGURE L27 P vs ε for Section UD3H

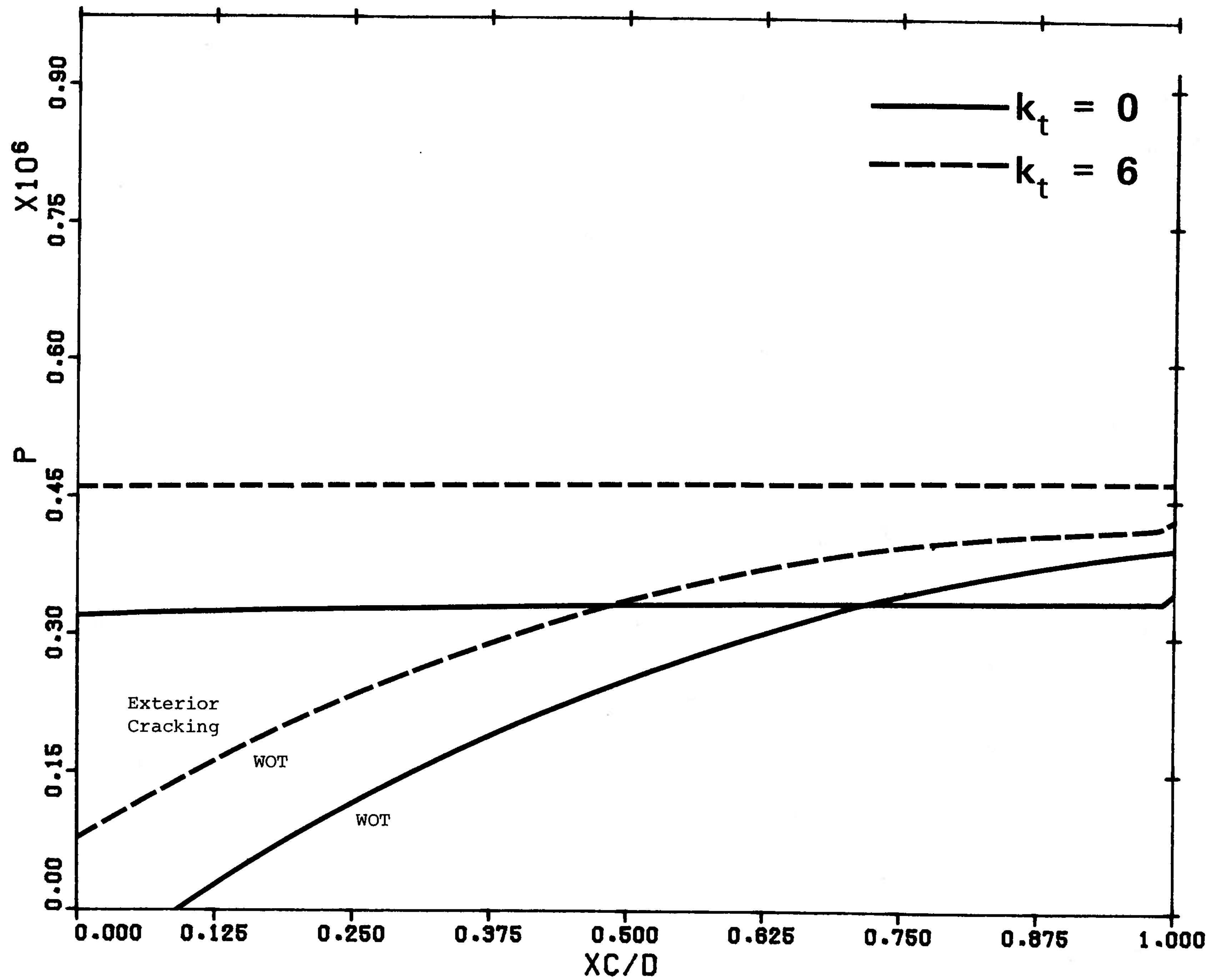

FIGURE L28 x_c/d for Section UD3H

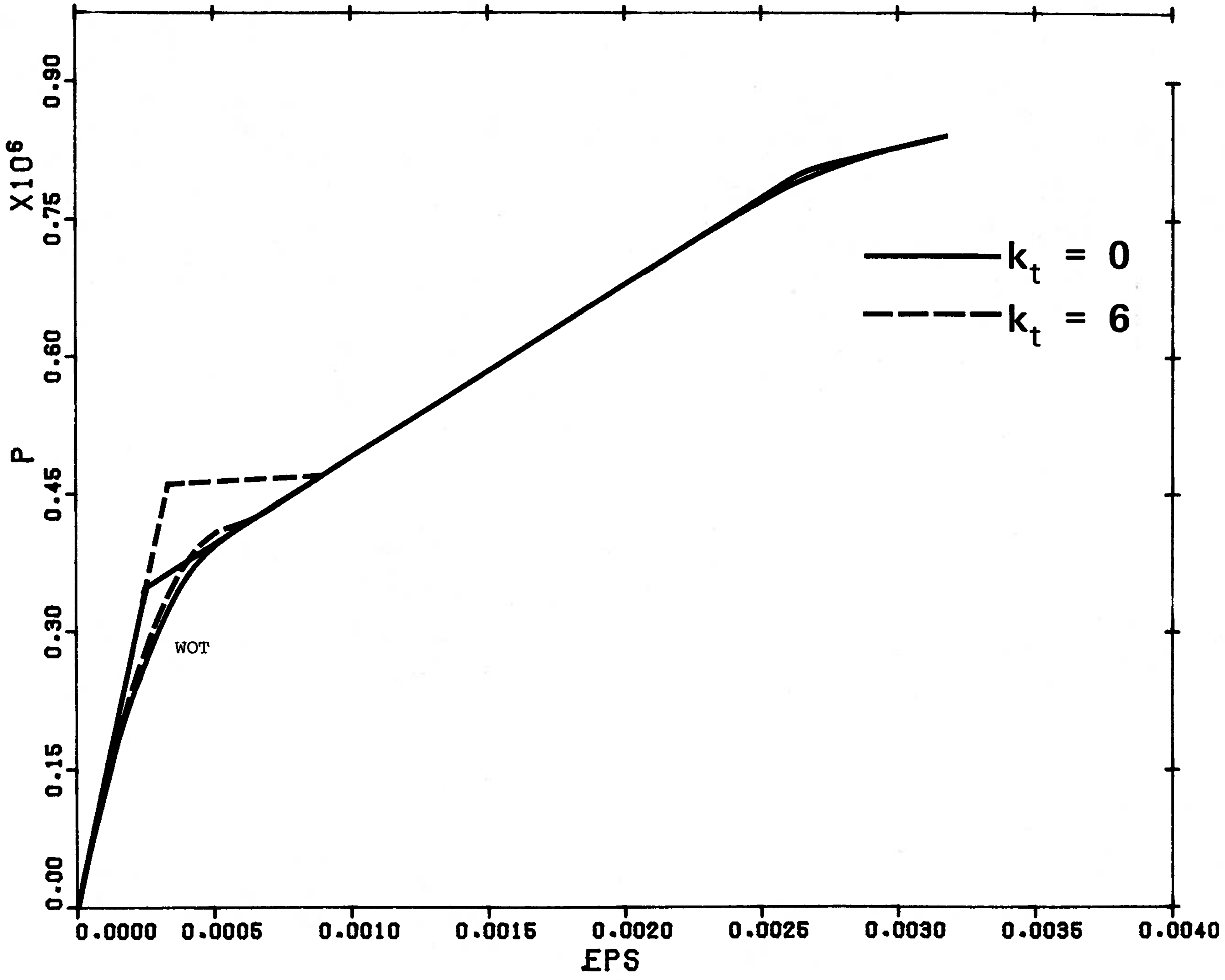

FIGURE L29 P vs ε for Section UD3V

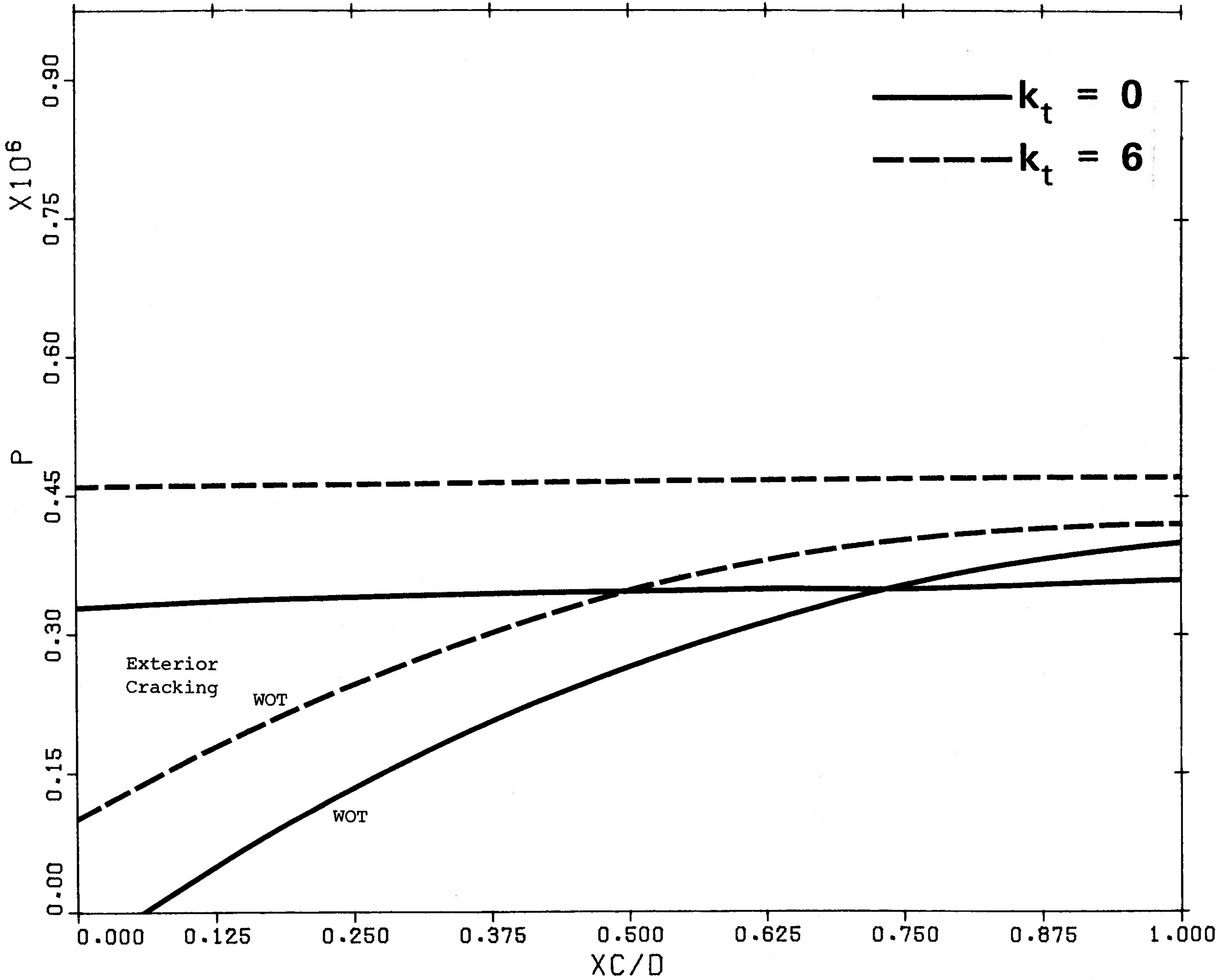

FIGURE L30 x_c/d for Section UD3V

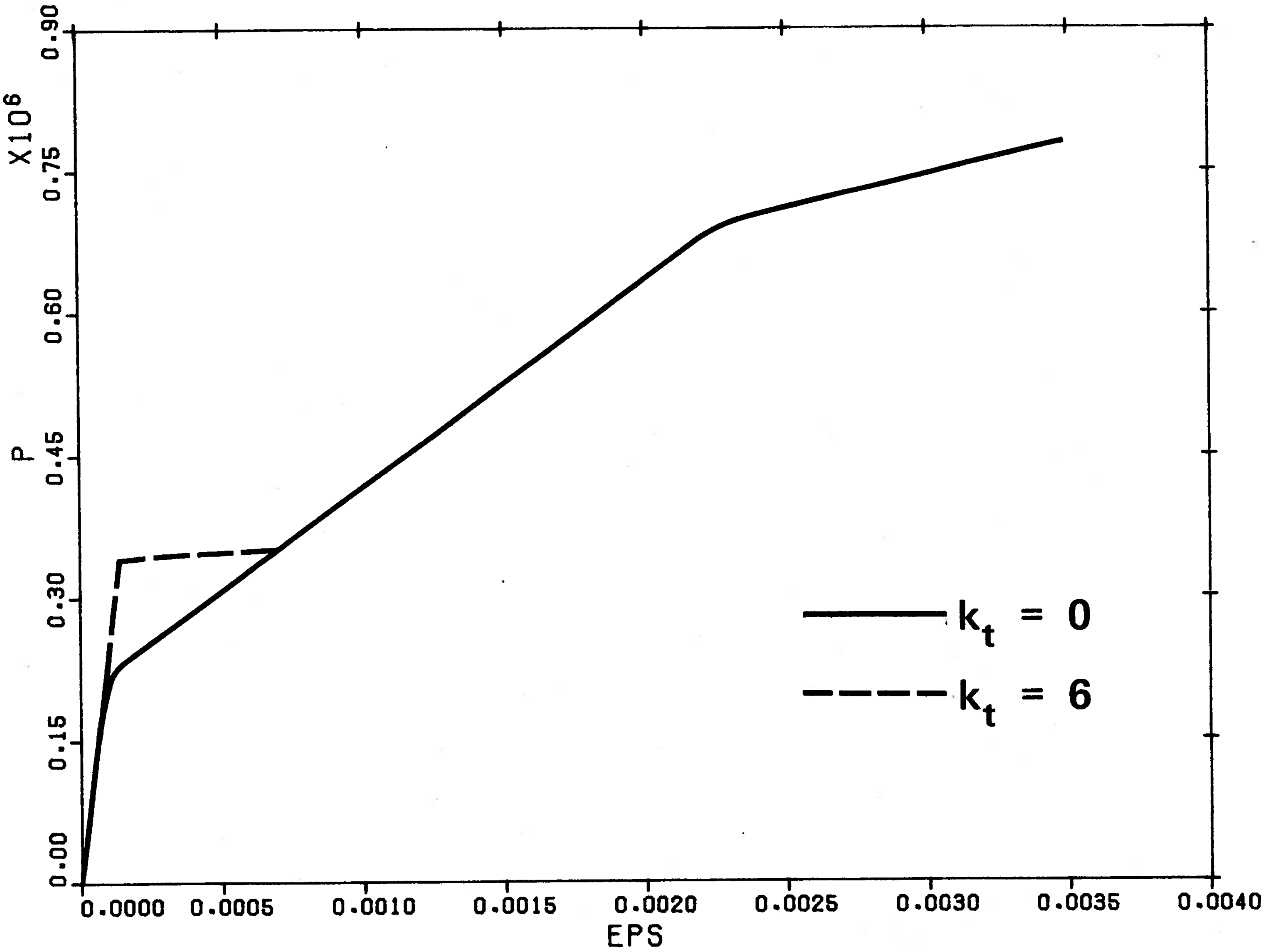

FIGURE L31 P vs ε for Section W2V (CH:Hp)

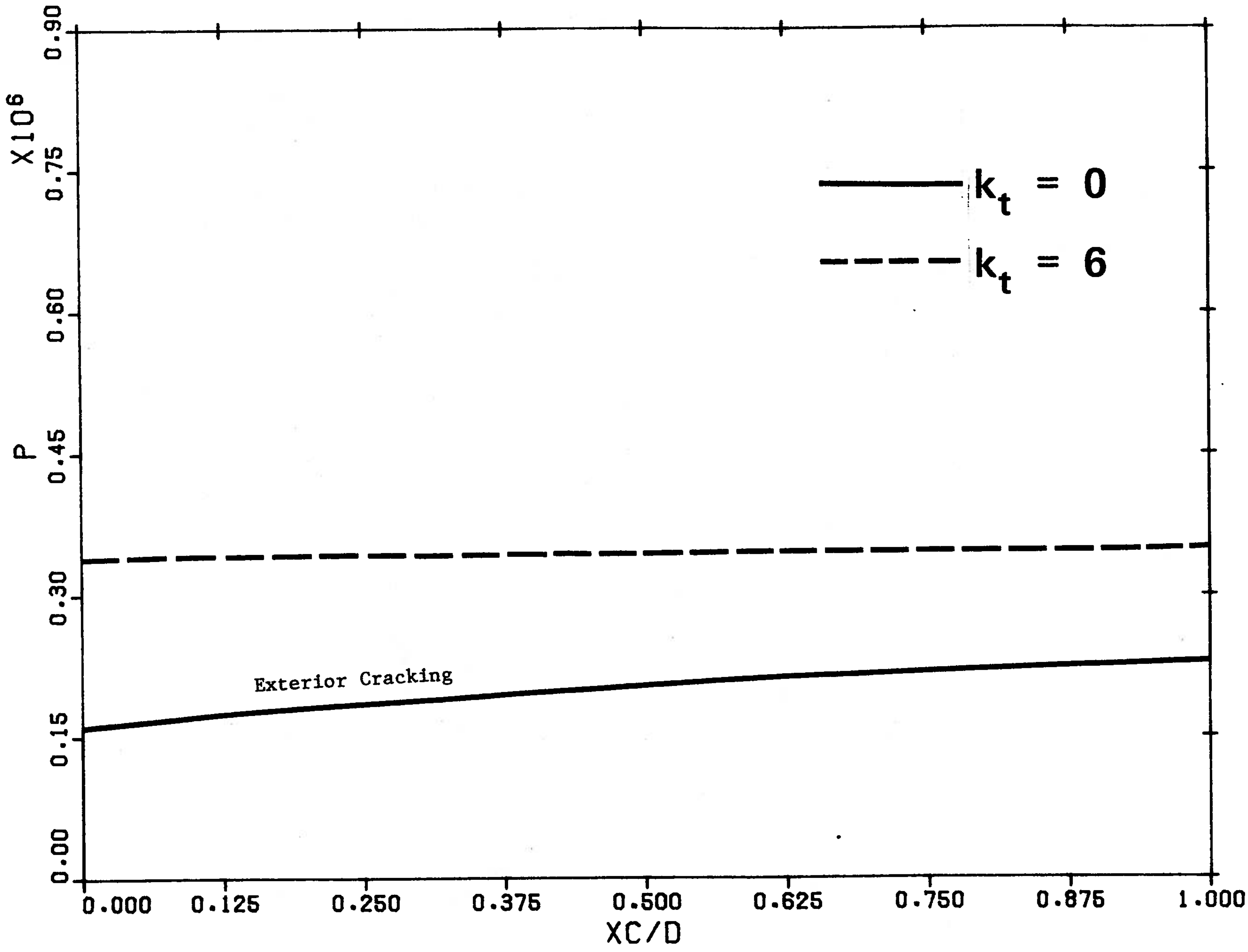

FIGURE L32 x_c/d for Section W2V (CH:Hp)

APPENDIX M

Approximate Determination of Hinge Forces

APPENDIX M

Approximate Determination of Hinge Forces

M.1 Method of Attack

Some difficulties associated with the analysis of section W1H, the hinge location, have been discussed in Sect. 4.5. The basic problem is that, in the BOSOR4 analyses, one may either assume there is continuity at the hinge or alternatively, that there is a pure hinge. The first assumption yields moments that are probably too high while the second yields moments that are unrealistically low until very high internal pressures exist. The object of this Appendix is to present an approximate analysis, based on the 'plane section' assumption, to estimate the moments that are likely to occur at the hinge when the sequence of loading is examined more closely.

The approximate procedure employed is similar to that used in developing the cracking analysis methodology. Thus, it is assumed that moments arise from curvatures, which are necessary to enforce geometric compatibility, but since moments are not a necessary part of the load carrying force system they are relieved by concrete cracking. Under these circumstances the geometric curvatures may be considered to be the primary effect and it is assumed that these remain constant while the section cracks to relieve the initial stresses due to the curvature. Although this assumption is approximate, it appears to be the most realistic 'plane section' assumption which can be made without attempting a full non-linear analysis.

The procedure to approximate the sequence of events at the hinge is also based upon the assumption that the vertical prestressing in the wall is the last long term load to be applied to the structure. This is a possible sequence consistent with the construction sequence outlined in Sect. 2.4, but a more detailed sequence is considered herein than in the gross load superposition analysis of Chapter 2.

M.2 Derivation of Linear Equations

Assuming a moment of M arises from a continuity analysis of the section the resulting curvature (ϕ) is

$$\phi = \frac{M}{EI} \tag{M-1}$$

If this curvature is assumed to remain constant during cracking the strains in the extreme concrete fibre and in the reinforcing steel may be expressed as

$$\varepsilon_c = \phi x \tag{M-2}$$

$$\varepsilon_s = \phi(d-x) \tag{M-3}$$

where x is the depth from the extreme compressive fibre to the neutral axis (tip of the crack) and d is the effective depth of the section.

If the section is at the same time subjected to a vertical compressive load of N, and linear stress-strain relations are assumed, the summation of vertical forces may be expressed as

$$E\phi \frac{bx^2}{2} - n\,E\phi\,A_s\,(d-x) = N \qquad \text{(M-4)}$$

where b is the width of the section, A_s is the area of reinforcing steel, E is the modulus of the concrete and n is the modular ratio. This equation can be put in the quadratic form.

$$x^2 + \frac{2nA_s}{b}\,x - \left(\frac{2N}{E\phi b} + \frac{2n\,A_s\,d}{b}\right) = 0 \qquad \text{(M-5)}$$

from which the depth of compression block (x) may be computed. The maximum concrete stress then becomes

$$f_c = E\phi x \qquad \text{(M-7)}$$

and the steel stress

$$f_s = nE\phi\,(d-x). \qquad \text{(M-7)}$$

Although the above formulation is essentially the same as the cracking analysis of Section 3.4, it has been simplified to allow a closed form solution. At the hinge the reinforcing consists of two layers of #9 bars at 12" on centers inclined at 45° each way, crossing the hinge surface at the center of the 18" section. This is assumed to be equivalent to 1.414 in^2 of vertical steel passing through the centre of the 18" section. Therefore, the values applicable are: $d = 9$ in. $A_s = 1.414$ in^2, $b = 12$ in. and $n = 17.95$ (for long term, see Sect. 3.5.1).

The BOSOR4 model assumes a continuous section of 12 inch thickness at the hinge. Therefore, for consistency, this thickness should be used in Eqn. M-1 to compute curvatures.

M.3 Sequenced Analysis at the Hinge

M.3.1 Dead Load Moment

The load superposition analysis of Chapter 2 predicts a moment of 82.8 ft.-kips and an axial force of 104.1 kips resulting from dead load effects (Tab.e 2.3). The curvature from the BOSOR4 analysis becomes

$$\phi = \frac{82800\text{x}12}{\text{Ex}1728} = \frac{575}{E} \text{ radians/inch}$$

Substituting into Eqn.M-5 yields

$$x^2 + 4.230x - 68.246 = 0$$

from which the solution for the depth of compression block is 6.42 inches. Stresses as computed by Eqs. M-6 and M-7 are $f_c = 3687$ psi and $f_s = 26{,}700$ psi, for which the resulting forces are $N = 104.1^k$ and $M = 81.1^{lk}$. Thus it is seen that the moment of 81.1^{lk}, arising by imposing the BOSOR4 curvatures on the hinge section, corresponds closely with that for dead loads arising from the BOSOR4 analysis. (This is a coincidence but it is indicative that the moments at the hinge from the BOSOR4 analysis are reasonably representative of those to be expected when the hinge response is elastic and the forces are of the order of those developed by dead load effects.)

M.3.2 Moment Prior to Vertical Prestressing

If all the prestressing, except the vertical wall prestressing, is now applied to the structure the BOSOR4 prediction of moment may be represented by the M1 moment for the Rf1 or Rs1 reference state of Table 2.3. To be conservative we select the Rs1 stress resultant of 135.6 ft.-kips. However, in the absence of vertical prestressing the N1 force remains at 104.1 kips. The following analysis then follows directly from the procedure in Sect. M.3.1.

$$\phi = \frac{135600}{144E} = \frac{942}{E} \text{ rad/inch}$$

$$x = 5.693 \text{ inches}$$

$$f_c = 5.693 \times 942 = 5360 \text{ psi} > 4250 \text{ psi } (0.85\, f_c')$$

$$f_s = 17.95\,(9 - 5.693) \times 942 = 55{,}900 \text{ psi}$$

From these stresses

$$N = 104.1^k$$

$$M = 104.8^{1k}$$

Therefore, on imposing the curvature from the continuous analysis on the hinge detail the moment arising from the stresses is 104.8 ft.-kips rather than the 135.6 ft.-kips predicted by BOSOR.

This linear analysis, however, predicts a concrete stress above 0.85 f'_c. Obviously, there must be some inelastic action. Assuming concrete has a bilinear response in compression with a horizontal yield plateau at 0.85 f'_c, a somewhat simpler analysis than that above, for an imposed curvature of 942/E, yields

$$x = 6.566 \text{ inches}$$
$$f_s = 41100 \text{ psi}$$
$$\varepsilon_c = 0.00375$$
$$f_c = 4250$$
$$N = 104.^{k}$$
$$M = 95.3^{1k}$$

Thus, when inelastic response is considered, the section resists only 95.3 ft.-kips rather than the initial 135.6 ft.-kips. This is reached at very high compressive strains (ε_c = 0.00375).

M.3.3 Application of Vertical Prestressing

The application of vertical prestressing now imposes an additional N1 force of 199.5 kips/ft. (The moment due to this force has already been considered in the 135.6 ft.-kip stress resultant of Sect. M.3.2.) After application of this prestressing force the final set of stress resultants on the section for the reference state Rs1, computed with a yield plateau for concrete, becomes, N1 = 303.6 kips and M = 146.5 ft.-kips. The depth of cracking for this condition becomes 8.67 inches which differs from that of Sect. 4.5 because the program computes curvatures using the full 18 inch depth of section rather than the 12 inches assumed herein.

M.3.4 Relation of Approximate Analysis to Interaction Curve

The points representing the stress resultants computed above are shown on Fig. K16. The sequence of BOSOR points are denoted as a, b, and S1, while the corresponding points from the cracking analysis are denoted as c, d and e, respectively, representing the conditions for dead load, dead load plus horizontal prestress, and dead load plus total prestress plus shrinkage, respectively. The load line for pressurization reverses the direction of moment and is plotted arising from point S1 and progressing through P18. Load factors from this line are contained in Table 4.6.

M.4 Concluding Remarks

The analysis contained herein indicates that some inelastic behavior is to be expected at the hinge in the reference states. This is not surprising since, if the connection is to act as a hinge, large strains are required to develop the necessary curvature. It should be noted, however, that preliminary finite element studies indicate that BOSOR4 overestimates the moment that will be developed at this section which implies that this connection detail is one where the classical 'plane section' type of analysis is inadequate to predict behavior properly. These preliminary studies also indicate that no cracking occurs at the hinge in the reference states.

ADDENDUM (August 1976)

List of Tables and Figures for ADDENDUM

ADDENDUM (August 1976)

AD.1 INTRODUCTION

The purpose of this addendum is to provide information to clarify some aspects of the report and to examine some additional factors of behaviour which were not included. It is possible to use the techniques of the report to examine a multitude of combinations but it is clearly impossible to examine all combinations. It was intended that sufficient detail be provided to allow a reader to extract the relevant information necessary to pursue his own investigation with respect to any aspect of behaviour, subject only to the limitations of the methodology. The reader should understand that the primary purpose of this report is to examine methodology and not to provide specific numerical results. At present, the investigation is continuing with an examination of more sophisticated methodologies.

This Addendum will deal with three questions raised by readers. The influence loadings and load combinations of Chapter 2 are more precisely defined in Section AD.2. In Sect. AD.3 the effect of the increased section thickness at the springing line of the upper dome is examined. In Sect. AD.4, the results of a BOSOR4 analysis of the Gentilly 1 powerhouse are compared with the field measurements reported in the literature.

AD.2 DEFINITIONS OF INFLUENCE LOADINGS AND LOAD COMBINATIONS

A general description of the influence loadings has been given in Section 2.4 of the report. The following are more precise definitions:

d = dead load at 150 pcf.

u = uniform strain associated with a 1° F temperature rise.

g = a uniform strain gradient associated with a linear temperature variation of 1° F per foot of thickness.

f = prestressing influence loads of one pound per square foot of inward pressure distributed over the middle surface of the structural component to represent the hoop prestressing of the walls and the dome prestressing; or

= a load of one pound per perimeter foot on the center-line of the section in the case of line loads, such as the vertical prestressing in the wall or the base prestressing.

(Note that all influence prestressing conditions must be self-equilibrating, and it may be necessary to add non-unit line loads to achieve this condition).

p = one pound per square foot on the interior surface.

Ld* = the weight of the upper dome applied to the lower dome during construction, which was used in computing the alternative sequencing of dead loads.

The numerical factors used to produce the load combinations of various loading conditions in Chapter 2, are specified in Table AD.1.

AD.3 SECTION ANALYSES AT UPPER DOME SPRINGING LINE

The loads and load factors presented in Chapter 4 (Table 4.3 to 4.7) and the associated plots for location UD1 did not take into account the thickening of the upper dome in the vicinity of the springing line. The results for location UD1 are, therefore, in error in the sense that they do not reflect conditions to be expected in the structure as it was constructed.

To indicate the change in response associated with this effect, cracking and interaction analyses were carried out for a new section, denoted as UD4, at location 276.43 (approximately four feet from location UD1). At this point the shell thickness is 25 inches and the reinforcing, prestressing and concrete cover are essentially the same as those at location UD1.

The stress resultants for loading conditions Rf1 and C:Cp at location UD4 are shown in Table AD.2. Plots of the cracking analysis for section UD4H are shown in Figures AD.1 and AD.2. Interaction plots at this location are shown in Figures AD.3 and AD.4. Limit state loads and load factors for section UD4H are tabulated in Tables AD.3 and AD.4.

A comparison of the load factors of Table AD.4 with those for section UD1H in Table 4.6 indicates that the values in the report do not accurately reflect the behaviour to be expected in the Gentilly 2 structure at the perimeter of the upper dome. The values tabulated for section UD1H in Tables 4.4 and 4.6 should, therefore, be replaced with those computed for section UD4H in Tables AD.3 and AD.4. The values of the interaction loads and load factors for section UD1H in Table 4.3 should also be replaced by those for section UD4H in Table AD.4. The lowest interaction ultimate strength load factor of Table 4.3 becomes 2.8 at section W3V instead of 2.0 at section UD1H. These changes do not alter any of the conclusions contained in the body of the report.

AD.4 BASE MODELLING

The connection between the cylinder wall and the base is an important aspect of Gentilly type structures. Comparative analyses indicate that the results in this area are sensitive to the details of modelling the foundation. The technique used in this report has been described in Sect. 2.3. However, preliminary finite element analyses have indicated that the rotational stiffness at this base connection is of more significance than the vertical stiffness and, since no attempt was made in this report to simulate rotational foundation stiffness, the results of the present BOSOR4 analysis in the region of this connection may require substantial revision.

Some indications of the accuracy of the present BOSOR4 analysis may be obtained by comparing the field measurements made during the proof testing of the Gentilly 1 containment building (16) and the results of a BOSOR4 analysis of that building.

The controlling feature of a Gentilly type building, from the point of view of correlating strains, is the simple state of cylinder stresses which must occur in the central region of the cylinder wall. This can be computed from elementary strength of materials considerations without the necessity of a shell analysis or a computer code. Thus, from simple statics, the axial force and hoop force for an internal pressure of 17 psi (2448 psf) may be computed as:

$$N_1 = \frac{p\ D_i}{4} = 73440 \text{ lb/ft.}$$

$$N_2 = \frac{p\ D_i}{2} = 146880 \text{ lb/ft.}$$

The average σ_1 and σ_2 stresses may be obtained by dividing these forces by the thickness of the wall. The average strains may be computed as

$$\begin{Bmatrix} \varepsilon_1 \\ \\ \varepsilon_2 \end{Bmatrix} = \frac{1}{E} \begin{bmatrix} 1 & -\nu \\ \\ -\nu & 1 \end{bmatrix} \begin{Bmatrix} \sigma_1 \\ \\ \sigma_2 \end{Bmatrix}$$

OR

$$\begin{Bmatrix} \varepsilon_1 \\ \\ \varepsilon_2 \end{Bmatrix} = \frac{p\ D_i}{4\ t} \frac{1}{E} \begin{Bmatrix} 1 - 2\nu \\ \\ 2 - \nu \end{Bmatrix}$$

For the case of a pressure of 17 psi in Gentilly 1, this reduces to

$$\begin{Bmatrix} \varepsilon_1 \\ \\ \varepsilon_2 \end{Bmatrix} = \frac{127.5}{E} \begin{Bmatrix} 1 - 2\nu \\ \\ 2 - \nu \end{Bmatrix}$$

For the proof tests of Gentilly 1, an E value of 6×10^6 psi and Poisson's ratio of 0.15 were considered representative of the structure in the range of stress under consideration (Ref. 16, pg. 13). Substitution of these values into the above expressions for strains (the constant becomes

2.125×10^{-5}) yields

$$\varepsilon_1 = 14.88 \times 10^{-6}$$

$$\varepsilon_2 = 39.31 \times 10^{-6}$$

The radial displacement of the inside of the perimeter wall, using these strains, is 28.3×10^{-3} in. and of the wall centerline is 29.25×10^{-3} in. If, on the other hand, Poisson's ratio is assumed zero, and E is maintained at 6×10^6 psi, the above values become $\varepsilon_1 = 21.25 \times 10^{-6}$, $\varepsilon_2 = 42.50 \times 10^{-6}$, $w_i = 30.6 \times 10^{-3}$ and $w_{\mathrm{C\!\!L}} = 31.62 \times 10^{-3}$ in. These values are summarized in Table AD.5.

Information from PLATES 7 and 8 of Ref. 16 is reproduced in Figs. AD.5, AD.6 and AD.7 where it is compared with some results from the present preliminary studies. The value of the strains and deflection at mid-height, from the analysis of Ref. 16, are also tabulated in Table AD.5. It is apparent that the analytical strain predictions of Ref. 16 correlate well with the strains of Column 1 of the table, predicted from the simple strength results for $E = 6 \times 10^6$ psi and $\nu = 0.15$. However, it appears as though the deflections of Fig. AD.5 have been predicted using $E = 6 \times 10^6$ psi and $\nu = 0$, since the deflection result correlates with column 2 of the table. In order to verify this, the investigators have run a BOSOR4 analysis in an attempt to reproduce the theoretical values of Fig. AD.5. By providing an ideal hinge at the base of the wall, applying to it an external moment of 66816 ft-lb. (inferred from PLATE 8 and the description on pg. 36 of Ref. 16), setting $E = 6 \times 10^6$ psi and $\nu = 0$, the BOSOR4 analysis yields displacement results, denoted as 'fixed hinge' results in Fig. AD.5, indistinguishable from the theoretical values reproduced from PLATE 7 of Ref. 16. Although BOSOR4 does not output strain values, but only stress resultants and displacements, approximate strains consistent with this 'fixed hinge' analysis may be obtained by numerical differentiation of the displacements. These strains have been computed from the BOSOR4 run and are shown on Figs. AD.6 and AD.7. The BOSOR4 strains correspond closely with those of Ref. 16 on Fig. AD.6 but produce the mid-height strain of 42.5×10^{-6}, as shown in column 2 of Table AD.5.

The strains in the vertical direction are plotted in Fig. AD.7. These do not correspond as well with those of Ref. 16 but are more consistent with those of column 2 of Table AD.5 than the results from Ref. 16. Since the results of Ref. 16 on Figs. AD.6 and AD.7 are consistent with column 1 of Table AD.5, while the deflections of Fig. AD.5 are consistent with column 2 of Table AD.5 one must make this adjustment in any attempted comparison.

It may be concluded that, for the base support conditions assumed in Ref. 16, the BOSOR4 analysis predicts exactly the same wall displacements if Poisson's ratios, ν, is taken as zero. The strains predicted by BOSOR4 are essentially the same as those from Ref. 16 if Poisson's Ratio, ν, is taken as 0.15.

All of this confirms, in our minds, the validity of the BOSOR4 technique for estimating the elastic response of a Gentilly type of containment shell.

The discussion above has centered around the analysis of a model with a pure hinge at the base of the wall which is fixed in space and to which a known moment can be applied to produce a set of deflections and strains which correlate with field measurements. Such a model may be referred to as a 'fixed hinge' model. The analysis upon which this report is based uses a considerably different approach for modelling the base connection of the structure, which attempts to include the base flexibility. The investigators recognize that a more detailed investigation of the base area is required before any definitive statements can be made with respect to the most satisfactory techniques of modelling this area. However, an analysis similar to that used in body of this report has been run for the Gentilly 1 structure, with elastic stiffnesses adjusted to produce a deflection of 31.6×10^{-3} in. at mid-height of the cylinder. Let us refer to this model as a 'rigid link' model. The displacements in the lower segment of the cylinder wall predicted by this analysis are plotted in Fig. AD.8. The analysis predicts a negative radial movement of the hinge of 7.12×10^{-3} inches. The first impression of these results indicates that they yield significant differences from the field measurements. However, the reader should bear in mind the extreme difficulty in measuring small absolute displacements in the field. A study of Ref. 16, (pg. 33) indicates that the displacements of the perimeter wall were measured relative to an interior wall which had a clearance of one foot from the perimeter wall. If this interior wall is subjected to a rotation of 18×10^{-6} radians, due to deformations of the base slab, the relative motion between the exterior and interior walls becomes, for all practical purposes, the same as the absolute displacement predicted with a fixed hinge. This relative displacement is also plotted on Fig. AD.8.

A prediction of strains using the rigid link modelling technique is shown on Figs. AD.9 and AD.10. There is no question that the 'fixed hinge' BOXOR4 strains of Fig. AD.6 correlate better with the field measurements of tangential strains than the 'rigid link' strains of Fig. AD.9. However, the 'rigid link' strains of Fig. AD.10 correlate considerably better with the field measurement of vertical strains than the theoretical strains from Ref. 16. Indeed the 'fixed hinge' strains of Ref. 16 appear to place the inflection point below the level of strain measurements, whereas the strain measurements themselves indicate the inflection point should be above this level. This observation has important implications with respect to the moment that may be developed in the base connection.

AD.5 CLOSURE

It is not the purpose of Sect. AD.4, nor is it the purpose of this report, to argue that any particular model under consideration is 'right'. Indeed such arguments are counterproductive, and generally inhibit a real understanding of behaviour. However, the investigators believe that the field measurements are open to interpretation and that there is no compelling case to establish the superiority of the 'fixed hinge' model over a suitably chosen 'rigid link' model. The 'best' parameters for a reliable modelling technique in the area of the base can probably only be determined by more sophisticated analytical techniques which are presently under study.

It is interesting to note the remark on pg. 36 of Ref. 16 about the nonlinear response of field measurements with respect to internal pressure. There are many sources from which such nonlinearities can arise, one of which is nonlinear material response or crack variation in localized areas of the structure. Correlation of linear predictions with field measurements is not totally conclusive evidence that linear behaviour is taking place.

The investigators do not wish to imply that they have any reason to believe that there is unsatisfactory response in the behaviour of the structure. Indeed they have been impressed with the thoroughness of the design and the excellent correlation that has been achieved in carrying out very difficult field measurements. On the other hand, they do not believe that definitive answers have been obtained to all aspects of the behaviour of such structures.

TABLE AD.1

NUMERICAL COEFFICIENTS FOR
LOAD COMBINATIONS

Struct.	Load	BDL	ADL	Tf(#)	Ts(^{o}F)	SST(^{o}F)	WOT(^{o}F)	SOT(^{o}F)
BW	Wd	1	1					
	LBd	1	1					
	Bf			276264				
	Whf			10580				
	Bu				-0.9692			
	Wu				-2.4615			
BD	LDd*		1					
	UBd	1	1					
	LDd		1					
	LBf			9624				
	Bu				-0.6462			
	Wu				-1.3538			
	LBu				-6.9231			
C	LDd	1						
	LDd*		-1					
	UDd	1	1					
	UBf			4559				
	Whf			4232				
	Wvf			199500				
	UDf			5197				
	Bu				-13.5692	2.5	13.0	20.0
	Wu				-12.9692	19.0	-12.0	36.5
	RBu				-13.8	19.0	-12.0	36.5
	UBu				- 2.3538			
	LDu				-11.7692	5.0	26.0	40.0
	UDu				-17.7692	19.0	-12.0	36.5
	Bg					- 1.0	- 5.2	- 8.0
	Wg					8.0	-21.7	- 2.0
	RBg					4.0	-10.9	- 1.0
	UDg					14.0	-38.0	- 3.5

Load Comb.	Rd1	Rf1	Rs1	Rd2	Rf2	Rs2
BDL	1	1	1			
ADL				1	1	1
Tf		1	1		1	1
Ts			1			1

BDL = Basic dead load　　Tf = Total prestress
ADL = Alternate dead load　　Ts = Total shrinkage.

NOTE: See also Chapter 2, and Tables 2.1 and 2.2, for terms not defined here.

TABLE AD.2

STRESS RESULTANTS AT LOCATION UD4

Stress Resultant	Load Condition		
		C:Cp	
	Rf1	@ 1 psf	@ 18 psi
N1	-353970	52.46	135,980
N2	-187870	-38.54	- 99,900
M1	- 47847	42.06	109,020
M2	- 1074	4.30	11,146

TABLE AD.3

PRESSURIZATION LIMIT LOADS AT SECTION UD4H

Limit State	Cracking Analysis				Interaction Analysis
	k=0	WOT, k=0	k=6	WOT, k=6	
FC	160	0-(210)-300	210	0-(50)-360	150
FY	600	620	600	620	330
TC	410	370	430	390	NA
ULT	720	720	720	720	410

TABLE AD.4

PRESSURIZATION LOAD FACTORS AT SECTION UD4H

Limit State	Cracking Analysis				Interaction Analysis
	k=0	WOT, k=0	k=6	WOT, k=6	
FC	1.2	0-(1.5)-2.2	1.5	0-(0.4)-2.6	1.1
FY	4.4	4.6	4.4	4.6	2.4
TC	3.0	2.7	3.2	2.9	NA
ULT	5.3	5.3	5.3	5.3	3.0

NOTE: For notation, see Chapters 2 and 4.

TABLE AD.5

MID-HEIGHT STRAINS AND DISPLACEMENTS FROM THIN CYLINDER ANALYSIS

Column	1	2	3
Variables	$E = 6 \times 10^6$ $\nu = 0.15$	$E = 6 \times 10^6$ $\nu = 0$	Ref. 16
ε_1 ε_2	14.88×10^{-6} 39.31×10^{-6}	21.25×10^{-6} 42.50×10^{-6}	14×10^{-6} 40.5×10^{-6}
w_i $w_{\pounds}$	28.30×10^{-3} 29.25×10^{-3}	30.6×10^{-3} 31.6×10^{-3}	31.6×10^{-3}

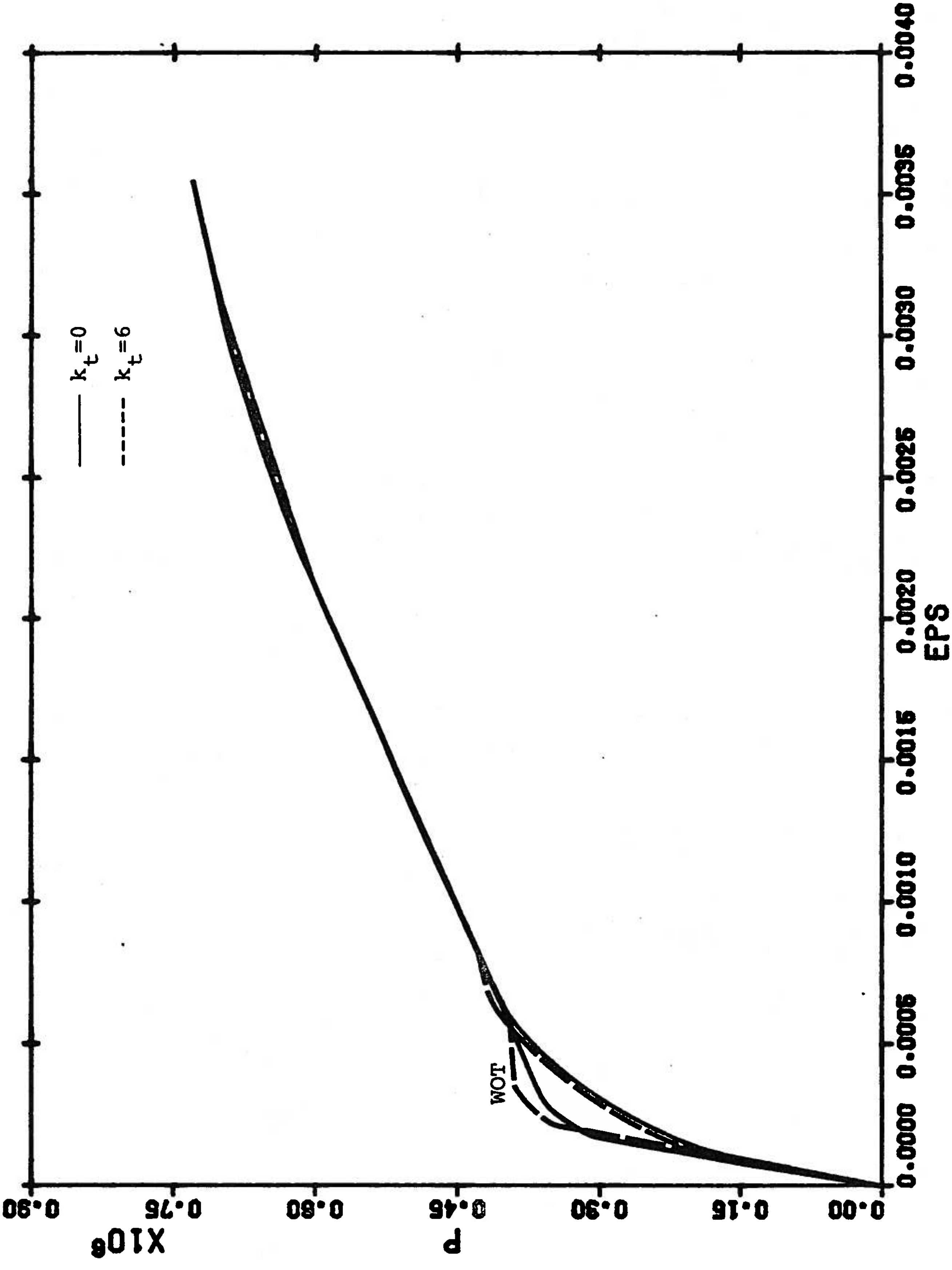

FIGURE AD.1 - P vs ε for Section W4H

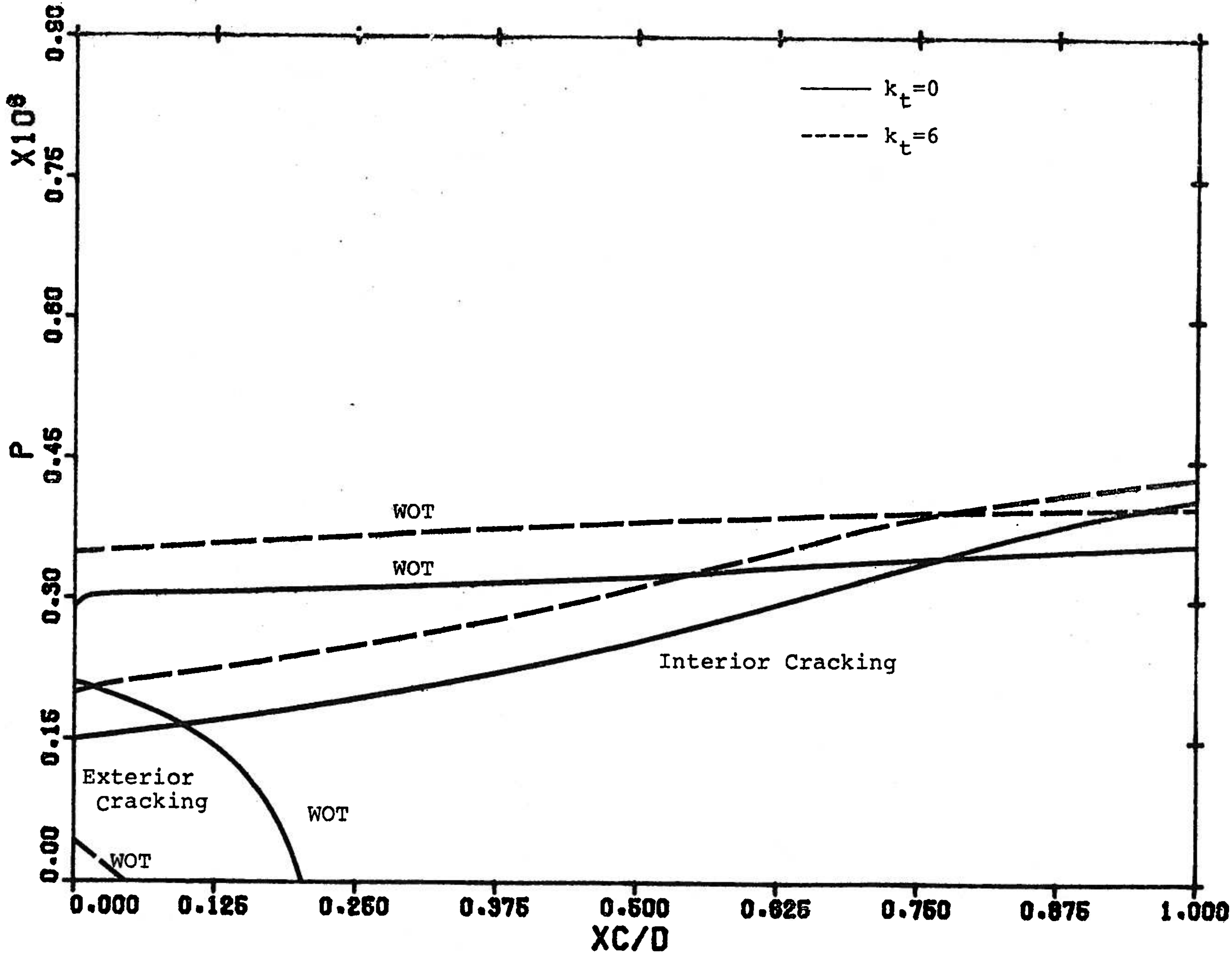

FIGURE AD.2 - x_c/d for Section W4H

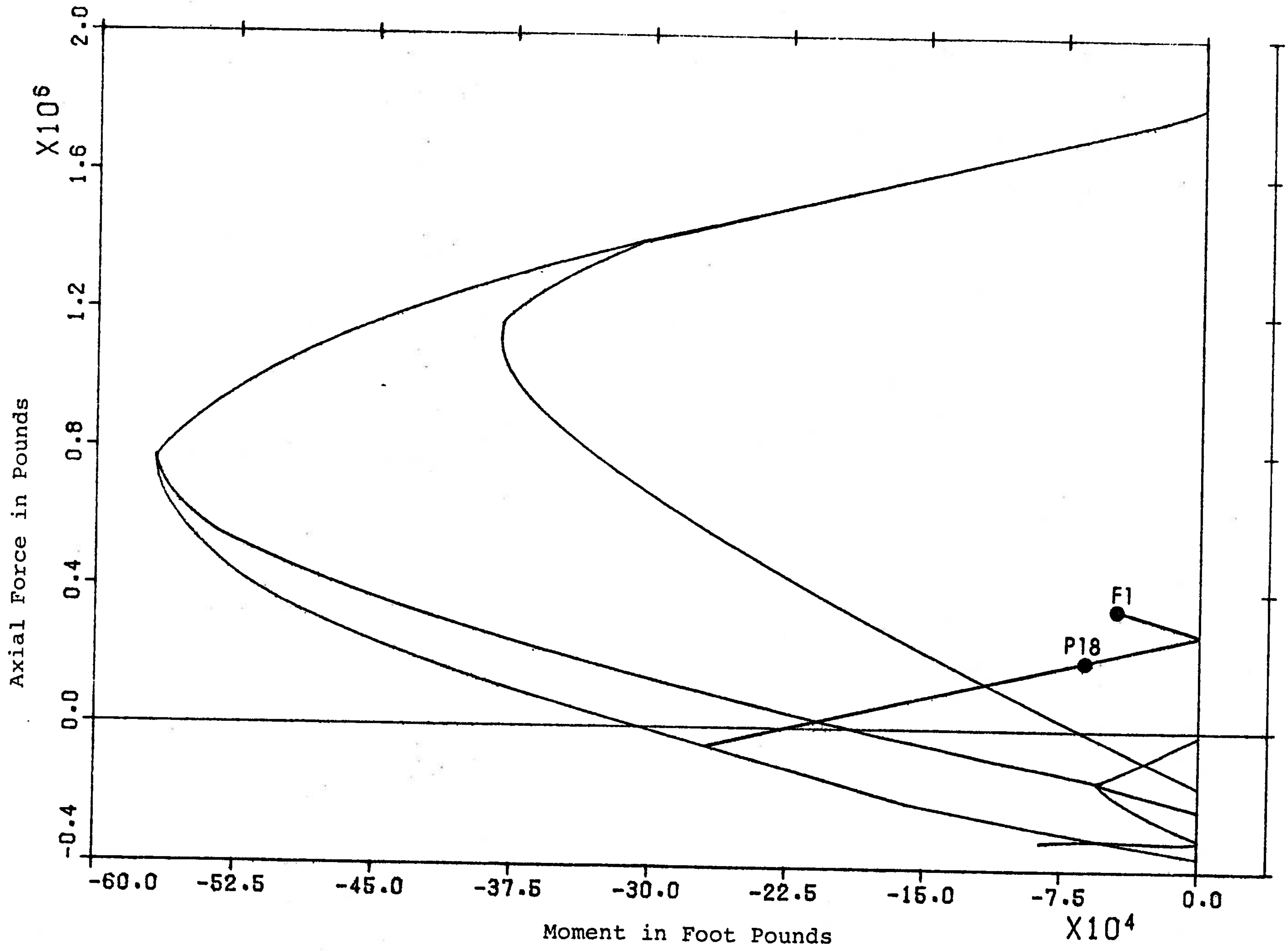

FIGURE AD.3 - Interaction Plot for Section UD4H

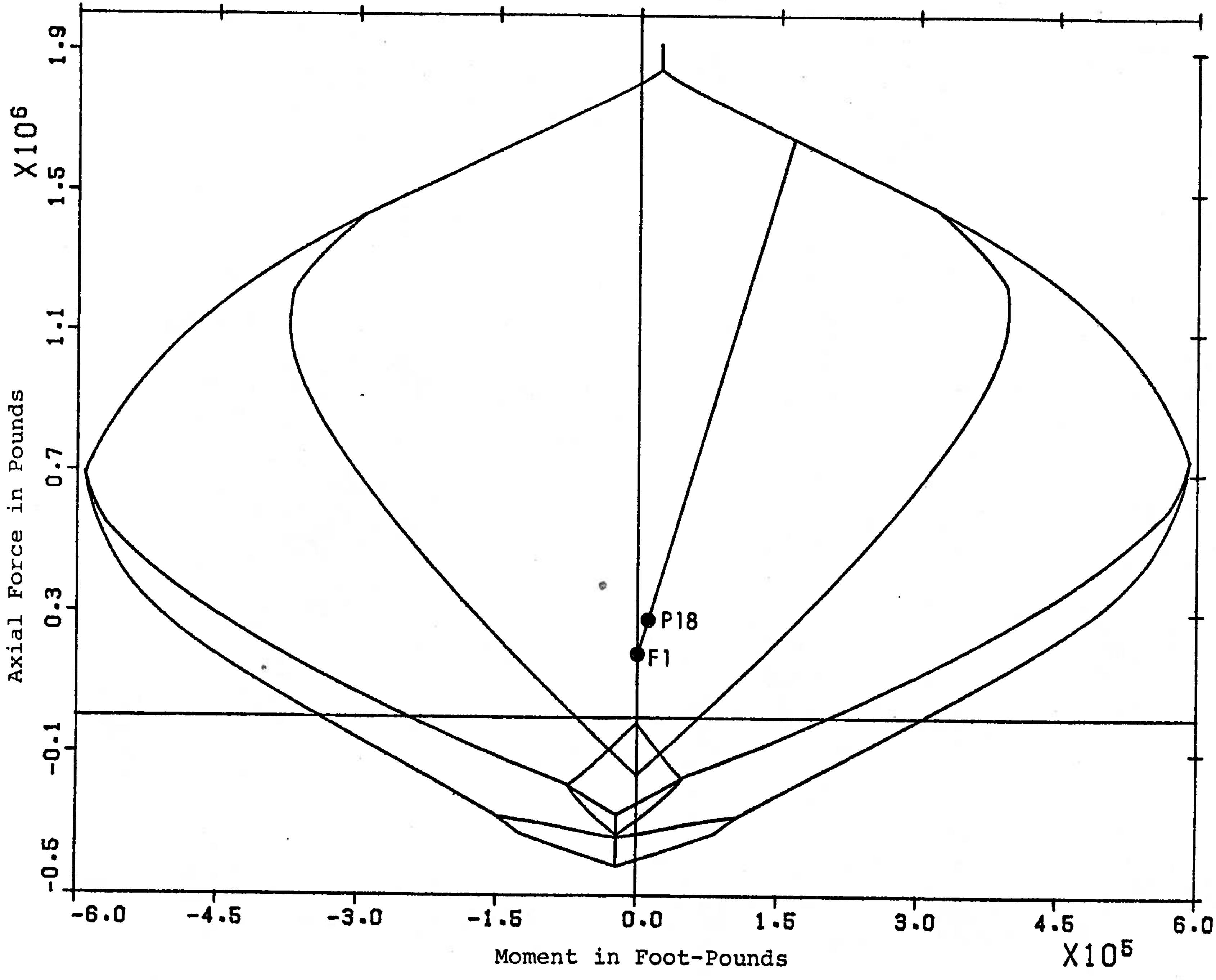

FIGURE AD.4 - Interaction Plot for Section UD4V

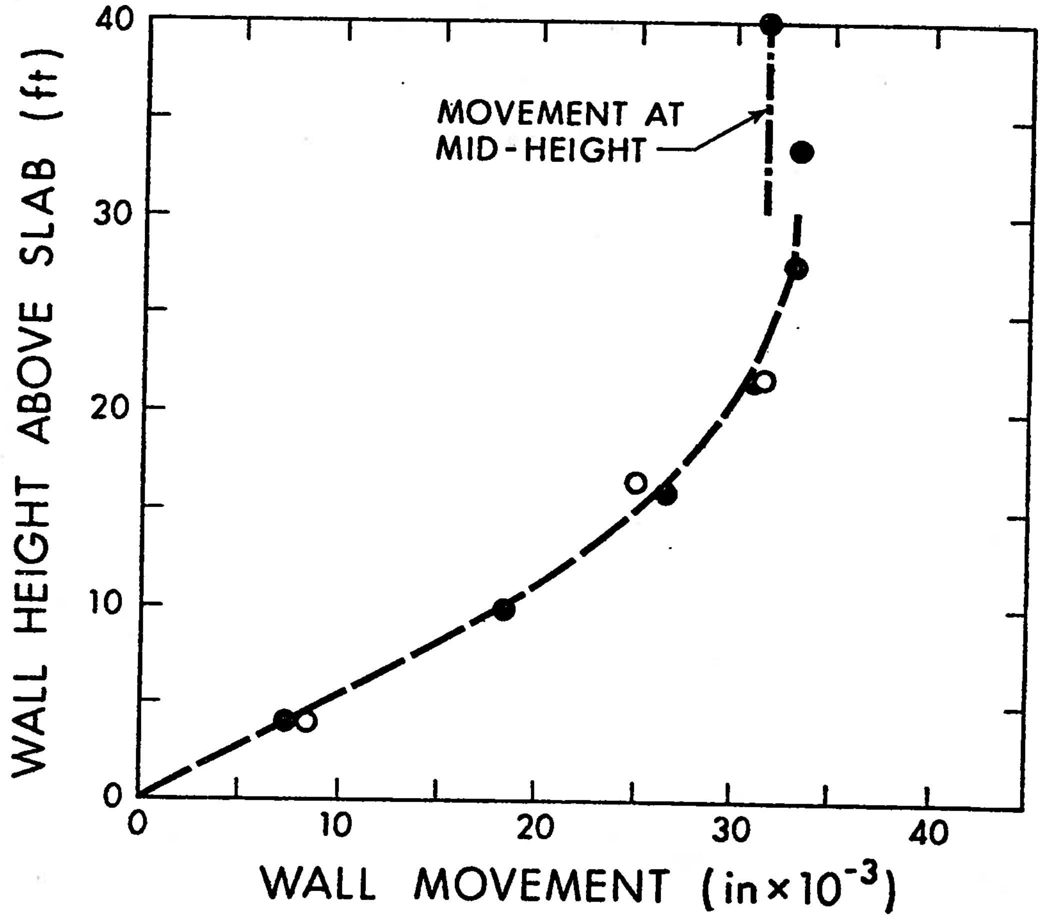

Legend

— — Ref. 16, theoretical value (fixed hinge).

○ Ref. 16, field measurement

● BOSOR4, fixed hinge model ($E = 6 \times 10^6$ psi, $\nu = 0$).

Figure AD5 - Radial Movement of Perimeter Wall (Fixed Hinge Model).

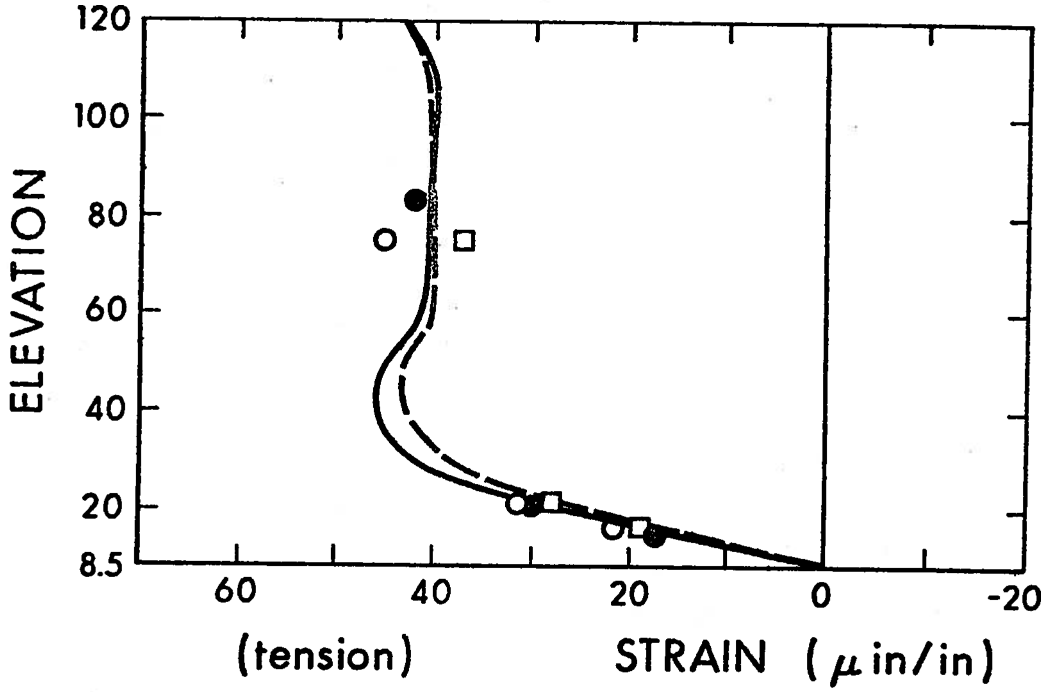

Legend

Ref. 16, theoretical value, exterior face

Ref. 16, theoretical value, interior face

Ref. 16, field measurement, exterior face

Ref. 16, field measurement, interior face

BOSOR4, fixed hinge model ($E = 6 \times 10^6$, $\nu = 0$)

Figure AD6 - Horizontal Strains in Perimeter Wall (Fixed Hinge Model).

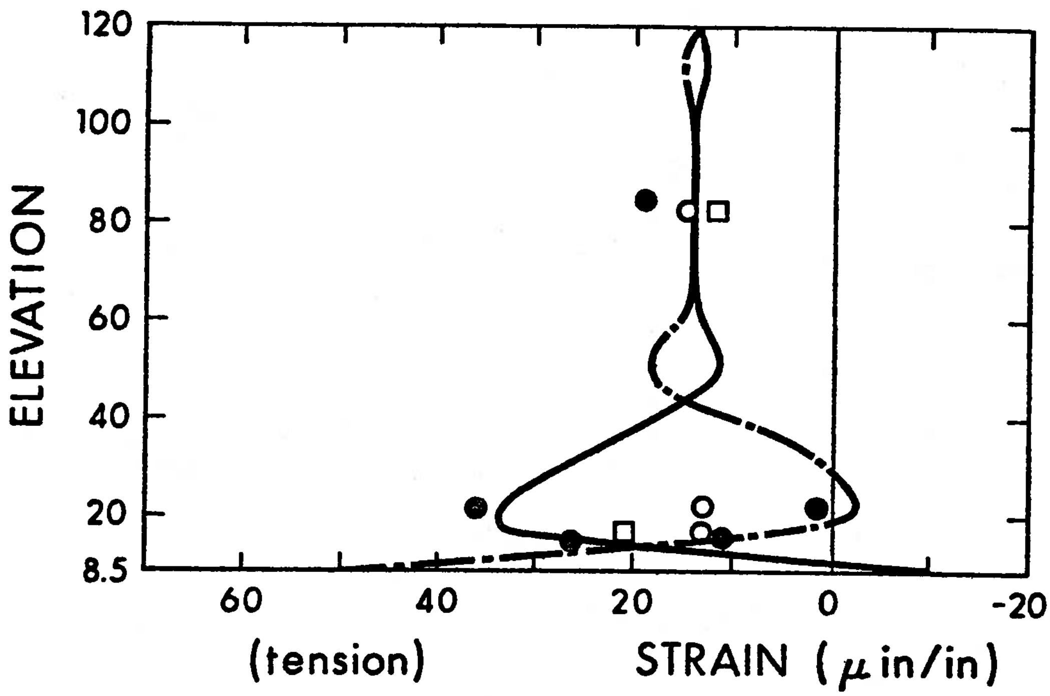

Legend

- Solid line: Ref. 16, theoretical value, external face.
- Dash-dot line: Ref. 16, theoretical value, interior face.
- O Ref. 16, field measurement, exterior face
- □ Ref. 16, field measurement, interior face
- ● BOSOR4, fixed hinge model ($E = 6 \times 10^6$ psi, $\nu = 0$)

Figure AD7 - Vertical Strains in Perimeter Wall (Fixed Hinge Model).

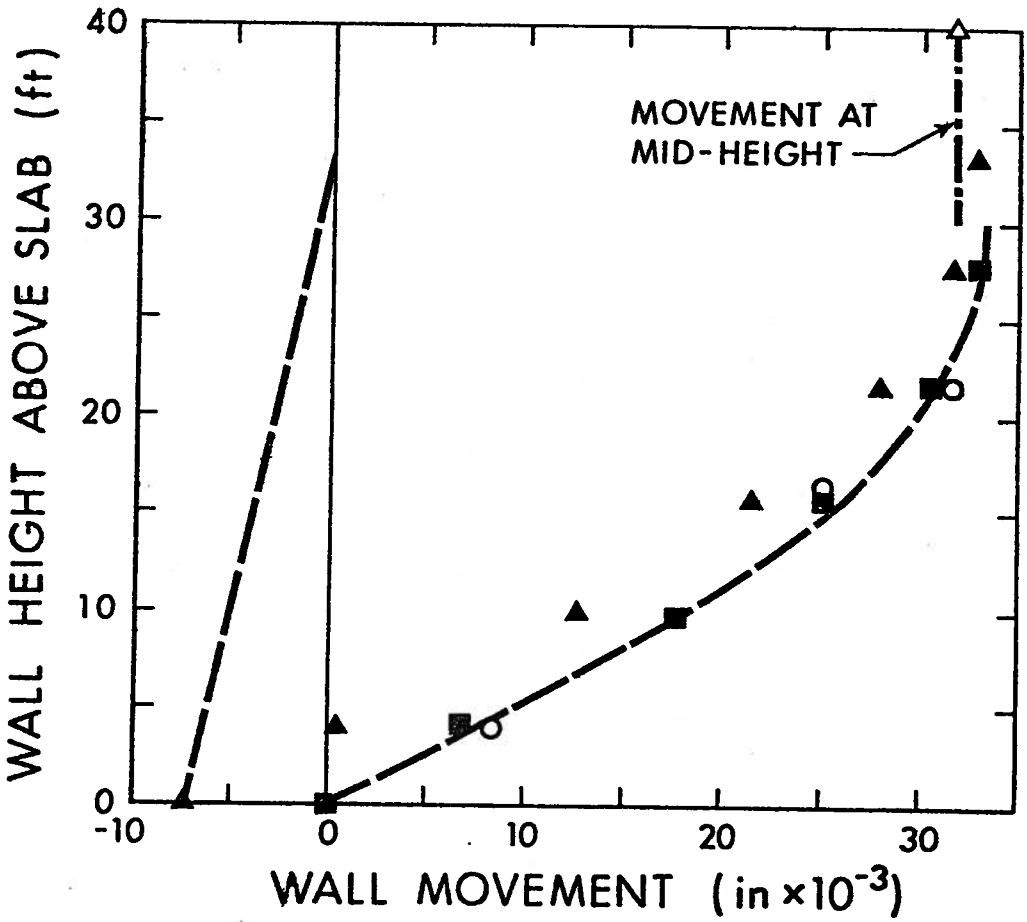

Legend

——— ———	Ref. 16, theoretical vlaue (fixed hinge)
○	Ref. 16, field measurements
▲	BOSOR4. rigid link, absolute displacements
■	BOSOR4, rigid link relative displacements
△	BOSOR4, midheight displacement (adjusted)

Figure AD8 - Radial Movement of Perimeter Wall (Rigid Link).

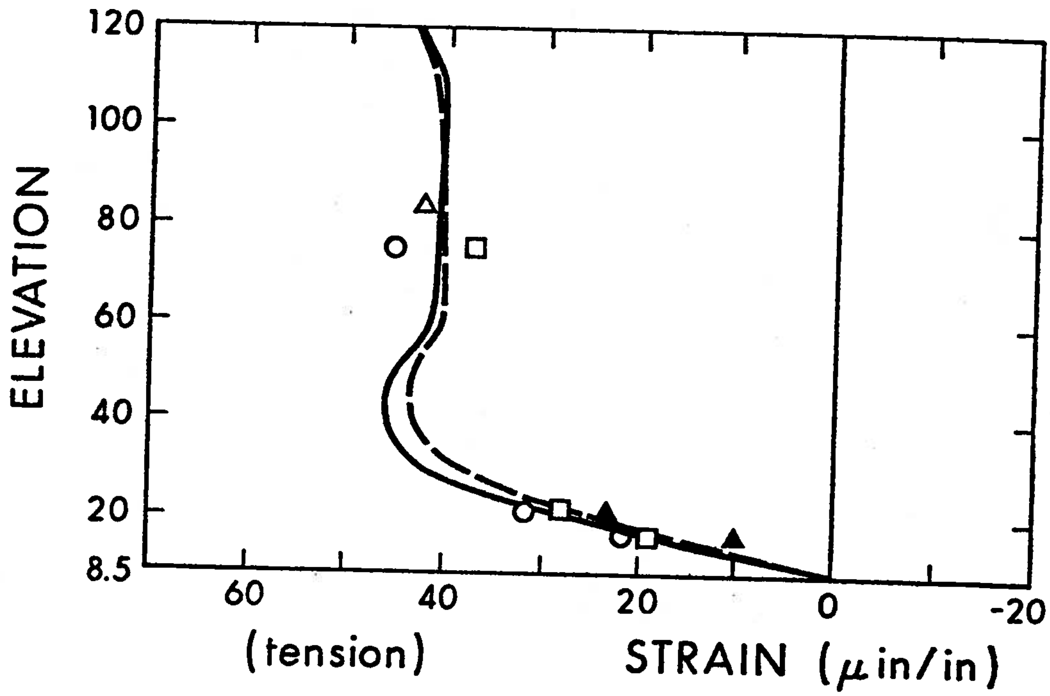

Legend

- Ref. 16, theoretical value, exterior face (solid line)
- Ref. 16, theoretical value, interior face (dashed line)
- ○ Ref. 16, field measurement, exterior face
- □ Ref. 16, field measurement, interior face
- ▲ BOSOR 4, rigid link model
- △ BOSOR 4, fixed hinge and rigid link models.

Figure AD9 - Horizontal Strains in Perimeter Wall (Rigid Link Model).

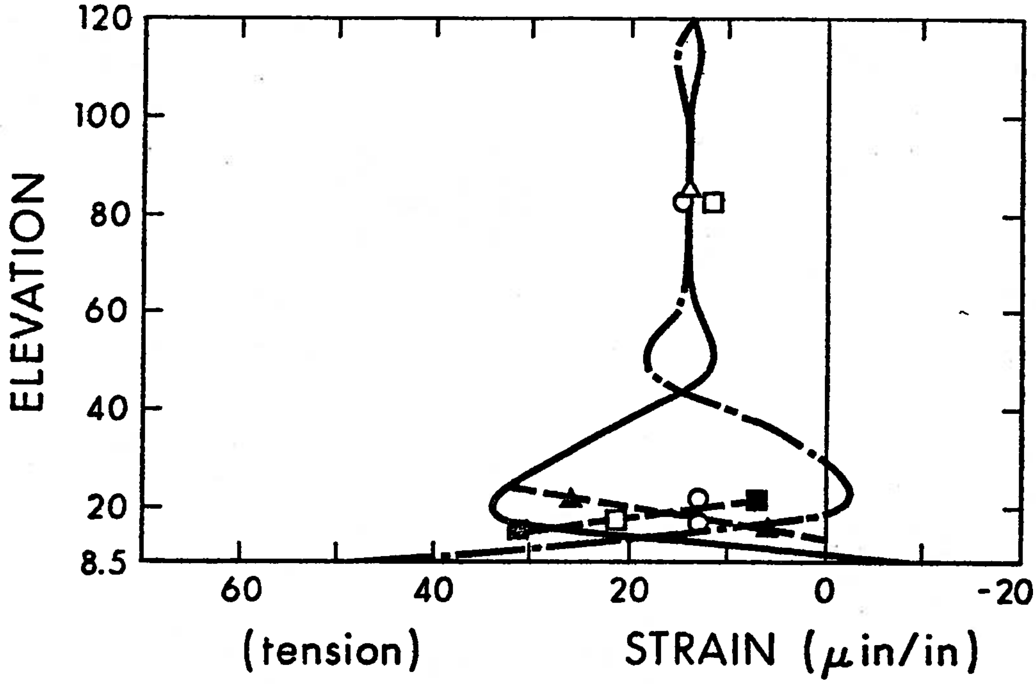

Legend

———	Ref. 16, theoretical value, exterior face
—·—	Ref. 16, theoretical value, interior face
○	Ref. 16, field measurement, exterior face
□	Ref. 16, field measurement, interior face
▲	BOSOR4, rigid link model, exterior face
■	BOSOR4, rigid link model, interior face
△	BOSOR4, rigid link model, both faces

Figure AD10 - Vertical Strains in Perimeter Wall (Rigid Link Model)